NASA
Technical
Paper
2447
C.2
December 1985

Effect of Underwing Aft-Mounted Nacelles on the Longitudinal Aerodynamic Characteristics of a High-Wing Transport Airplane

William K. Abeyounis and
James C. Patterson, Jr.

NASA

NASA Technical Paper 2447

1985

Effect of Underwing Aft-Mounted Nacelles on the Longitudinal Aerodynamic Characteristics of a High-Wing Transport Airplane

William K. Abeyounis and
James C. Patterson, Jr.

Langley Research Center
Hampton, Virginia

National Aeronautics
and Space Administration

**Scientific and Technical
Information Branch**

SUMMARY

As part of a propulsion/airframe integration program at Langley Research Center, tests have been conducted in the Langley 16-Foot Transonic Tunnel to determine the longitudinal aerodynamic effects of installing flow-through mixed-flow engine nacelles in the aft underwing position of a high-wing transonic transport airplane. Both circular and D-shaped inlet nacelles were tested. In search of a structurally adequate low-drag pylon configuration, antishock bodies installed on the wing and nacelle upper surfaces were also tested. Data were obtained for a free-stream Mach number range from 0.70 to 0.85 and a model angle-of-attack range from -2.5° to 4.0°. The design cruise conditions were a free-stream Mach number of 0.80 and a lift coefficient of 0.43 (at an angle of attack of approximately 1°).

Installation of nacelles in the aft underwing position produced lift increases, as opposed to the loss in lift typical of forward wing-mounted nacelle configurations. The longitudinal aerodynamic characteristics of the aft-mounted nacelle configurations were better than those of a conventional, forward, underwing pylon-mounted nacelle configuration. The D-shaped inlet nacelles had the lower nacelle installation drag. It was also demonstrated that properly configured antishock bodies, proposed to house the structure required to attach the nacelles in the aft underwing position, could be installed on the wing and nacelle upper surfaces without a deterioration of the longitudinal aerodynamic cruise performance at a Mach number of 0.80. At the highest test Mach number of 0.85, at which a higher shock loss occurs, one of the antishock-body/pylon configurations reduced the nacelle installation drag approximately 80 percent at cruise lift.

INTRODUCTION

The installation of engine nacelles on the wing, fuselage, or tail of an airplane has a decided effect on the aerodynamic performance of the airplane. In particular, the installed drag of the propulsion system directly affects the fuel consumption at cruise conditions. Previous studies (ref. 1) have shown the difficulty of reducing interference drag for conventional, forward, underwing pylon-mounted nacelles on supercritical wings. Conversely, it has been shown theoretically that a lower installation drag may be obtained by placing the nacelles in the underwing aft-mounted position (ref. 2) where they inherently cause fewer wing upper-surface flow disturbances and minimize channeling effects of the wing/pylon/nacelle juncture. Also, the aft installation lends itself to blending D-shaped inlets into the wing lower surface, a result which may have a favorable effect on interference drag.

One important concern related to aft-mounted nacelles is the problem of providing structurally adequate nacelle supports that do not negate the drag benefits of the aft installation. The application of antishock bodies similar to those reported in reference 3 has been proposed as one potentially fruitful approach to this problem.

To determine the aerodynamic effects of this unconventional nacelle installation, nacelles with both circular and D-shaped inlets (referred to herein as "circular nacelles" and "D-nacelles," respectively) were tested in a wind-tunnel

investigation. Configurations with antishock bodies were also included to explore the feasibility of configuring low-drag supports that are structurally adequate for mounting nacelles in the aft underwing position.

SYMBOLS AND ABBREVIATIONS

A	cross-sectional area, in^2
A_0	capture area, in^2
ABL	buttline for highlight diverter (fig. 8), in.
AWL	waterline for highlight diverter (fig. 8), in.
BL	buttline of model (lateral dimension), in.
b	wing span, in.
C_D	drag coefficient, $\text{Drag}/q_\infty S$
ΔC_D	nacelle installation drag
C_L	lift coefficient, $\text{Lift}/q_\infty S$
$\mathbb{C}_L$	centerline
C_m	pitching-moment coefficient, $\text{Pitching moment}/q_\infty \bar{c} S$
C_n	normal-force coefficient, $(\text{Normal force to WRP})/q_\infty S$
C_p	pressure coefficient, $(p - p_\infty)/q_\infty$
c	chord measured in wing reference plane, in.
$\bar{c}$	mean geometric chord, $\frac{2}{3}\left(c_T + c_R - \frac{c_T c_R}{c_T + c_R}\right)$, in.
c_{av}	average wing chord, in.
c_R	reference root chord at model centerline, in.
c_T	reference tip chord, in.
D_{exit}	nacelle-exit diameter, in.
FS	fuselage station (axial dimension from nose of model), in.
h	length of vertical superelliptic axis for top half of D-nacelle internal transition section, in.
L	length, in.
LER	leading-edge radius, in.
M_∞	free-stream Mach number

MHB maximum half-breadth, in.

NBL D-nacelle buttline (fig. 9), in.

NS nacelle station, in.

NWL D-nacelle waterline (fig. 9), in.

n exponent for superelliptic equation for top half of D-nacelle internal transition section

PBL pylon buttline for circular nacelle, in.

PWL pylon waterline for circular nacelle, in.

p pressure, lb/in^2

p_∞ free-stream static pressure, lb/in^2

q_∞ free-stream dynamic pressure, lb/in^2

$\mathcal{R}$ D-nacelle radial distance from top (fig. 9), in. (denoted by "SCRIPT-$\mathcal{R}$" in table 10)

r_c radius of curvature, in.

r_m radius from model local centerline, in.

r_n radius from nacelle centerline, in.

r_{SB} cross-sectional radius of antishock body, in.

S wing reference area, in^2

t wing thickness, in.

WL waterline of model (vertical dimension), in.

WRP wing reference plane (WL 3.25), in.

x local axial dimension, in.

y local lateral dimension, in.

z vertical dimension, in.

α angle of attack, deg

ε wing twist angle, deg

η semispan location, 2y/b

θ circumferential angular dimension for D-nacelle (fig. 9), deg

μ rotation angle of 4.573° between coordinate axes of model and circular nacelle (fig. 8), deg

τ nacelle forebody thickness, in.

ϕ rotation angle between highlight diverter for circular nacelle and coordinate axes of model (fig. 8), deg

ψ circumferential angular dimension from vertical axis through nacelle centerline (fig. 8), deg

Subscripts:

cn circular nacelle

HL highlight

lip inlet-forebody lip

max maximum cross section

EXPERIMENTAL APPARATUS AND PROCEDURE

Wind Tunnel

The experimental investigation was conducted in the Langley 16-Foot Transonic Tunnel (refs. 4 and 5). This facility is a single-return, continuous-flow, atmospheric wind tunnel. It has a 47-ft-long octagonal test section with eight longitudinal slots and a throat cross-sectional area of 199.15 ft^2. The tunnel has continuous air exchange for cooling. The wall divergence in the test section is adjusted as a function of the airstream dew point and Mach number to minimize any longitudinal static-pressure gradients in the test section. The free-stream Mach number is continuously variable to a maximum of 1.30 with an accuracy of ±0.005. The average Reynolds number per foot varies from approximately 1.46×10^6 at a free-stream Mach number of 0.20 to approximately 4.10×10^6 at a free-stream Mach number of 1.30.

Model and Support System

General arrangement.- The experimental apparatus used in this investigation is shown in figure 1. The 1/24th-scale model was representative of a wide-body transport. The model was fully metric and sting supported on a six-component strain-gauge balance. It had a high wing consisting of supercritical airfoil sections and a T-shaped tail (T-tail). Both circular nacelles and D-nacelles were tested in the aft underwing position. A sketch showing the general arrangement of the transport model is given in figure 2. The model blockage was 0.36 percent of the test-section cross section.

Model support system.- The transport model was sting mounted in the test section of the tunnel. The centerline of the model was aligned with the test-section centerline at an angle of attack of 0°. The moment center of the balance at a fuselage station of 30.203 in. (FS 30.203) was located at tunnel station 132.51 ft with the model nose at tunnel station 129.99 ft.

Fuselage.- The fuselage geometry of the model is shown in figure 3. This fuselage was 62.0 in. in length with circular cross sections and a maximum diameter of 9.0 in. The model had an ellipsoidal nose, a cylindrical centerbody, and an upswept aft section. Wing-fuselage fairings shown in figure 4 were added to fill the gap between the fuselage and the wing lower surface. Table 1 presents coordinates of the wing-fuselage fairings.

Wing.- The wing geometry is presented in figure 5(a). In addition to the dimensions shown, the wing was defined by specifying the airfoil sections used at the three spanwise stations shown in figure 5(b). The airfoil section at the fuselage side was a supercritical airfoil section modified to have reduced curvature on the aft upper surface. The maximum thickness of this airfoil section was located at a chordwise station x/c of approximately 0.30 as opposed to the normal x/c of 0.40. These modifications were incorporated to compensate for adverse fuselage interference that tends to move wing isobars aft, thereby unsweeping the shock wave in this region. The airfoil sections at the planform break and at the wing tip were supercritical sections. A thickness ratio t/c of 0.144 was specified at the fuselage side, 0.12 at the planform break, and 0.10 at the wing tip. As shown in figure 5(c), the wing twist ε was specified to be 2.4622° at the fuselage side, 0.2564° at the planform break, and -1.2294° at the wing tip with a linear variation between these spanwise locations. The wing sections were oriented so that the leading-edge points were collinear. The wing sweep was 32.81° at the leading edge, 30.00° at $x/c = 0.25$, and 20.58° at the trailing edge (outboard the planform break). Intermediate spanwise sections were obtained by linearly interpolating along lines of constant percent chord. The wing definition at the intersection with the fuselage was obtained by extrapolating the airfoil coordinates from the two most inboard airfoil sections specified. Fillets were added to the fuselage-wing leading-edge junctures (fig. 4). The wing-tip leading edges also were faired and rounded. Wing streamwise coordinates relative to the wing reference plane (WRP) 3.25 in. above the model waterline are presented in table 2 for selected span stations. Chordwise rows of pressure orifices were located at 10 spanwise locations η as shown in figure 5(d) and listed in table 3.

Tail.- The model had a T-tail with a bullet fairing at the juncture of the horizontal and vertical stabilizers. A sketch of the vertical stabilizer and bullet fairing is shown in figure 6, and a sketch of the horizontal stabilizer is shown in figure 7.

The vertical stabilizer had a symmetrical airfoil section. The coordinates for this airfoil section are presented in figure 6. The airfoil had a ratio of leading-edge radius to chord of 0.0100 and a ratio of maximum thickness to chord of 0.1126. The reference planform was trapezoidal with a height of 11.500 in. The root was at a waterline of 4.5 in. (WL 4.500) and had a chord of 15.119 in. with the leading edge located at a fuselage station of 45.688 in. (FS 45.688). The tip was at WL 16.000 and had a chord of 9.800 in. Thus, the taper ratio was 0.6482; the sweep angle was 49.60° at the leading edge, 35.47° at the trailing edge, and 46.65° at the quarter-chord line. The vertical stabilizer extended past WL 4.500 to intersect the curved fuselage surface. A fairing, smoothing the intersection of the leading edge and fuselage, extended forward to FS 42.938.

The bullet fairing is also shown in figure 6. It had circular cross sections centered about WL 15.840. Its length was 14.000 in., extending from FS 58.000 to FS 72.000. It consisted of a 1.750-in-diameter cylindrical centerbody and two 3.638-in-long ogive tips with longitudinal radii of 8.000 in.

The horizonal stabilizer had an inverted-camber airfoil section with no dihedral or twist. The incidence angle was variable by ±2°, but it was tested only at the 0° setting. The coordinates for this airfoil section at the 0° incidence setting are presented in figure 7 with the reference plane located at WL 16.000. The airfoil section had a ratio of leading-edge radius to chord of 0.0188 and a ratio of maximum thickness to chord of 0.1168. The reference planform was trapezoidal with a span of 24.000 in. The root chord was 9.000 in. with the leading edge located at FS 60.000. The tip chord was 3.400 in. Thus, the taper ratio was 0.3778; the sweep angle was 36.25° at the leading edge, 14.93° at the trailing edge, and 31.66° at the quarter-chord line. The tip leading edges were faired and rounded in the same manner as the wing tips.

Nacelle and pylon.- Two flow-through, long-duct, mixed-flow nacelles were tested, a circular nacelle shown in figure 8 and a D-nacelle shown in figure 9. Both nacelles were designed to have a mass flow ratio A_0/A_{HL} of 0.70 at the free-stream Mach number of 0.80. The centerlines of both nacelles were located at $\eta = 0.370$, the same as for a similar forward-mounted nacelle previously tested (ref. 6). The inlet highlights were located at $x/c = 0.714$ (at FS 33.65). The local Mach number for the clean wing at this location was 0.72. Both nacelles had a maximum diameter of 4.500 in. and a length of 15.750 in. with smooth exterior and interior surfaces. (Both had continuous first and second derivatives in the axial direction.) Reference 7 presents a geometric description of both configurations. Much of the geometric information presented in the tables herein was extracted from reference 7.

Circular nacelle.- The centerline of the circular nacelle was located at WL 0.80 and $\eta = 0.370$. The exterior consisted of a forebody, a cylindrical section, and an afterbody. The forebody was a shaped ellipse 2.713 in. long that was followed by a 5.087-in. cylindrical section with a diameter of 4.500 in. The 7.95-in. afterbody consisted of two sections. The first section had an elliptic distribution of the inverse of the longitudinal radius of curvature with a peak value of r_{max}/r_c of 0.061. It faired into a second section, a 2.200-in. conical section with a half-cone angle of 7.01° and an external exit diameter of 3.2228 in. Coordinates for the exterior of the circular nacelle are presented in table 4.

The interior of the circular nacelle also consisted of three sections. The inlet lip was 0.342 in. long and had a contraction ratio of 1.21. Its shape was a lemniscate with an aspect ratio of 2.0 and with specified radii of curvature at the highlight and throat. The diameter of the highlight was 3.748 in., and the diameter of the throat was 3.406 in. The inlet was followed by a 13.2709-in-long cylindrical section and a 2.1371-in-long conical section with a half-cone angle of 3° and an exit diameter of 3.182 in. Interior coordinates are presented in table 5.

Diverter.- The two diverters shown in figure 8 were used to fair the gap between the circular nacelle and the wing lower surface. The gap was designed to have flow with no adverse pressure gradient and with minimum entrainment of air into the boundary layer. The recessed diverter was designed to start where the wing and nacelle boundary layers filled the gap, with its contour defined to be the intersection of the two boundary layers. The highlight diverter originated 0.100 in. aft of the nacelle highlight. Both diverters had cross sections symmetric about a rotated vertical axis, with sides parallel to that axis. Coordinates for the two diverters are presented in table 6.

Circular-nacelle pylon.- The basic pylon started at FS 30.3751 at approximately the wing crest. It had elliptical cross sections symmetric about the rotated

vertical axis of the pylon coordinate system shown in figure 8. The pylon faired smoothly into the circular-nacelle afterbody at a boattail angle of 6.73°. Coordinates of the basic pylon are presented in table 7. The pressure pylon was larger to allow sufficient area to route pressure tubes to the nacelle. The pressure pylon originated at FS 26.50 near the wing leading edge. Coordinates of the pressure pylon are presented in table 8. Static-pressure orifice locations for the pressure pylon and the exterior and interior of the circular nacelle are presented in table 9.

D-nacelle.- The centerline of the D-nacelle was located at WL 1.224 and $\eta = 0.370$. The exterior consisted of a forebody, a centerbody, and an afterbody. The forebody contours were developed in planes of constant θ (fig. 9). The length of the forebody varied sinusoidally from 3.811 in. in the $\theta = 0°$ plane to 2.713 in. in planes with $\theta \geq \arctan(4/\pi)$. At the highlight, the bottom was a 1.874-in-radius semicircle; at the end of the forebody, it was a 2.25-in-radius semicircle. Forebody coordinates are presented in table 10. The straight sidewalls formed a flat surface from a nacelle station of 2.713 to 7.8 in. (NS 2.713 to NS 7.8), the end of the centerbody. This surface extended from the nacelle centerline (WL 1.224) upward to the wing lower surface or the pylon aft of the wing. Coordinates of the pylon/flat-sidewall boundary are presented in table 11. The bottom centerbody surface from NS 3.811 aft to NS 7.8 was a semicircular cylinder with a 2.25 in. radius. The afterbody was the same as the circular-nacelle afterbody in table 4 with the pylon faired into the top half.

The interior of the D-nacelle consisted of an inlet, a transition section, a cylindrical section, and a conical section. The D-nacelle had the same highlight, throat, and exit areas as the circular nacelle. The cylindrical and conical sections were the same as those of the circular nacelle starting at NS 7.8 (table 5). The inlet lip was 0.4804 in. long. Its shape was proportioned to the circular-nacelle inlet geometry by using the D-nacelle external forebody length and thickness for each value of θ. Thus,

$$\frac{x_{lip}}{x_{lip,cn}} = \frac{L_{lip}}{L_{lip,cn}}$$

$$\frac{y_{lip}}{y_{lip,cn}} = \frac{y}{y_{cn}}$$

The coordinates are presented in table 10. As shown in figure 9, the flat top of the inlet extended forward to the highlight plane and intersected the wing lower surface. The coordinates of this intersection line are presented in table 12. A constant-area transition section connected the inlet and the cylindrical section. The bottom of the section had 1.703-in-radius semicircular cross sections. The maximum longitudinal wall angle was 6.3°. The top of the transition section had superelliptic cross sections of the form

$$\left(\frac{NBL}{1.703}\right)^n + \left[\frac{NWL - (NWL)_{\mathbb{C}}}{h}\right]^n = 1.0$$

Centerline and upper-contour parameters for the transition section are presented in table 13.

D-nacelle pylon.- The D-nacelle pylons had the same characteristics as the circular-nacelle pylons. The basic pylon originated at FS 30.5615, which was approximately the wing crest (fig. 9). It had symmetric, elliptical cross sections and faired smoothly into the axisymmetric nacelle afterbody. Coordinates are presented in table 14. The pressure pylon was larger to allow sufficient area to route pressure tubes to the nacelle. The pressure pylon originated at FS 26.65 near the wing leading edge. Coordinates are presented in table 15. Static-pressure orifice locations for the pressure pylon and the exterior and interior of the D-nacelle are presented in table 16.

Antishock bodies.- Two sets of bodies having semiconical forebodies and streamlined boattail afterbodies were tested on the D-nacelle/basic-pylon configuration (fig. 10). The bodies were mounted on the wing upper surface with the cone apex location (FS 31.2; $x/c = 0.47$) approximately at the wing maximum thickness location. The antishock bodies were designed to relieve the shock formation on the wing upper surface and reduce the shock-associated wave drag (ref. 3). Both sets of antishock bodies had semicircular cross sections, but they differed in the lengths of their cone forebodies. The short-cone antishock body was canted inboard approximately 2° relative to the nacelle centerline, and its centerline intersected the nacelle plane of symmetry at approximately FS 36.9. It had a total length of approximately 16.8 in. and a conic forebody length of about 4.7 in. The long-cone antishock body was canted inboard approximately 1° and intersected the nacelle symmetry plane at approximately FS 43.05. It had a total length of approximately 15.5 in. and a conic forebody length of about 8.0 in. that extended past the wing trailing edge. Nominal coordinates for both antishock bodies are presented in table 17.

INSTRUMENTATION

The model aerodynamic force and moment data were obtained by an internally mounted six-component strain-gauge balance (balance 838). The model surface static pressures were measured by scanning electrical strain-gauge transducers. These instruments were located in the model nose to reduce the lag time required between data points. Sting cavity pressures were measured by electrical strain-gauge transducers and were used to correct the cavity static pressure to the free-stream static pressure for force coefficients. Instruments were calibrated to an accuracy of at least ±0.5 percent of their maximum load.

TESTS

This experimental wind-tunnel investigation was conducted in the Langley 16-Foot Transonic Tunnel at free-stream Mach numbers from 0.70 to 0.85. The model angle of attack was varied from -2.5° to 4.0° at zero sideslip. The Reynolds number based on the mean geometric chord varied from approximately 2.5×10^6 to 3.0×10^6. Boundary-layer transition on the model was fixed by using a grit transition-strip procedure (ref. 8). A 0.1-in-wide strip of No. 100 silicon carbide grit was attached 1.0 in. behind the nose of the fuselage. The vertical-tail bullet fairing had a transition strip applied 1.0 in. behind its nose by using No. 120 silicon carbide grit. The horizontal and vertical tails had No. 100 strips applied at 0.10c. The transition strips on the wing were applied in an aft position in order to match the boundary-layer thickness at the trailing edge (ref. 9). Figure 11 shows the location of the

transition strips on the wing upper and lower surfaces. A strip of No. 90 silicon carbide grit was applied on the upper surface, whereas No. 80 was used on the lower surface. Strips of No. 120 silicon carbide grit were applied both externally and internally to the nacelles 0.375 in. aft of the nacelle highlight.

DATA REDUCTION

All wind-tunnel parameters and model data were recorded simultaneously on magnetic tape. Except for scanning valve pressures, averaged values were used to compute all parameters. The model angle of attack was computed by correcting the support-strut angle both for sting deflections based on balance loads and for tunnel upflow determined from inverted model runs in a previous tunnel entry (ref. 6). Sting cavity pressures were used to correct the longitudinal balance components for pressure forces in the sting cavity. Nacelle internal drag corrections were made by using internal static pressures to determine the mass flow for a one-dimensional flow calculation, and then by integrating the computed internal pressure and friction forces. Skin-friction drag was calculated by using the method of Frankl and Voishel (ref. 10) for compressible turbulent flow on a flat plate. No corrections were made for model blockage since it was 0.36 percent of the test-section cross section. Forces and moments were transferred to the model moment center, the quarter-chord point of the mean geometric chord on the model waterline.

PRESENTATION OF RESULTS

RESULTS AND DISCUSSION

Basic Longitudinal Aerodynamic Data

The basic longitudinal aerodynamic data for the clean wing-body configuration and the various underwing aft-mounted configurations are presented in figures 12 to 19. Plots of lift coefficient versus angle of attack and plots of drag coefficient and pitching-moment coefficient versus lift coefficient are shown for free-stream Mach numbers from 0.70 to 0.85. Data are presented for the clean wing-body configuration in figure 12, for the circular-nacelle configurations in figures 13 to 15, for the D-nacelle configurations in figures 16 and 17, and for the D-nacelle configurations with antishock bodies in figures 18 and 19. The analysis of these data is made primarily at the design cruise conditions of $M_\infty = 0.80$ and $C_L = 0.43$ at $\alpha \approx 1°$. (See also ref. 11.)

Aft-Mounted Nacelle Characteristics

There was an expected increase in the drag coefficient over that for the clean wing-body configuration at the cruise Mach number of 0.80 associated with the installation of both the circular and D-shaped aft-mounted flow-through nacelles (fig. 20). This drag increase was throughout the cruise lift range. Rotation of the drag polars was mainly the result of an almost constant increase in lift throughout the angle-of-attack range, resulting from the favorable interference effects of the aft-mounted nacelles pressurizing the wing lower surface. In addition, a portion of this lift increase may be attributed to the possible underwing fencing effect of aft nacelles in the cusp region on the lower surface of the wing. By retarding the large underwing spanwise flow associated with the cusp region of the supercritical airfoil, there was a reduction in the induced drag of the wing that was manifested as an increase in lift at a constant angle of attack. An increase in nose-up pitching moment also resulted from the lift increments.

Wing chordwise pressure-coefficient distributions at span stations inboard, along the centerline, and outboard of the aft-mounted nacelles are presented in figure 21 for basic-pylon configurations. These data indicate that a large increase in the wing lower-surface pressure coefficients resulted from a favorable interaction between the nacelle and wing pressure fields. The effect extended from the nacelle inlet ($x/c = 0.714$) forward to the wing leading edge. The presence of the D-nacelle pylon on the wing upper surface caused a small loss in lift as indicated by the increase in pressure coefficient occurring just behind the wing upper-surface shock wave (at approximately 45 percent of the local chord). The circular nacelle pylon caused a decrease in pressure coefficients. This resulted not only in an increase in lift but also in drag since the pressures were aft of the wing maximum thickness.

Wing, pylon, and external-nacelle pressure-coefficient distributions are presented in figures 22 to 24 for the circular-nacelle configurations and in figures 25 to 27 for the D-nacelle configurations. The wing pressure-coefficient distributions indicate that the favorable lift effect resulting from the aft-nacelle installations includes practically the entire wing. This effect is more prominent over the wing lower surface and indicates that the favorable lift effect afforded by the nacelle is

possibly reinforced by the flow being turned from a partially spanwise direction to a streamwise direction. Just outboard of the nacelle, the underwing pressure coefficients indicate that there is an acceleration of the flow at the nacelle inlet-lip location. Again, this flow acceleration is possibly due to the large flow angles that occur when the large spanwise flow of the cusp region of the supercritical wing accelerates around the inlet lip of an aft-mounted nacelle.

Pressure-Pylon Effect

Pressure pylons with larger cross-sectional areas than those of the basic pylons were used to route pressure tubes to the nacelles and pylons. An examination of the wing upper-surface pressure coefficients in figures 22, 23, 25, and 26 reveals that the primary effect of the larger pylon was to move the location of the shock forward. This resulted in small lift losses and pitching-moment reductions as shown in figures 28 and 29. The drag polars of these configurations indicate that the lift-drag ratios of the basic-pylon configurations are reduced by the pressure pylon.

Diverter Effect

Both a highlight and a recessed diverter were tested on the underwing aft-mounted circular-nacelle configuration with the basic pylon (fig. 8). The longitudinal characteristics are presented at a free-stream Mach number of 0.80 for these two configurations in figure 30. These data indicate that the drag associated with the recessed diverter is less than that of the highlight diverter throughout the lift range. This could possibly be the result of the higher lift produced by the wing when the recessed diverter, with its lower sweep, was used.

Antishock Bodies

Structurally, the installation of nacelles in an aft position as proposed herein is an extremely difficult task since the forward attachment points would be located well behind the aft structural member of the wing. Pylons of sufficient size to provide adequate structural volume (such as the pressure pylons tested here) have an associated installation drag as previously shown. It was proposed, therefore, that the structural volume required for this type of installation might be obtained by employing antishock bodies similar to those reported in reference 3. The forward portion of the bodies was a semiconical shape designed to reduce the wing upper-surface shock strength by reducing the local flow velocities. The aft portion was a minimum-drag afterbody terminating at approximately three body (maximum) diameters behind the wing trailing edge.

The antishock bodies investigated in the present study were tested only on the D-nacelle/basic-pylon configuration with the semiconical forebody apex located near the wing crest. Two antishock-body configurations were tested; one had a short-cone forebody that terminated ahead of the wing trailing edge, and the other had a long-cone forebody that extended beyond the wing trailing edge. (See fig. 10.) Chordwise pressure distributions and aerodynamic data for these two configurations are compared in figures 31 to 34 at free-stream Mach numbers of 0.80 and 0.85. The installation of the antishock bodies resulted in moving the shock location forward as indicated in the pressure distributions of figures 31 and 32. The short-cone bodies provided the greater shock relief. Characteristic of a supercritical airfoil, the forward movement of the shock location indicated a lower upper-surface Mach number and a

reduction in wave drag. However, the more negative pressure coefficients measured over the aft portion of the wing with the short-cone bodies installed increased the pressure drag to the extent that there was a net drag increase at the design lift coefficient at both the lower Mach number (fig. 33(b)) and the higher Mach number (fig. 34(b)). Although installation of the long-cone antishock bodies provided less shock relief than the short-cone bodies, the trailing-edge losses were reduced to the extent that the long-cone bodies caused no additional drag at a Mach number of 0.8 over a wide range of lift coefficients. In addition, the effectiveness of both antishock-body configurations in providing shock relief increased at the higher Mach number (0.85). In fact, the addition of the long-cone body at $M_\infty = 0.85$ resulted in reducing the drag of the complete configuration to that of the wing-body configurations alone at the design lift coefficient of 0.43 (fig. 34(b)). Also, the increase in lift associated with the installation of the aft-mounted nacelles was partially negated by the addition of the antishock bodies at a Mach number of 0.80 as shown in figure 33(a). However, at a Mach number of 0.85 (fig. 34(a)), there was essentially no lift loss associated with the antishock bodies at the cruise angle of attack.

The more negative pressure coefficients on the aft portion of the wing, which resulted in higher pressure drag for the short-cone antishock bodies, resulted from the location of the forebody/afterbody juncture near the curved portion of the wing aft upper surface. This location, in effect, created a compound curvature that caused an acceleration and separation of the flow. The long-cone forebody/afterbody juncture, on the other hand, occurs aft of the wing trailing edge and avoids this condition.

Span-Load Distribution

Generally, there is a large loss in lift associated with the pylon-nacelle installation in the conventional forward underwing position. This loss in lift increases as the relative size increases between the nacelle and wing. Such is the case for the more efficient high-aspect-ratio wings advocated for future airplanes, in which the local wing chord is reduced but the nacelle size remains the same. The span-load distributions for the wing-body configuration and for the forward and aft nacelle installations are presented in figure 35. The maximum loss in lift load associated with the conventional nacelle installation occurs at the nacelle span location and extends both inboard and outboard over the complete semispan of the wing. The amount of lift loss can be seen by comparing these data to the wing-body configuration. This lift must be recovered through an increase in angle of attack, with a resulting increase in induced drag. The aft-mounted nacelle configuration, on the other hand, develops an increase in lift relative to the wing-body configuration, thus allowing a decrease in angle of attack and induced drag of the configuration.

The rate of change in the span loading is indicative of the strength of the vorticity shed from a wing and its effect on induced drag. The large lift on the inboard section of the wing due to the aft-mounted nacelle indicates that a large part of the total vorticity is shed at the engine nacelle location. The nacelle, operating as an underwing fence, will possibly tend to dissipate the vorticity, with a resulting reduction in induced drag as shown in figure 20(b). The powered nacelle will possibly have a greater effect than is shown here.

Installation Drag

The difference between the drag of the complete model configuration and that of the model without nacelles is the nacelle installation drag ΔC_D. The installed drags of the D-nacelle and circular nacelle at the cruise Mach number and lift coefficient are compared (fig. 36) along with the installed drag of a comparable nacelle that is pylon mounted beneath the wing in a forward position. The shaded area of each bar on this chart indicates the amount of the installed drag that may be attributed to nacelle skin-friction drag (calculated skin-friction drag shown). The remaining area represents the combined value of form, wave, and interference drag of the configuration. With the skin-friction drag of each nacelle configuration being comparable, these data indicate that a maximum reduction in the drag above skin-friction drag is obtained by the aft-mounted D-nacelle installation. Its drag is approximately 60 percent of that of the conventional pylon-mounted nacelle in the forward position.

The installed drag, above skin friction, of the circular nacelle shown in figure 36 is higher than that of the D-nacelle, but it is still approximately one-half that of the conventional pylon-nacelle combination. This difference between the two aft-mounted nacelles may possibly be a result of the interference associated with the boundary-layer diverter required for the installation of the circular nacelle, and also the fact that the outboard portion of the D-nacelle is closer to the wing planform break where vorticity is shed.

CONCLUSIONS

An investigation to determine the effects of installing engine nacelles in the aft underwing position on a transonic transport airplane model has been conducted. Flow-through mixed-flow nacelles with circular and D-shaped inlets were tested over a free-stream Mach number range from 0.70 to 0.85 and an angle-of-attack range from -2.5° to 4.0°. The following conclusions are presented:

1. Underwing aft-mounted nacelles generate a lift gain over almost the entire span by pressurizing much of the lower wing surface in front of the nacelle. This lift increase allows lower incidence angles and, therefore, even lower trim drag than conventional forward-mounted nacelle configurations.

2. Underwing aft-mounted nacelles act like a fence to retard spanwise flow in the cusp region of the supercritical wing, thereby reducing induced drag.

3. Pylons sufficiently large for structurally mounting nacelles in the aft underwing position can be shaped like antishock bodies with the result of minimal performance loss at cruise conditions.

NASA Langley Research Center
Hampton, VA 23665-5225
July 8, 1985

REFERENCES

1. Henderson, William P.; and Patterson, James C., Jr.: Propulsion Installation Characteristics for Turbofan Transports. AIAA-83-0087, Jan. 1983.

2. Kuchemann, Dietrich; and Weber, Johanna: Aerodynamics of Propulsion, First ed. McGraw-Hill Book Co., Inc., 1953.

3. Whitcomb, Richard T.: Special Bodies Added on a Wing To Reduce Shock-Induced Boundary-Layer Separation at High Subsonic Speeds. NACA TN 4293, 1958.

4. Corson, Blake W., Jr.; Runckel, Jack F.; and Igoe, William B.: Calibration of the Langley 16-Foot Transonic Tunnel With Test Section Air Removal. NASA TR R-423, 1974.

5. Peddrew, Kathryn H., compiler: A User's Guide to the Langley 16-Foot Transonic Tunnel. NASA TM-83186, 1981.

6. Lee, Edwin E., Jr.; and Pendergraft, Odis C., Jr.: Installation Effects of Long-Duct, Pylon-Mounted Nacelles on a Twin-Jet Transport Model with Swept, Supercritical Wing. NASA TP-2457, 1985.

7. Krivec, D. K.; and Bangert, L. H.: Effects of Nacelle Configuration/Position on Performance of Subsonic Transport: Tabulated Coordinates of Model Nacelles. LR 29906 (Contract NAS1-16644), Lockheed California Co., July 1981. (Available as NASA CR-177931.)

8. Braslow, Albert L.; Hicks, Raymond M.; and Harris, Roy V., Jr.: Use of Grit-Type Boundary-Layer-Transition Trips on Wind-Tunnel Models. NASA TN D-3579, 1966.

9. Blackwell, James A., Jr.: Preliminary Study of Effects of Reynolds Number and Boundary-Layer Transition Location on Shock-Induced Separation. NASA TN D-5003, 1969.

10. Frankl, F.; and Voishel, V.: Turbulent Friction in the Boundary Layer of a Flat Plate in a Two-Dimensional Compressible Flow at High Speeds. NACA TM 1053, 1943.

11. Bangert, L. H.; Krivec, D. K.; and Segall, R. N.: Effects of Nacelle Configuration/Position on Performance of Subsonic Transport. NASA CR-3743, 1983.

TABLE 1.- WING-FUSELAGE FAIRINGS

(a) Forward fairing

FS, in.	BL, in.	WL, in.
19.02	3.14	3.22
19.50	2.83	3.50
	2.96	3.43
	3.11	3.32
	3.24	3.19
	3.34	3.02
20.00	2.58	3.69
	2.80	3.62
	2.98	3.54
	3.19	3.40
	3.36	3.22
	3.41	3.09
	3.43	2.91
20.50	2.35	3.84
	2.55	3.79
	2.74	3.73
	2.93	3.68
	3.12	3.60
	3.30	3.49
	3.45	3.33
	3.53	3.14
	3.54	2.97
	3.51	2.82
21.00	2.14	3.96
	2.40	3.91
	2.65	3.86
	2.91	3.79
	3.14	3.71
	3.37	3.61
	3.56	3.47
	3.67	3.30
	3.69	3.10
	3.67	2.90
	3.60	2.70

FS, in.	BL, in.	WL, in.
21.50	1.96	4.05
	2.27	4.00
	2.58	3.96
	2.89	3.90
	3.18	3.82
	3.43	3.74
	3.65	3.63
	3.81	3.50
	3.91	3.38
	3.96	3.23
	3.97	3.09
	3.93	2.94
	3.87	2.82
	3.77	2.69
	3.67	2.60
22.0	1.84	4.11
	2.16	4.08
	2.51	4.04
	2.87	3.98
	3.22	3.93
	3.57	3.87
	3.87	3.79
	4.11	3.72
	4.33	3.63
	4.50	3.51
	4.60	3.40
	4.65	3.26
	4.63	3.12
	4.56	3.01
	4.43	2.91
	4.26	2.81
	4.08	2.73
	3.90	2.65
	3.82	2.57
	3.74	2.50

TABLE 1.- Continued

(a) Concluded

FS, in.	BL, in.	WL, in.
23.00	1.59	4.21
	2.00	4.18
	2.41	4.15
	2.80	4.12
	3.21	4.08
	3.61	4.04
	4.02	4.00
	4.43	3.94
	4.82	3.88
	5.22	3.81
	5.56	3.73
	5.85	3.63
	6.01	3.53
	6.13	3.43
	6.19	3.34
	6.20	3.24
	6.18	3.15
	6.10	3.03
	5.93	2.90
	5.75	2.81
	5.47	2.70
	5.09	2.58
	4.70	2.47
	4.36	2.40
	4.07	2.34
	3.86	2.31

TABLE 1.- Continued

(b) Underwing rear fairing

FS, in.	BL, in.	WL, in.
27.86	4.04	1.98
28.00	4.05 4.05	1.98 1.96
29.00	4.11 4.11	2.05 1.83
30.00	4.20 4.20	2.16 1.61
31.00	4.31 4.31	2.31 1.29
32.00	4.40 4.40	2.47 .94
33.00	4.46 4.46	2.60 .60

(c) Flat vertical section

FS, in.	BL, in.	WL, in.
34.00	4.50 4.50	2.69 0
35.00	4.50 4.50	2.71 0
36.00	4.50 4.50	2.64 0
36.50	4.50 4.50	2.57 0

TABLE 1.- Concluded

(d) Rear fairing

FS, in.	BL, in.	WL, in.
36.50	3.67	2.61
	3.89	2.62
	4.09	2.63
	4.31	2.65
	4.50	2.66
	↓	2.40
		2.00
		1.60
		1.20
		.80
		.40
		0
37.00	3.75	2.49
	4.00	2.51
	4.25	2.53
	4.40	2.54
	4.46	2.53
	4.49	2.49
	4.50	2.45
	↓	2.40
		2.00
		1.60
		1.20
		.80
		.40
		0
38.00	3.86	2.31
	4.09	2.32
	4.29	2.33
	4.39	2.30
	4.45	2.25
	4.48	2.17
	↓	2.00
		1.60
		1.20
		.80
		.42

FS, in.	BL, in.	WL, in.
39.00	3.97	2.12
	4.12	2.13
	4.22	2.10
	4.31	2.05
	4.36	2.00
	4.42	1.90
	4.44	1.80
	↓	1.60
		1.20
		.73
40.00	4.07	1.92
	4.15	1.87
	4.22	1.81
	4.28	1.72
	4.32	1.63
	4.36	1.57
	4.37	1.39
	4.37	1.20
	4.37	1.07
41.00	4.17	1.69
	4.22	1.61
	4.26	1.53
	4.29	1.45
	4.30	1.33
41.29	4.23	1.54

TABLE 2. WING STREAMWISE AIRFOIL COORDINATES

(a) η = 0.127 (fuselage side); c = 14.921 in.; ε = 2.462°; t/c = 0.144

x/c	z/c	
	Upper surface	Lower surface
0	-0.0016	-0.0016
.002	.0104	-.0136
.005	.0164	-.0196
.010	.0229	-.0266
.020	.0304	-.0351
.030	.0359	-.0401
.040	.0394	-.0446
.050	.0419	-.0486
.060	.0441	-.0521
.070	.0460	-.0553
.080	.0477	-.0581
.090	.0492	-.0607
.100	.0506	-.0632
.110	.0518	-.0655
.120	.0529	-.0676
.130	.0539	-.0695
.140	.0548	-.0713
.150	.0556	-.0730
.160	.0563	-.0746
.170	.0570	-.0760
.180	.0576	-.0773
.190	.0582	-.0785
.200	.0587	-.0796
.210	.0591	-.0805
.220	.0593	-.0813
.230	.0595	-.0820
.240	.0596	-.0826
.250	.0596	-.0832
.260	.0596	-.0837
.270	.0595	-.0842
.280	.0593	-.0846
.290	.0591	-.0850
.300	.0588	-.0853
.310	.0585	-.0856
.320	.0581	-.0858
.330	.0577	-.0860
.340	.0572	-.0862
.350	.0567	-.0863

x/c	z/c	
	Upper surface	Lower surface
0.360	0.0561	-0.0864
.370	.0555	-.0864
.380	.0548	-.0863
.390	.0541	-.0862
.400	.0534	-.0860
.410	.0526	-.0858
.420	.0518	-.0855
.430	.0510	-.0852
.440	.0501	-.0848
.450	.0492	-.0843
.460	.0483	-.0838
.470	.0473	-.0832
.480	.0463	-.0825
.490	.0453	-.0817
.500	.0442	-.0809
.510	.0431	-.0800
.520	.0420	-.0790
.530	.0408	-.0779
.540	.0396	-.0767
.550	.0384	-.0754
.560	.0371	-.0741
.570	.0358	-.0727
.580	.0345	-.0713
.590	.0331	-.0698
.600	.0317	-.0683
.610	.0303	-.0668
.620	.0289	-.0652
.630	.0274	-.0636
.640	.0259	-.0620
.650	.0244	-.0604
.660	.0229	-.0588
.670	.0213	-.0573
.680	.0197	-.0558
.690	.0181	-.0543
.700	.0164	-.0529
.710	.0147	-.0515
.720	.0130	-.0502
.730	.0113	-.0489

TABLE 2.- Continued

(a) Concluded

x/c	z/c	
	Upper surface	Lower surface
0.740	0.0095	-0.0477
.750	.0077	-.0465
.760	.0059	-.0454
.770	.0041	-.0444
.780	.0022	-.0434
.790	.0003	-.0425
.800	-.0016	-.0417
.810	-.0036	-.0410
.820	-.0056	-.0404
.830	-.0076	-.0399
.840	-.0096	-.0394
.850	-.0116	-.0390
.860	-.0136	-.0387
.870	-.0156	-.0385
.880	-.0176	-.0384
.890	-.0196	-.0385
.900	-.0216	-.0387
.910	-.0236	-.0390
.920	-.0256	-.0394
.930	-.0276	-.0400
.940	-.0296	-.0407
.950	-.0316	-.0415
.960	-.0336	-.0424
.970	-.0356	-.0435
.980	-.0376	-.0447
.990	-.0396	-.0460
1.000	-.0416	-.0476

TABLE 2.- Continued

(b) η = 0.410 (planform break); c = 9.153 in.; ε = 0.256°; t/c = 0.12

x/c	z/c	
	Upper surface	Lower surface
0	-0.0044	-0.0044
.002	.0049	-.0131
.005	.0099	-.0181
.010	.0148	-.0230
.020	.0210	-.0290
.030	.0253	-.0329
.040	.0286	-.0360
.050	.0312	-.0386
.060	.0336	-.0408
.070	.0357	-.0427
.080	.0376	-.0444
.090	.0393	-.0459
.100	.0409	-.0473
.110	.0424	-.0487
.120	.0436	-.0499
.130	.0448	-.0510
.140	.0460	-.0520
.150	.0471	-.0529
.160	.0481	-.0538
.170	.0491	-.0546
.180	.0500	-.0554
.190	.0508	-.0561
.200	.0516	-.0567
.210	.0523	-.0573
.220	.0530	-.0579
.230	.0537	-.0584
.240	.0543	-.0588
.250	.0548	-.0593
.260	.0554	-.0597
.270	.0559	-.0600
.280	.0563	-.0603
.290	.0568	-.0605
.300	.0571	-.0607
.310	.0575	-.0609
.320	.0577	-.0611
.330	.0580	-.0612
.340	.0582	-.0612
.350	.0585	-.0612
0.360	0.0587	-0.0611
.370	.0589	-.0610
.380	.0590	-.0609
.390	.0590	-.0608
.400	.0591	-.0606
.410	.0591	-.0603
.420	.0591	-.0601
.430	.0591	-.0597
.440	.0591	-.0593
.450	.0590	-.0589
.460	.0588	-.0584
.470	.0587	-.0578
.480	.0585	-.0572
.490	.0584	-.0562
.500	.0582	-.0558
.510	.0579	-.0549
.520	.0577	-.0541
.530	.0573	-.0531
.540	.0570	-.0520
.550	.0567	-.0508
.560	.0563	-.0496
.570	.0559	-.0482
.580	.0555	-.0468
.590	.0550	-.0454
.600	.0544	-.0438
.610	.0539	-.0422
.620	.0534	-.0405
.630	.0528	-.0387
.640	.0522	-.0369
.650	.0515	-.0351
.660	.0509	-.0332
.670	.0500	-.0314
.680	.0493	-.0294
.690	.0485	-.0275
.700	.0476	-.0255
.710	.0467	-.0235
.720	.0458	-.0215
.730	.0448	-.0195

TABLE 2.- Continued

(b) Concluded

x/c	z/c	
	Upper surface	Lower surface
0.740	0.0438	-0.0175
.750	.0427	-.0155
.760	.0415	-.0135
.770	.0404	-.0116
.780	.0391	-.0098
.790	.0378	-.0081
.800	.0365	-.0064
.810	.0351	-.0048
.820	.0336	-.0034
.830	.0320	-.0020
.840	.0304	-.0008
.850	.0288	.0003
.860	.0271	.0011
.870	.0253	.0017
.880	.0235	.0021
.890	.0215	.0024
.900	.0195	.0025
.910	.0174	.0023
.920	.0152	.0019
.930	.0130	.0011
.940	.0107	.0001
.950	.0083	-.0012
.960	.0058	-.0027
.970	.0033	-.0046
.980	.0005	-.0067
.990	-.0025	-.0092
1.000	-.0056	-.0120

TABLE 2.- Continued

(c) η = 1.000 (tip); c = 4.142 in.; ε = 1.229°; t/c = 0.10

x/c	z/c	
	Upper surface	Lower surface
0	-0.0175	-0.0175
.002	-.0095	-.0240
.005	-.0053	-.0284
.010	-.0012	-.0323
.020	.0041	-.0367
.030	.0079	-.0397
.040	.0109	-.0420
.050	.0134	-.0439
.060	.0157	-.0455
.070	.0177	-.0468
.080	.0195	-.0480
.090	.0213	-.0491
.100	.0229	-.0500
.110	.0245	-.0509
.120	.0258	-.0516
.130	.0272	-.0523
.140	.0284	-.0530
.150	.0296	-.0535
.160	.0308	-.0540
.170	.0318	-.0544
.180	.0329	-.0548
.190	.0339	-.0551
.200	.0349	-.0554
.210	.0357	-.0557
.220	.0366	-.0559
.230	.0374	-.0561
.240	.0382	-.0562
.250	.0390	-.0563
.260	.0397	-.0563
.270	.0404	-.0564
.280	.0410	-.0564
.290	.0417	-.0563
.300	.0422	-.0563
.310	.0428	-.0561
.320	.0433	-.0560
.330	.0437	-.0558
.340	.0442	-.0556
.350	.0446	-.0553

x/c	z/c	
	Upper surface	Lower surface
0.360	0.0451	-0.0551
.370	.0455	-.0548
.380	.0459	-.0544
.390	.0462	-.0541
.400	.0465	-.0536
.410	.0468	-.0532
.420	.0470	-.0527
.430	.0473	-.0522
.440	.0475	-.0516
.450	.0478	-.0510
.460	.0479	-.0503
.470	.0481	-.0495
.480	.0482	-.0488
.490	.0483	-.0479
.500	.0484	-.0471
.510	.0484	-.0462
.520	.0485	-.0451
.530	.0485	-.0441
.540	.0486	-.0429
.550	.0485	-.0418
.560	.0485	-.0405
.570	.0484	-.0392
.580	.0484	-.0378
.590	.0482	-.0364
.600	.0481	-.0348
.610	.0479	-.0333
.620	.0477	-.0316
.630	.0475	-.0299
.640	.0472	-.0281
.650	.0470	-.0264
.660	.0467	-.0245
.670	.0464	-.0227
.680	.0460	-.0208
.690	.0457	-.0189
.700	.0452	-.0170
.710	.0448	-.0150
.720	.0443	-.0131
.730	.0437	-.0111

TABLE 2.- Concluded

(c) Concluded

x/c	z/c	
	Upper surface	Lower surface
0.740	0.0432	-0.0092
.750	.0426	-.0072
.760	.0420	-.0052
.770	.0413	-.0034
.780	.0406	-.0015
.790	.0398	.0003
.800	.0391	.0020
.810	.0382	.0037
.820	.0372	.0052
.830	.0362	.0067
.840	.0351	.0081
.850	.0340	.0094
.860	.0328	.0104
.870	.0316	.0113
.880	.0302	.0119
.890	.0288	.0123
.900	.0273	.0127
.910	.0258	.0127
.920	.0241	.0126
.930	.0224	.0122
.940	.0207	.0114
.950	.0188	.0104
.960	.0168	.0091
.970	.0146	.0076
.980	.0123	.0057
.990	.0097	.0036
1.000	.0069	.0012

TABLE 3.- WING AND FUSELAGE PRESSURE-ORIFICE LOCATIONS

x/c	z/c for values of η of -									
	0	0.154	0.250	0.328	0.370	0.440	0.550	0.750	0.850	0.950
Upper surface										
0.0000		-0.00180	-0.00251	-0.00327	-0.00378	-0.00468	-0.00597	-0.00934	-0.01182	-0.01522
.0125		.02491	.02267	.02026	.01866	.01643	.01482			
.0250		.03276	.03013	.02729	.02541	.02284	.02115	.01672	.01346	.00899
.0500	0.07143	.04122	.03846	.03548	.03350	.03080	.02904	.02445	.02107	.01644
.0750	↓	.04623	.04358	.04073	.03884	.03623	.03445			
.1000		.04998	.04746	.04473	.04292	.04042	.03865	.03403	.03064	.02598
.1500		.05505	.05285	.05047	.04889	.04666	.04494	.04045	.03714	.03261
.2000		.05824	.05640	.05442	.05311	.05120	.04954	.04523	.04205	.03770
0.2500	0.07143	0.05928	0.05805	0.05673	0.05584	.05445	0.05289	0.04880	0.04580	0.04169
.3000	↓	.05866	.05822	.05775	.05743	.05671	.05524	.05141	.04859	.04473
.3500		.05678	.05725	.05777	.05811	.05816	.05679	.05322	.05059	.04699
.4000		.05371	.05521	.05683	.05790	[a].05881	.05757	.05433	.05195	.04868
.4500		.04976	.05230	.05505	.05687	.05868	.05757	.05469	.05257	.04866
.5000		.04501	.04866	.05259	.05520	.05794	.05697	.05445	.05260	.05006
.5500		.03948	.04425	[b].04848	.05281	.05651	.05570	.05359	.05204	.04991
.6000		.03304	.03897	.04536	.04960	.05428	.05365	.05201	.05080	.04914
0.6500	0.07143	0.02601	0.03305	0.04066	0.04571	0.05136	0.05092	0.04976	0.04891	0.04774
.7000	↓	.01826	.02638	.03514	.04096	.04754	.04730	.04669	.04623	.04561
.7500		.00979	.01891	.02875	.03528	.04273	.04272			
.8000		.00067	.01058	.02127	.02836	.03652	.03678	.03745	.03794	.03861
.8500		-.00919	.00133	.01268	.02021	.02893	.02944			
.9000		-.01915	-.00846	.00307	.01072	.01964	.02042			
.9500		-.02922	-.01883	-.00763	-.00019	.00856	.00960	.01230	.01429	
Lower surface										
0.0125		-0.02918	-0.02802	-0.02677	-0.02594	-0.02520	-0.02608			
.0250		-.03729	-.03556	-.03369	-.03245	-.03121	-.03192	-0.03379	-0.03516	-0.03704
.0500		-.04802	-.04540	-.04257	-.04069	-.03868	-.03921			
.0750		-.05596	-.05253	-.04883	-.04637	-.04366	-.04404	-.04504	-.04577	-.04678
.1000		-.06227	-.05814	-.05367	-.05071	-.04740	-.04766	-.04835	-.04886	-.04956
.1500		-.07182	-.06658	-.06094	-.05719	-.05292	-.05298	-.05314	-.05325	-.05341
.2000		-.07824	-.07228	-.06583	-.06156	-.05665	-.05652	-.05619	-.05595	-.05562
0.2500		-0.08178	-0.07555	-0.06881	-0.06435	-0.05918	-0.05889	-0.05812	-0.05756	-0.05679
.3000		-.08384	-.07745	-.07054	-.06596	-.06062	-.06018			
.3500		-.08481	-.07828	-.07122	-.06654	-.06106	-.06048	-.05897	-.05786	-.05634
.4000		-.08449	-.07787	-.07072	-.06598	[a]-.06003	-.05971			
.4500		-.08280	-.07619	-.06907	-.06434	-.05875	-.05796	-.05592	-.05442	-.05236
.5000		-.07941	-.07288	-.06583	-.06115	-.05560	-.05474			
.5500		-.07394	-.06754	[b]-.05913	-.05604	-.05058	-.04969	-.04736	-.04565	-.04331
0.6000		-0.06685	-0.06046	-0.05357	-0.04899	-0.04355	-0.04267			
.6500		-.05890	-.05232	-.04522	-.04051	-.03492	-.03405	-0.03179	-0.03014	-0.02786
.7000		-.05127	-.04413	-.03643	-.03131	-.02527	-.02443			
.7500		-.04466	-.03660	-.02789	-.02212	-.01533	-.01450			
.8000		-.03959	-.03040	-.02047	-.01389	-.00616	-.00534	-.00318	-.00159	.00058
.8500		-.03666	-.02643	-.01540	-.00808	.00049	.00139			
.9000		-.03624	-.02552	-.01395	-.00627	.00274	.00375	.00637	.00830	.01095
.9500		-.03909	-.02860	-.01727	-.00976	-.00090	.00024			

[a] x/c = 0.414.
[b] x/c = 0.562.

TABLE 4.- CIRCULAR-NACELLE EXTERIOR COORDINATES

[All dimensions are in inches]

FOREBODY EXTERNAL CONTOUR

NS	r_n	NS	r_n
0.0	1.8740	0.6748	2.1182
0.0015	1.8815	0.7238	2.1260
0.0022	1.8890	0.7755	2.1338
0.0049	1.8963	0.8302	2.1416
0.0087	1.9036	0.8882	2.1494
0.0136	1.9108	0.9498	2.1572
0.0196	1.9179	1.0153	2.1651
0.0267	1.9250	1.0852	2.1729
0.0350	1.9320	1.1666	2.1814
0.0443	1.9391	1.2480	2.1893
0.0548	1.9462	1.3294	2.1966
0.0665	1.9533	1.4108	2.2033
0.0793	1.9604	1.4922	2.2095
0.0933	1.9676	1.5735	2.2152
0.1085	1.9749	1.6549	2.2204
0.1250	1.9821	1.7363	2.2252
0.1427	1.9894	1.8177	2.2296
0.1616	1.9968	1.8991	2.2335
0.1819	2.0042	1.9805	2.2370
0.2035	2.0116	2.0619	2.2401
0.2265	2.0190	2.1433	2.2428
0.2509	2.0265	2.2247	2.2451
0.2767	2.0340	2.3061	2.2470
0.3041	2.0415	2.3874	2.2485
0.3330	2.0491	2.4688	2.2494
0.3635	2.0567	2.5502	2.2499
0.3956	2.0643	2.6316	2.2500
0.4296	2.0719	2.7130	2.2500
0.4653	2.0796	3.0000	2.2500
0.5029	2.0873	4.0000	2.2500
0.5426	2.0950	5.0000	2.2500
0.5844	2.1027	6.0000	2.2500
0.6284	2.1104		

AFTERBODY EXTERNAL CONTOUR

NS	r_n	NS	r_n
7.8000	2.2500	12.0000	2.0633
8.0000	2.2498	12.2000	2.0432
8.2000	2.2492	12.4000	2.0222
8.4000	2.2479	12.6000	2.0004
8.6000	2.2459	12.8000	1.9779
8.8000	2.2432	13.0000	1.9546
9.0000	2.2396	13.2000	1.9307
9.2000	2.2351	13.4000	1.9064
9.4000	2.2296	13.5500	1.8819
9.6000	2.2232	13.6000	1.8757
9.8000	2.2157	13.8000	1.8512
10.0000	2.2072	14.0000	1.8266
10.2000	2.1976	14.2000	1.8020
10.4000	2.1870	14.4000	1.7774
10.6000	2.1753	14.6000	1.7528
10.8000	2.1625	14.8000	1.7282
11.0000	2.1486	15.0000	1.7036
11.2000	2.1336	15.2000	1.6790
11.4000	2.1175	15.4000	1.6544
11.6000	2.1005	15.6000	1.6298
11.8000	2.0823	15.7500	1.6114

TABLE 5.- CIRCULAR-NACELLE INTERIOR COORDINATES

[All dimensions are in inches]

NS	r_n	NS	r_n
0.0000	1.8740	0.2804	1.7034
0.0003	1.8686	0.3010	1.7031
0.0011	1.8632	0.3215	1.7030
0.0025	1.8576	0.3420	1.7030
0.0044	1.8518	1.0000	1.7030
0.0069	1.8458	2.0000	1.7030
0.0100	1.8395	3.0000	1.7030
0.0137	1.8329	4.0000	1.7030
0.0180	1.8261	5.0000	1.7030
0.0229	1.8190	6.0000	1.7030
0.0286	1.8116	7.0000	1.7030
0.0349	1.8040	8.0000	1.7030
0.0420	1.7960	9.0000	1.7030
0.0499	1.7879	10.0000	1.7030
0.0587	1.7796	11.0000	1.7030
0.0684	1.7712	12.0000	1.7030
0.0792	1.7627	13.0000	1.7030
0.0912	1.7542	13.6129	1.7030
0.1047	1.7458	13.7500	1.6958
0.1197	1.7376	14.0000	1.6827
0.1368	1.7297	14.2500	1.6696
0.1573	1.7220	14.5000	1.6565
0.1778	1.7160	14.7500	1.6434
0.1984	1.7114	15.0000	1.6303
0.2189	1.7080	15.2500	1.6172
0.2394	1.7057	15.5000	1.6041
0.2599	1.7043	15.7500	1.5910

TABLE 6.- DIVERTER COORDINATES

(a) Recessed diverter

FS, in.	±PBL, in.	μ, deg
35.1221	0.0000	4.573
35.1300	.0384	
35.1500	.0762	
35.2000	.1375	
35.2500	.1857	
35.5000	.3775	
35.7500	.5434	
36.0000	.7002	
36.2500	.8522	
36.5000	1.0015	

(b) Highlight diverter

FS, in.	±ABL, in.	ϕ, deg
33.7500	0.0000	0.0000
33.8000	.0688	.0003
33.9000	.1233	.0068
34.0000	.1633	.0298
34.2500	.2434	.2054
34.5000	.3123	.5896
34.7500	.3773	1.1740
35.0000	.4418	1.8989
35.2500	.5082	2.6741
35.5000	.5789	3.3990
35.7500	.6572	3.9834
36.0000	.7485	4.3677
36.2500	.8612	4.5432
36.5000	1.0015	4.5730

TABLE 7.- CIRCULAR-NACELLE BASIC-PYLON COORDINATES

(a) Over wing

FS, in.	PBL, in.	PWL, in.
30.3751	0.0022	3.0451
30.4000	0.0012	3.0452
	.1000	3.0403
	.2000	3.0256
	.2298	3.0192
30.6000	0.0011	3.0445
	.1000	3.0417
	.2000	3.0329
	.3000	3.0180
	.3691	3.0083
31.0000	-0.0069	3.0406
	0.0000	3.0406
	.2000	3.0320
	.4000	3.0052
	.4636	2.9921
32.0000	-0.1283	3.0159
	-.1000	3.0172
	0.0000	3.0191
	.3000	3.0014
	.5178	2.9633
33.0000	-0.3444	2.9568
	-.2000	2.9763
	0.0000	2.9859
	.3000	2.9640
	.5660	2.9017
34.0000	-0.5344	2.8505
	-.3000	2.9165
	0.0000	2.9491
	.4000	2.8939
	.6476	2.7991
35.0000	-0.7291	2.6978
	-.4000	2.8443
	0.0000	2.8955
	.4000	2.8443
	.7918	2.6491
36.0000	-0.9011	2.4977
	-.5000	2.7658
	0.0000	2.8411
	.5000	2.7658
	.9279	2.4465
36.5000	-0.9317	2.4401
	-.5000	2.7540
	0.0000	2.8267
	.5000	2.7540
	.9480	2.3867

TABLE 7.- Concluded

(b) Over nacelle

FS, in.	±PBL, in.	PWL, in.
36.5000	0.0000	2.8119
	.5000	2.7425
	1.0000	2.3204
	1.0015	2.8119
37.0000	0.0000	2.7815
	.5000	2.7193
	1.0000	2.4883
	1.2905	1.8431
38.0000	0.0000	2.7172
	.5000	2.6631
	1.0000	2.4846
	1.5000	2.0880
	1.7488	1.4157
38.7070	0.0000	2.6689
	.5000	2.6173
	1.0000	2.4492
	1.5000	2.0981
	1.8714	1.2491
39.0000	0.0000	2.6483
	.5000	2.5974
	1.0000	2.4316
	1.5000	2.0852
	1.8714	1.2491
40.0000	0.0000	2.5749
	.5000	2.5257
	1.0000	2.3654
	1.5000	2.0306
	1.8714	1.2491
41.0000	0.0000	2.4971
	.5000	2.4485
	1.0000	2.2904
	1.5000	1.9605
	1.8714	1.2491

FS, in.	±PBL, in.	PWL, in.
41.4500	0.0000	2.4606
	.5000	2.4120
	1.0000	2.2537
	1.5000	1.9244
	1.8714	1.2491
41.8500	0.0000	2.4274
	.5000	2.3785
	1.0000	2.2195
	1.5000	1.8899
	1.8707	1.2486
42.8500	0.0000	2.3408
	.5000	2.2906
	1.0000	2.1277
	1.5000	1.7930
	1.8590	1.2408
43.8500	0.0000	2.2488
	.5000	2.1962
	1.0000	2.0261
	1.5000	1.6802
	1.8279	1.2200
44.8500	0.0000	2.1508
	.5000	2.0947
	1.0000	1.9139
	1.5000	1.5492
	1.7746	1.1845
45.8500	0.0000	2.0459
	.5000	1.9845
	1.0000	1.7894
	1.5000	1.3958
	1.6994	1.1343
46.6500	0.0000	1.9546
	.5000	1.8896
	1.0000	1.6794
	1.5000	1.2532
	1.6257	1.0851

TABLE 8.- CIRCULAR-NACELLE PRESSURE-PYLON COORDINATES

(a) Over wing

FS, in.	PBL, in.	PWL, in.
26.5000	0.0000	2.6243
26.6000	-0.0044	2.6945
	0.0000	2.6946
	.1000	2.6583
	.1534	2.6087
26.7500	-0.0311	2.7696
	0.0000	2.7707
	.2000	2.7215
	.3784	2.5888
27.0000	-0.1054	2.8584
	0.0000	2.8682
	.3000	2.7866
	.4223	2.7020
27.5000	-0.2553	2.9664
	-.2000	2.9858
	0.0000	3.0162
	.3000	2.9469
	.5090	2.8053
28.0000	-0.3846	3.0308
	-.2000	3.1056
	0.0000	3.1321
	.4000	3.0222
	.6102	2.8559
29.0000	-0.5947	3.1019
	-.3000	3.2607
	0.0000	3.3087
	.4000	3.2214
	.7784	2.9080
30.0000	-0.7358	3.1282
	-.4000	3.3550
	0.0000	3.4318
	.5000	3.3082
	.8712	2.9342
31.0000	-0.8062	3.1154
	-.5000	3.3815
	0.0000	3.5054
	.5000	3.3815
	.8993	2.9444

FS, in.	PBL, in.	PWL, in.
31.6500	-0.8257	3.0875
	-.5000	3.3929
	0.0000	3.5214
	.5000	3.3929
	.8998	2.9382
32.0000	-0.8312	3.0664
	-.5000	3.3859
	0.0000	3.5165
	.5000	3.3859
	.8977	2.9295
33.0000	-0.8294	2.9819
	-.5000	3.3235
	0.0000	3.4645
	.5000	3.3235
	.8788	2.8803
34.0000	-0.8281	2.8610
	-.5000	3.2290
	0.0000	3.3819
	.5000	3.2290
	.8627	2.7881
35.0000	-0.8552	2.7009
	-.5000	3.1301
	0.0000	3.2850
	.5000	3.1301
	.8779	2.6457
36.0000	-0.9220	2.4981
	-.5000	3.0458
	0.0000	3.1805
	.5000	3.0458
	.9340	2.4462
36.5000	-0.9959	2.3802
	-.5000	3.0150
	0.0000	3.1265
	.5000	3.0150
	1.0009	2.3213

TABLE 8.- Concluded

(b) Over nacelle

FS, in.	±PBL, in.	PWL, in.
36.5000	0.0000	3.1265
	.5000	3.0150
	1.0000	2.3375
	1.0015	2.0148
37.0000	0.0000	3.0716
	.5000	2.9852
	1.0000	2.6646
	1.2905	1.8431
38.0000	0.0000	2.9601
	.5000	2.8971
	1.0000	2.6894
	1.5000	2.2278
	1.7488	1.4157
38.7070	0.0000	2.8800
	.5000	2.8208
	1.0000	2.6277
	1.5000	2.2243
	1.8714	1.2491
39.0000	0.0000	2.8467
	.5000	2.7874
	1.0000	2.5943
	1.5000	2.1911
	1.8714	1.2491
40.0000	0.0000	2.7320
	.5000	2.6728
	1.0000	2.4799
	1.5000	2.0785
	1.8714	1.2491
41.0000	0.0000	2.6165
	.5000	2.5572
	1.0000	2.3649
	1.5000	1.9686
	1.8714	1.2491

FS, in.	±PBL, in.	PWL, in.
41.4500	0.0000	2.5643
	.5000	2.5050
	1.0000	2.3131
	1.5000	1.9204
	1.8714	1.2491
41.8500	0.0000	2.5178
	.5000	2.4585
	1.0000	2.2670
	1.5000	1.8782
	1.8707	1.2486
42.8500	0.0000	2.4011
	.5000	2.3418
	1.0000	2.1512
	1.5000	1.7717
	1.8590	1.2408
43.8500	0.0000	2.2840
	.5000	2.2245
	1.0000	2.0339
	1.5000	1.6596
	1.8279	1.2200
44.8500	0.0000	2.1666
	.5000	2.1063
	1.0000	1.9136
	1.5000	1.5356
	1.7746	1.1845
45.8500	0.0000	2.0489
	.5000	1.9869
	1.0000	1.7876
	1.5000	1.3912
	1.6994	1.1343
46.5000	0.0000	1.9546
	.5000	1.8896
	1.0000	1.6794
	1.5000	1.2532
	1.6257	1.0851

TABLE 9.- CIRCULAR-NACELLE AND PYLON STATIC-PRESSURE ORIFICE LOCATIONS

NS, in.	x/c	Orifice locations at angles of ψ of -							
		0°	15°	30°	90°	180°	270°	330°	345°
Pressure pylon									
-4.650	0.248	X							
-3.300	.383	X							
-2.000	.514	X	X						X
-.650	.649	X							
.650	.779	X	X						X
2.000	0.915	X							
3.100	1.025	X	X	X				X	X
4.600	1.176	X		X				X	
6.200	1.336	X		X				X	
9.300	1.647	X		X				X	
Exterior of circular nacelle									
0.030	0.717	X		X	X	X	X	X	
.100	.724	X		X	X	X	X	X	
.200	.734	X		X	X	X	X	X	
.300	.744	X		X	X	X	X	X	
.500	.764	X		X	X	X	X	X	
0.700	0.784	X		X	X	X	X	X	
1.200	.835	X		X	X	X	X	X	
1.500	.865			X	X	X	X	X	
2.300	.945			X	X	X	X	X	
3.100	1.025				X	X	X		
4.600	1.176				X	X	X		
5.400	1.256				X	X	X		
6.200	1.336				X	X	X		
7.100	1.426				X	X	X		
8.100	1.527				X	X	X		
9.300	1.647				X	X	X		
10.700	1.787				X	X	X		
12.100	1.928				X	X	X		
13.500	2.068	X		X	X	X	X	X	
14.800	2.198	X			X	X	X		
15.500	2.269	X			X	X	X		
Interior of circular nacelle									
2.500	0.965	X			X	X	X		
13.000	2.018	X			X	X	X		
15.000	2.219	X			X	X	X		

TABLE 10.- D-NACELLE FOREBODY COORDINATES

[All dimensions are in inches]

(a) $\theta = 0°$; $R_{HL} = 3.3458$ in.; $L_{lip} = 3.8110$ in.; $\tau = 0.6713$ in.; $x_{lip} = 0.4804$ in.; $y_{lip} = 0.3053$ in.

FOREBODY EXTERNAL CONTOUR						INTERNAL CONTOUR		
WS	+-WBL	WWL SCRIPT-R	WS	+-WBL	WWL SCRIPT-R	WS	+-WBL	WWL SCRIPT-R
0.0	0.0	6.6542 3.3458	1.0153	0.0	6.2046 3.7954	0.0	0.0	6.6542 3.3458
0.0005	0.0	6.6428 3.3572	1.0852	0.0	6.1912 3.8088	0.0003	0.0	6.6622 3.3378
0.0022	0.0	6.6316 3.3684	1.1666	0.0	6.1764 3.8236	0.0011	0.0	6.6704 3.3296
0.0049	0.0	6.6204 3.3796	1.2480	0.0	6.1624 3.8376	0.0025	0.0	6.6788 3.3212
0.0087	0.0	6.6094 3.3906	1.3294	0.0	6.1493 3.8507	0.0044	0.0	6.6874 3.3126
0.0136	0.0	6.5984 3.4016	1.4108	0.0	6.1368 3.8632	0.0069	0.0	6.6962 3.3038
0.0196	0.0	6.5876 3.4124	1.4921	0.0	6.1250 3.8750	0.0100	0.0	6.7054 3.2946
0.0267	0.0	6.5768 3.4232	1.5735	0.0	6.1138 3.8862	0.0137	0.0	6.7149 3.2851
0.0350	0.0	6.5662 3.4338	1.6549	0.0	6.1032 3.8968	0.0180	0.0	6.7248 3.2752
0.0443	0.0	6.5555 3.4445	1.7363	0.0	6.0932 3.9068	0.0229	0.0	6.7351 3.2649
0.0548	0.0	6.5449 3.4551	1.8177	0.0	6.0838 3.9162	0.0286	0.0	6.7458 3.2542
0.0665	0.0	6.5342 3.4658	1.8991	0.0	6.0748 3.9252	0.0349	0.0	6.7569 3.2431
0.0793	0.0	6.5235 3.4765	1.9805	0.0	6.0663 3.9337	0.0420	0.0	6.7685 3.2315
0.0933	0.0	6.5127 3.4873	2.0619	0.0	6.0584 3.9416	0.0499	0.0	6.7805 3.2195
0.1085	0.0	6.5018 3.4982	2.1433	0.0	6.0508 3.9492	0.0587	0.0	6.7929 3.2071
0.1250	0.0	6.4909 3.5091	2.2247	0.0	6.0437 3.9563	0.0684	0.0	6.8058 3.1942
0.1427	0.0	6.4799 3.5201	2.3060	0.0	6.0371 3.9629	0.0792	0.0	6.8190 3.1810
0.1616	0.0	6.4688 3.5312	2.3874	0.0	6.0308 3.9692	0.0912	0.0	6.8326 3.1674
0.1819	0.0	6.4577 3.5423	2.4688	0.0	6.0250 3.9750	0.1047	0.0	6.8465 3.1535
0.2035	0.0	6.4465 3.5535	2.5502	0.0	6.0195 3.9805	0.1197	0.0	6.8607 3.1393
0.2265	0.0	6.4352 3.5648	2.6316	0.0	6.0145 3.9855	0.1368	0.0	6.8751 3.1249
0.2509	0.0	6.4239 3.5761	2.7130	0.0	6.0098 3.9902	0.1573	0.0	6.8904 3.1096
0.2767	0.0	6.4124 3.5876	2.7808	0.0	6.0062 3.9938	0.1778	0.0	6.9036 3.0964
0.3041	0.0	6.4010 3.5990	2.8486	0.0	6.0028 3.9972	0.1984	0.0	6.9150 3.0850
0.3330	0.0	6.3894 3.6106	2.9184	0.0	5.9995 4.0005	0.2189	0.0	6.9246 3.0754
0.3635	0.0	6.3777 3.6223	2.9882	0.0	5.9966 4.0034	0.2394	0.0	6.9327 3.0673
0.3956	0.0	6.3660 3.6340	3.0581	0.0	5.9939 4.0061	0.2599	0.0	6.9394 3.0606
0.4296	0.0	6.3542 3.6458	3.1279	0.0	5.9914 4.0086	0.2804	0.0	6.9449 3.0551
0.4653	0.0	6.3423 3.6577	3.1933	0.0	5.9894 4.0106	0.3010	0.0	6.9493 3.0507
0.5029	0.0	6.3303 3.6697	3.2587	0.0	5.9876 4.0124	0.3215	0.0	6.9527 3.0473
0.5426	0.0	6.3183 3.6817	3.3241	0.0	5.9862 4.0138	0.3420	0.0	6.9552 3.0448
0.5844	0.0	6.3061 3.6939	3.3895	0.0	5.9850 4.0150	0.3591	0.0	6.9568 3.0432
0.6284	0.0	6.2939 3.7061	3.4549	0.0	5.9841 4.0159	0.3767	0.0	6.9579 3.0421
0.6748	0.0	6.2815 3.7185	3.5195	0.0	5.9835 4.0165	0.3943	0.0	6.9587 3.0413
0.7238	0.0	6.2690 3.7310	3.5841	0.0	5.9831 4.0169	0.4149	0.0	6.9592 3.0408
0.7755	0.0	6.2564 3.7436	3.6487	0.0	5.9829 4.0171	0.4355	0.0	6.9594 3.0406
0.8302	0.0	6.2437 3.7563	3.7133	0.0	5.9829 4.0171	0.4518	0.0	6.9595 3.0405
0.8882	0.0	6.2308 3.7692	3.8110	0.0	5.9829 4.0171	0.4681	0.0	6.9595 3.0405
0.9498	0.0	6.2178 3.7822				0.4804	0.0	6.9595 3.0405

TABLE 10.- Continued

(b) $\theta = 10°$; $R_{HL} = 3.3060$ in.; $L_{lip} = 3.7133$ in.; $\tau = 0.6633$ in.; $x_{lip} = 0.4681$ in.; $y_{lip} = 0.3017$ in.

FOREBODY EXTERNAL CONTOUR				INTERNAL CONTOUR			
NS	ϕ-NBL	NWL SCRIPT-R		NS	ϕ-NBL	NWL SCRIPT-R	
0.0	0.5741	6.7443	3.3060	1.0153	0.6521	6.3017	3.7553
0.0005	0.5760	6.7331	3.3173	1.0852	0.6544	6.2866	3.7687
0.0022	0.5780	6.7220	3.3286	1.1666	0.6570	6.2741	3.7833
0.0049	0.5799	6.7110	3.3397	1.2480	0.6594	6.2605	3.7972
0.0087	0.5819	6.7001	3.3508	1.3294	0.6616	6.2477	3.8102
0.0136	0.5838	6.6893	3.3617	1.4108	0.6638	6.2355	3.8226
0.0196	0.5856	6.6787	3.3726	1.4921	0.6658	6.2240	3.8342
0.0267	0.5875	6.6681	3.3833	1.5735	0.6677	6.2132	3.8453
0.0350	0.5894	6.6576	3.3940	1.6549	0.6695	6.2029	3.8557
0.0443	0.5912	6.6471	3.4047	1.7363	0.6712	6.1932	3.8655
0.0548	0.5931	6.6366	3.4153	1.8177	0.6729	6.1840	3.8748
0.0665	0.5949	6.6261	3.4260	1.8991	0.6744	6.1754	3.8836
0.0793	0.5968	6.6155	3.4367	1.9805	0.6758	6.1672	3.8919
0.0933	0.5987	6.6048	3.4475	2.0619	0.6772	6.1596	3.8997
0.1085	0.6005	6.5941	3.4584	2.1433	0.6784	6.1524	3.9070
0.1250	0.6024	6.5833	3.4694	2.2247	0.6796	6.1456	3.9139
0.1427	0.6044	6.5725	3.4804	2.3060	0.6808	6.1392	3.9203
0.1616	0.6063	6.5616	3.4915	2.3874	0.6818	6.1333	3.9264
0.1819	0.6082	6.5506	3.5026	2.4688	0.6828	6.1278	3.9320
0.2035	0.6102	6.5396	3.5138	2.5502	0.6837	6.1226	3.9372
0.2265	0.6121	6.5285	3.5251	2.6316	0.6845	6.1179	3.9420
0.2509	0.6141	6.5173	3.5365	2.7130	0.6853	6.1135	3.9464
0.2767	0.6161	6.5060	3.5479	2.7808	0.6859	6.1102	3.9499
0.3041	0.6181	6.4947	3.5594	2.8486	0.6864	6.1070	3.9530
0.3330	0.6201	6.4833	3.5710	2.9184	0.6870	6.1041	3.9560
0.3635	0.6221	6.4718	3.5826	2.9882	0.6874	6.1014	3.9587
0.3956	0.6241	6.4603	3.5943	3.0581	0.6878	6.0990	3.9611
0.4296	0.6262	6.4487	3.6061	3.1279	0.6882	6.0969	3.9633
0.4653	0.6283	6.4370	3.6180	3.1933	0.6885	6.0952	3.9650
0.5029	0.6303	6.4252	3.6300	3.2587	0.6888	6.0938	3.9664
0.5426	0.6324	6.4133	3.6420	3.3241	0.6890	6.0927	3.9675
0.5844	0.6345	6.4014	3.6542	3.3895	0.6891	6.0919	3.9683
0.6284	0.6367	6.3893	3.6664	3.4549	0.6892	6.0914	3.9689
0.6748	0.6388	6.3772	3.6787	3.5195	0.6892	6.0912	3.9691
0.7238	0.6410	6.3649	3.6912	3.5841	0.6893	6.0911	3.9692
0.7755	0.6431	6.3526	3.7037	3.6487	0.6893	6.0910	3.9693
0.8302	0.6453	6.3401	3.7164	3.7133	0.6893	6.0910	3.9693
0.8882	0.6476	6.3274	3.7292	3.8110	0.6893	6.0910	3.9693
0.9498	0.6498	6.3147	3.7422				

INTERNAL CONTOUR			
NS	ϕ-NBL	NWL SCRIPT-R	
0.0	0.5741	6.7443	3.3060
0.0003	0.5727	6.7522	3.2979
0.0011	0.5712	6.7603	3.2897
0.0025	0.5698	6.7685	3.2813
0.0044	0.5683	6.7770	3.2727
0.0069	0.5668	6.7858	3.2638
0.0100	0.5652	6.7948	3.2546
0.0137	0.5635	6.8042	3.2451
0.0180	0.5618	6.8140	3.2352
0.0229	0.5600	6.8242	3.2248
0.0286	0.5581	6.8348	3.2141
0.0349	0.5562	6.8458	3.2029
0.0420	0.5542	6.8572	3.1913
0.0499	0.5521	6.6691	3.1792
0.0587	0.5499	6.8813	3.1668
0.0684	0.5477	6.8940	3.1539
0.0792	0.5454	6.9070	3.1407
0.0912	0.5430	6.9204	3.1271
0.1047	0.5406	6.9340	3.1133
0.1197	0.5382	6.9479	3.0992
0.1368	0.5357	6.9620	3.0848
0.1573	0.5331	6.9769	3.0697
0.1778	0.5308	6.9897	3.0568
0.1984	0.5289	7.0006	3.0457
0.2189	0.5273	7.0098	3.0363
0.2394	0.5259	7.0175	3.0286
0.2599	0.5248	7.0238	3.0221
0.2804	0.5239	7.0288	3.0170
0.3010	0.5232	7.0328	3.0129
0.3215	0.5227	7.0359	3.0099
0.3420	0.5223	7.0381	3.0076
0.3591	0.5220	7.0394	3.0063
0.3767	0.5219	7.0403	3.0054
0.3943	0.5218	7.0409	3.0048
0.4149	0.5217	7.0412	3.0044
0.4355	0.5217	7.0413	3.0043
0.4518	0.5217	7.0413	3.0043
0.4681	0.5217	7.0413	3.0043
0.4804	0.5217	7.0413	3.0043

TABLE 10.- Continued

(c) $\theta = 20°$; $R_{HL} = 3.1882$ in.; $L_{lip} = 3.4549$ in.; $\tau = 0.6397$ in.; $x_{lip} = 0.4355$ in.; $y_{lip} = 0.2909$ in.

FOREBODY EXTERNAL CONTOUR						INTERNAL CONTOUR		
NS	ϕ-NBL	NWL SCRIPT-R	NS	ϕ-NBL	NWL SCRIPT-R	NS	ϕ-NBL	NWL SCRIPT-R
0.0	1.0904	7.0041 3.1882	1.0153	1.2434	6.5838 3.6355	0.0	1.0904	7.0041 3.1882
0.0005	1.0943	6.9934 3.1995	1.0852	1.2479	6.5715 3.6485	0.0003	1.0877	7.0117 3.1801
0.0022	1.0982	6.9829 3.2108	1.1666	1.2528	6.5581 3.6628	0.0011	1.0849	7.0194 3.1719
0.0049	1.1020	6.9724 3.2219	1.2480	1.2574	6.5454 3.6763	0.0025	1.0820	7.0273 3.1635
0.0087	1.1057	6.9620 3.2330	1.3294	1.2617	6.5335 3.6889	0.0044	1.0790	7.0354 3.1549
0.0136	1.1095	6.9517 3.2439	1.4108	1.2658	6.5223 3.7009	0.0069	1.0760	7.0438 3.1460
0.0196	1.1132	6.9416 3.2547	1.4921	1.2696	6.5118 3.7121	0.0100	1.0728	7.0524 3.1367
0.0267	1.1168	6.9315 3.2654	1.5735	1.2732	6.5019 3.7226	0.0137	1.0695	7.0615 3.1271
0.0350	1.1205	6.9215 3.2761	1.6549	1.2766	6.4925 3.7326	0.0180	1.0661	7.0709 3.1171
0.0443	1.1241	6.9115 3.2867	1.7363	1.2798	6.4838 3.7419	0.0229	1.0625	7.0807 3.1067
0.0548	1.1278	6.9015 3.2974	1.8177	1.2828	6.4755 3.7507	0.0286	1.0588	7.0909 3.0958
0.0665	1.1314	6.8914 3.3081	1.8991	1.2856	6.4678 3.7589	0.0349	1.0550	7.1014 3.0846
0.0793	1.1351	6.8813 3.3188	1.9805	1.2882	6.4606 3.7666	0.0420	1.0510	7.1124 3.0729
0.0933	1.1388	6.8712 3.3296	2.0619	1.2907	6.4538 3.7738	0.0499	1.0468	7.1238 3.0608
0.1085	1.1425	6.8609 3.3405	2.1433	1.2930	6.4475 3.7805	0.0587	1.0426	7.1355 3.0483
0.1250	1.1463	6.8506 3.3515	2.2247	1.2951	6.4416 3.7867	0.0684	1.0382	7.1476 3.0354
0.1427	1.1500	6.8403 3.3625	2.3060	1.2971	6.4362 3.7925	0.0792	1.0337	7.1600 3.0222
0.1616	1.1538	6.8299 3.3736	2.3874	1.2989	6.4312 3.7979	0.0912	1.0291	7.1727 3.0088
0.1819	1.1576	6.8194 3.3847	2.4688	1.3006	6.4266 3.8028	0.1047	1.0244	7.1855 2.9951
0.2035	1.1615	6.8089 3.3959	2.5502	1.3022	6.4224 3.8072	0.1197	1.0197	7.1985 2.9813
0.2265	1.1653	6.7983 3.4072	2.6316	1.3035	6.4185 3.8113	0.1368	1.0149	7.2115 2.9674
0.2509	1.1692	6.7876 3.4185	2.7130	1.3048	6.4151 3.8150	0.1573	1.0100	7.2251 2.9530
0.2767	1.1731	6.7769 3.4299	2.7808	1.3057	6.4125 3.8177	0.1778	1.0058	7.2366 2.9408
0.3041	1.1770	6.7661 3.4414	2.8486	1.3066	6.4102 3.8201	0.1984	1.0023	7.2462 2.9305
0.3330	1.1810	6.7553 3.4530	2.9184	1.3073	6.4082 3.8223	0.2189	0.9994	7.2541 2.9221
0.3635	1.1850	6.7444 3.4646	2.9882	1.3079	6.4065 3.8242	0.2394	0.9971	7.2606 2.9152
0.3956	1.1889	6.7334 3.4762	3.0581	1.3084	6.4051 3.8256	0.2599	0.9952	7.2657 2.9097
0.4296	1.1930	6.7224 3.4880	3.1279	1.3088	6.4041 3.8267	0.2804	0.9937	7.2697 2.9055
0.4653	1.1970	6.7113 3.4998	3.1933	1.3090	6.4035 3.8273	0.3010	0.9927	7.2726 2.9024
0.5029	1.2011	6.7001 3.5117	3.2587	1.3091	6.4032 3.8277	0.3215	0.9919	7.2747 2.9002
0.5426	1.2052	6.6888 3.5237	3.3241	1.3092	6.4030 3.8278	0.3420	0.9914	7.2761 2.8987
0.5844	1.2093	6.6775 3.5357	3.3895	1.3092	6.4030 3.8279	0.3591	0.9912	7.2768 2.8980
0.6284	1.2134	6.6661 3.5478	3.4549	1.3092	6.4030 3.8279	0.3767	0.9910	7.2772 2.8975
0.6748	1.2176	6.6547 3.5600	3.5195	1.3092	6.4030 3.8279	0.3943	0.9909	7.2774 2.8973
0.7238	1.2218	6.6431 3.5723	3.5841	1.3092	6.4030 3.8279	0.4149	0.9909	7.2774 2.8973
0.7755	1.2260	6.6315 3.5847	3.6487	1.3092	6.4030 3.8279	0.4355	0.9909	7.2774 2.8973
0.8302	1.2303	6.6197 3.5972	3.7133	1.3092	6.4030 3.8279	0.4518	0.9909	7.2774 2.8973
0.8882	1.2346	6.6079 3.6098	3.8110	1.3092	6.4030 3.8279	0.4681	0.9909	7.2774 2.8973
0.9498	1.2390	6.5959 3.6226				0.4804	0.9909	7.2774 2.8973

TABLE 10.- Continued

(d) $\theta = 30°$; $R_{HL} = 2.9981$ in.; $L_{lip} = 3.1279$ in.; $\tau = 0.6015$ in.; $x_{lip} = 0.3943$ in.; $y_{lip} = 0.2736$ in.

FOREBODY EXTERNAL CONTOUR								INTERNAL CONTOUR			
NS	+-NBL	NWL SCRIPT-R		NS	+-NBL	NWL SCRIPT-R		NS	+-NBL	NWL SCRIPT-R	
0.0	1.4991	7.4036	2.9981	1.0153	1.7185	7.0234	3.4371	0.0	1.4991	7.4036	2.9981
0.0005	1.5046	7.3939	3.0093	1.0852	1.7248	7.0126	3.4495	0.0003	1.4951	7.4105	2.9901
0.0022	1.5102	7.3842	3.0204	1.1666	1.7316	7.0009	3.4631	0.0011	1.4910	7.4175	2.9820
0.0049	1.5157	7.3747	3.0314	1.2480	1.7379	6.9898	3.4758	0.0025	1.4868	7.4247	2.9737
0.0087	1.5212	7.3653	3.0423	1.3294	1.7439	6.9795	3.4877	0.0044	1.4826	7.4321	2.9651
0.0136	1.5265	7.3560	3.0531	1.4108	1.7494	6.9699	3.4989	0.0069	1.4781	7.4398	2.9562
0.0196	1.5319	7.3467	3.0637	1.4921	1.7546	6.9609	3.5093	0.0100	1.4735	7.4478	2.9470
0.0267	1.5371	7.3376	3.0743	1.5735	1.7595	6.9525	3.5190	0.0137	1.4687	7.4561	2.9374
0.0350	1.5424	7.3285	3.0848	1.6549	1.7640	6.9446	3.5280	0.0180	1.4637	7.4648	2.9274
0.0443	1.5477	7.3194	3.0953	1.7363	1.7682	6.9373	3.5365	0.0229	1.4585	7.4738	2.9170
0.0548	1.5529	7.3103	3.1058	1.8177	1.7722	6.9305	3.5443	0.0286	1.4531	7.4832	2.9062
0.0665	1.5582	7.3011	3.1164	1.8991	1.7758	6.9242	3.5516	0.0349	1.4475	7.4929	2.8949
0.0793	1.5635	7.2919	3.1270	1.9805	1.7792	6.9184	3.5583	0.0420	1.4416	7.5030	2.8832
0.0933	1.5689	7.2826	3.1378	2.0619	1.7823	6.9130	3.5645	0.0499	1.4356	7.5135	2.8712
0.1085	1.5743	7.2733	3.1485	2.1433	1.7851	6.9081	3.5702	0.0587	1.4294	7.5242	2.8588
0.1250	1.5797	7.2639	3.1594	2.2247	1.7877	6.9036	3.5754	0.0684	1.4231	7.5352	2.8461
0.1427	1.5851	7.2545	3.1702	2.3060	1.7900	6.8996	3.5801	0.0792	1.4166	7.5464	2.8332
0.1616	1.5906	7.2450	3.1812	2.3874	1.7922	6.8959	3.5843	0.0912	1.4101	7.5577	2.8201
0.1819	1.5961	7.2355	3.1922	2.4688	1.7940	6.8927	3.5881	0.1047	1.4035	7.5691	2.8070
0.2035	1.6016	7.2259	3.2033	2.5502	1.7957	6.8898	3.5913	0.1197	1.3969	7.5805	2.7938
0.2265	1.6072	7.2162	3.2144	2.6316	1.7970	6.8874	3.5941	0.1368	1.3904	7.5918	2.7808
0.2509	1.6128	7.2066	3.2256	2.7130	1.7982	6.8855	3.5963	0.1573	1.3838	7.6032	2.7675
0.2767	1.6184	7.1968	3.2368	2.7808	1.7989	6.8843	3.5977	0.1778	1.3783	7.6127	2.7566
0.3041	1.6241	7.1870	3.2481	2.8486	1.7994	6.8834	3.5987	0.1984	1.3739	7.6204	2.7478
0.3330	1.6297	7.1772	3.2595	2.9164	1.7997	6.8829	3.5993	0.2189	1.3704	7.6265	2.7407
0.3635	1.6355	7.1673	3.2709	2.9682	1.7998	6.8827	3.5996	0.2394	1.3676	7.6312	2.7353
0.3956	1.6412	7.1574	3.2824	3.0581	1.7998	6.8826	3.5996	0.2599	1.3656	7.6347	2.7312
0.4296	1.6470	7.1474	3.2939	3.1279	1.7998	6.8826	3.5996	0.2804	1.3642	7.6372	2.7283
0.4653	1.6527	7.1374	3.3055	3.1933	1.7998	6.8826	3.5996	0.3010	1.3632	7.6388	2.7264
0.5029	1.6586	7.1273	3.3171	3.2587	1.7998	6.8826	3.5996	0.3215	1.3627	7.6398	2.7253
0.5426	1.6644	7.1172	3.3288	3.3241	1.7998	6.8826	3.5996	0.3420	1.3624	7.6403	2.7248
0.5844	1.6703	7.1070	3.3406	3.3895	1.7998	6.8826	3.5996	0.3591	1.3623	7.6404	2.7246
0.6284	1.6762	7.0968	3.3524	3.4549	1.7998	6.8826	3.5996	0.3767	1.3623	7.6405	2.7245
0.6748	1.6821	7.0865	3.3643	3.5195	1.7998	6.8826	3.5996	0.3943	1.3623	7.6405	2.7245
0.7238	1.6881	7.0761	3.3762	3.5841	1.7998	6.8826	3.5996	0.4149	1.3623	7.6405	2.7245
0.7755	1.6941	7.0657	3.3882	3.6487	1.7998	6.8826	3.5996	0.4355	1.3623	7.6405	2.7245
0.8302	1.7002	7.0552	3.4003	3.7133	1.7998	6.8826	3.5996	0.4518	1.3623	7.6405	2.7245
0.8882	1.7062	7.0447	3.4125	3.8110	1.7998	6.8826	3.5996	0.4661	1.3623	7.6405	2.7245
0.9498	1.7124	7.0341	3.4247					0.4804	1.3623	7.6405	2.7245

TABLE 10.- Continued

(e) $\theta = 40°$; $R_{HL} = 2.7451$ in.; $L_{lip} = 2.8486$ in.; $\tau = 0.5508$ in.; $x_{lip} = 0.3591$ in.; $y_{lip} = 0.2505$ in.

FOREBODY EXTERNAL CONTOUR								INTERNAL CONTOUR			
NS	ϕ-NBL	NWL SCRIPT-R		NS	ϕ-NBL	NWL SCRIPT-R		NS	ϕ-NBL	NWL SCRIPT-R	
0.0	1.7645	7.6971	2.7451	1.0153	2.0332	7.5769	3.1631	0.0	1.7645	7.8971	2.7451
0.0005	1.7714	7.8889	2.7559	1.0852	2.0406	7.5681	3.1746	0.0003	1.7596	7.9030	2.7375
0.0022	1.7783	7.8807	2.7666	1.1666	2.0486	7.5586	3.1871	0.0011	1.7546	7.9089	2.7297
0.0049	1.7851	7.6726	2.7771	1.2480	2.0561	7.5497	3.1987	0.0025	1.7495	7.9151	2.7217
0.0087	1.7918	7.8646	2.7875	1.3294	2.0630	7.5414	3.2095	0.0044	1.7441	7.9214	2.7134
0.0136	1.7984	7.8567	2.7978	1.4108	2.0694	7.5338	3.2195	0.0069	1.7386	7.9280	2.7048
0.0196	1.8050	7.8489	2.8080	1.4921	2.0754	7.5266	3.2287	0.0100	1.7329	7.9348	2.6959
0.0267	1.8115	7.8412	2.8181	1.5735	2.0809	7.5201	3.2373	0.0137	1.7269	7.9419	2.6866
0.0350	1.8179	7.8335	2.8282	1.6549	2.0860	7.5140	3.2452	0.0180	1.7207	7.9494	2.6769
0.0443	1.8244	7.8258	2.8383	1.7363	2.0907	7.5084	3.2525	0.0229	1.7142	7.9571	2.6668
0.0548	1.8309	7.8180	2.8484	1.8177	2.0950	7.5033	3.2592	0.0286	1.7074	7.9652	2.6563
0.0665	1.8374	7.8102	2.8585	1.8991	2.0989	7.4986	3.2653	0.0349	1.7004	7.9735	2.6454
0.0793	1.8440	7.8024	2.8687	1.9805	2.1025	7.4944	3.2709	0.0420	1.6932	7.9821	2.6341
0.0933	1.8506	7.7945	2.8790	2.0619	2.1057	7.4905	3.2759	0.0499	1.6857	7.9910	2.6225
0.1085	1.8573	7.7866	2.8894	2.1433	2.1086	7.4871	3.2803	0.0587	1.6781	8.0001	2.6106
0.1250	1.8639	7.7786	2.8998	2.2247	2.1111	7.4841	3.2843	0.0684	1.6703	8.0094	2.5985
0.1427	1.8707	7.7706	2.9102	2.3060	2.1133	7.4815	3.2877	0.0792	1.6624	8.0188	2.5863
0.1616	1.8774	7.7626	2.9207	2.3874	2.1151	7.4793	3.2906	0.0912	1.6545	8.0282	2.5740
0.1819	1.8842	7.7545	2.9313	2.4688	2.1166	7.4775	3.2929	0.1047	1.6467	8.0376	2.5618
0.2035	1.8910	7.7464	2.9419	2.5502	2.1177	7.4763	3.2945	0.1197	1.6389	8.0468	2.5497
0.2265	1.8979	7.7382	2.9525	2.6316	2.1183	7.4755	3.2955	0.1368	1.6314	8.0558	2.5380
0.2509	1.9047	7.7300	2.9633	2.7130	2.1185	7.4752	3.2958	0.1573	1.6239	8.0647	2.5263
0.2767	1.9117	7.7218	2.9740	2.7808	2.1186	7.4752	3.2959	0.1778	1.6179	8.0718	2.5170
0.3041	1.9186	7.7135	2.9848	2.8486	2.1186	7.4752	3.2959	0.1984	1.6133	8.0774	2.5098
0.3330	1.9256	7.7052	2.9957	2.9184	2.1186	7.4752	3.2959	0.2189	1.6097	8.0816	2.5043
0.3635	1.9326	7.6969	3.0065	2.9882	2.1186	7.4752	3.2959	0.2394	1.6072	8.0846	2.5003
0.3956	1.9396	7.6885	3.0175	3.0581	2.1186	7.4752	3.2959	0.2599	1.6055	8.0867	2.4977
0.4296	1.9466	7.6801	3.0284	3.1279	2.1186	7.4752	3.2959	0.2804	1.6044	8.0880	2.4960
0.4653	1.9537	7.6717	3.0394	3.1933	2.1186	7.4752	3.2959	0.3010	1.6038	8.0886	2.4951
0.5029	1.9608	7.6632	3.0505	3.2587	2.1186	7.4752	3.2959	0.3215	1.6036	8.0889	2.4947
0.5426	1.9679	7.6547	3.0616	3.3241	2.1186	7.4752	3.2959	0.3420	1.6035	8.0890	2.4947
0.5844	1.9751	7.6462	3.0727	3.3855	2.1186	7.4752	3.2959	0.3591	1.6035	8.0890	2.4947
0.6284	1.9823	7.6376	3.0839	3.4549	2.1186	7.4752	3.2959	0.3767	1.6035	8.0890	2.4947
0.6748	1.9895	7.6290	3.0951	3.5195	2.1186	7.4752	3.2959	0.3943	1.6035	8.0890	2.4947
0.7238	1.9967	7.6204	3.1063	3.5841	2.1186	7.4752	3.2959	0.4149	1.6035	8.0890	2.4947
0.7755	2.0039	7.6118	3.1176	3.6487	2.1186	7.4752	3.2959	0.4355	1.6035	8.0890	2.4947
0.8302	2.0112	7.6031	3.1289	3.7133	2.1186	7.4752	3.2959	0.4518	1.6035	8.0890	2.4947
0.8882	2.0185	7.5944	3.1403	3.8110	2.1186	7.4752	3.2959	0.4681	1.6035	8.0890	2.4947
0.9498	2.0258	7.5857	3.1517					0.4804	1.6035	8.0890	2.4947

TABLE 10.- Continued

(f) $\theta = 51.8540°$; $R_{HL} = 2.3829$ in.; $L_{lip} = 2.7130$ in.; $\tau = 0.4781$ in.; $x_{lip} = 0.3420$ in.; $y_{lip} = 0.2174$ in.

FOREBODY EXTERNAL CONTOUR						INTERNAL CONTOUR			
NS	ϕ-NBL	NWL SCRIPT-R		NS	ϕ-NBL	NWL SCRIPT-R		NS	ϕ-NBL	NWL SCRIPT-R	
0.0	1.8740	8.5282	2.3629	1.0153	2.1651	8.2996	2.7530	0.0	1.8740	8.5282	2.3829
0.0005	1.8815	8.5223	2.3924	1.0852	2.1729	8.2934	2.7630	0.0003	1.8686	8.5324	2.3761
0.0022	1.8890	8.5164	2.4019	1.1666	2.1814	8.2867	2.7738	0.0011	1.8632	8.5367	2.3691
0.0049	1.8963	8.5106	2.4113	1.2480	2.1893	8.2805	2.7838	0.0025	1.8576	8.5411	2.3620
0.0087	1.9036	8.5049	2.4206	1.3294	2.1966	8.2748	2.7931	0.0044	1.8518	8.5456	2.3546
0.0136	1.9108	8.4992	2.4297	1.4108	2.2033	8.2695	2.8016	0.0069	1.8458	8.5503	2.3470
0.0196	1.9179	8.4937	2.4388	1.4921	2.2095	8.2647	2.8095	0.0100	1.8395	8.5553	2.3390
0.0267	1.9250	8.4881	2.4477	1.5735	2.2152	8.2602	2.8168	0.0137	1.8329	8.5604	2.3307
0.0350	1.9320	8.4826	2.4567	1.6549	2.2204	8.2561	2.8234	0.0180	1.8261	8.5658	2.3220
0.0443	1.9391	8.4770	2.4657	1.7363	2.2252	8.2523	2.8295	0.0229	1.8190	8.5713	2.3130
0.0548	1.9462	8.4715	2.4746	1.8177	2.2296	8.2489	2.8350	0.0286	1.8116	8.5772	2.3036
0.0665	1.9533	8.4659	2.4837	1.8991	2.2335	8.2458	2.8400	0.0349	1.8040	8.5832	2.2938
0.0793	1.9604	8.4603	2.4928	1.9805	2.2370	8.2431	2.8445	0.0420	1.7960	8.5894	2.2838
0.0933	1.9676	8.4546	2.5019	2.0619	2.2401	8.2406	2.8484	0.0499	1.7879	8.5958	2.2734
0.1085	1.9749	8.4490	2.5111	2.1433	2.2428	8.2385	2.8519	0.0587	1.7796	8.6023	2.2629
0.1250	1.9821	8.4432	2.5204	2.2247	2.2451	8.2367	2.8548	0.0684	1.7712	8.6089	2.2522
0.1427	1.9894	8.4375	2.5297	2.3060	2.2470	8.2352	2.8572	0.0792	1.7627	8.6156	2.2414
0.1616	1.9968	8.4317	2.5390	2.3874	2.2485	8.2340	2.8591	0.0912	1.7542	8.6222	2.2306
0.1819	2.0042	8.4259	2.5484	2.4688	2.2494	8.2333	2.8602	0.1047	1.7458	8.6288	2.2199
0.2035	2.0116	8.4201	2.5578	2.5502	2.2499	8.2330	2.8608	0.1197	1.7376	8.6353	2.2095
0.2265	2.0190	8.4143	2.5673	2.6316	2.2500	8.2329	2.8610	0.1368	1.7297	8.6415	2.1995
0.2509	2.0265	8.4084	2.5768	2.7130	2.2500	8.2329	2.8610	0.1573	1.7220	8.6475	2.1896
0.2767	2.0340	8.4025	2.5864	2.7808	2.2500	8.2329	2.8610	0.1778	1.7160	8.6523	2.1820
0.3041	2.0415	8.3966	2.5959	2.8486	2.2500	8.2329	2.8610	0.1984	1.7114	8.6559	2.1761
0.3330	2.0491	8.3906	2.6056	2.9164	2.2500	8.2329	2.8610	0.2189	1.7080	8.6585	2.1719
0.3635	2.0567	8.3847	2.6152	2.9882	2.2500	8.2329	2.8610	0.2394	1.7057	8.6603	2.1669
0.3956	2.0643	8.3787	2.6249	3.0581	2.2500	8.2329	2.8610	0.2599	1.7043	8.6615	2.1670
0.4296	2.0719	8.3727	2.6346	3.1279	2.2500	8.2329	2.8610	0.2804	1.7034	8.6621	2.1660
0.4653	2.0796	8.3667	2.6443	3.1933	2.2500	8.2329	2.8610	0.3010	1.7031	8.6624	2.1656
0.5029	2.0873	8.3607	2.6541	3.2587	2.2500	8.2329	2.8610	0.3215	1.7030	8.6625	2.1655
0.5426	2.0950	8.3546	2.6639	3.3241	2.2500	8.2329	2.8610	0.3420	1.7030	8.6625	2.1655
0.5844	2.1027	8.3485	2.6737	3.3895	2.2500	8.2329	2.8610	0.3591	1.7030	8.6625	2.1655
0.6284	2.1104	8.3425	2.6835	3.4549	2.2500	8.2329	2.8610	0.3767	1.7030	8.6625	2.1655
0.6748	2.1182	8.3364	2.6934	3.5195	2.2500	8.2329	2.8610	0.3943	1.7030	8.6625	2.1655
0.7238	2.1260	8.3303	2.7033	3.5841	2.2500	8.2329	2.8610	0.4149	1.7030	8.6625	2.1655
0.7755	2.1338	8.3241	2.7132	3.6487	2.2500	8.2329	2.8610	0.4355	1.7030	8.6625	2.1655
0.8302	2.1416	8.3180	2.7231	3.7133	2.2500	8.2329	2.8610	0.4518	1.7030	8.6625	2.1655
0.8882	2.1494	8.3119	2.7331	3.8110	2.2500	8.2329	2.8610	0.4681	1.7030	8.6625	2.1655
0.9498	2.1572	8.3057	2.7430					0.4804	1.7030	8.6625	2.1655

TABLE 10.- Concluded

(g) $\theta = 90°$; $R_{HL} = 1.8740$ in.; $L_{lip} = 2.7130$ in.; $\tau = 0.3760$ in.; $x_{lip} = 0.3420$ in.; $y_{lip} = 0.1710$ in.

FOREBODY EXTERNAL CONTOUR								INTERNAL CONTOUR			
NS	ϕ-NBL	NWL SCRIPT-R		NS	ϕ-NBL	NWL SCRIPT-R		NS	ϕ-NBL	NWL SCRIPT-R	
0.0	1.8740	10.0000	1.8740	1.0153	2.1651	10.0000	2.1651	0.0	1.8740	10.0000	1.8740
0.0005	1.8815	10.0000	1.8815	1.0852	2.1729	10.0000	2.1729	0.0003	1.8686	10.0000	1.8686
0.0022	1.8890	10.0000	1.8890	1.1666	2.1814	10.0000	2.1814	0.0011	1.8632	10.0000	1.8632
0.0049	1.8963	10.0000	1.8963	1.2480	2.1893	10.0000	2.1893	0.0025	1.8576	10.0000	1.8576
0.0087	1.9036	10.0000	1.9036	1.3294	2.1966	10.0000	2.1966	0.0044	1.8518	10.0000	1.8518
0.0136	1.9108	10.0000	1.9108	1.4108	2.2033	10.0000	2.2033	0.0069	1.8458	10.0000	1.8458
0.0196	1.9179	10.0000	1.9179	1.4921	2.2095	10.0000	2.2095	0.0100	1.8395	10.0000	1.8395
0.0267	1.9250	10.0000	1.9250	1.5735	2.2152	10.0000	2.2152	0.0137	1.8329	10.0000	1.8329
0.0350	1.9320	10.0000	1.9320	1.6549	2.2204	10.0000	2.2204	0.0180	1.8261	10.0000	1.8261
0.0443	1.9391	10.0000	1.9391	1.7363	2.2252	10.0000	2.2252	0.0229	1.8190	10.0000	1.8190
0.0548	1.9462	10.0000	1.9462	1.8177	2.2296	10.0000	2.2296	0.0286	1.8116	10.0000	1.8116
0.0665	1.9533	10.0000	1.9533	1.8991	2.2335	10.0000	2.2335	0.0349	1.8040	10.0000	1.8040
0.0793	1.9604	10.0000	1.9604	1.9805	2.2370	10.0000	2.2370	0.0420	1.7960	10.0000	1.7960
0.0933	1.9676	10.0000	1.9676	2.0619	2.2401	10.0000	2.2401	0.0499	1.7879	10.0000	1.7879
0.1085	1.9749	10.0000	1.9749	2.1433	2.2428	10.0000	2.2428	0.0587	1.7796	10.0000	1.7796
0.1250	1.9821	10.0000	1.9821	2.2247	2.2451	10.0000	2.2451	0.0684	1.7712	10.0000	1.7712
0.1427	1.9894	10.0000	1.9894	2.3060	2.2470	10.0000	2.2470	0.0792	1.7627	10.0000	1.7627
0.1616	1.9968	10.0000	1.9968	2.3874	2.2485	10.0000	2.2485	0.0912	1.7542	10.0000	1.7542
0.1819	2.0042	10.0000	2.0042	2.4688	2.2494	10.0000	2.2494	0.1047	1.7458	10.0000	1.7458
0.2035	2.0116	10.0000	2.0116	2.5502	2.2499	10.0000	2.2499	0.1197	1.7376	10.0000	1.7376
0.2265	2.0190	10.0000	2.0190	2.6316	2.2500	10.0000	2.2500	0.1368	1.7297	10.0000	1.7297
0.2509	2.0265	10.0000	2.0265	2.7130	2.2500	10.0000	2.2500	0.1573	1.7220	10.0000	1.7220
0.2767	2.0340	10.0000	2.0340	2.7808	2.2500	10.0000	2.2500	0.1778	1.7160	10.0000	1.7160
0.3041	2.0415	10.0000	2.0415	2.8486	2.2500	10.0000	2.2500	0.1984	1.7114	10.0000	1.7114
0.3330	2.0491	10.0000	2.0491	2.9184	2.2500	10.0000	2.2500	0.2189	1.7080	10.0000	1.7080
0.3635	2.0567	10.0000	2.0567	2.9882	2.2500	10.0000	2.2500	0.2394	1.7057	10.0000	1.7057
0.3956	2.0643	10.0000	2.0643	3.0581	2.2500	10.0000	2.2500	0.2599	1.7043	10.0000	1.7043
0.4296	2.0719	10.0000	2.0719	3.1279	2.2500	10.0000	2.2500	0.2804	1.7034	10.0000	1.7034
0.4653	2.0796	10.0000	2.0796	3.1933	2.2500	10.0000	2.2500	0.3010	1.7031	10.0000	1.7031
0.5029	2.0873	10.0000	2.0873	3.2587	2.2500	10.0000	2.2500	0.3215	1.7030	10.0000	1.7030
0.5426	2.0950	10.0000	2.0950	3.3241	2.2500	10.0000	2.2500	0.3420	1.7030	10.0000	1.7030
0.5844	2.1027	10.0000	2.1027	3.3895	2.2500	10.0000	2.2500	0.3591	1.7030	10.0000	1.7030
0.6284	2.1104	10.0000	2.1104	3.4549	2.2500	10.0000	2.2500	0.3767	1.7030	10.0000	1.7030
0.6748	2.1182	10.0000	2.1182	3.5195	2.2500	10.0000	2.2500	0.3943	1.7030	10.0000	1.7030
0.7238	2.1260	10.0000	2.1260	3.5841	2.2500	10.0000	2.2500	0.4149	1.7030	10.0000	1.7030
0.7755	2.1338	10.0000	2.1338	3.6487	2.2500	10.0000	2.2500	0.4355	1.7030	10.0000	1.7030
0.8302	2.1416	10.0000	2.1416	3.7133	2.2500	10.0000	2.2500	0.4518	1.7030	10.0000	1.7030
0.8882	2.1494	10.0000	2.1494	3.8110	2.2500	10.0000	2.2500	0.4681	1.7030	10.0000	1.7030
0.9498	2.1572	10.0000	2.1572					0.4804	1.7030	10.0000	1.7030

TABLE 11.- BOUNDARY BETWEEN PYLON AND D-NACELLE FLAT SIDEWALL

FS, in.	NS, in.	NWL, in.	WL, in.
36.5000	2.8500	10.0089	3.0000
36.7500	3.1000	9.9794	2.9705
36.8548	3.2048	9.9538	2.9449
37.0000	3.3500	9.9073	2.8984
37.2500	3.6000	9.8021	2.7932
37.4610	3.8110	9.6940	2.6852
37.5000	3.8500	9.6725	2.6637
37.7500	4.1000	9.5265	2.5176
38.0000	4.3500	9.3711	2.3622
38.2500	4.6000	9.2125	2.2037
38.5000	4.8500	9.0563	2.0475
38.7500	5.1000	8.9071	1.8983
39.0000	5.3500	8.7687	1.7579
39.2500	5.6000	8.6440	1.6352
39.5000	5.8500	8.5353	1.5265
39.7500	6.1000	8.4440	1.4351
40.0000	6.3500	8.3705	1.3617
40.2500	6.6000	8.3146	1.3058
40.5000	6.8500	8.2753	1.2664
40.7500	7.1000	8.2506	1.2417
41.0000	7.3500	8.2378	1.2289
41.2500	7.6000	8.2333	1.2244
41.4500	7.8000	8.2329	1.2240

TABLE 12.- INTERSECTION BETWEEN WING LOWER SURFACE AND D-NACELLE INTERIOR

[All dimensions are in inches]

FS	BL(inner)	BL(outer)	WL
33.6500	12.9480	12.9480	2.9911
33.6600	12.7683	12.9709	2.9911
33.6700	12.6070	12.9939	2.9911
33.6800	12.4573	13.0168	2.9911
33.6900	12.3155	13.0398	2.9911
33.7000	12.1795	13.0629	2.9911
33.7100	12.0481	13.0859	2.9911
33.7200	11.9206	13.1090	2.9911
33.7300	11.7964	13.1321	2.9911
33.7400	11.6753	13.1552	2.9911
33.7500	11.5573	13.1784	2.9911
33.7600	11.4423	13.2016	2.9911
33.7700	11.3305	13.2248	2.9911
33.7800	11.2218	13.2481	2.9911
33.7900	11.1164	13.2714	2.9911
33.8000	11.0145	13.2947	2.9911
33.8100	10.9159	13.3180	2.9911
33.8200	10.8209	13.3414	2.9911
33.8300	10.7293	13.3648	2.9911
33.8400	10.6412	13.3882	2.9911
33.8415	10.6286	13.3917	2.9911
33.8500	10.5565		2.9911
33.8600	10.4751		2.9911
33.8700	10.3970		2.9911
33.8800	10.3219		2.9911
33.8900	10.2499		2.9911
33.9000	10.1807		2.9911
33.9100	10.1142		2.9911
33.9200	10.0504		2.9911
33.9300	9.9891		2.9911
33.9326	9.9736		2.9911

TABLE 13.- D-NACELLE UPPER-CONTOUR PARAMETERS FOR TRANSITION SECTION

$$\left[\left(\frac{NBL}{1.703}\right)^n + \left[\frac{NWL - (NWL)_{\text{℄}}}{h}\right]^n = 1.0\right]$$

FS, in.	NS, in.	$(NWL)_{\text{℄}}$	Top NWL, in.	Upper contour	
				h, in.	n
34.1304	0.4804	8.6625	10.0000	1.3375	50 000.0000
34.2500	.6000	8.6624	10.0000	1.3376	369.7916
34.5000	.8500	8.6620	10.0000	1.3380	65.1874
34.7500	1.1000	8.6602	10.0000	1.3398	30.3554
35.0000	1.3500	8.6565	10.0000	1.3435	18.4949
35.2500	1.6000	8.6504	9.9991	1.3487	13.3586
35.5000	1.8500	8.6416	9.9942	1.3526	11.4353
35.7500	2.1000	8.6300	9.9843	1.3543	10.7914
36.0000	2.3500	8.6155	9.9710	1.3555	10.4181
36.2500	2.6000	8.5982	9.9569	1.3587	9.5304
36.5000	2.8500	8.5783	9.9453	1.3670	7.9998
36.7500	3.1000	8.5561	9.9382	1.3821	6.4012
37.0000	3.3500	8.5320	9.9359	1.4039	5.1520
37.1063	3.4563	8.5212	↓	1.4147	4.7478
37.2500	3.6000	8.5063	↓	1.4296	4.3073
37.5000	3.8500	8.4795	↓	1.4564	3.7401
37.7500	4.1000	8.4521	9.9359	1.4838	3.3334
38.0000	4.3500	8.4246	↓	1.5113	3.0286
38.2500	4.6000	8.3976	↓	1.5383	2.7938
38.5000	4.8500	8.3715	↓	1.5644	2.6094
38.7500	5.1000	8.3468	↓	1.5891	2.4630
39.0000	5.3500	8.3239	↓	1.6120	2.3461
39.2500	5.6000	8.3032	↓	1.6327	2.2530
39.5000	5.8500	8.2851	↓	1.6508	2.1792
39.7500	6.1000	8.2697	9.9359	1.6662	2.1217
40.0000	6.3500	8.2571	↓	1.6788	2.0779
40.2500	6.6000	8.2474	↓	1.6885	2.0458
40.5000	6.8500	8.2405	↓	1.6954	2.0237
40.7500	7.1000	8.2361	↓	1.6998	2.0099
41.0000	7.3500	8.2338	↓	1.7021	2.0028
41.2500	7.6000	8.2329	↓	1.7030	2.0003
41.4500	7.8000	8.2329	↓	1.7030	2.0000

TABLE 14.- D-NACELLE BASIC-PYLON COORDINATES

[NBL 0.0 at BL 11.6770]

(a) Over wing

FS, in.	NBL, in.	WL, in.
30.5615	0.0000	3.8278
30.6500	-0.0034	3.8278
	0.0000	3.8278
	.2000	3.8241
	.3479	3.8164
30.7500	-0.0159	3.8278
	0.0000	3.8278
	.2000	3.8244
	.3750	3.8158
31.0000	-0.0902	3.8271
	0.0000	3.8276
	.3000	3.8215
	.4653	3.8128
31.5000	-0.3951	3.8186
	-.2000	3.8248
	0.0000	3.8269
	.4000	3.8184
	.6626	3.8032
32.0000	-0.7739	3.7936
	-.4000	3.8172
	0.0000	3.8255
	.5000	3.8124
	.8200	3.7896
33.0000	-1.4214	3.6944
	-1.0000	3.7623
	-.5000	3.8068
	0.0000	3.8209
	.5000	3.8068
	1.0000	3.7623
	1.1362	3.7439
34.0000	-1.8297	3.5472
	-1.5000	3.6512
	-1.0000	3.7470
	-.5000	3.7974
	0.0000	3.8133
	.5000	3.7974
	1.0000	3.7470
	1.4265	3.6690
35.0000	-2.0747	3.3634
	-2.0000	3.4143
	-1.5000	3.6200
	-1.0000	3.7278
	-.5000	3.7845
	0.0000	3.8024
	.5000	3.7845
	1.0000	3.7278
	1.5000	3.6200
	1.6980	3.5561
36.0000	-2.2180	3.1466
	-2.0000	3.3702
	-1.5000	3.5915
	-1.0000	3.7074
	-.5000	3.7684
	0.0000	3.7877
	.5000	3.7684
	1.0000	3.7074
	1.5000	3.5915
	1.9614	3.3947

TABLE 14.- Continued

(a) Concluded

FS, in.	NBL, in.	WL, in.
36.5000	-2.2500	[a]3.0000
	-2.2487	[b]3.0268
	-2.0000	3.3567
	-1.5000	3.5804
	-1.0000	3.6976
	-.5000	3.7592
	0.0000	3.7787
	.5000	3.7592
	1.0000	3.6976
	1.5000	3.5804
	2.0000	3.3567
	2.0851	3.2926
36.8548	-2.2500	[c]2.9449
	-2.0000	3.3237
	-1.5000	3.5611
	-1.0000	3.6855
	-.5000	3.7510
	0.0000	3.7716
	.5000	3.7510
	1.0000	3.6855
	1.5000	3.5611
	2.0000	3.3237
	2.1807	[d]3.1486
	2.2500	[c]2.9449

[a]Flat sidewall.
[b]Wing.
[c]Sidewall.
[d]Wing trailing-edge bottom.

TABLE 14.- Concluded

(b) Over nacelle

FS, in.	±NBL, in.	WL, in.
36.8548	0.0000	3.7716
	.5000	3.7510
	1.0000	3.6855
	1.5000	3.5611
	2.0000	3.3237
	2.2500	2.9449
37.0000	0.0000	3.7686
	.5000	3.7468
	1.0000	3.6779
	1.5000	3.5470
	2.0000	3.2971
	2.5000	2.8984
37.4610	0.0000	3.7581
	.5000	3.7312
	1.0000	3.6463
	1.5000	3.4849
	2.0000	3.1767
	2.2500	2.6852
38.0000	0.0000	3.7443
	.5000	3.7098
	1.0000	3.6003
	1.5000	3.3924
	2.0000	2.9954
	2.2500	2.3622
39.0000	0.0000	3.7143
	.5000	3.6654
	1.0000	3.5106
	1.5000	3.2166
	2.0000	2.6552
	2.2500	1.7598
40.0000	0.0000	3.6774
	.5000	3.6195
	1.0000	3.4362
	1.5000	3.0877
	2.0000	2.4226
	2.2500	1.3617
41.0000	0.0000	3.6328
	.5000	3.5727
	1.0000	3.3824
	1.5000	3.0207
	2.0000	2.3302
	2.2500	1.2289

FS, in.	±NBL, in.	WL, in.
41.4500	0.0000	3.6099
	.5000	3.5503
	1.0000	3.3613
	1.5000	3.0024
	2.0000	2.3171
	2.2500	1.2240
41.8500	0.0000	3.5880
	.5000	3.5288
	1.0000	3.3415
	1.5000	2.9855
	2.0000	2.3055
	2.2492	1.2240
42.8500	0.0000	3.5260
	.5000	3.4677
	1.0000	3.2827
	1.5000	2.9306
	2.0000	2.2516
	2.3510	1.2240
43.8500	0.0000	3.4528
	.5000	3.3944
	1.0000	3.2087
	1.5000	2.8529
	2.0000	2.1478
	2.1976	1.2240
44.8500	0.0000	3.3673
	.5000	3.3076
	1.0000	3.1173
	1.5000	2.7482
	2.0000	1.9704
	2.1336	1.2240
45.8500	0.0000	3.2682
	.5000	3.2061
	1.0000	3.0066
	1.5000	2.6120
	2.0000	1.6421
	2.0432	1.2240
46.6500	0.0000	3.1786
	.5000	3.1136
	1.0000	2.9034
	1.5000	2.4772
	1.9546	1.2240

TABLE 15.- D-NACELLE PRESSURE-PYLON COORDINATES

[NBL 0.0 at BL 11.6770]

(a) Over wing

FS, in.	NBL, in.	WL, in.
26.6500	0.0000	3.4227
26.7500	-0.0041	3.4850
	0.0000	3.4851
	.1000	3.4603
	.1765	3.4077
27.0000	-0.0676	3.5910
	0.0000	3.5951
	.2000	3.5585
	.3434	3.4868
27.5000	-0.2793	3.7124
	-.2000	3.7322
	0.0000	3.7531
	.3000	3.7061
	.5506	3.5931
28.0000	-0.4870	3.7790
	-.3000	3.8395
	0.0000	3.8760
	.4000	3.8108
	.7303	3.6544
29.0000	-0.8352	3.8444
	-.5000	3.9886
	0.0000	4.0663
	.5000	3.9886
	1.0000	3.7427
	1.0234	3.7264
30.0000	-1.1163	3.8635
	-1.0000	3.9346
	-.5000	4.1390
	0.0000	4.2035
	.5000	4.1390
	1.0000	3.9346
	1.2571	3.7631
31.0000	-1.3700	3.8430
	-1.0000	4.0647
	-.5000	4.2900
	0.0000	4.2359
	.5000	4.2900
	1.0000	4.0647
	1.4518	3.7797
31.6500	-1.5272	3.8078
	-1.5000	3.8286
	-1.0000	4.1131
	-.5000	4.2629
	0.0000	4.3102
	.5000	4.2629
	1.0000	4.1131
	1.5000	3.8286
	1.5616	3.7805
32.0000	-1.6076	3.7816
	-1.5000	3.8613
	-1.0000	4.1236
	-.5000	4.2616
	0.0000	4.3052
	.5000	4.2616
	1.0000	4.1236
	1.5000	3.8613
	1.6133	3.7771
33.0000	-1.8483	3.6783
	-1.5000	3.9183
	-1.0000	4.1245
	-.5000	4.2331
	0.0000	4.2673
	.5000	4.2331
	1.0000	4.1245
	1.5000	3.9183
	1.7630	3.7483
34.0000	-2.0676	3.5341
	-2.0000	3.6058
	-1.5000	3.9291
	-1.0000	4.0984
	-.5000	4.1876
	0.0000	4.2157
	.5000	4.1876
	1.0000	4.0984
	1.5000	3.9291
	1.9105	3.6846

TABLE 15.- Continued

(a) Concluded

FS, in.	NBL, in.	WL, in.
35.0000	-2.1918	3.3559
	-2.0000	3.5961
	-1.5000	3.8934
	-1.0000	4.0491
	-.5000	4.1311
	0.0000	4.1570
	.5000	4.1311
	1.0000	4.0491
	1.5000	3.8934
	2.0000	3.5961
	2.0230	3.5750
36.0000	-2.2376	3.1453
	-.0000	3.5195
	-1.5000	3.8237
	-1.0000	3.9830
	-.5000	4.0669
	0.0000	4.0934
	.5000	4.0669
	1.0000	3.9830
	1.5000	3.8237
	2.0000	3.5195
	2.1058	3.4074
36.5000	-2.2500	[a]3.0000
	-2.2493	[b]3.0268
	-2.0000	3.4856
	-1.5000	3.7901
	-1.0000	3.9496
	-.5000	4.0335
	0.0000	4.0600
	.5000	4.0335
	1.0000	3.9496
	1.5000	3.7901
	2.0000	3.4856
	2.1579	[b]3.3001
36.8660	-2.2500	[a]2.9418
	-2.0000	3.4426
	-1.5000	3.7566
	-1.0000	3.9211
	-.5000	4.0077
	0.0000	4.0350
	.5000	4.0077
	1.0000	3.9211
	1.5000	3.7566
	2.0000	3.4426
	2.2094	[c]3.1486
	2.2500	[a]2.9418

[a]Sidewall.
[b]Wing.
[c]Wing trailing-edge bottom.

TABLE 15.- Continued

(b) Over nacelle

FS, in.	±NBL, in.	WL, in.
36.8660	0.0000	4.0350
	.5000	4.0077
	1.0000	3.9211
	1.5000	3.7566
	2.0000	3.4426
	2.2500	2.9418
37.0000	0.0000	4.0257
	.5000	3.9975
	1.0000	3.9083
	1.5000	3.7387
	2.0000	3.4149
	2.2500	2.8984
37.4610	0.0000	3.9934
	.5000	3.9607
	1.0000	3.8571
	1.5000	3.6602
	2.0000	3.2845
	2.2500	2.6852
38.0000	0.0000	3.9546
	.5000	3.9148
	1.0000	3.7887
	1.5000	3.5491
	2.0000	3.0917
	2.2500	2.3622
39.0000	0.0000	3.8802
	.5000	3.8272
	1.0000	3.6593
	1.5000	3.3403
	2.0000	2.7312
	2.2500	1.7598
40.0000	0.0000	3.8026
	.5000	3.7416
	1.0000	3.5483
	1.5000	3.1810
	2.0000	2.4799
	2.2500	1.3617

FS, in.	±NBL, in.	WL, in.
41.0000	0.0000	3.7217
	.5000	3.6593
	1.0000	3.4619
	1.5000	3.0869
	2.0000	2.3709
	2.2500	1.2289
41.4500	0.0000	3.6841
	.5000	3.6226
	1.0000	3.4278
	1.5000	3.0577
	2.0000	2.3510
	2.2500	1.2240
41.8500	0.0000	3.6501
	.5000	3.5894
	1.0000	3.3971
	1.5000	3.0318
	2.0000	2.3339
	2.2492	1.2240
42.8500	0.0000	3.5624
	.5000	3.5031
	1.0000	3.3153
	1.5000	2.9576
	2.0000	2.2679
	2.2351	1.2240
43.8500	0.0000	3.4703
	.5000	3.4114
	1.0000	3.2243
	1.5000	2.8657
	2.0000	2.1550
	2.1976	1.2240
44.8500	0.0000	3.3730
	.5000	3.3132
	1.0000	3.1223
	1.5000	2.7523
	2.0000	1.9724
	2.1336	1.2240

TABLE 15.- Concluded

(b) Concluded

FS, in.	±NBL, in.	WL, in.
45.8500	0.0000	3.2689
	.5000	3.2067
	1.0000	3.0072
	1.5000	2.6124
	2.0000	1.6423
	2.0432	1.2240
46.6500	0.0000	3.1786
	.5000	3.1136
	1.0000	2.9034
	1.5000	2.4772
	1.9546	1.2240

TABLE 16.- D-NACELLE AND PRESSURE PYLON STATIC-PRESSURE ORIFICE LOCATIONS

NS, in.	x/c	Orifice locations at angles of ψ of -							
		0°	15°	30°	90°	180°	270°	330°	345°
Pressure pylon									
-4.650	0.248	X							
-3.300	.383	X							
-2.000	.514	X	X						X
-.650	.649	X							
0.650	0.779	X	X	X				X	X
2.000	.915	X							
3.100	1.025	X		X				X	
4.600	1.176	X		X				X	
6.200	1.336	X		X				X	
Exterior of D-nacelle									
0.030	0.717			(a)	X	X	X	(a)	
.100	.724			(a)	X	X	X	(a)	
.200	.734			(a)	X	X	X	(a)	
.300	.744			(a)	X	X	X	(a)	
.500	.764			(a)	X	X	X	(a)	
0.700	0.784			(a)	X	X	X	(a)	
1.200	.835			(a)	X	X	X	(a)	
1.500	.865			(a)	X	X	X	(a)	
2.300	.945			(a)	X	X	X	(a)	
3.100	1.025			(a)	X	X	X	(a)	
4.600	1.176				X	X	X		
5.400	1.256				X	X	X		
6.200	1.336				X	X	X		
7.100	1.426				X	X	X		
8.100	1.527				X	X	X		
9.300	1.647	X		X	X	X	X	X	
10.700	1.787				X	X	X		
12.100	1.928				X	X	X		
13.500	2.068	X		X	X	X	X	X	
14.800	2.198	X			X	X	X		
15.500	2.269	X			X	X	X		
Interior of D-nacelle									
2.500	0.965	X			X	X	X		
7.800	1.496	X			X	X	X		
13.000	2.018	X			X	X	X		
15.000	2.219	X			X	X	X		

[a]Waterline, 2.725 in.

TABLE 17.- NOMINAL COORDINATES FOR BOTH ANTISHOCK BODIES

(a) Short-cone antishock body

FS, in.	r_{SB}, in.
31.2	0.00
32.0	.23
33.0	.50
34.0	.77
35.0	1.04
36.0	1.25
37.0	1.34
38.0	1.39
39.0	1.39
40.0	1.36
41.0	1.30
42.0	1.22
43.0	1.09
44.0	.94
45.0	.74
46.0	.52
46.7	.35
47.0	.28
48.0	0.00

(b) Long-cone antishock body

FS, in.	r_{SB}, in.
31.2	0.00
32.0	.15
33.0	.33
34.0	.50
35.0	.67
36.0	.84
37.0	1.01
38.0	1.17
39.0	1.31
40.0	1.38
41.0	1.40
42.0	1.29
43.0	1.08
44.0	.84
45.0	.54
46.0	.24
46.7	0.00

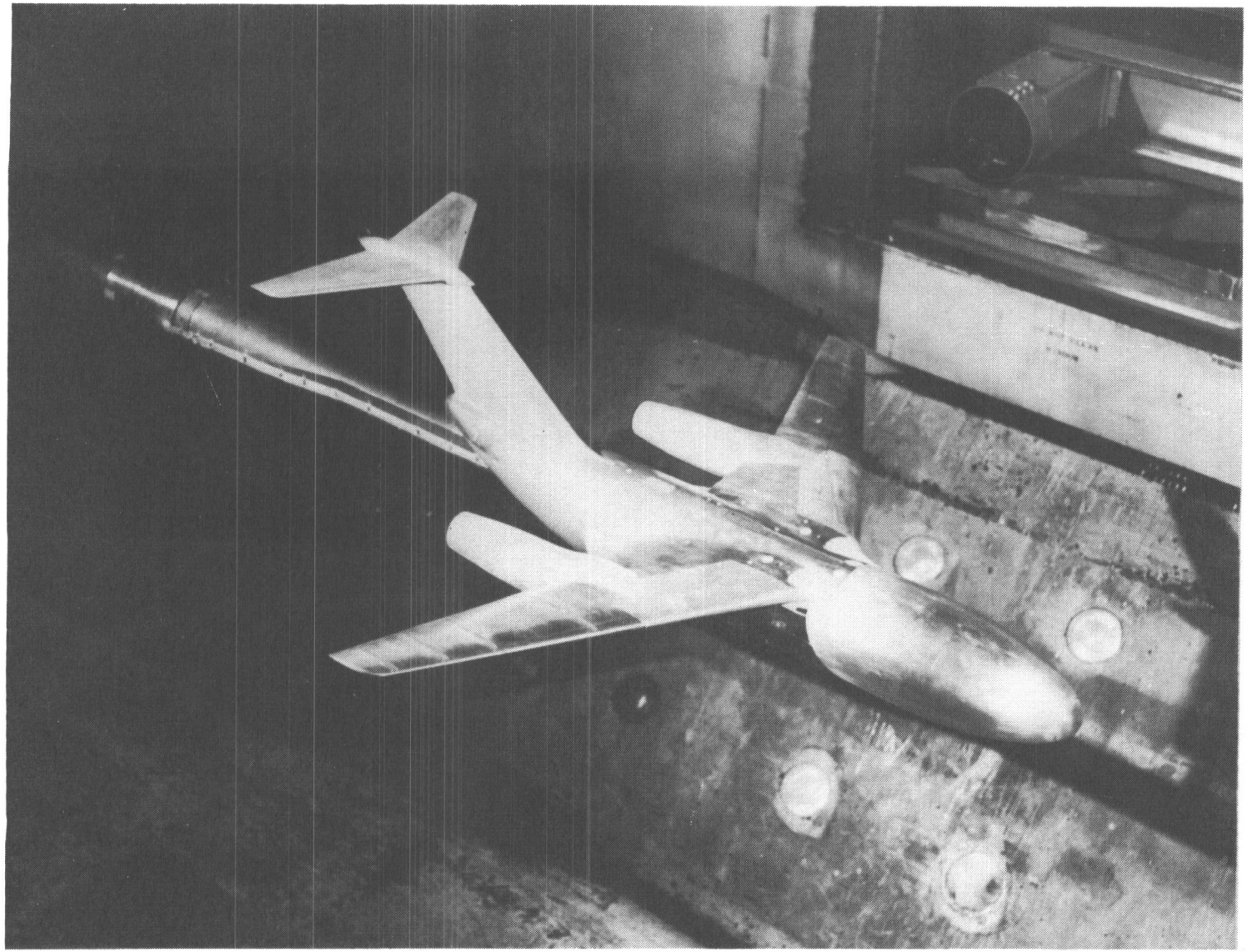

L-82-6460

Figure 1.- Transonic transport airplane with aft-mounted D-nacelles.

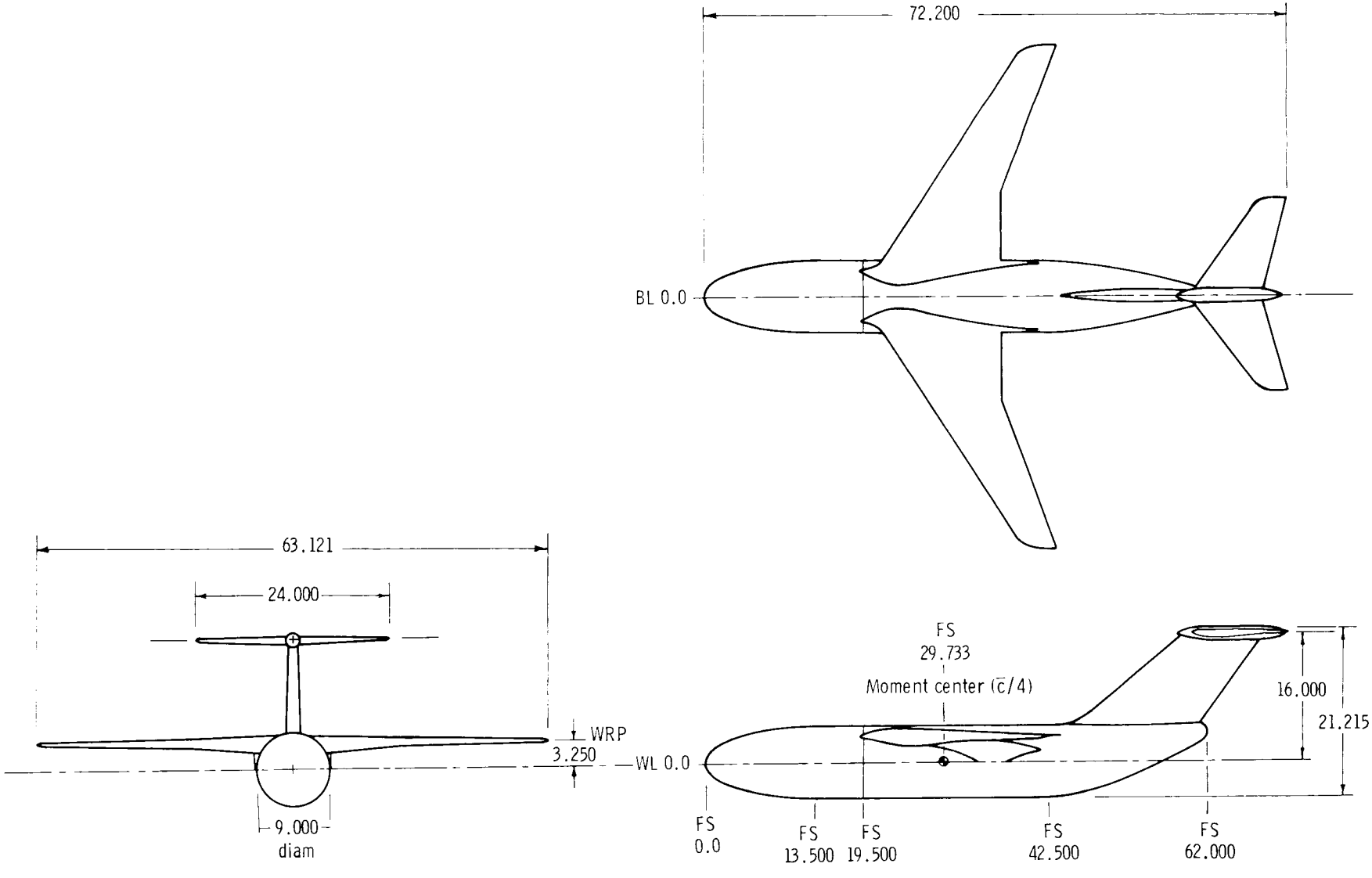

Figure 2.- General arrangement of transport model. All dimensions are in inches.

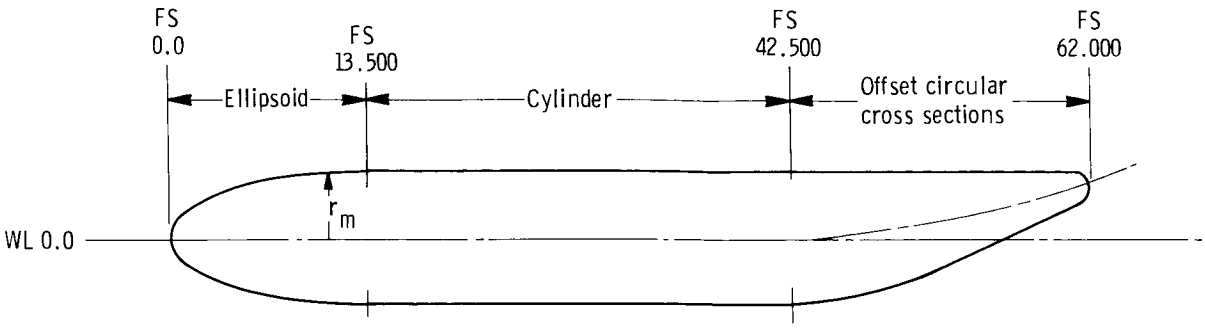

Closure detail

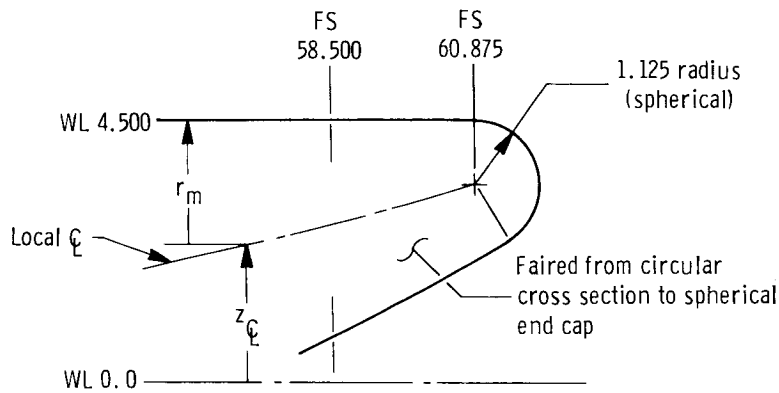

Ellipsoidal-nose coordinates	
FS	r_m
0	0
.100	.547
.200	.772
.250	.862
.375	1.053
.500	1.213
.750	1.479
1.000	1.700
1.250	1.891
1.500	2.062
2.000	2.357
2.500	2.609
3.500	3.023
4.500	3.354
5.500	3.625
6.500	3.848
7.500	4.031
9.500	4.298
11.500	4.450
13.500	4.500

Afterbody coordinates		
FS	$z_{℄}$	r_m
42.500	0	4.500
44.500	.100	4.400
46.500	.280	4.220
48.500	.550	3.950
50.500	.860	3.640
52.500	1.225	3.275
54.500	1.660	2.840
56.500	2.130	2.370
58.500	2.650	1.850
60.875	3.375	1.125

(a) General description.

Figure 3.- Fuselage geometry. All dimensions are in inches.

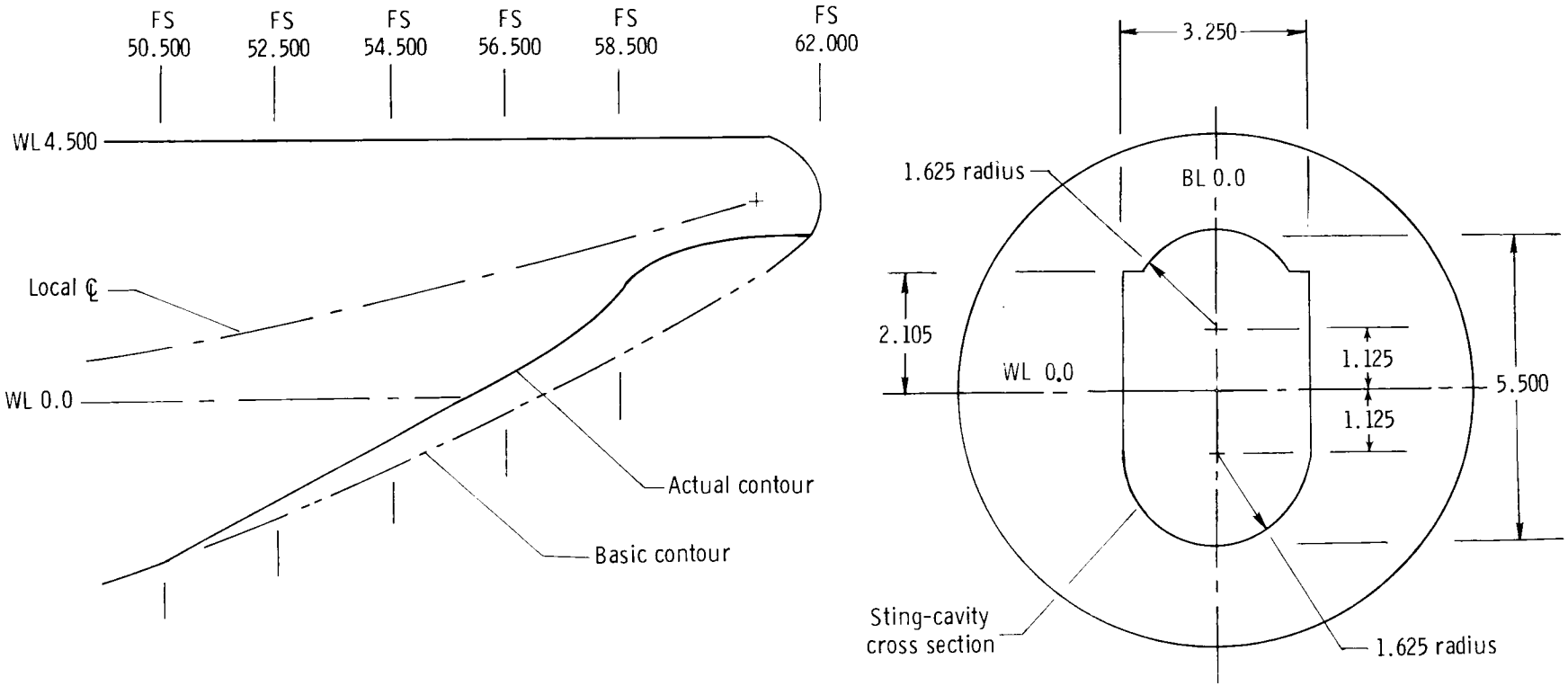

(b) Sting cavity detail.

Figure 3.- Concluded.

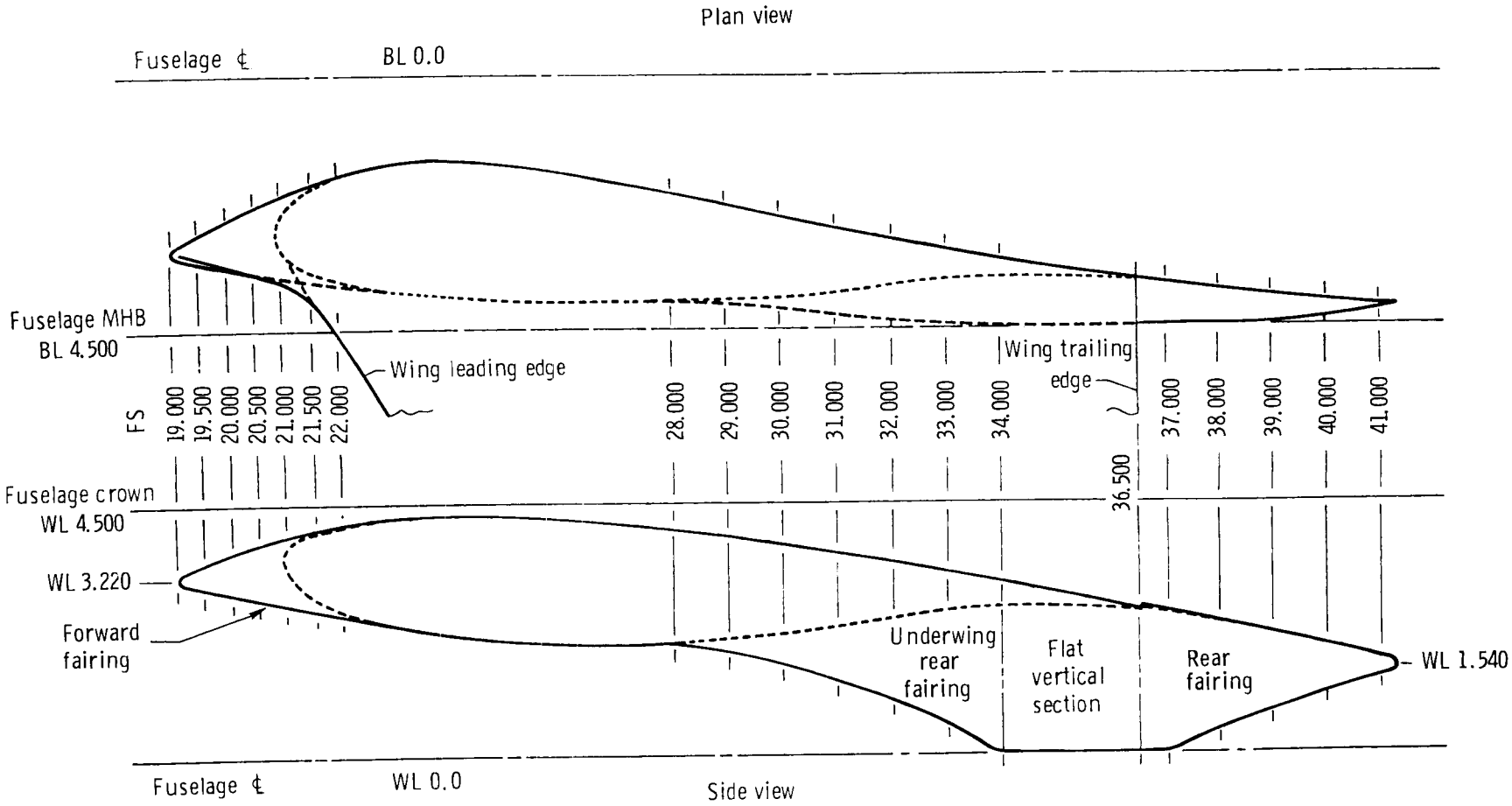

(a) Top and side profiles.

Figure 4.- Details of wing-fuselage fairings. All dimensions are in inches.

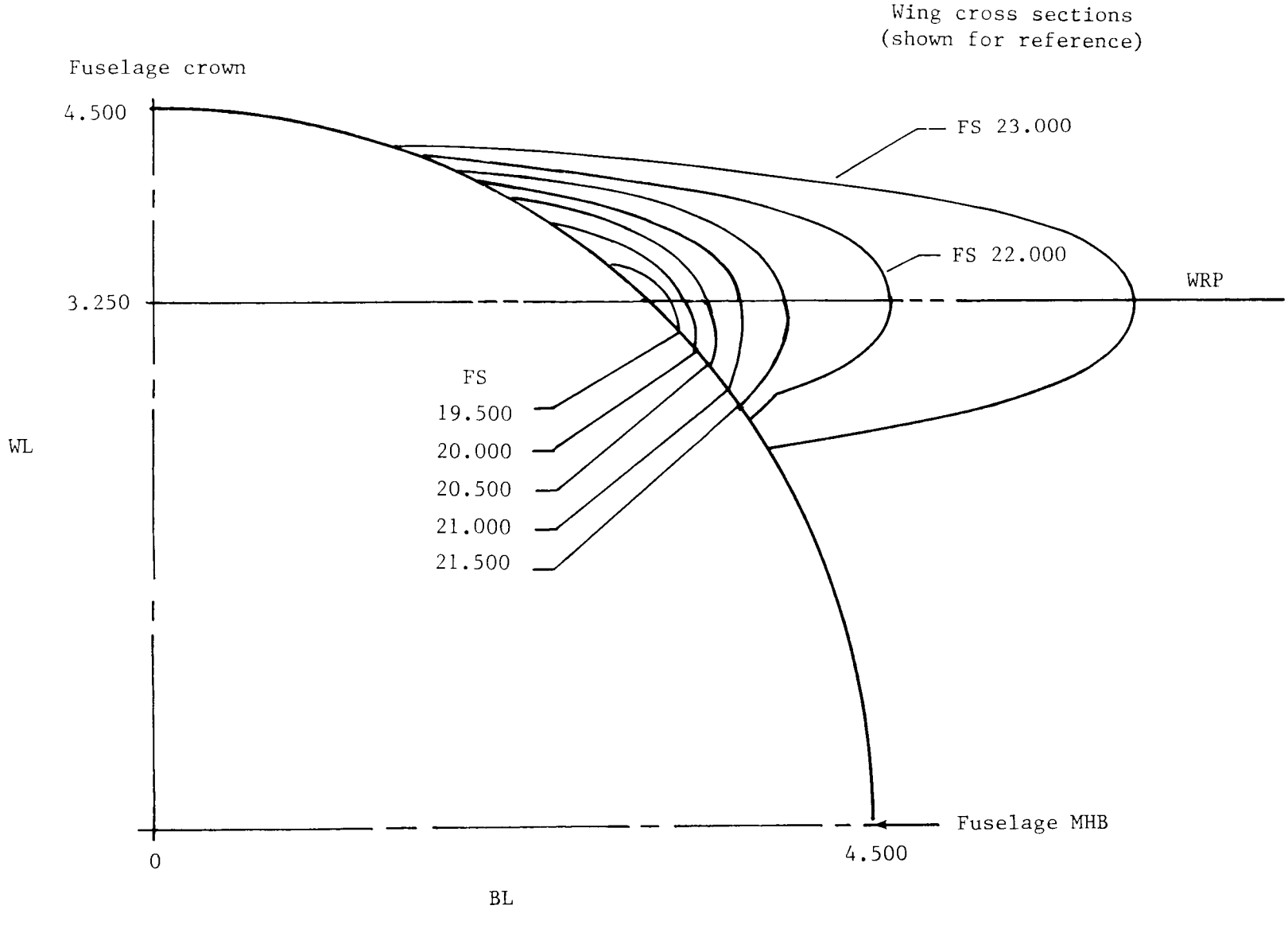

(b) Forward-fairing cross sections.

Figure 4.- Continued.

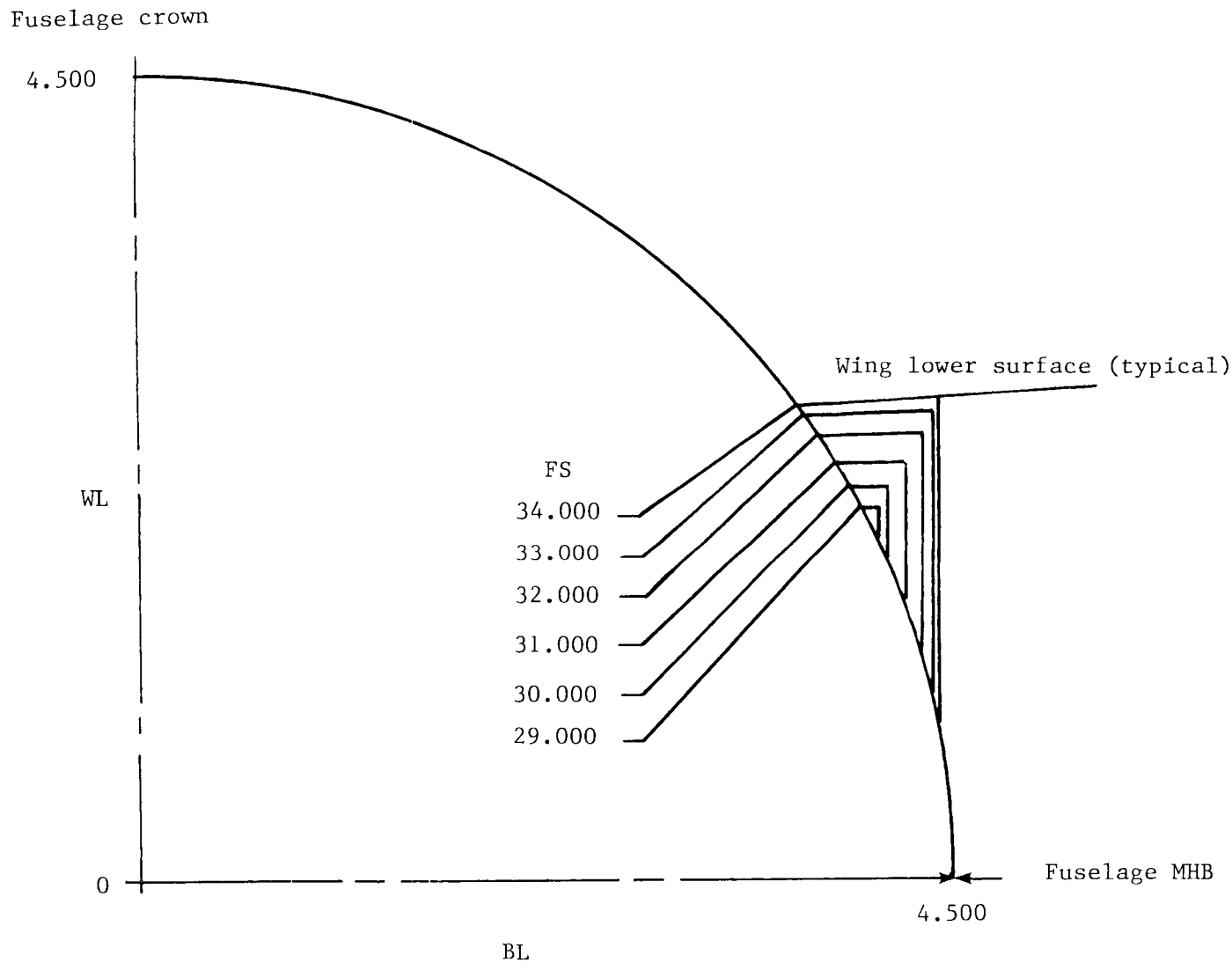

(c) Underwing rear-fairing cross sections.

Figure 4.- Continued.

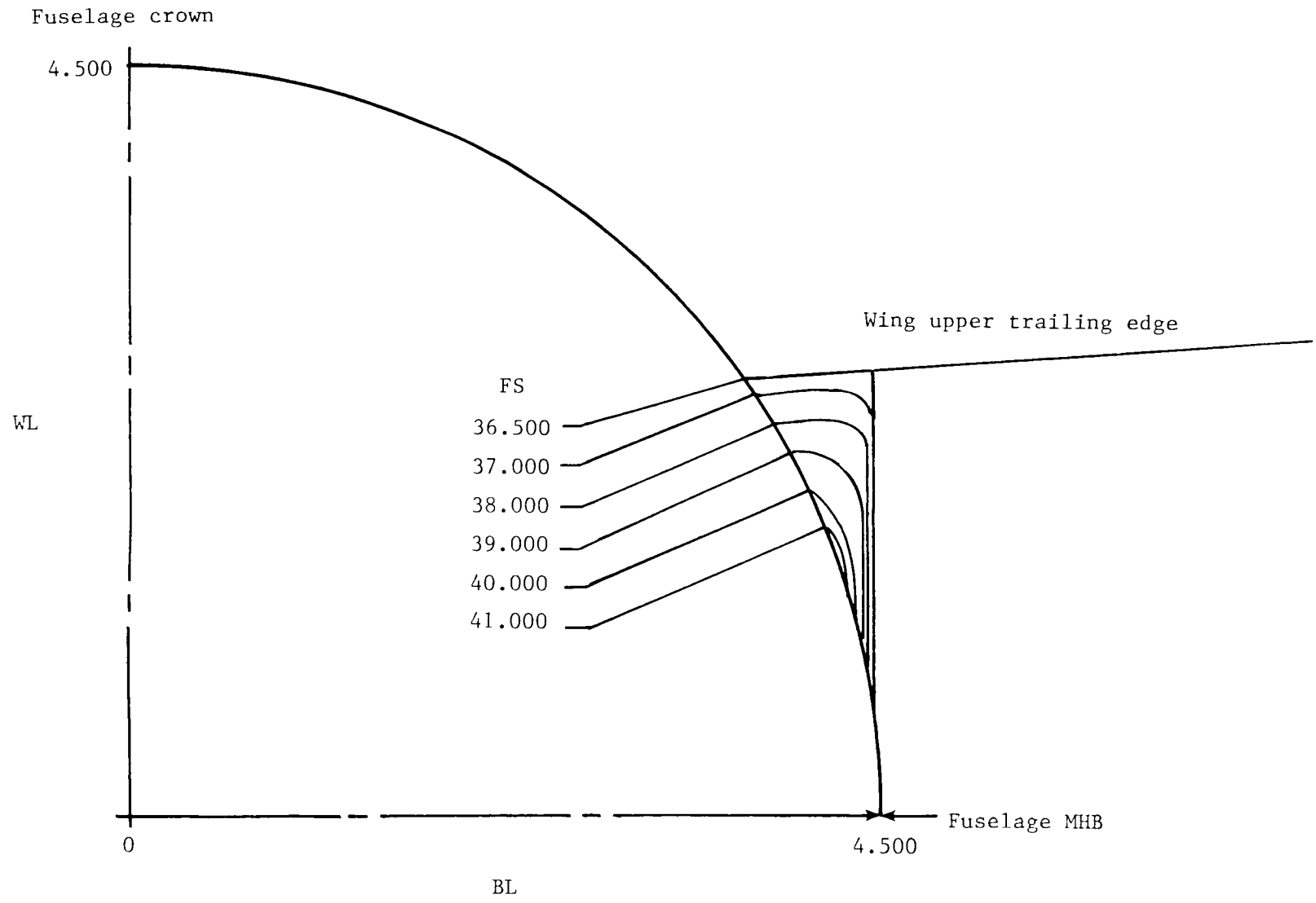

(d) Rear-fairing cross sections aft of wing.

Figure 4.- Concluded.

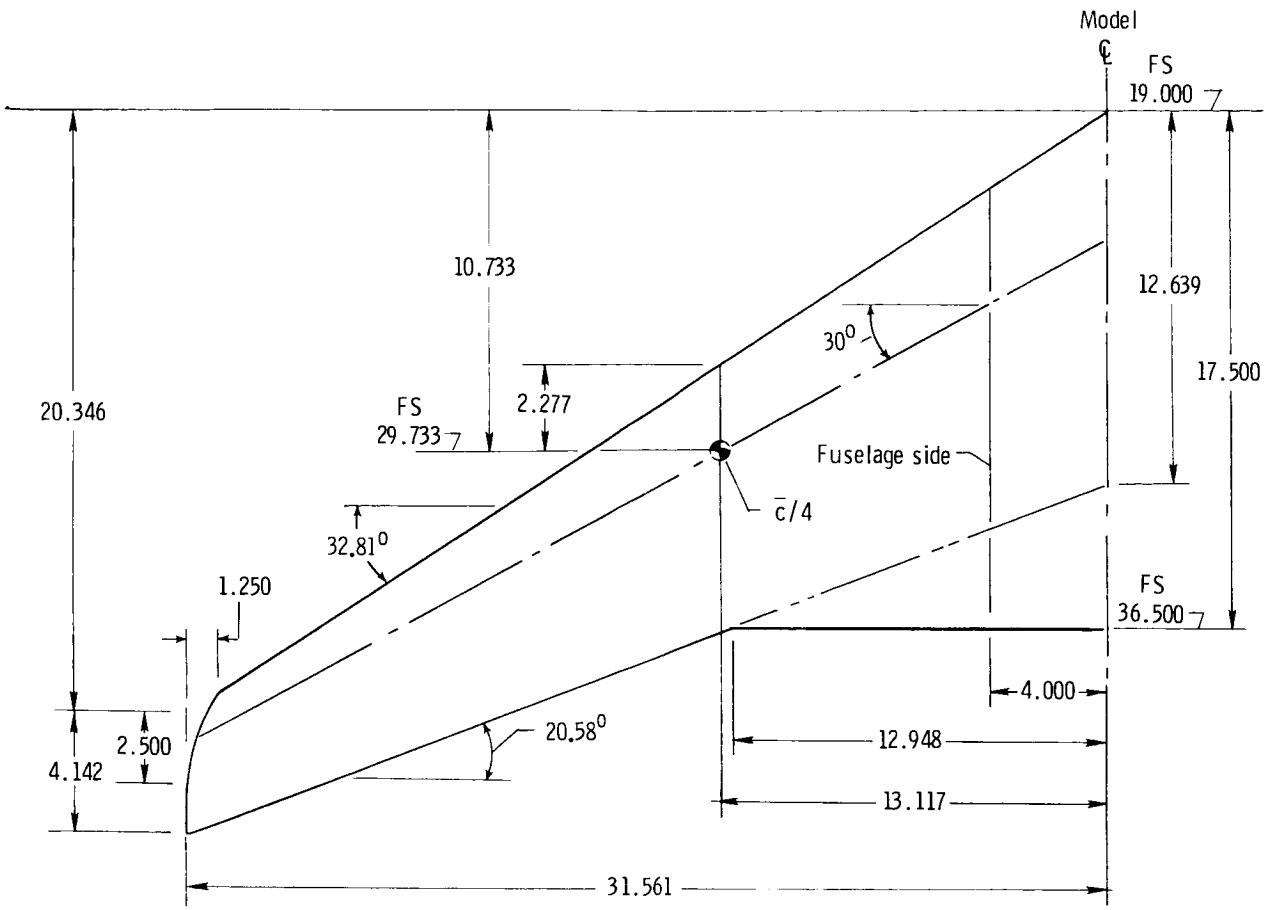

Aspect ratio	7.52
Taper ratio	0.328
Area (trapezoid), in^2 ..	529.590
$\bar{c}$, in.	9.107
c_{av}, in.	8.390
Incidence, deg.....	0
Dihedral, deg.....	0

(a) Wing planform. All dimensions are in inches unless otherwise specified.

Figure 5.- Wing geometry.

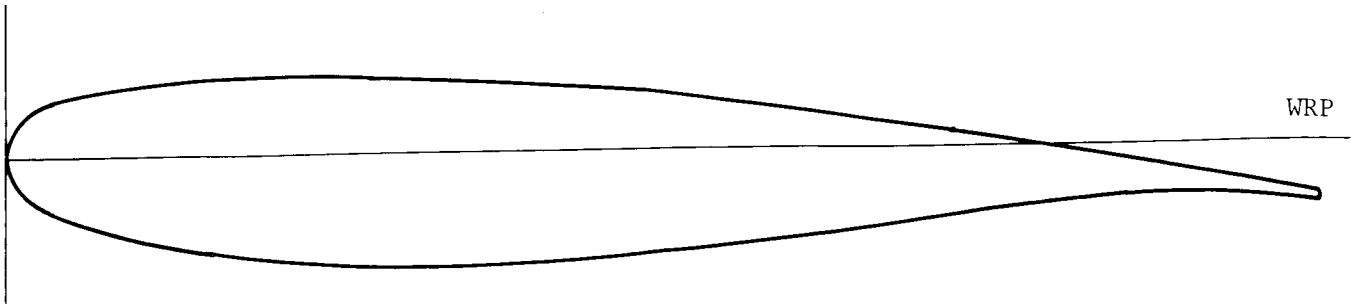

Fuselage side (BL 4.000; η = 0.127); t/c = 0.144

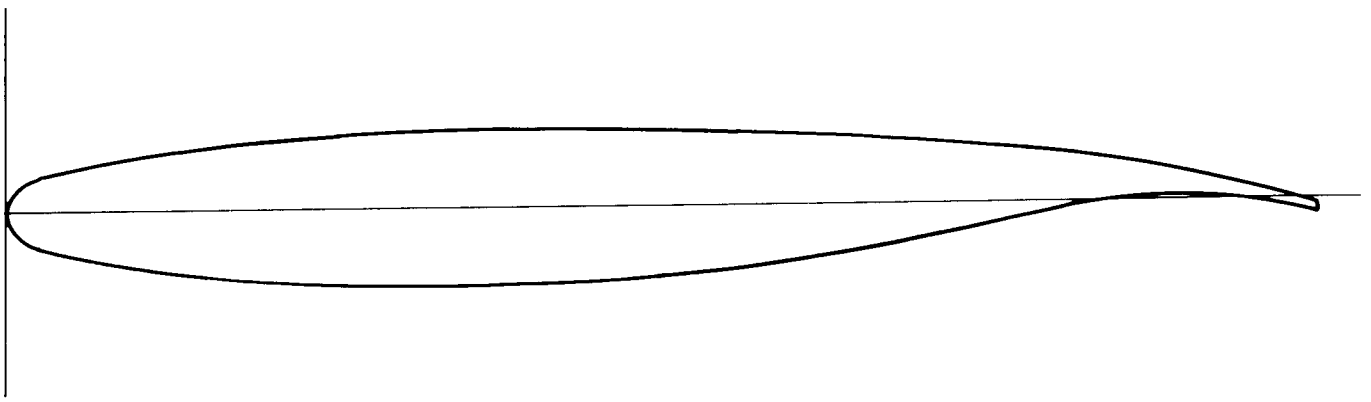

Planform break (BL 12.948; η = 0.410); t/c = 0.120

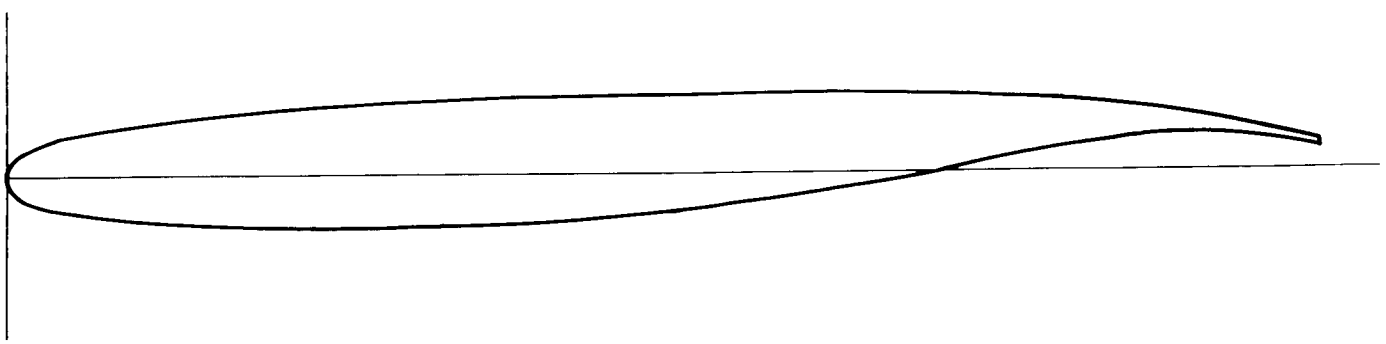

Tip (BL 31.561; η = 1.000); t/c = 0.100

(b) Defining airfoil sections of model wing. All dimensions are in inches.

Figure 5.- Continued.

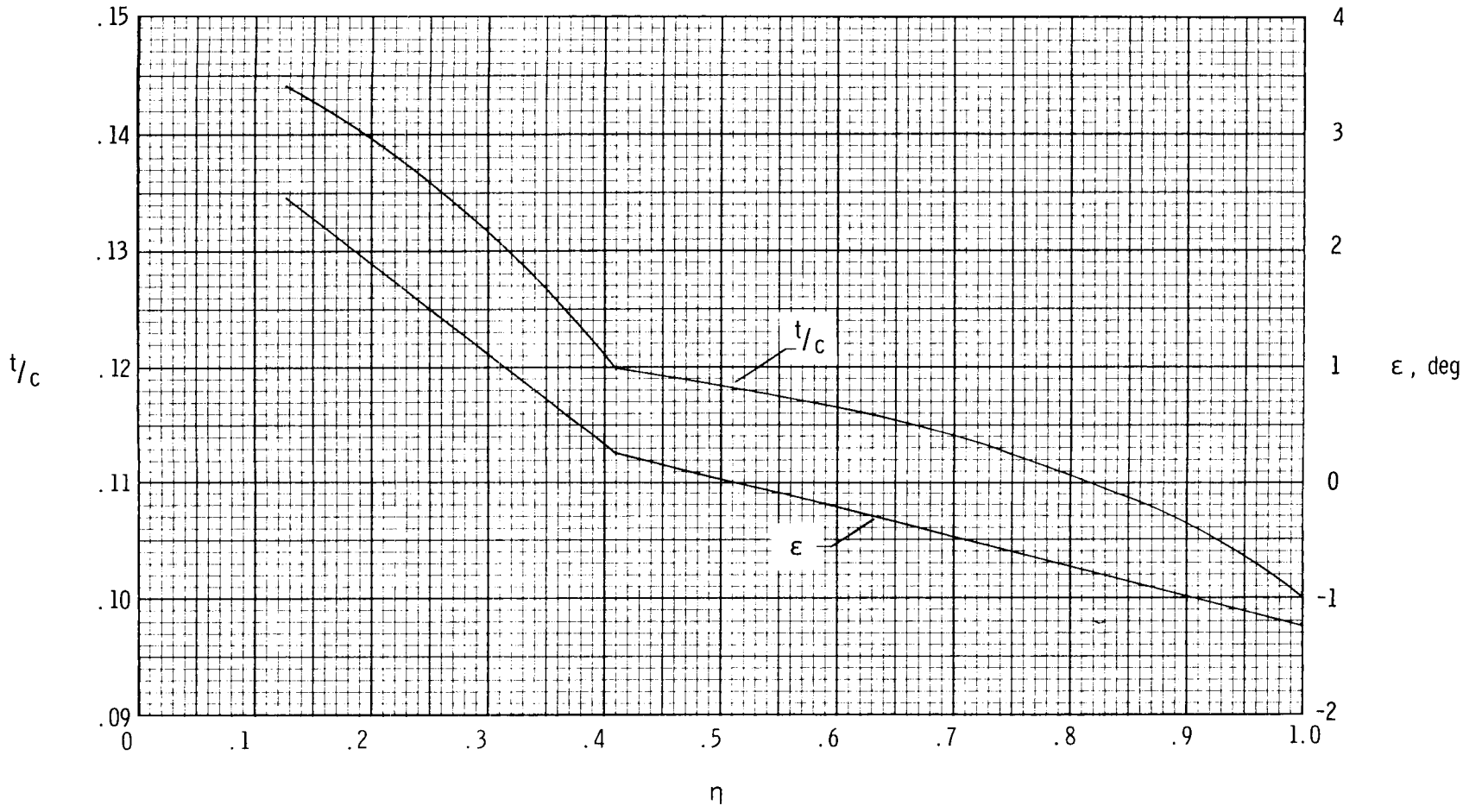

(c) Spanwise thickness and twist distributions of wing.

Figure 5.- Continued.

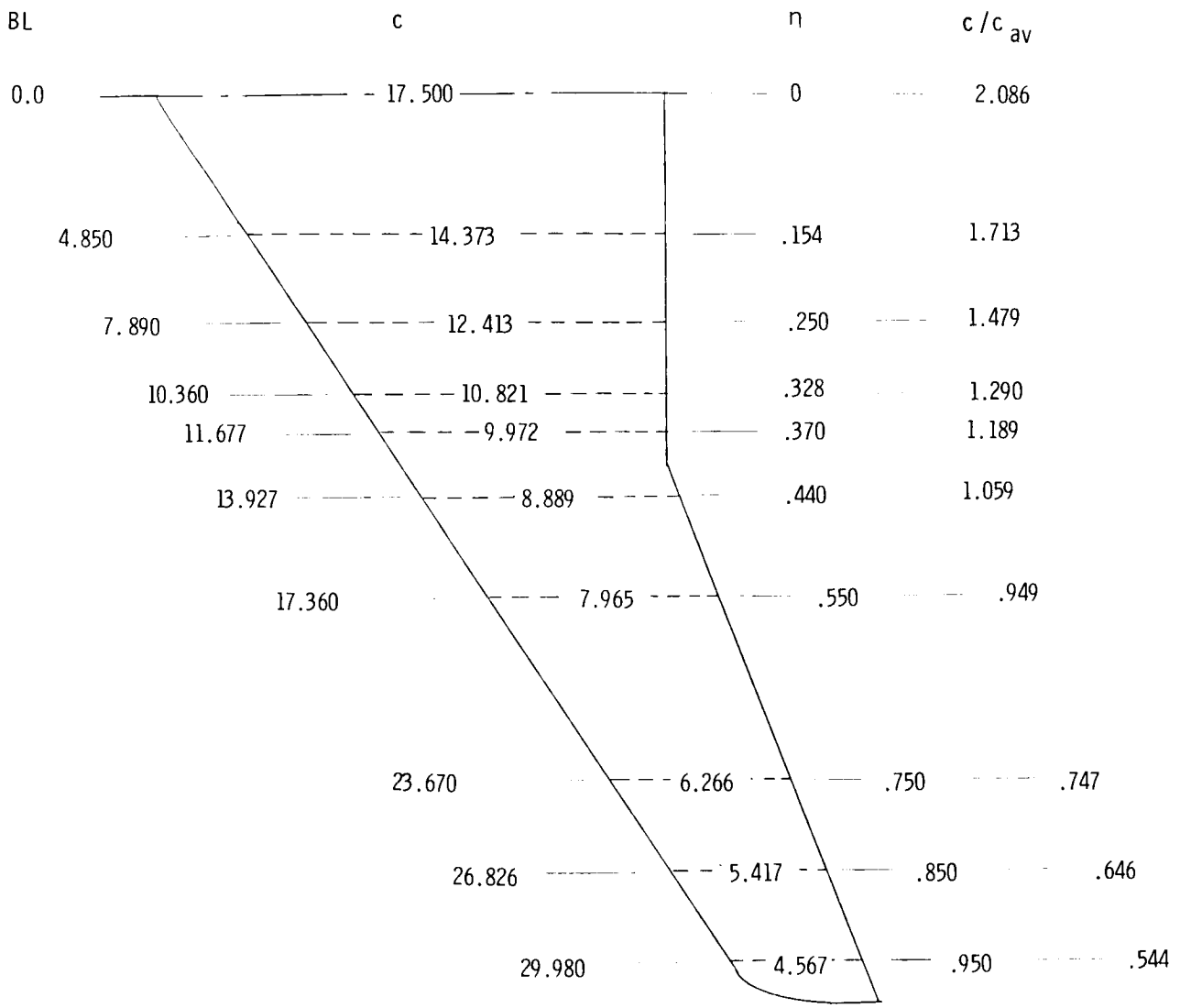

(d) Wing pressure-orifice row locations. All dimensions are in inches.

Figure 5.- Concluded.

Streamwise airfoil ordinates	
x/c	± y/c
0	0
.0025	.0066
.0050	.0099
.0075	.0108
.0100	.0122
.0125	.0132
.0250	.0181
.0500	.0248
.0750	.0304
.1000	.0351
.1500	.0423
.2000	.0475
.2500	.0513
.3000	.0540
.3500	.0556
.4000	.0563
.4500	.0563
.5000	.0555
.6000	.0499
.7000	.0394
.7500	.0328
1.0000	.0004

LER/c = 0.0100

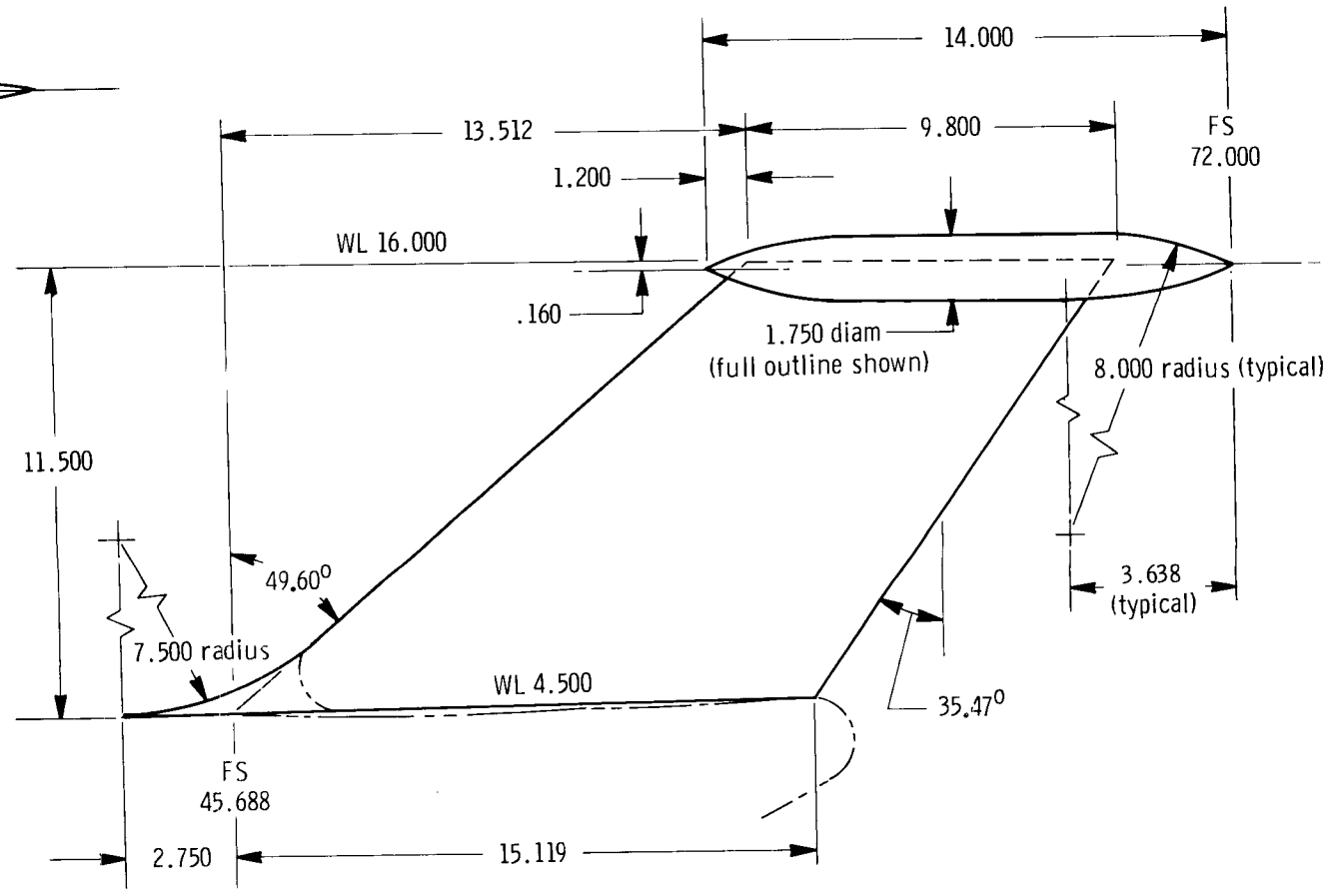

Figure 6.- Vertical stabilizer and bullet fairing. All dimensions are in inches unless otherwise specified.

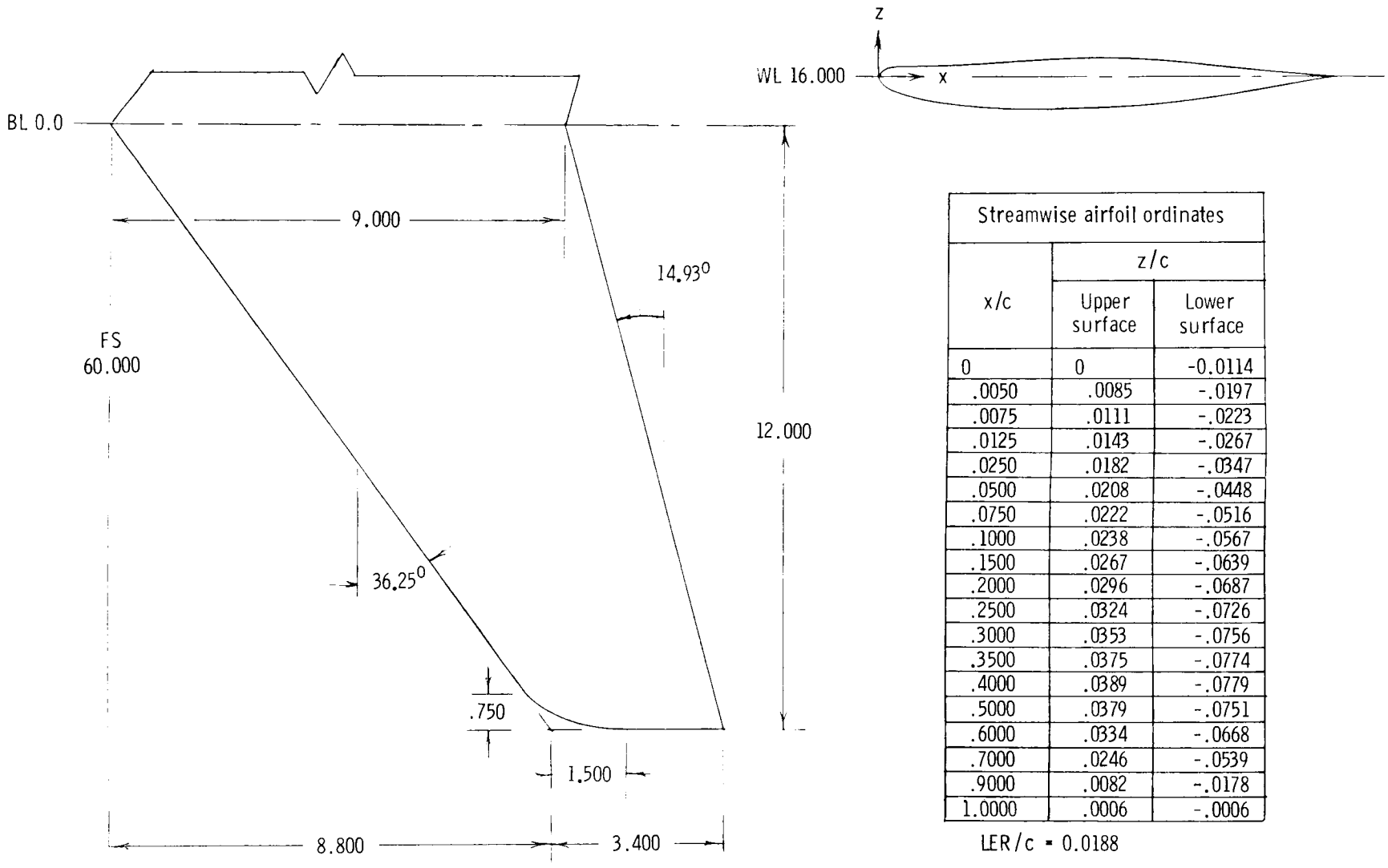

Streamwise airfoil ordinates		
x/c	z/c	
	Upper surface	Lower surface
0	0	-0.0114
.0050	.0085	-.0197
.0075	.0111	-.0223
.0125	.0143	-.0267
.0250	.0182	-.0347
.0500	.0208	-.0448
.0750	.0222	-.0516
.1000	.0238	-.0567
.1500	.0267	-.0639
.2000	.0296	-.0687
.2500	.0324	-.0726
.3000	.0353	-.0756
.3500	.0375	-.0774
.4000	.0389	-.0779
.5000	.0379	-.0751
.6000	.0334	-.0668
.7000	.0246	-.0539
.9000	.0082	-.0178
1.0000	.0006	-.0006

LER/c = 0.0188

Figure 7.- Horizontal stabilizer. All dimensions are in inches unless otherwise specified.

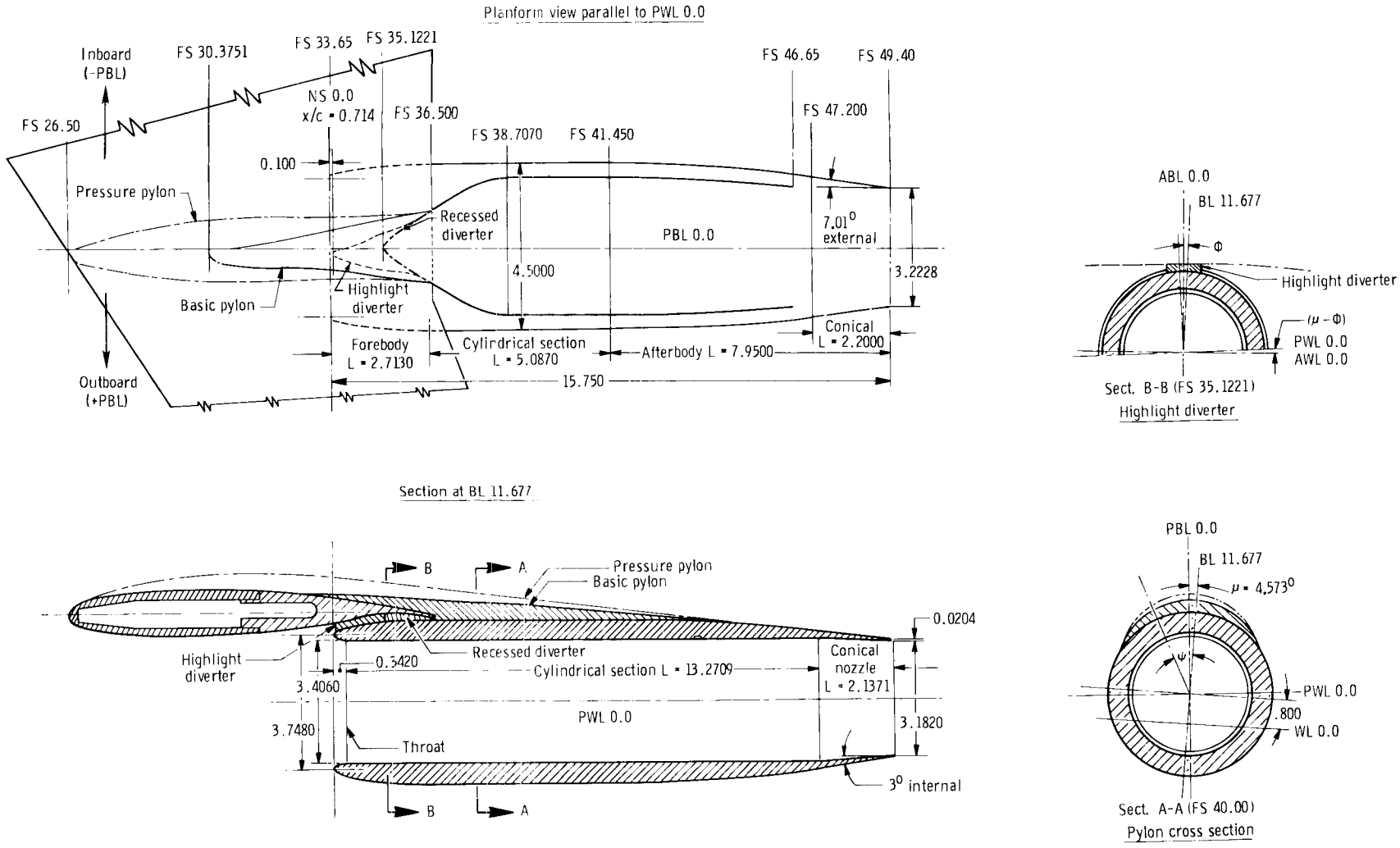

Figure 8.- Aft wing-mounted circular nacelle. A_0/A_{HL} = 0.70; A_{HL} = 11.03 in^2; A_{max} = 15.90 in^2; D_{exit} = 3.182 in. All dimensions are in inches unless otherwise specified.

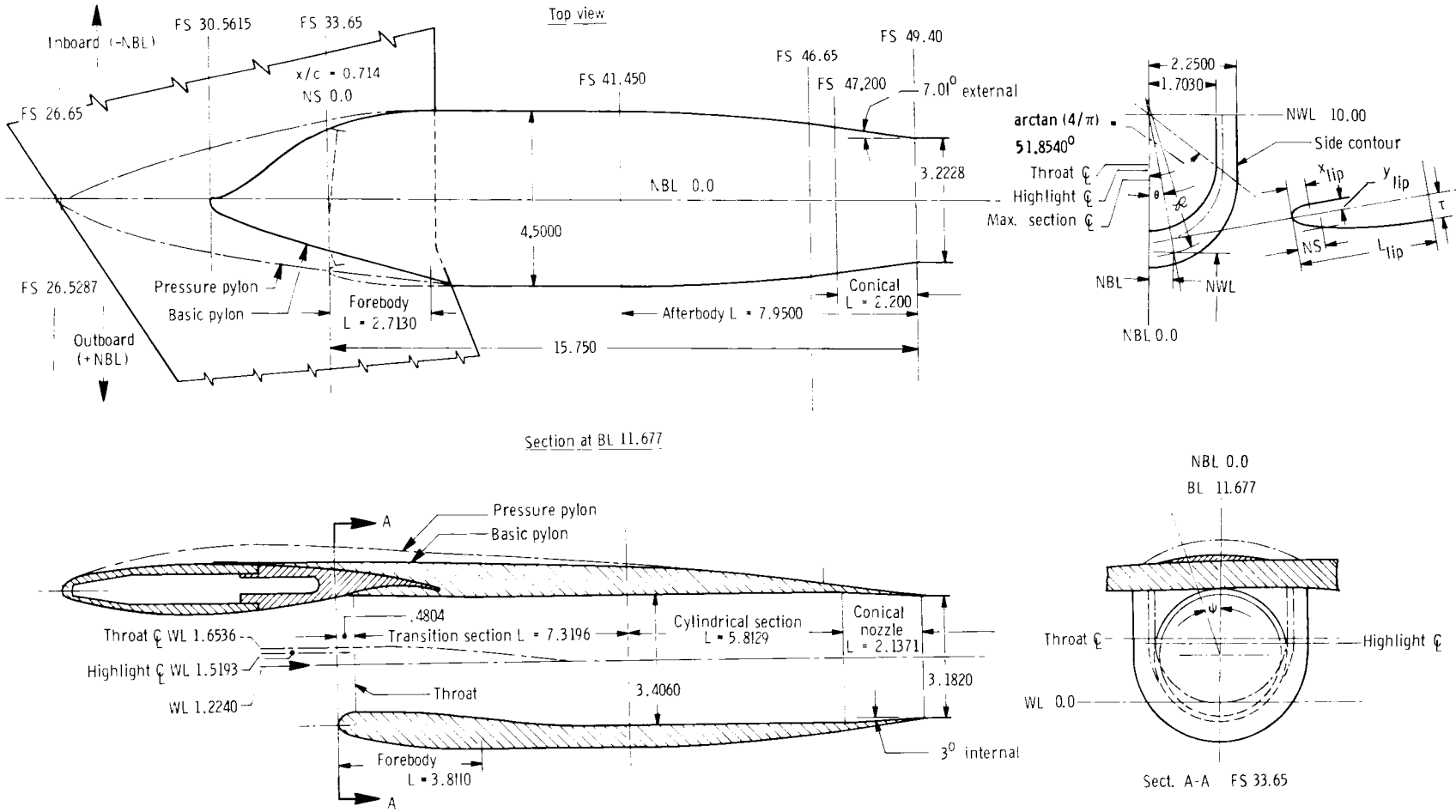

Figure 9.- Aft wing-mounted D-nacelle. A_0/A_{HL} = 0.70; A_{HL} = 11.03 in^2; A_{max} = 15.90 in^2; D_{exit} = 3.182 in. All dimensions are in inches unless otherwise specified.

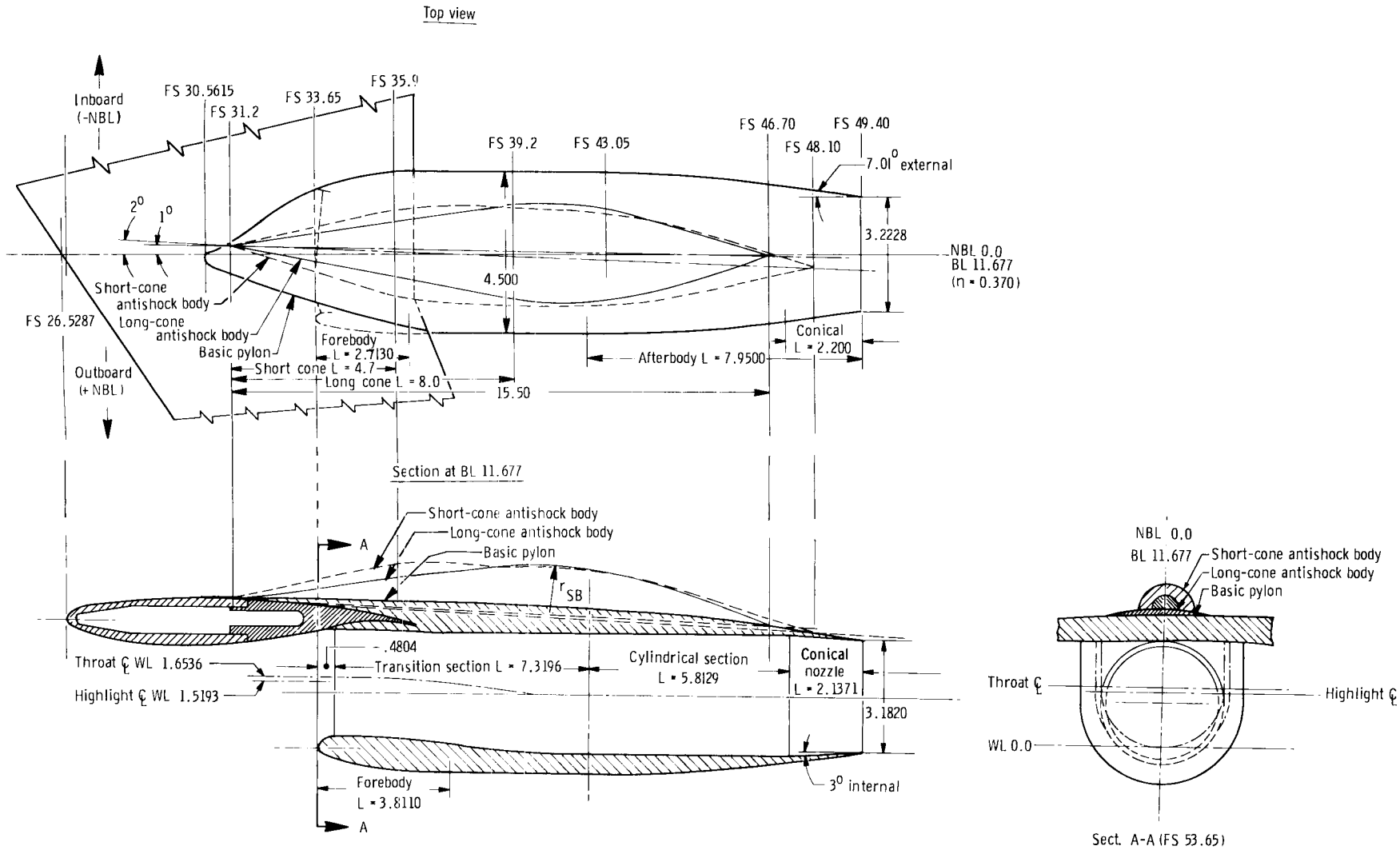

Figure 10.- Antishock body configurations. All dimensions are in inches unless otherwise specified.

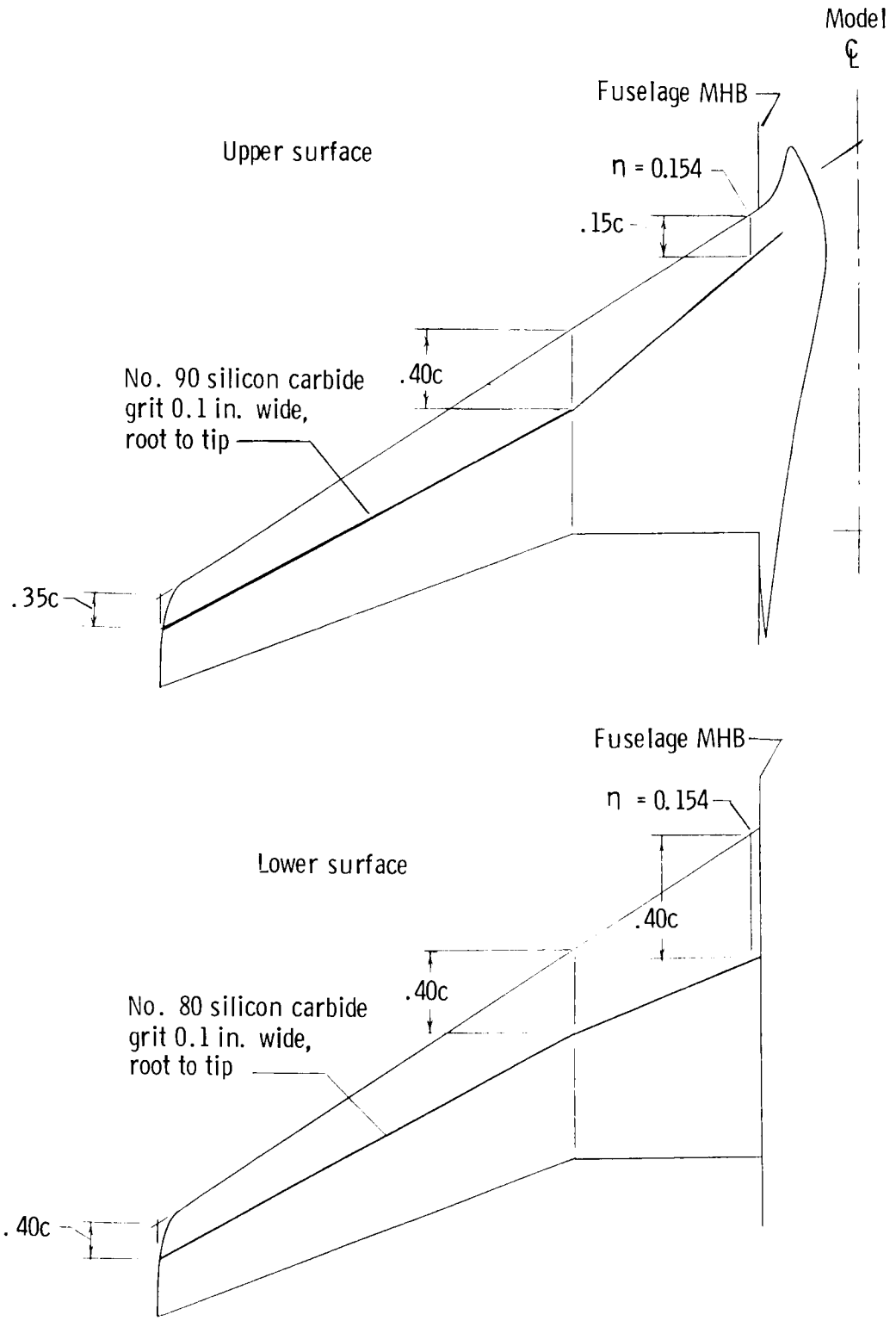

Figure 11.- Wing transition-strip locations.

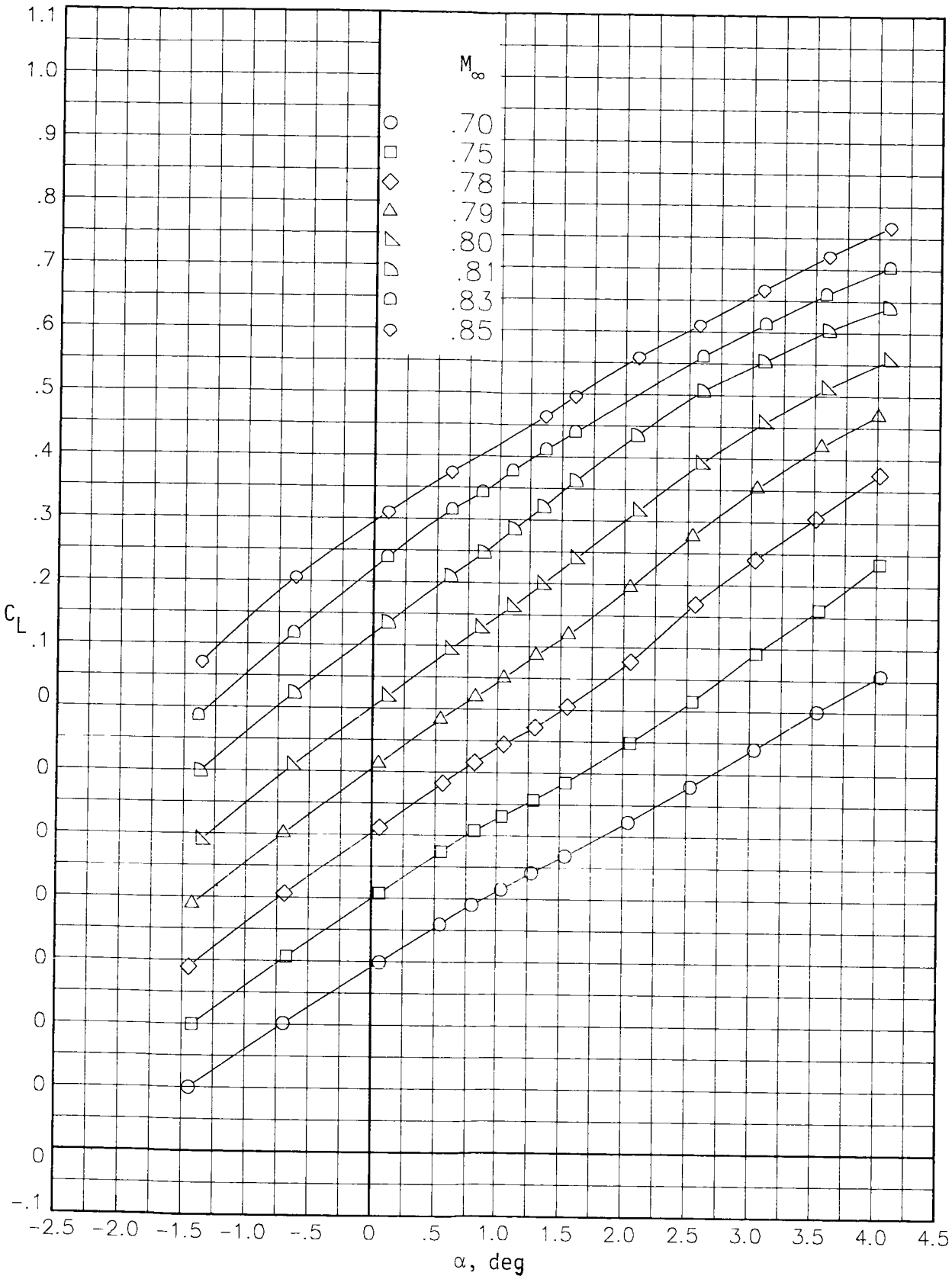

(a) Lift coefficient plotted against angle of attack.

Figure 12.- Longitudinal aerodynamic characteristics for clean wing-body configuration.

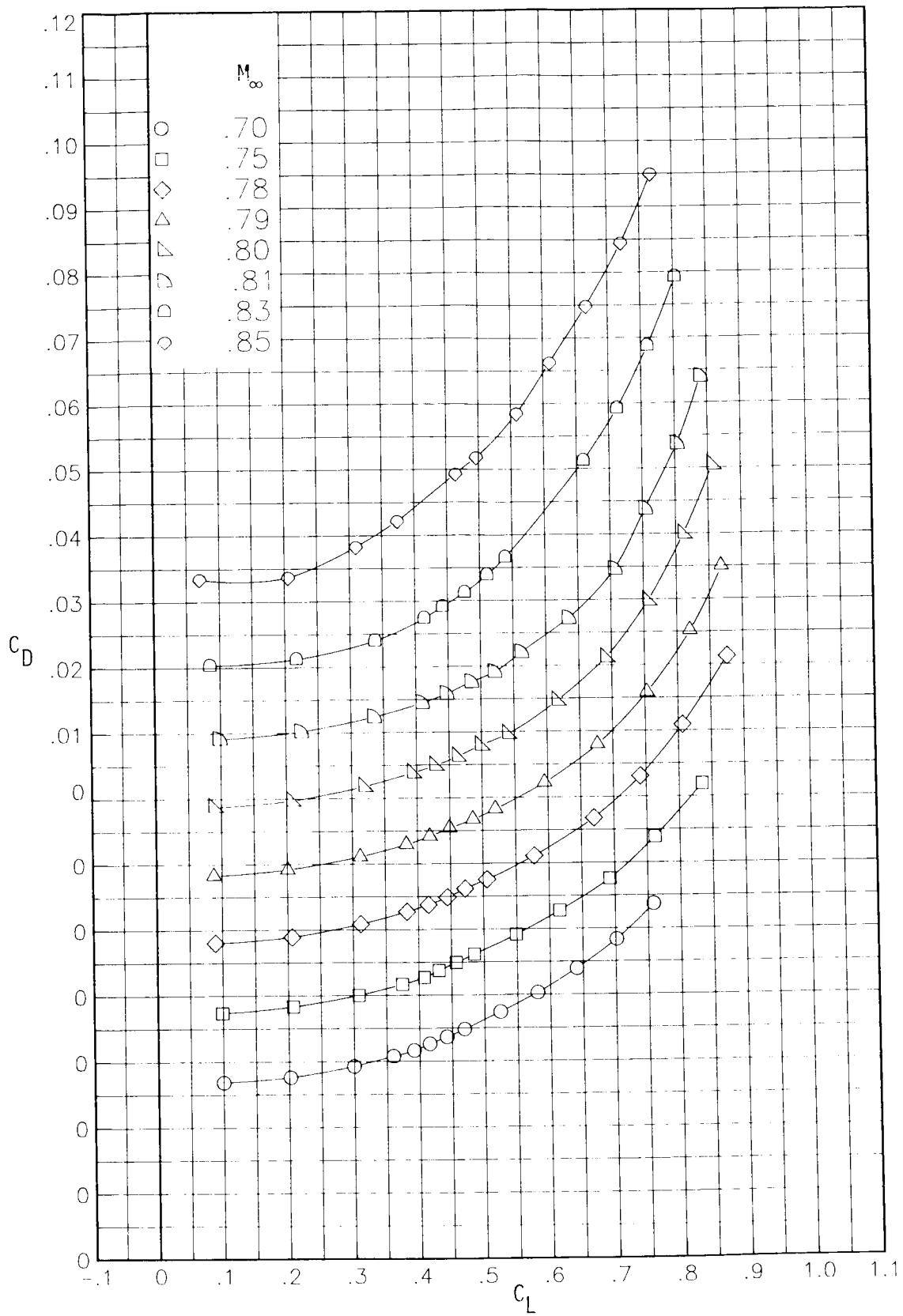

(b) Drag polar.

Figure 12.- Continued.

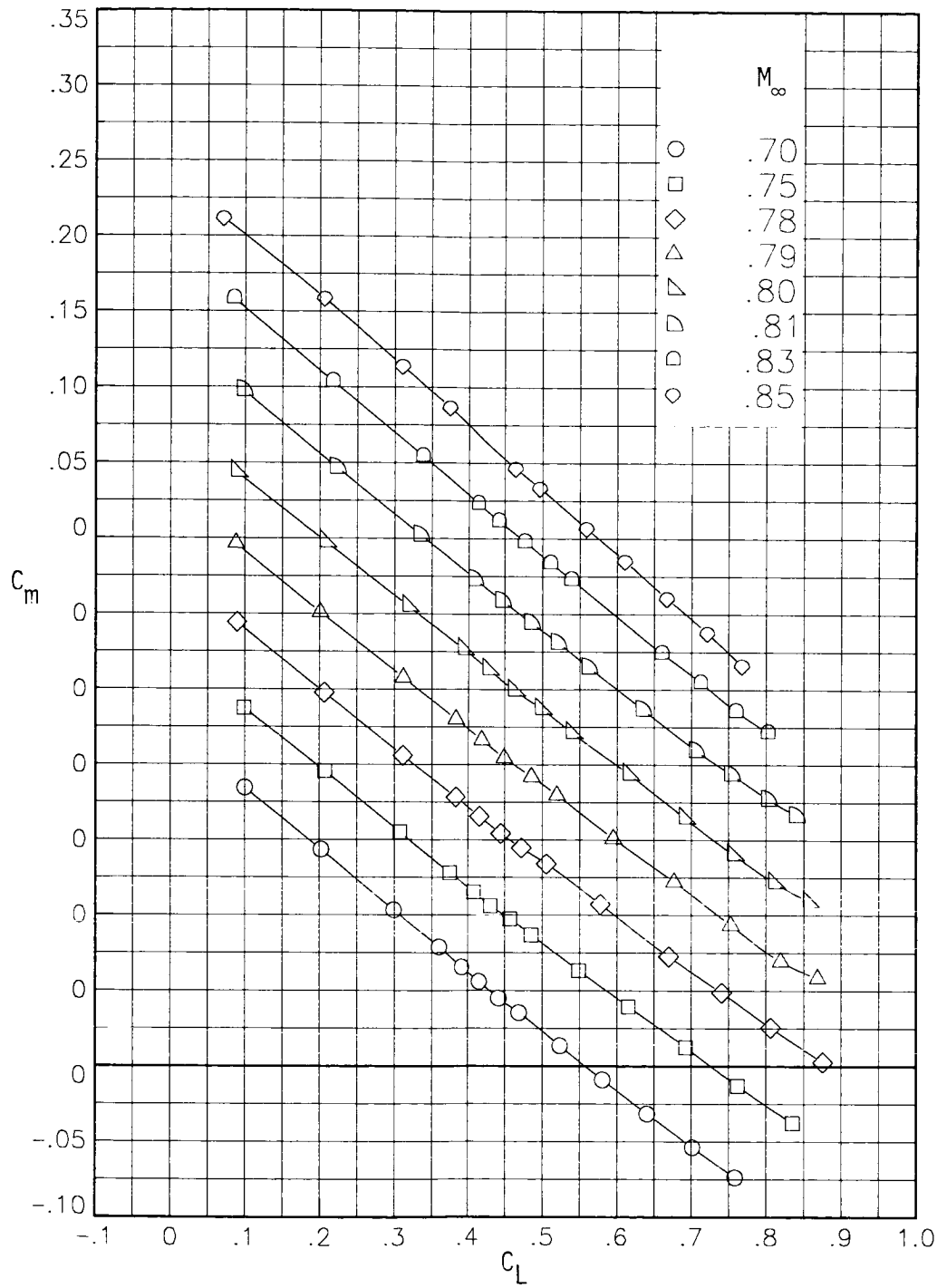

(c) Pitching-moment coefficient plotted against lift coefficient.

Figure 12.- Concluded.

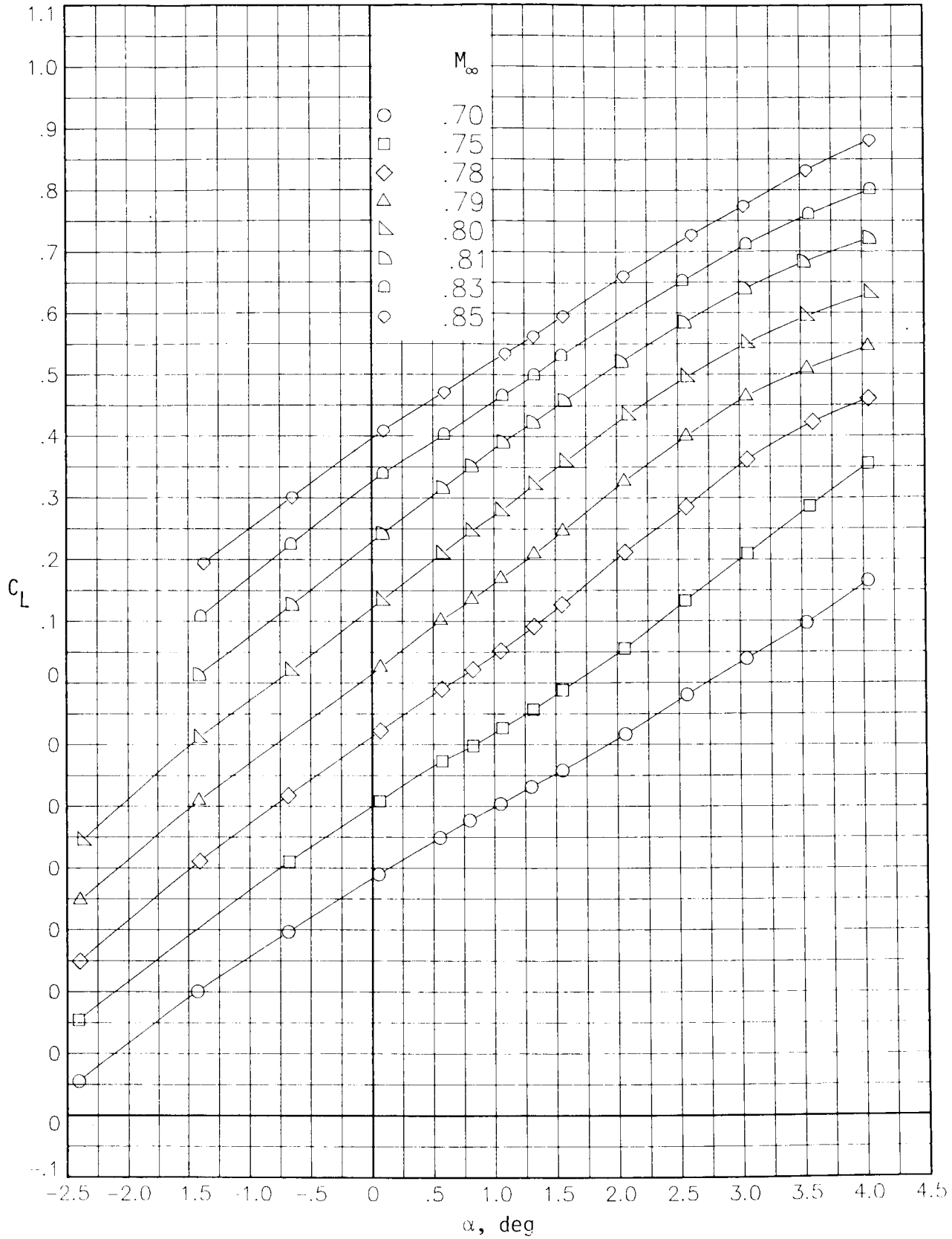

(a) Lift coefficient plotted against angle of attack.

Figure 13.- Longitudinal aerodynamic characteristics for underwing aft-mounted circular-nacelle configuration with basic pylon and recessed diverter.

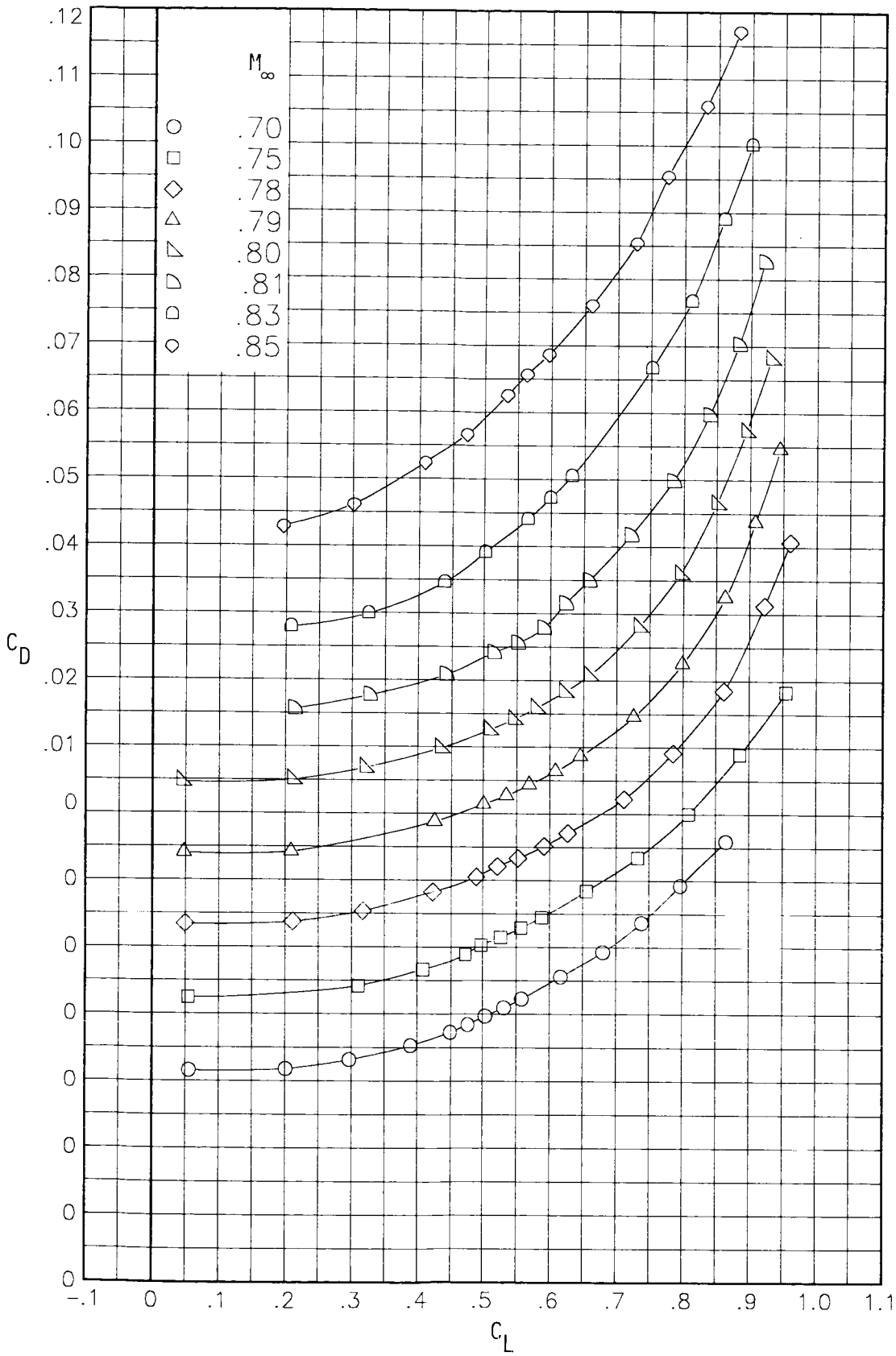

(b) Drag polar.

Figure 13.- Continued.

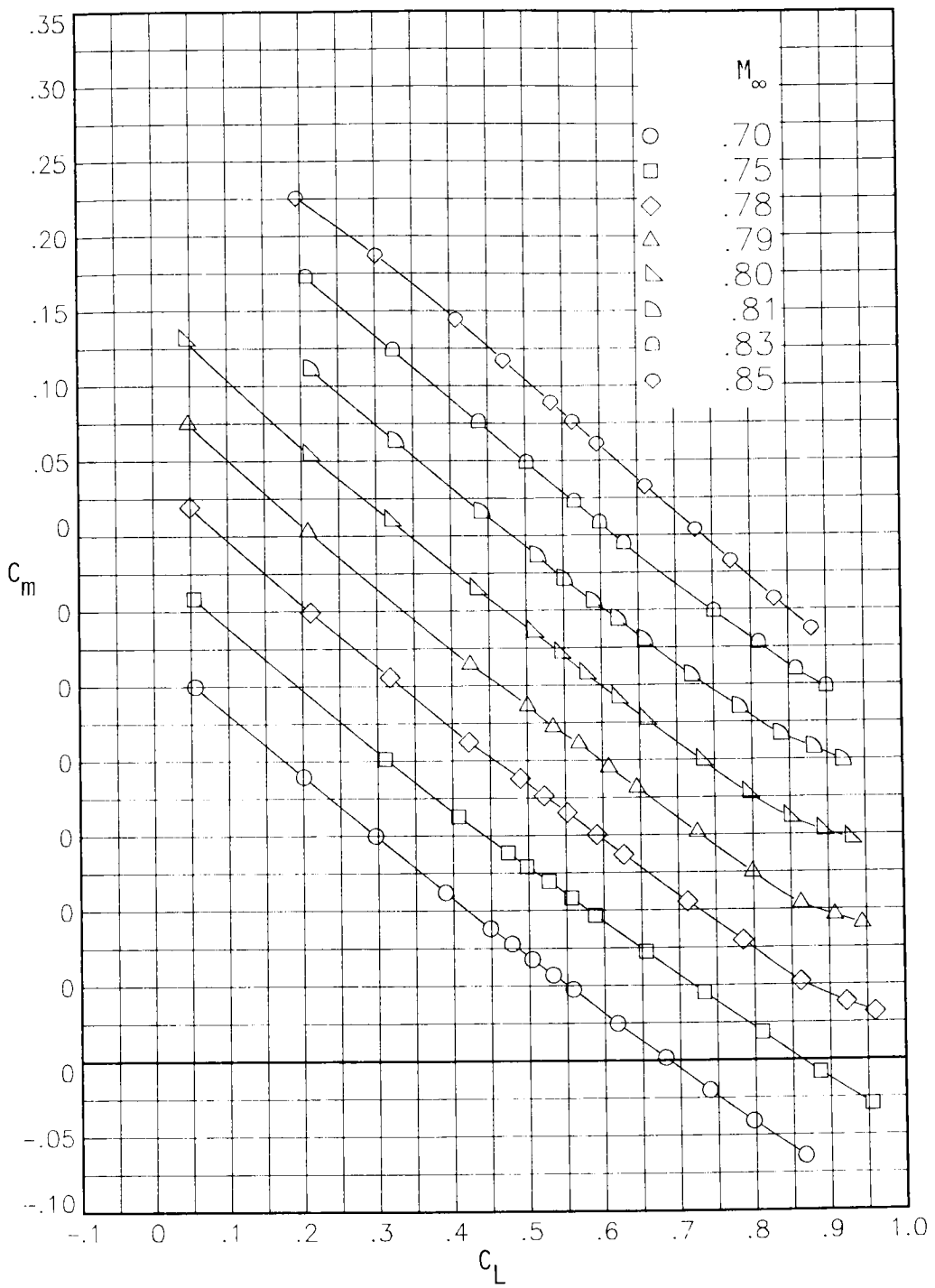

(c) Pitching-moment coefficient plotted against lift coefficient.

Figure 13.- Concluded.

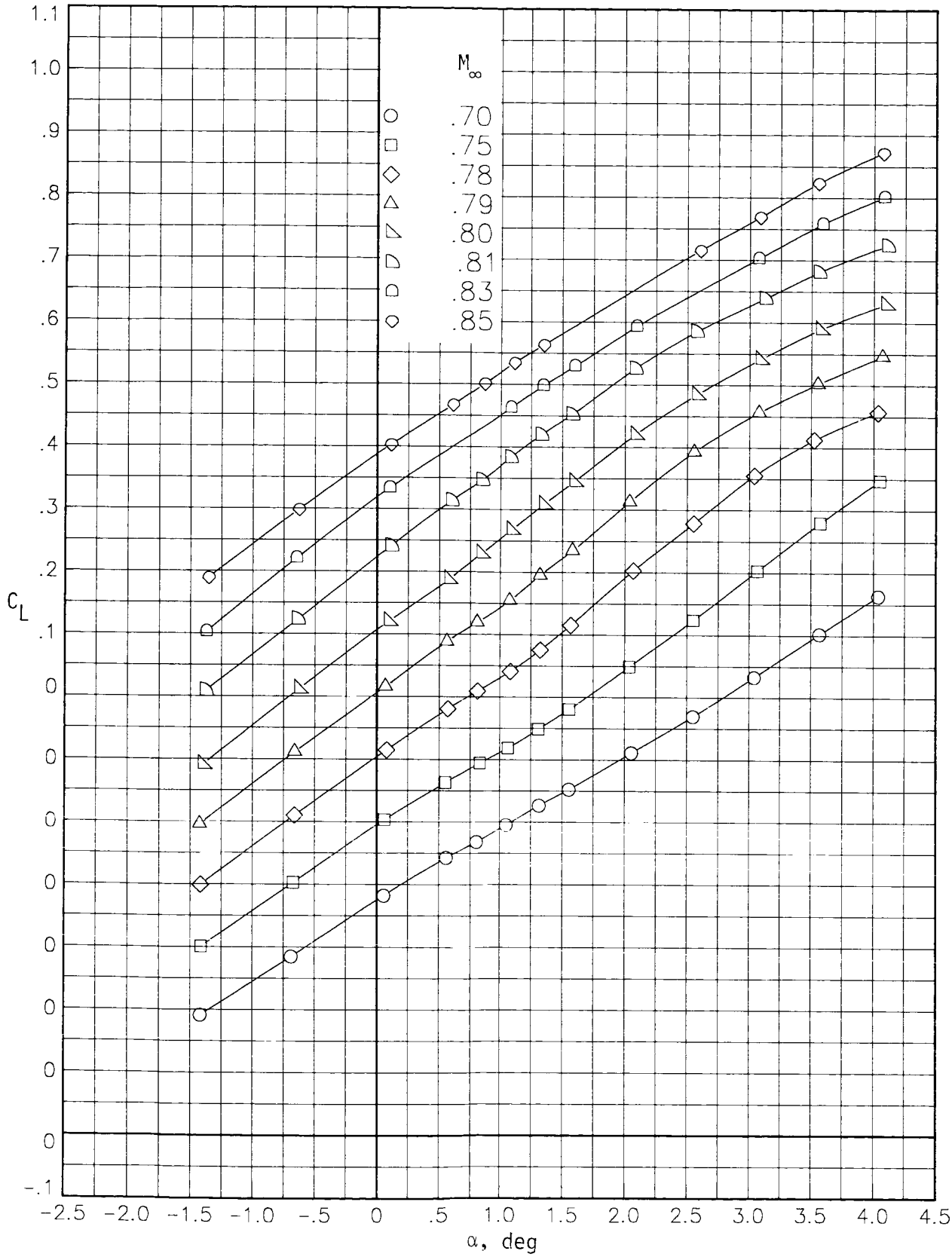

(a) Lift coefficient plotted against angle of attack.

Figure 14.- Longitudinal aerodynamic characteristics for underwing aft-mounted circular-nacelle configuration with basic pylon and highlight diverter.

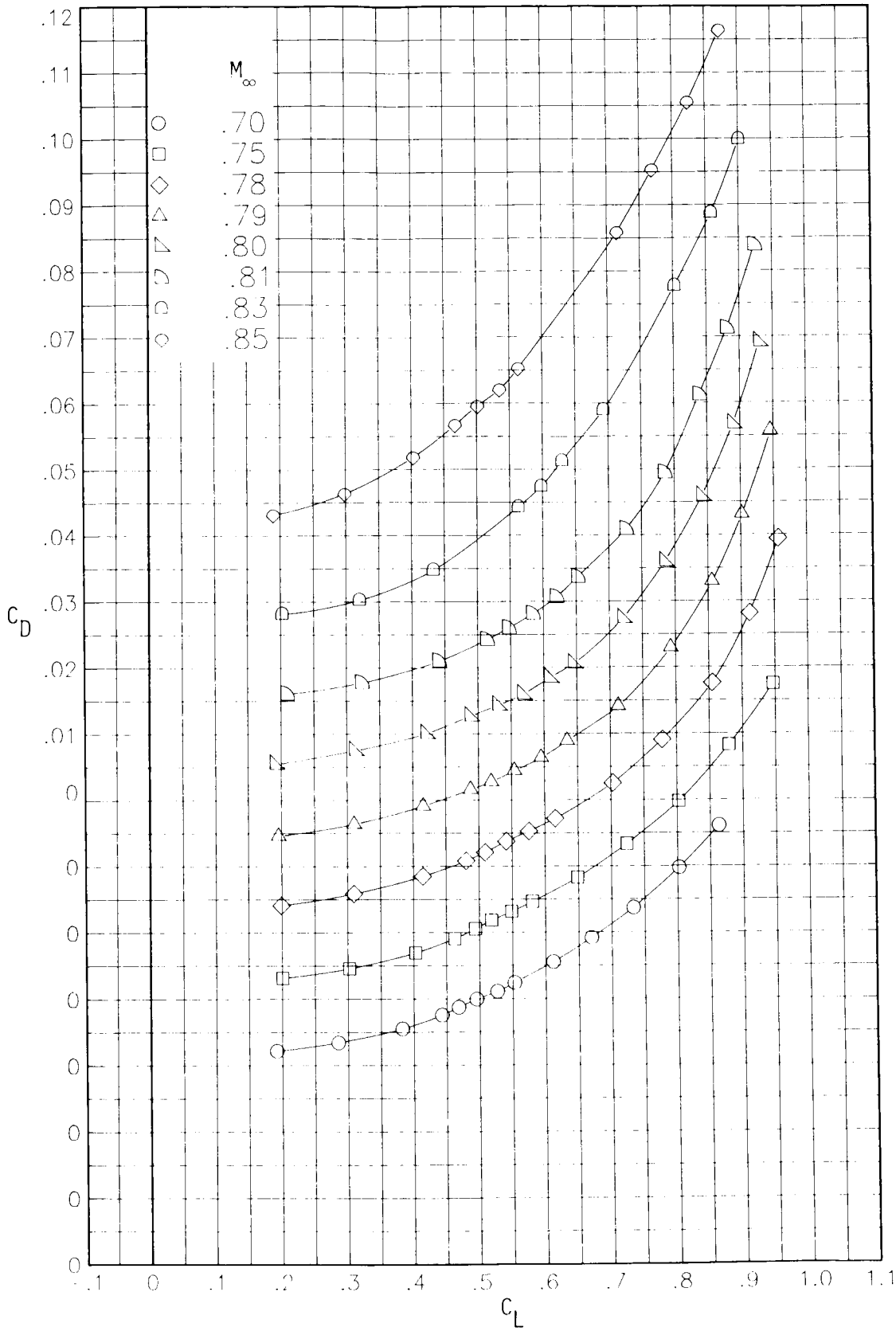

(b) Drag polar.

Figure 14.- Continued.

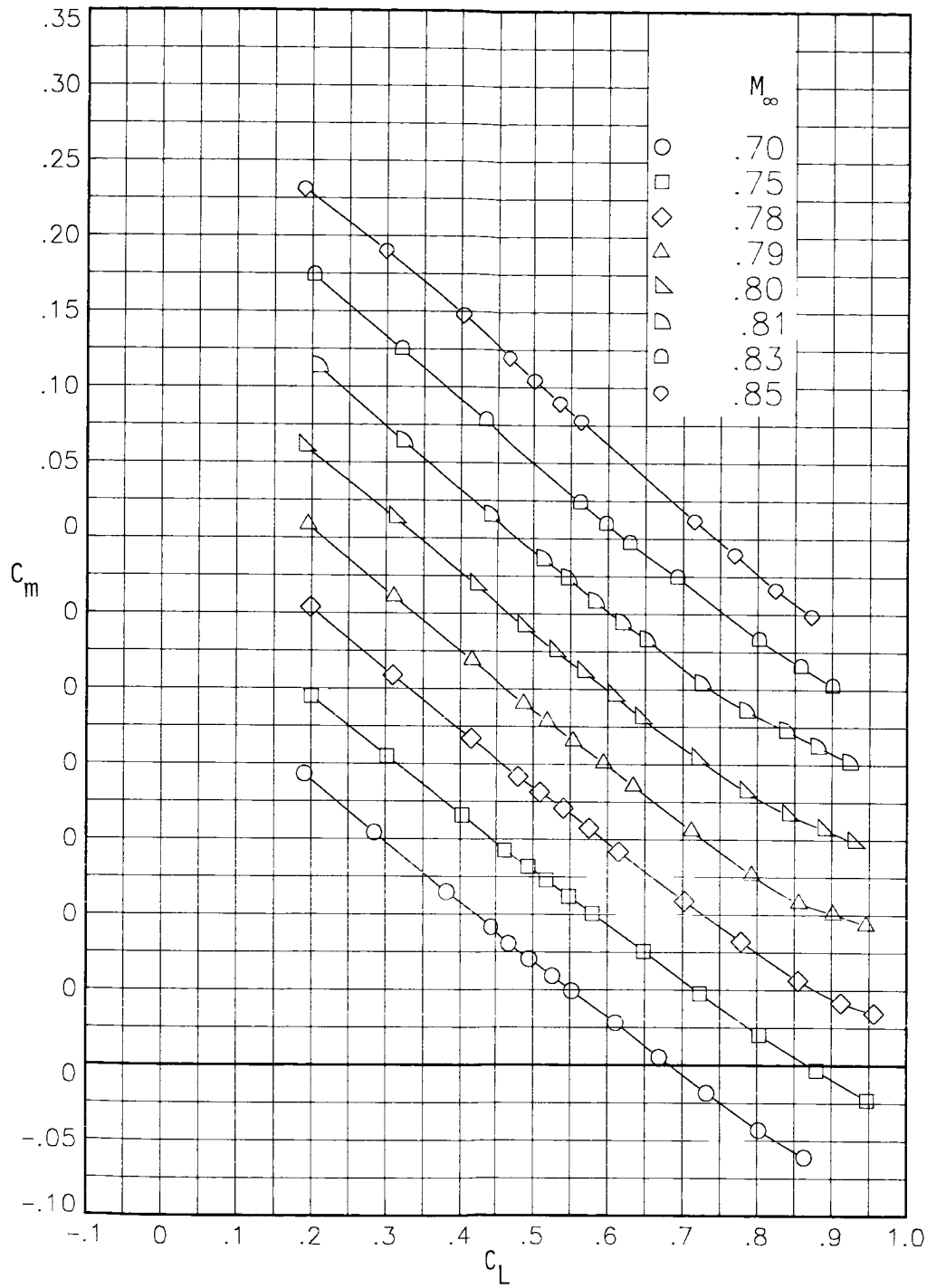

(c) Pitching-moment coefficient plotted against lift coefficient.

Figure 14.- Concluded.

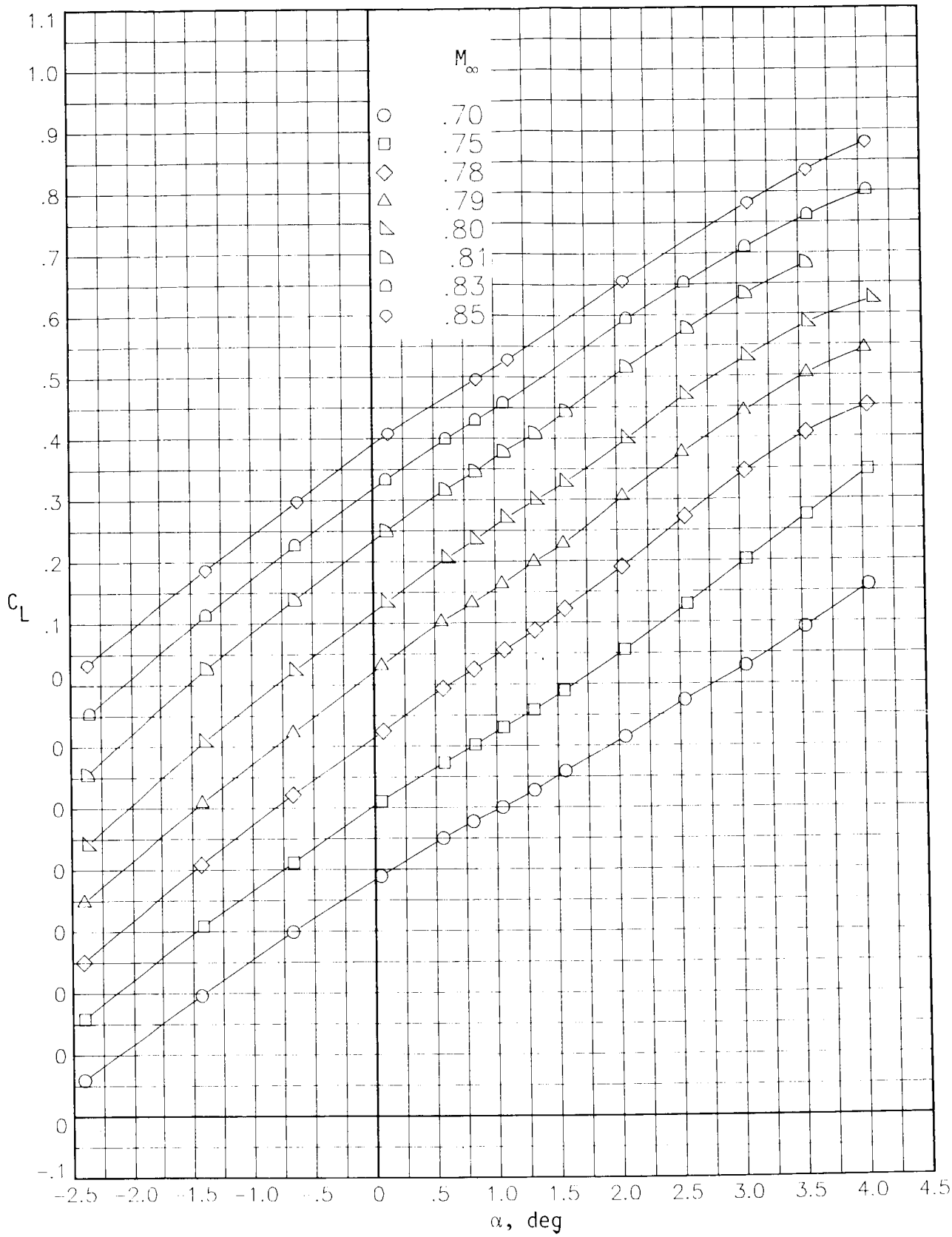

(a) Lift coefficient plotted against angle of attack.

Figure 15.- Longitudinal aerodynamic characteristics for underwing aft-mounted circular-nacelle configuration with pressure pylon and recessed diverter.

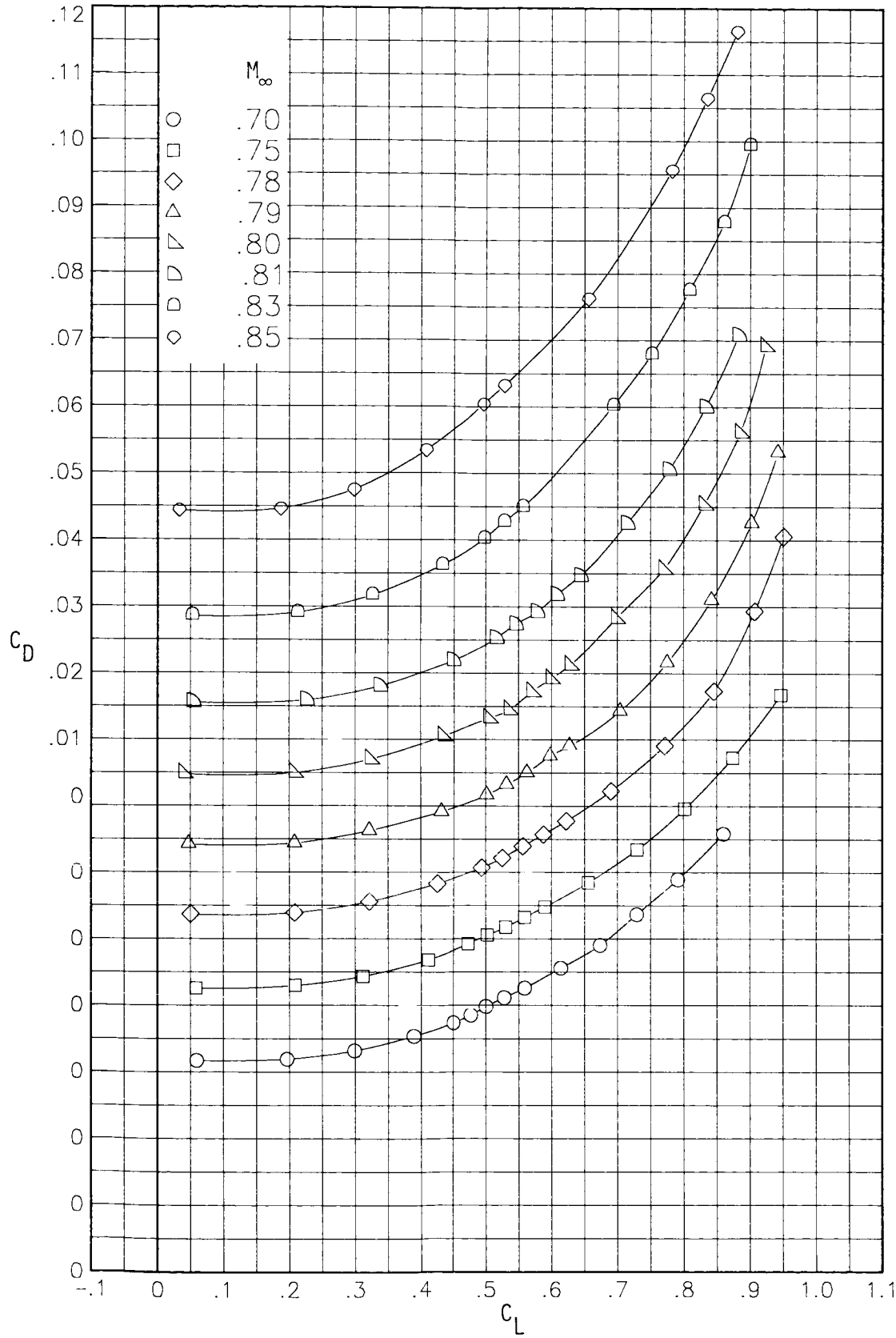

(b) Drag polar.

Figure 15.- Continued.

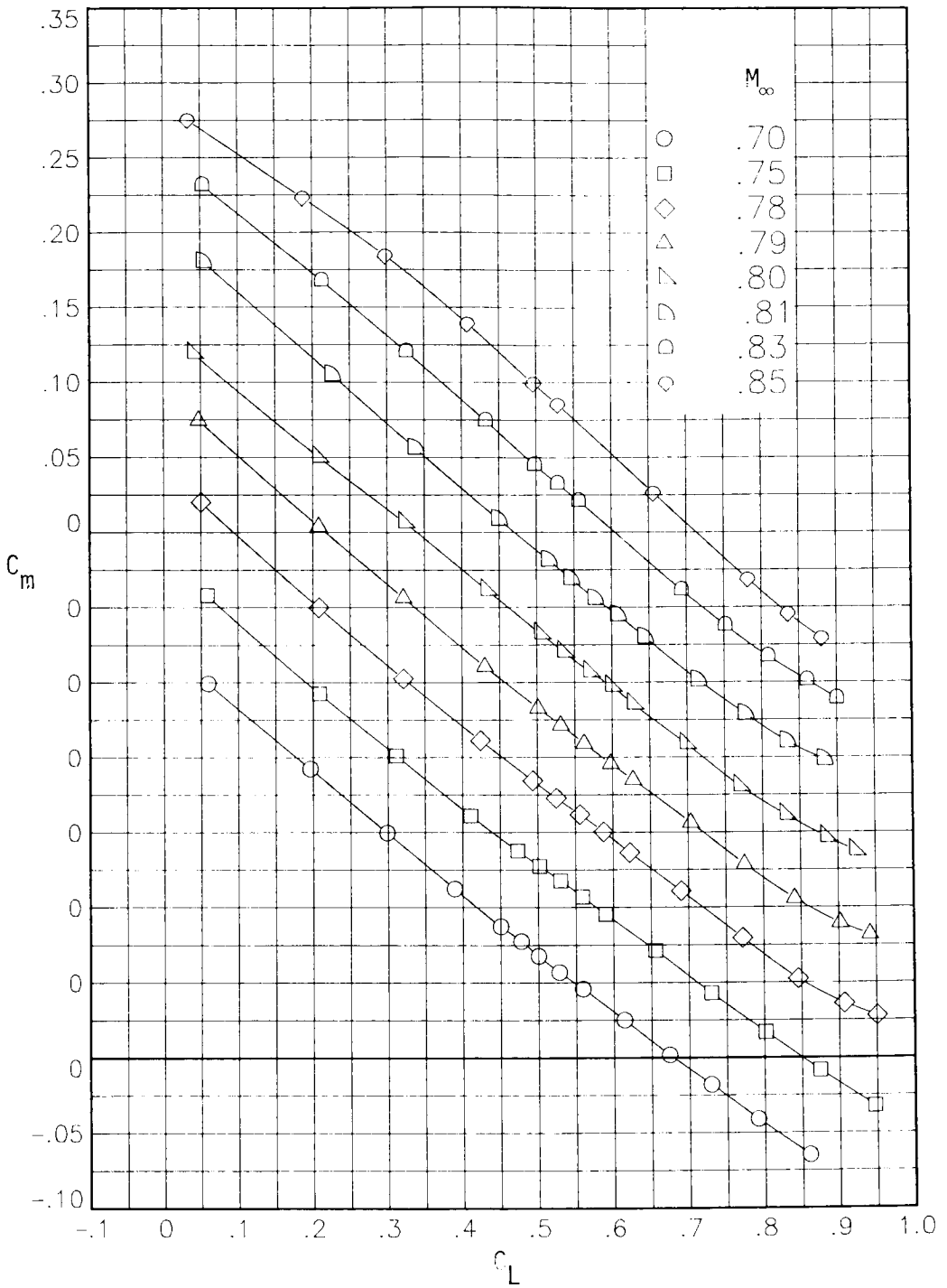

(c) Pitching-moment coefficient plotted against lift coefficient.

Figure 15.- Concluded.

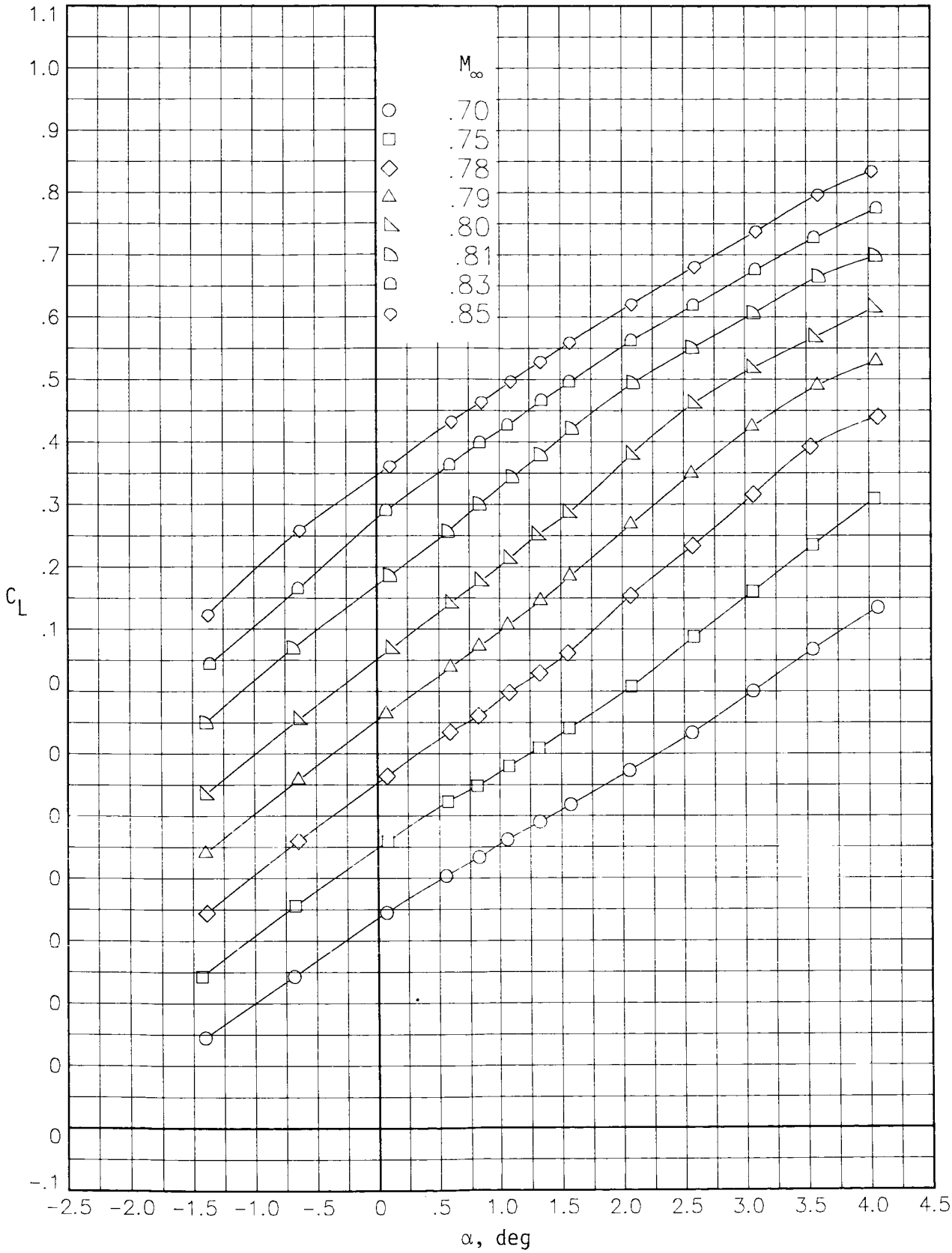

(a) Lift coefficient plotted against angle of attack.

Figure 16.- Longitudinal aerodynamic characteristics for underwing D-nacelle with basic pylon.

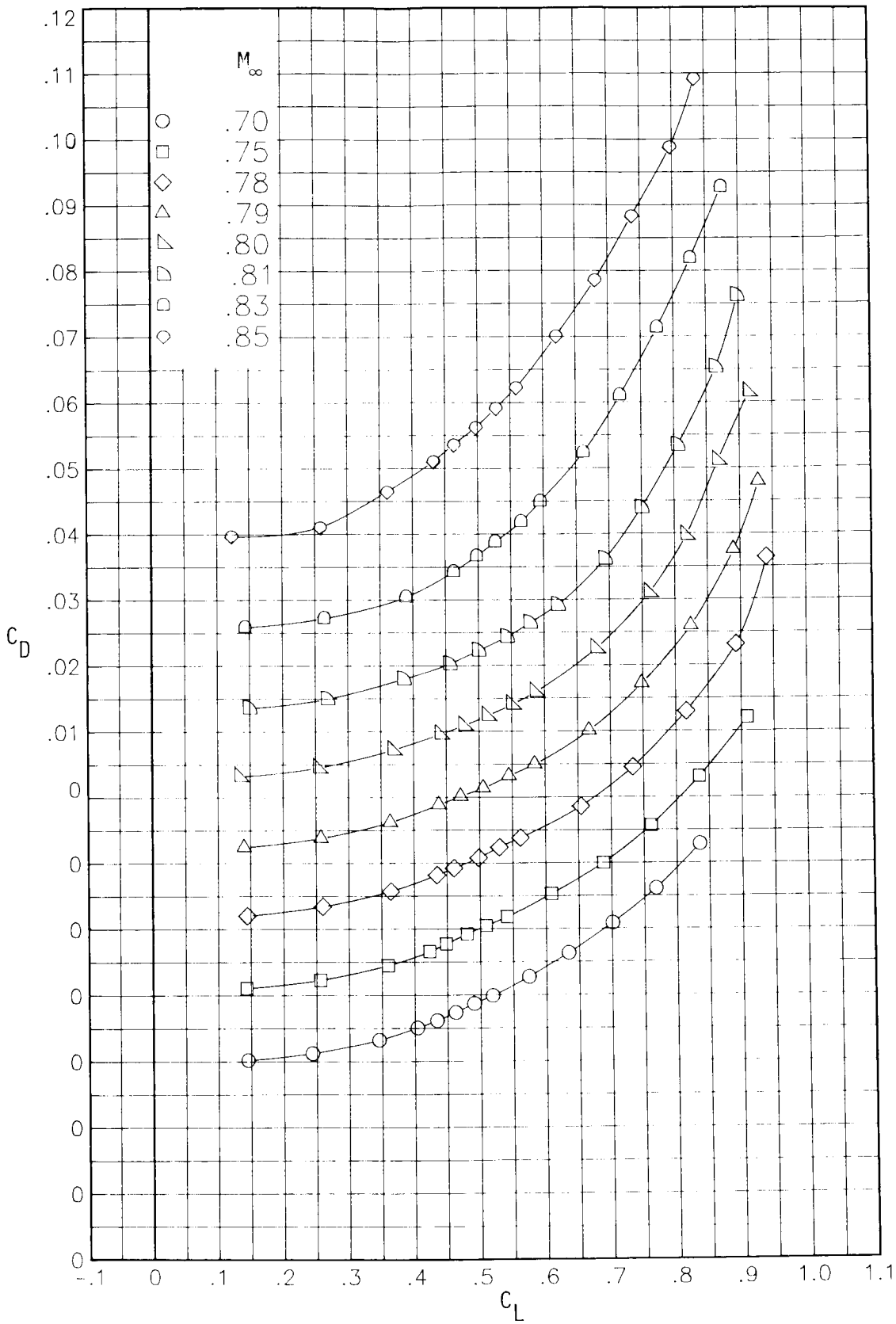

(b) Drag polar.

Figure 16.- Continued.

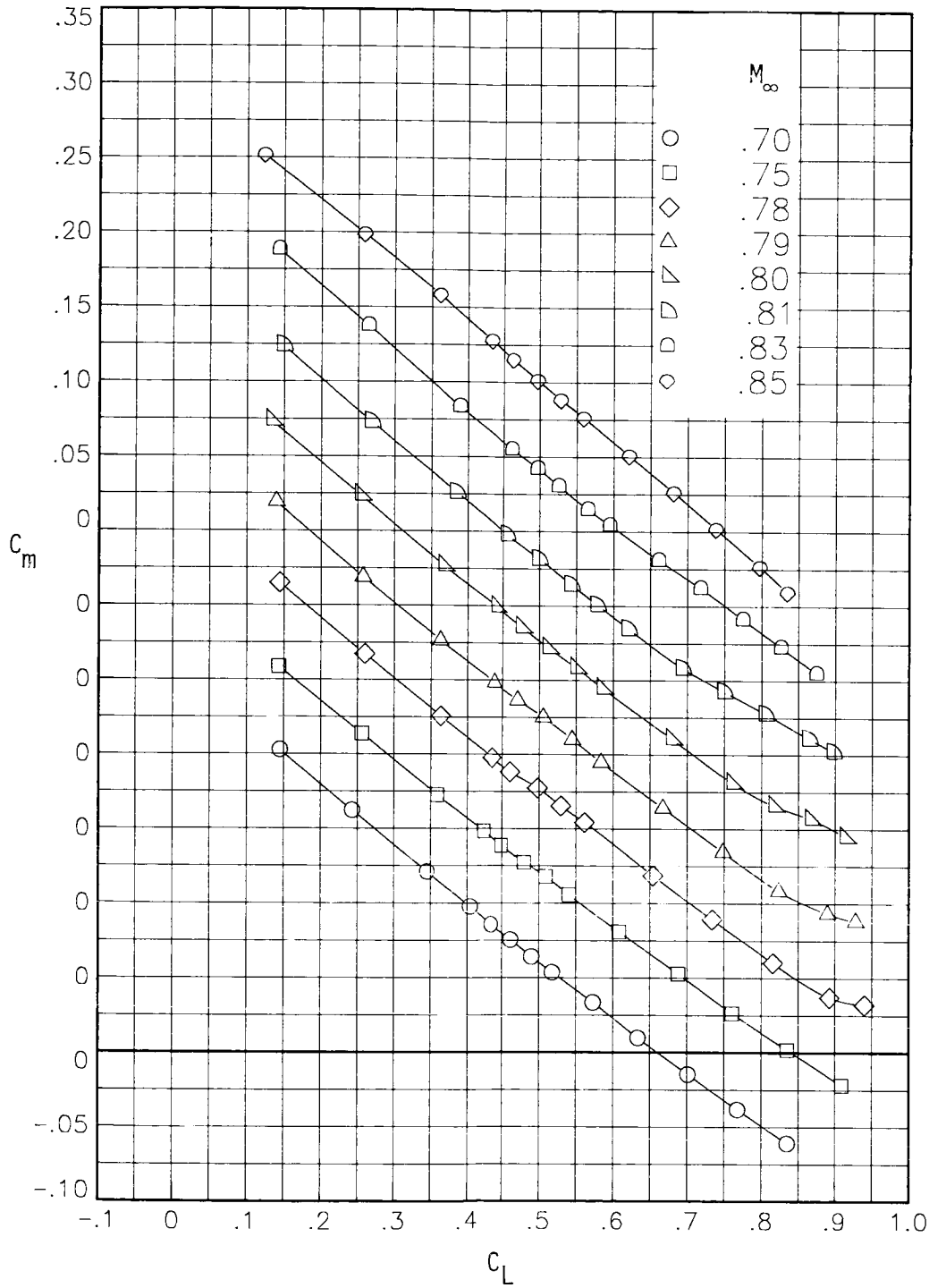

(c) Pitching-moment coefficient plotted against lift coefficient.

Figure 16.- Concluded.

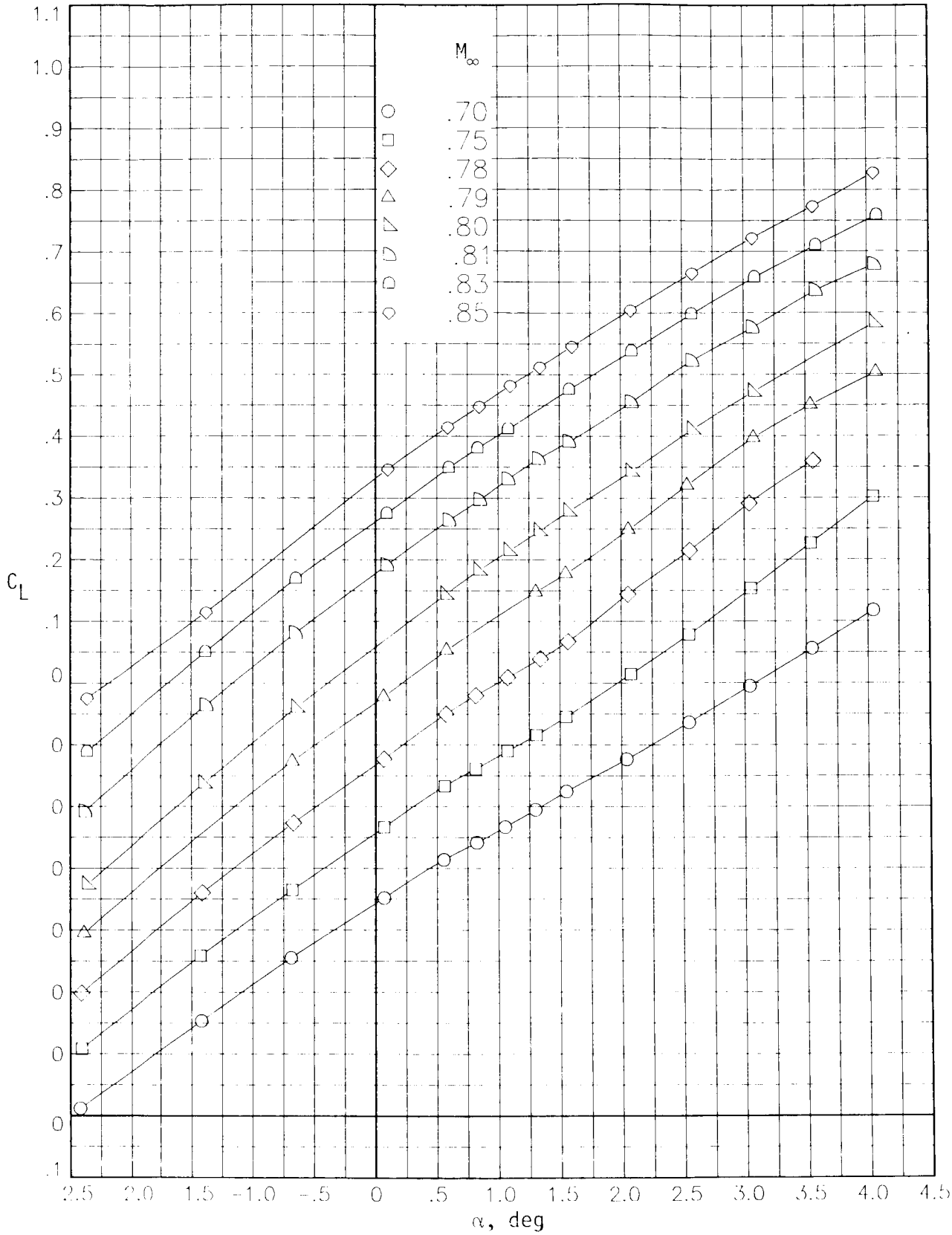

(a) Lift coefficient plotted against angle of attack.

Figure 17.- Longitudinal aerodynamic characteristics for underwing D-nacelle with pressure pylon.

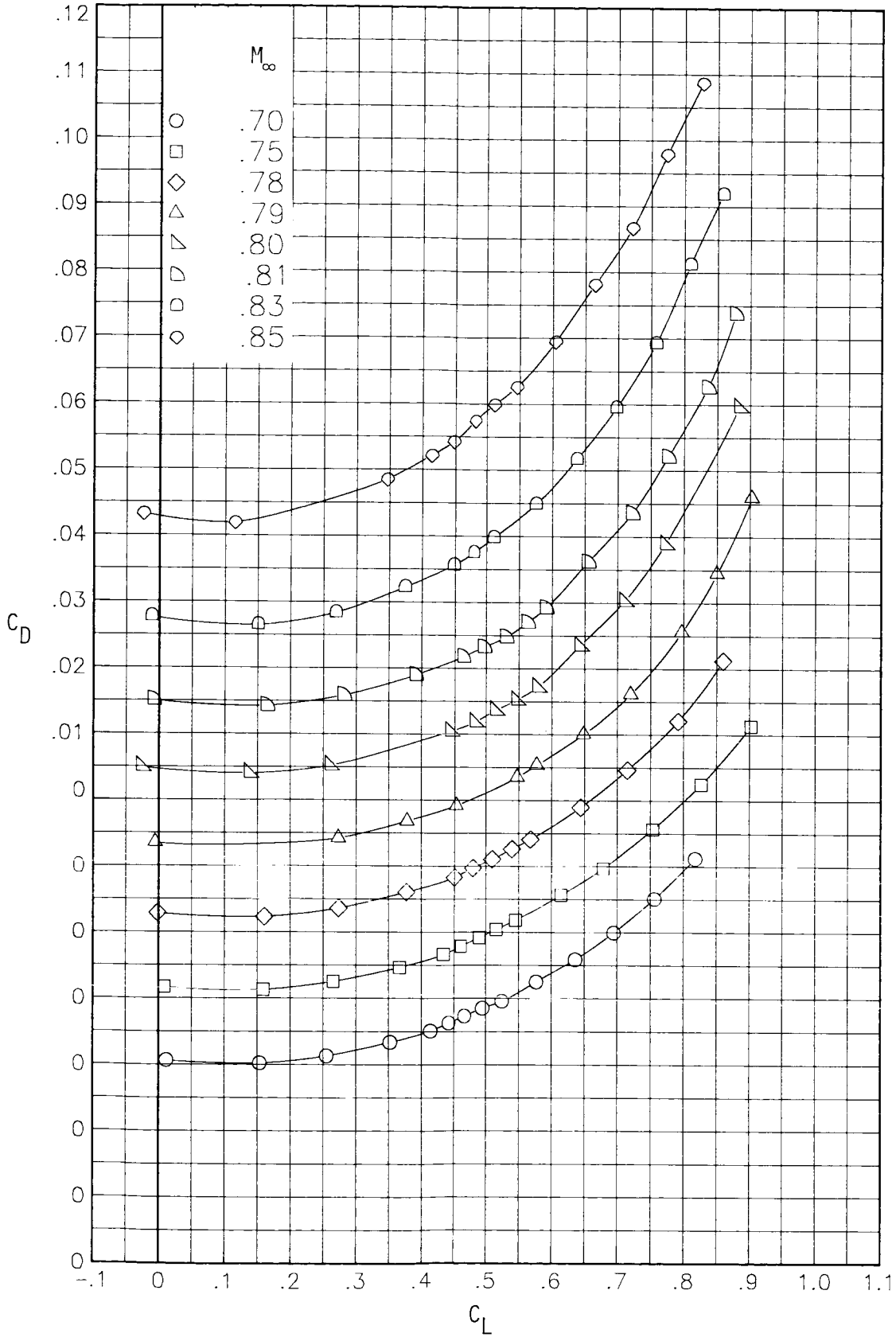

(b) Drag polar.

Figure 17.- Continued.

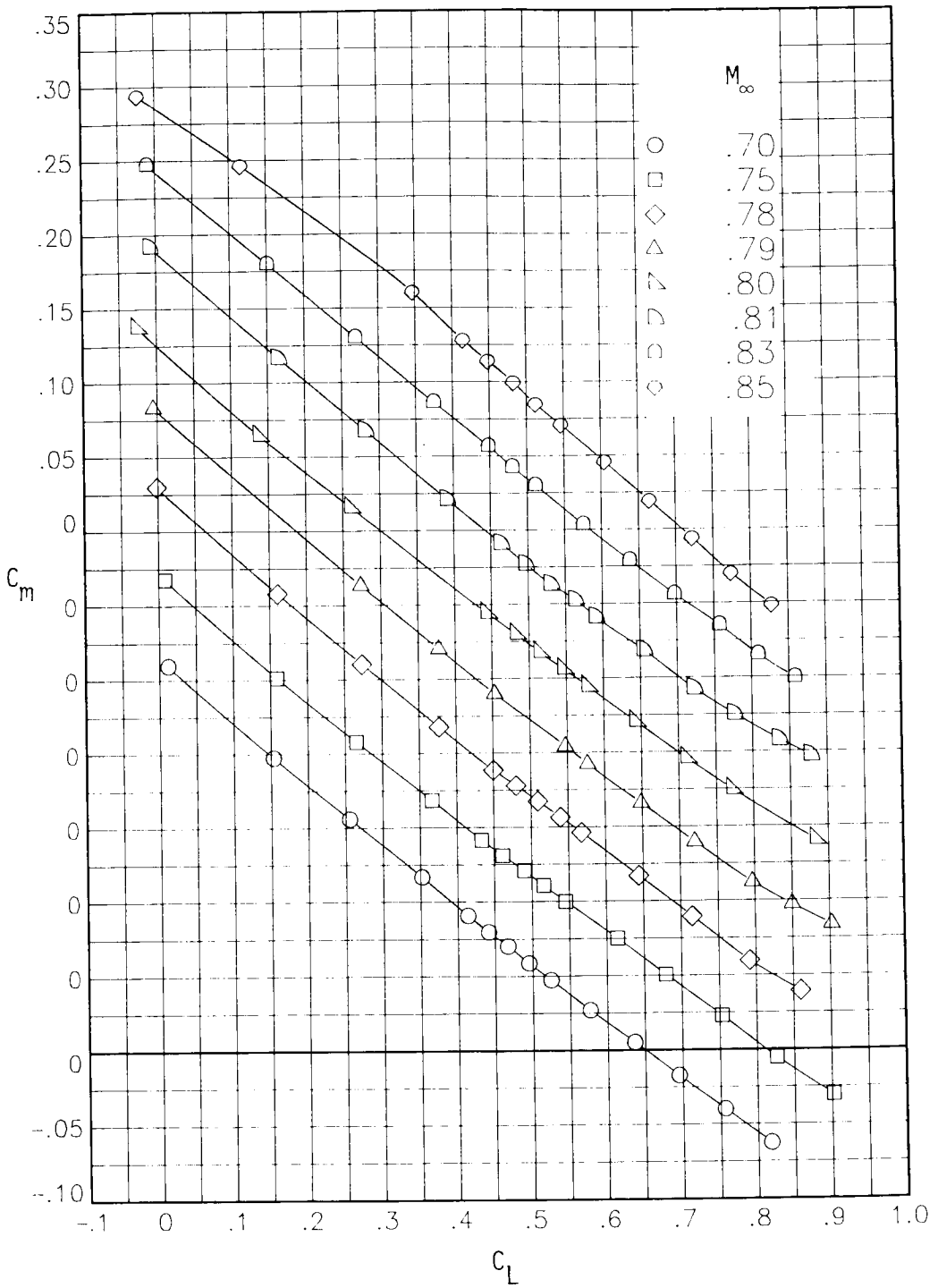

(c) Pitching-moment coefficient plotted against lift coefficient.

Figure 17.- Concluded.

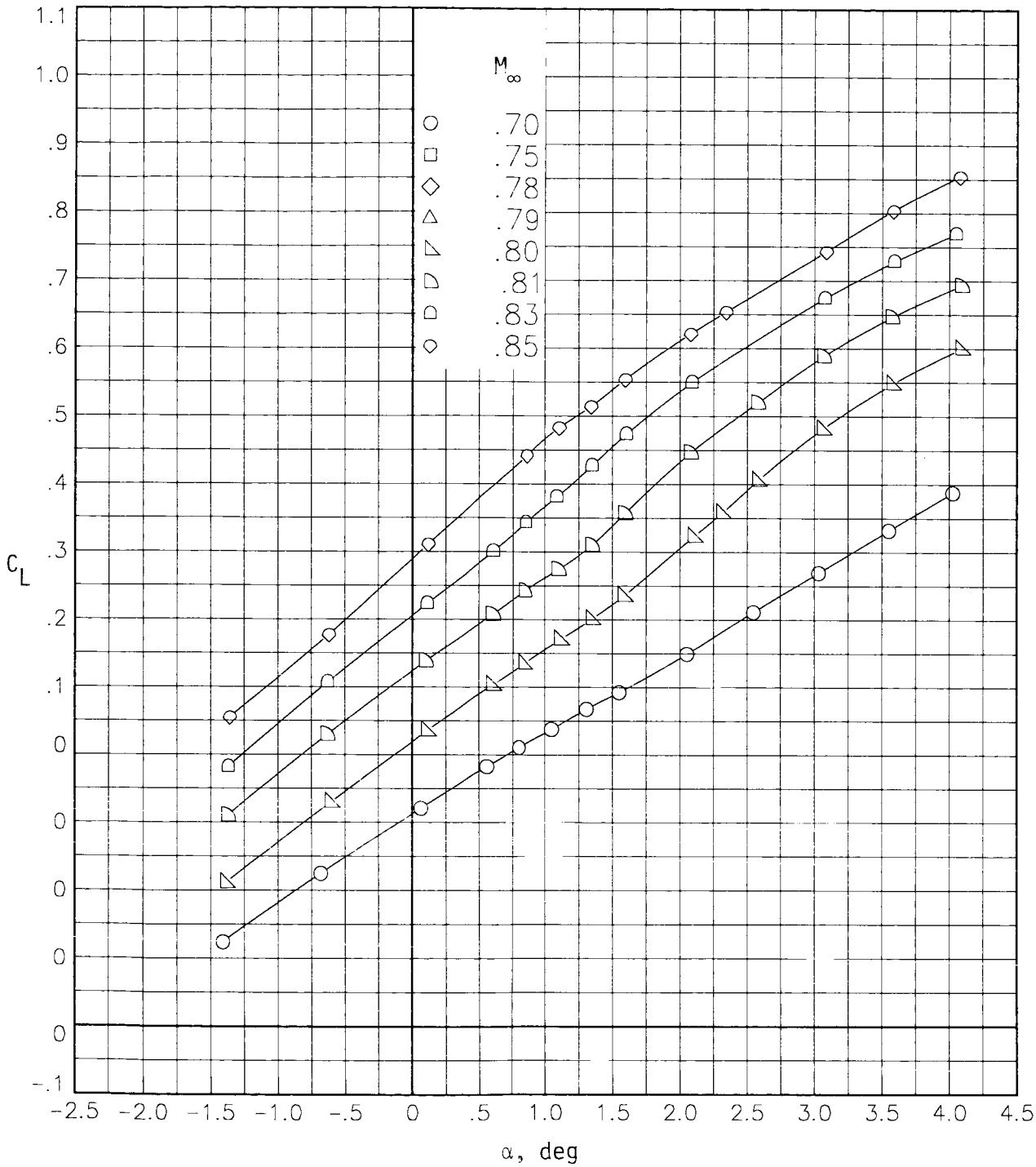

(a) Lift coefficient plotted against angle of attack.

Figure 18.- Longitudinal aerodynamic characteristics for underwing D-nacelle with basic pylon and short-cone antishock body.

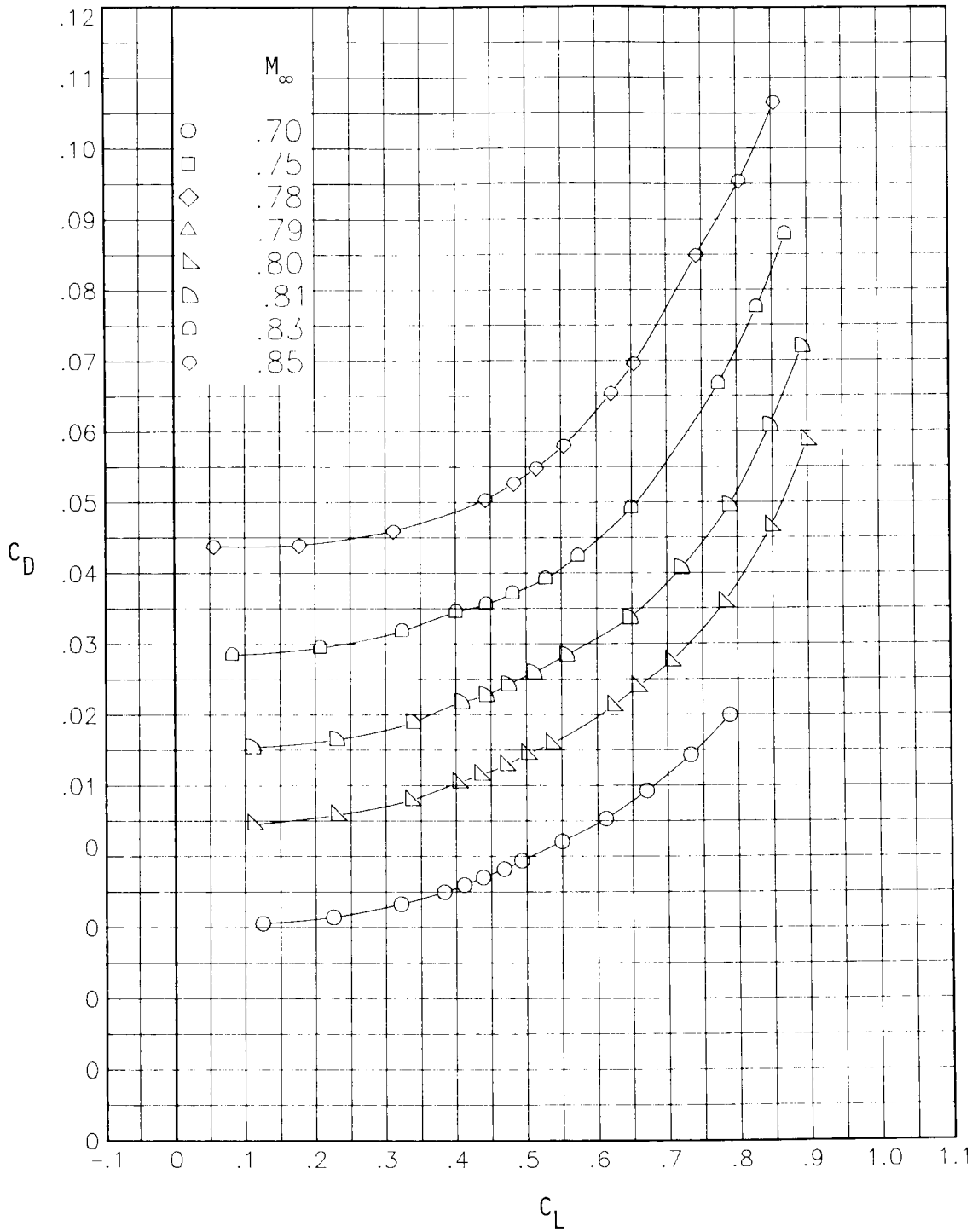

(b) Drag polar.

Figure 18.- Continued.

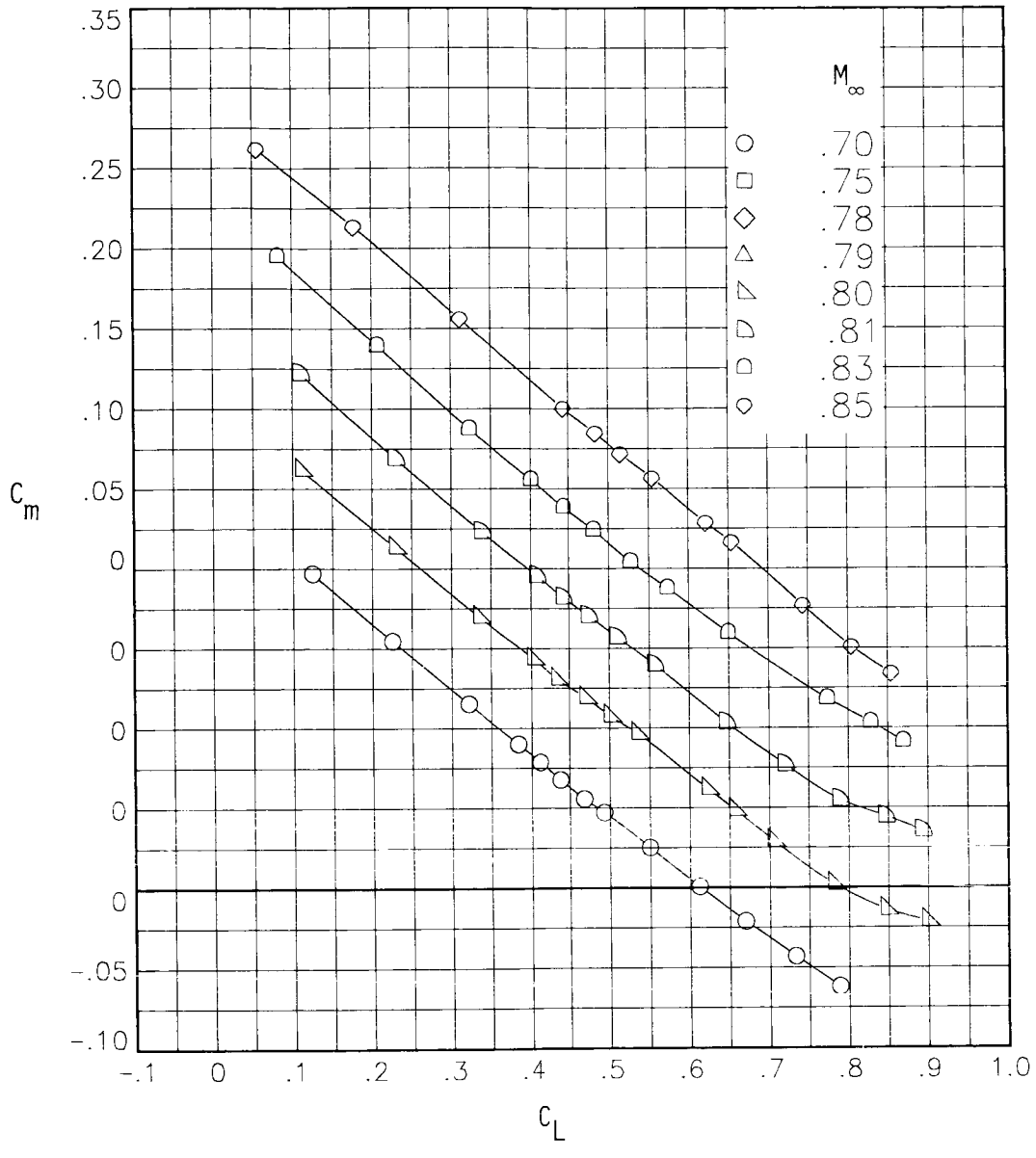

(c) Pitching-moment coefficient plotted against lift coefficient.

Figure 18.- Concluded.

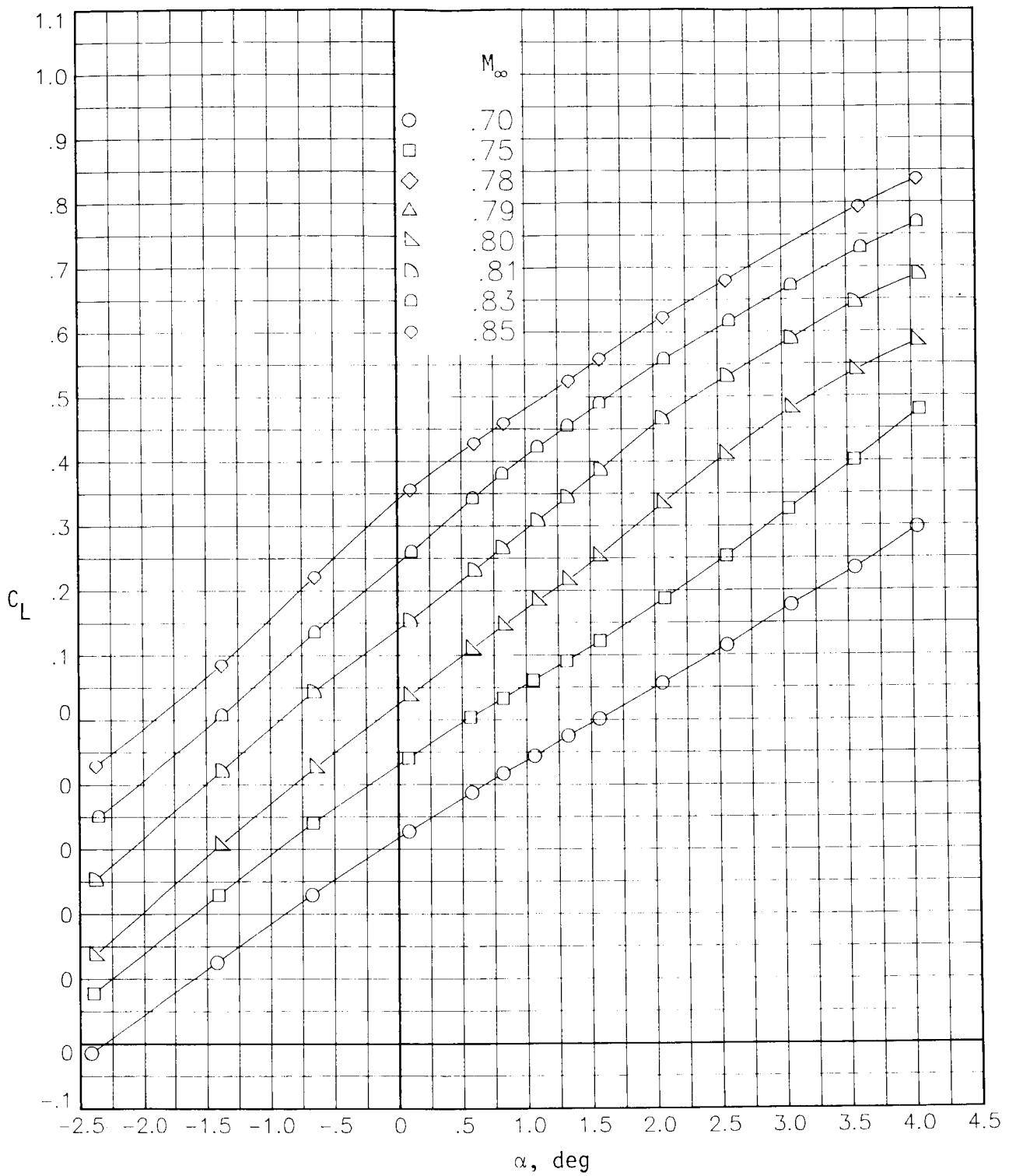

(a) Lift coefficient plotted against angle of attack.

Figure 19.- Longitudinal aerodynamic characteristics for underwing D-nacelle with basic pylon and long-cone antishock body.

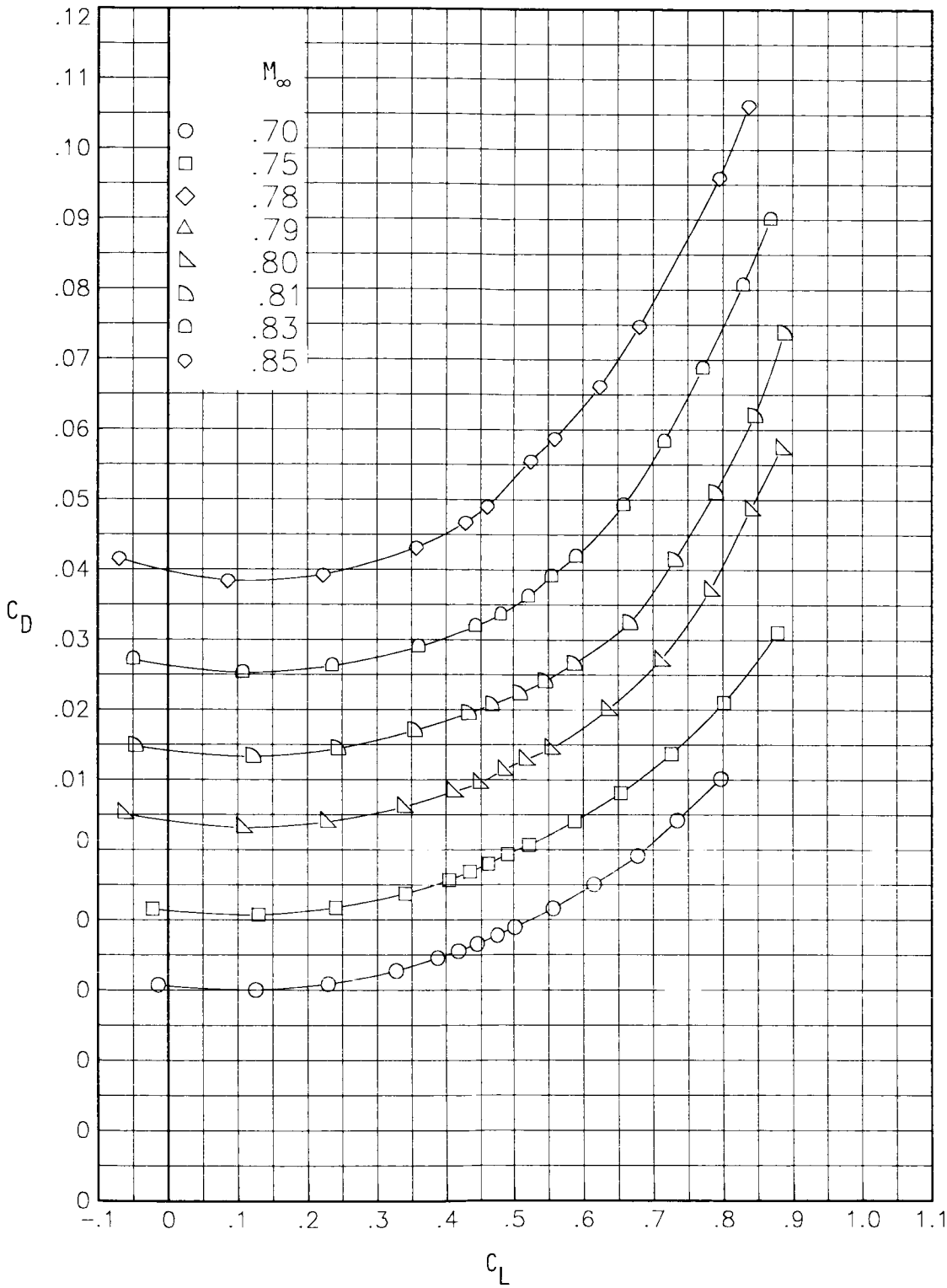

(b) Drag polar.

Figure 19.- Continued.

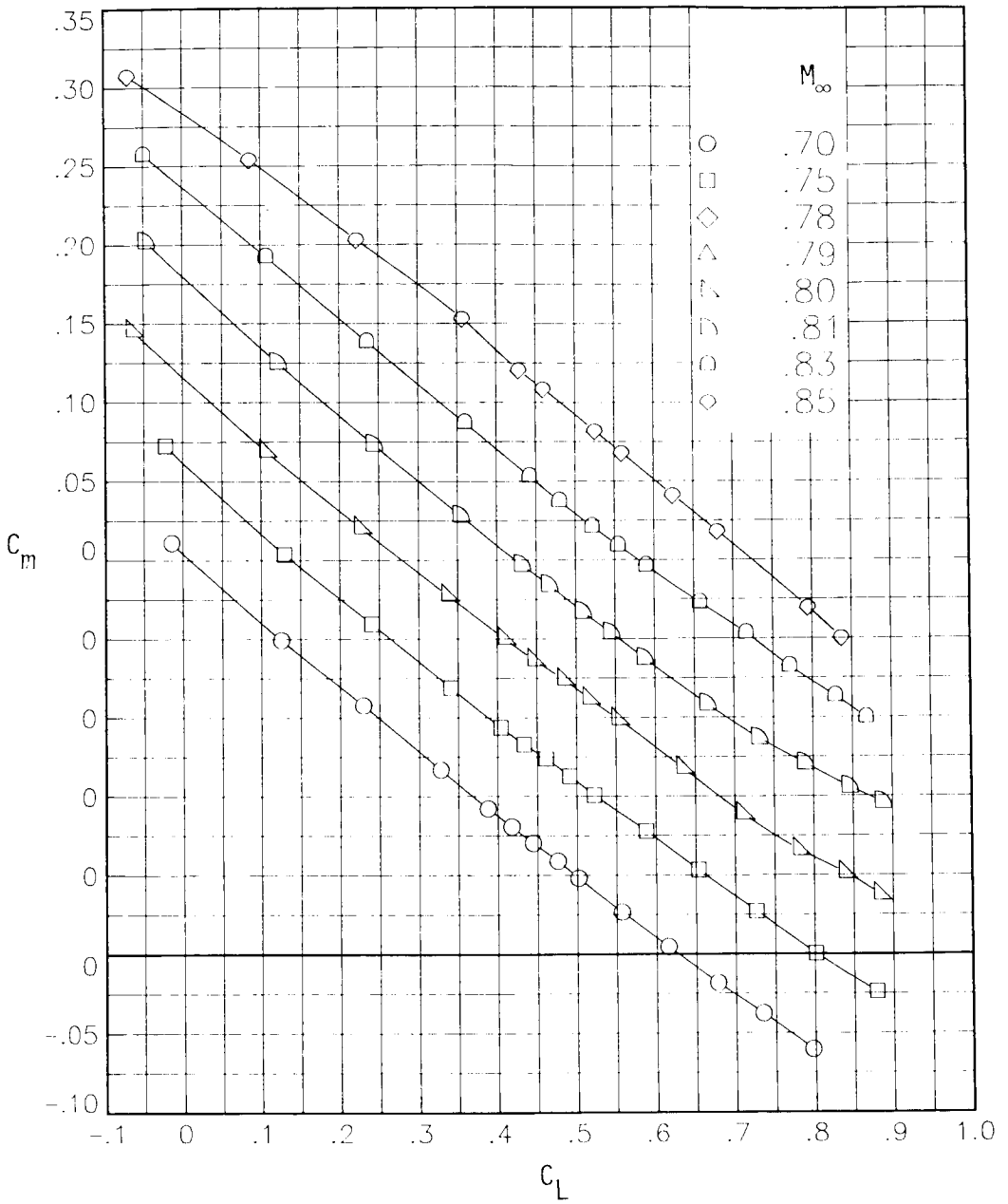

(c) Pitching-moment coefficient plotted against lift coefficient.

Figure 19.- Concluded.

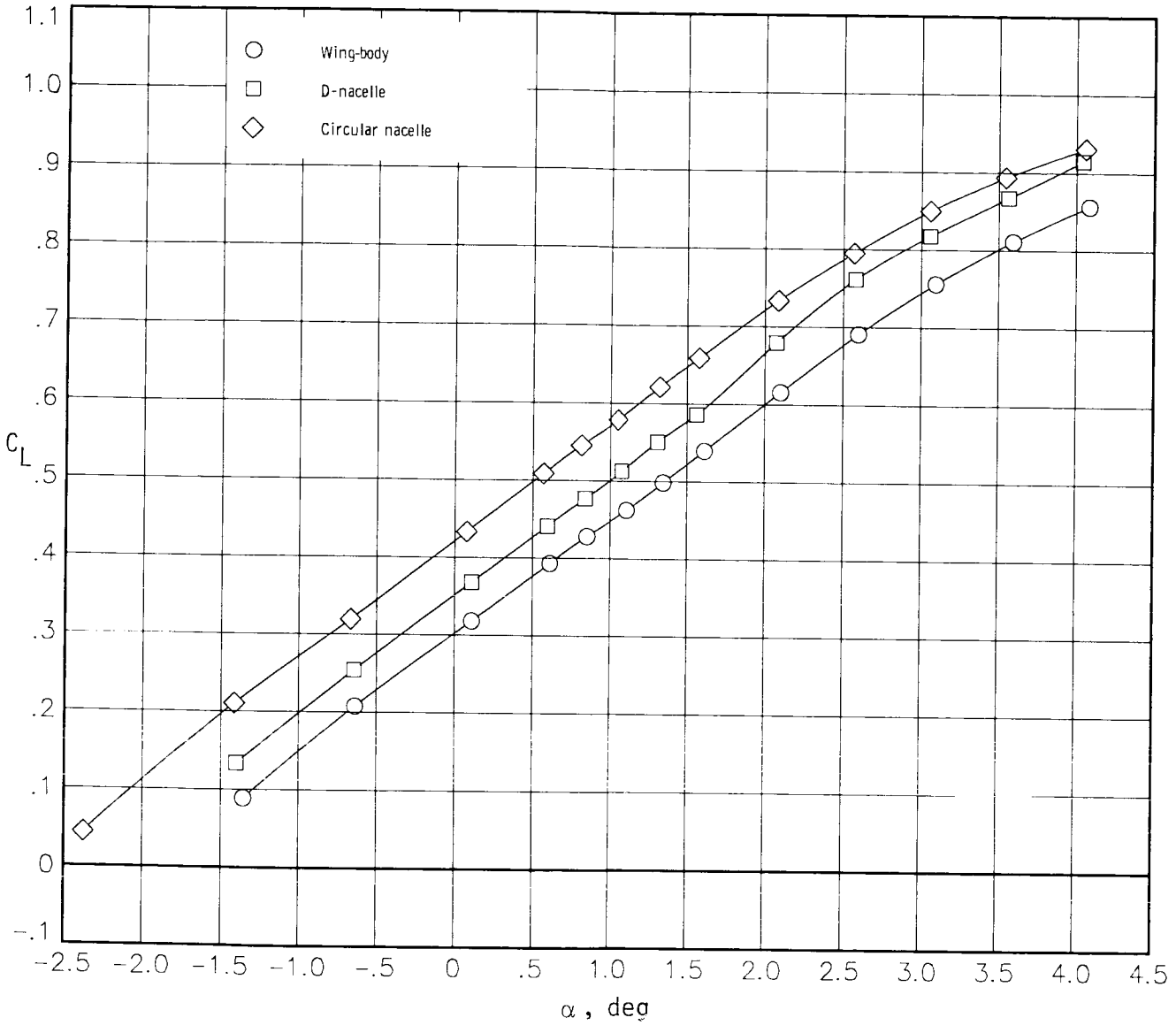

(a) Lift coefficient plotted against angle of attack.

Figure 20.- Comparison of longitudinal characteristics at $M_\infty = 0.80$ for underwing aft-mounted circular nacelles and D-nacelles.

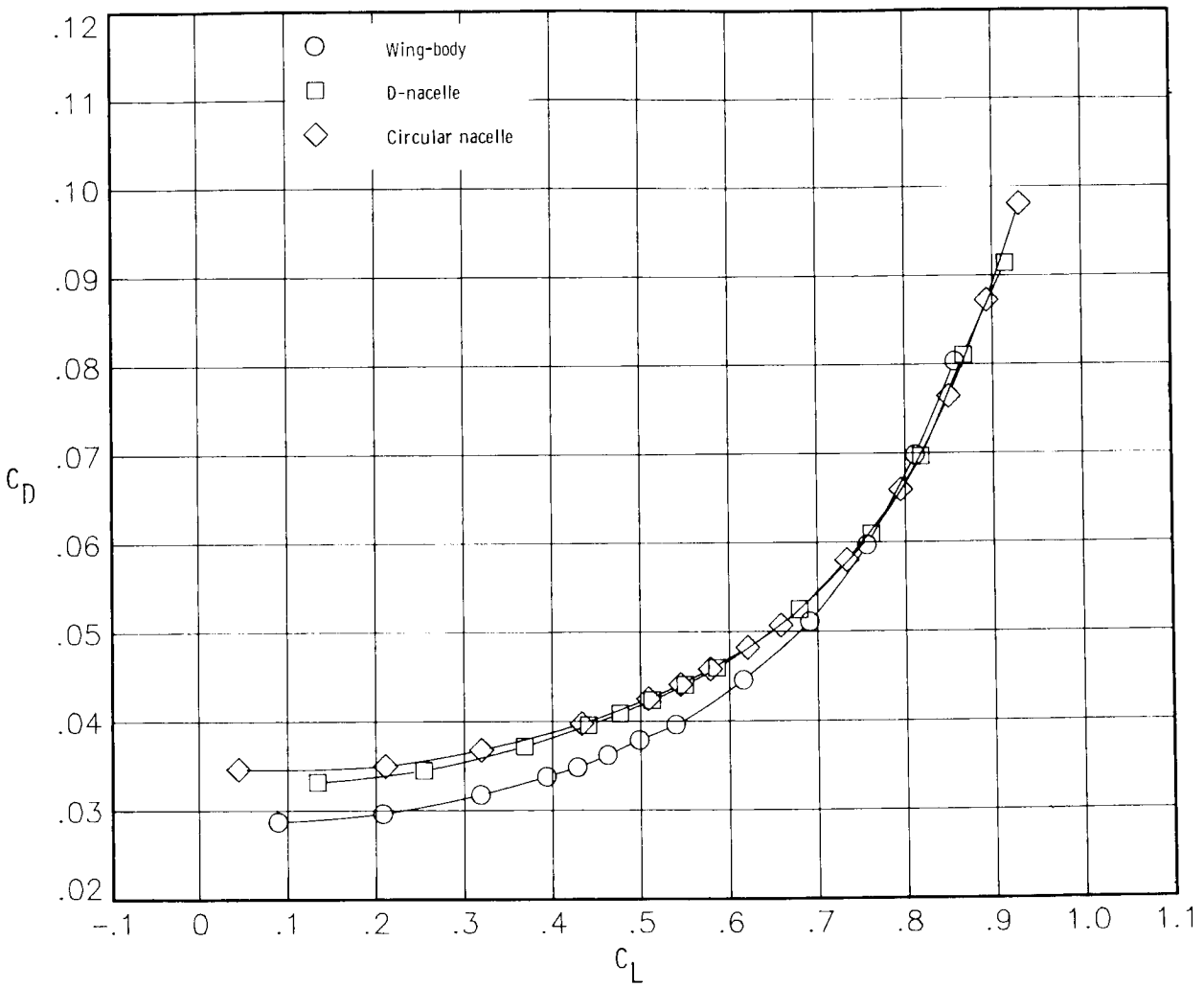

(b) Drag polar.

Figure 20.- Continued.

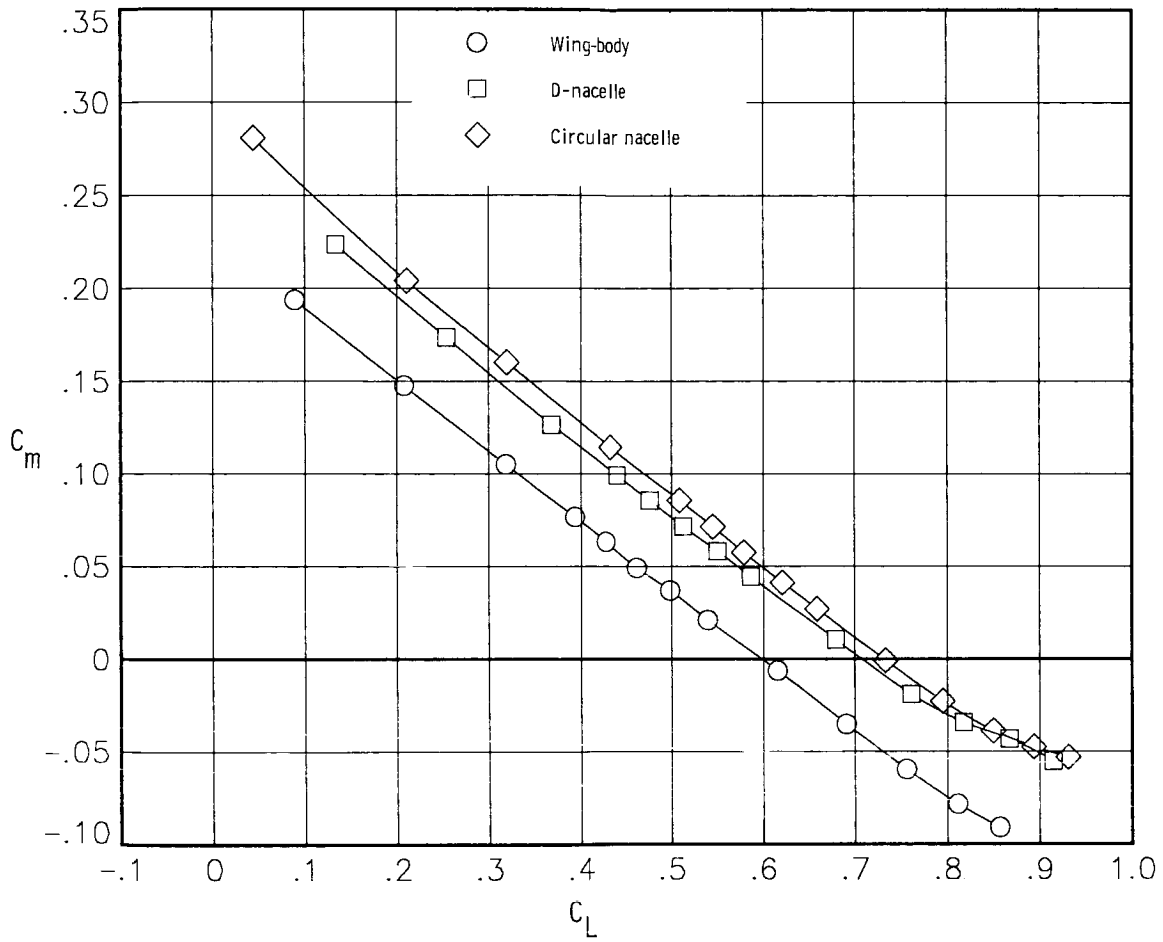

(c) Pitching-moment coefficient plotted against lift coefficient.

Figure 20.- Concluded.

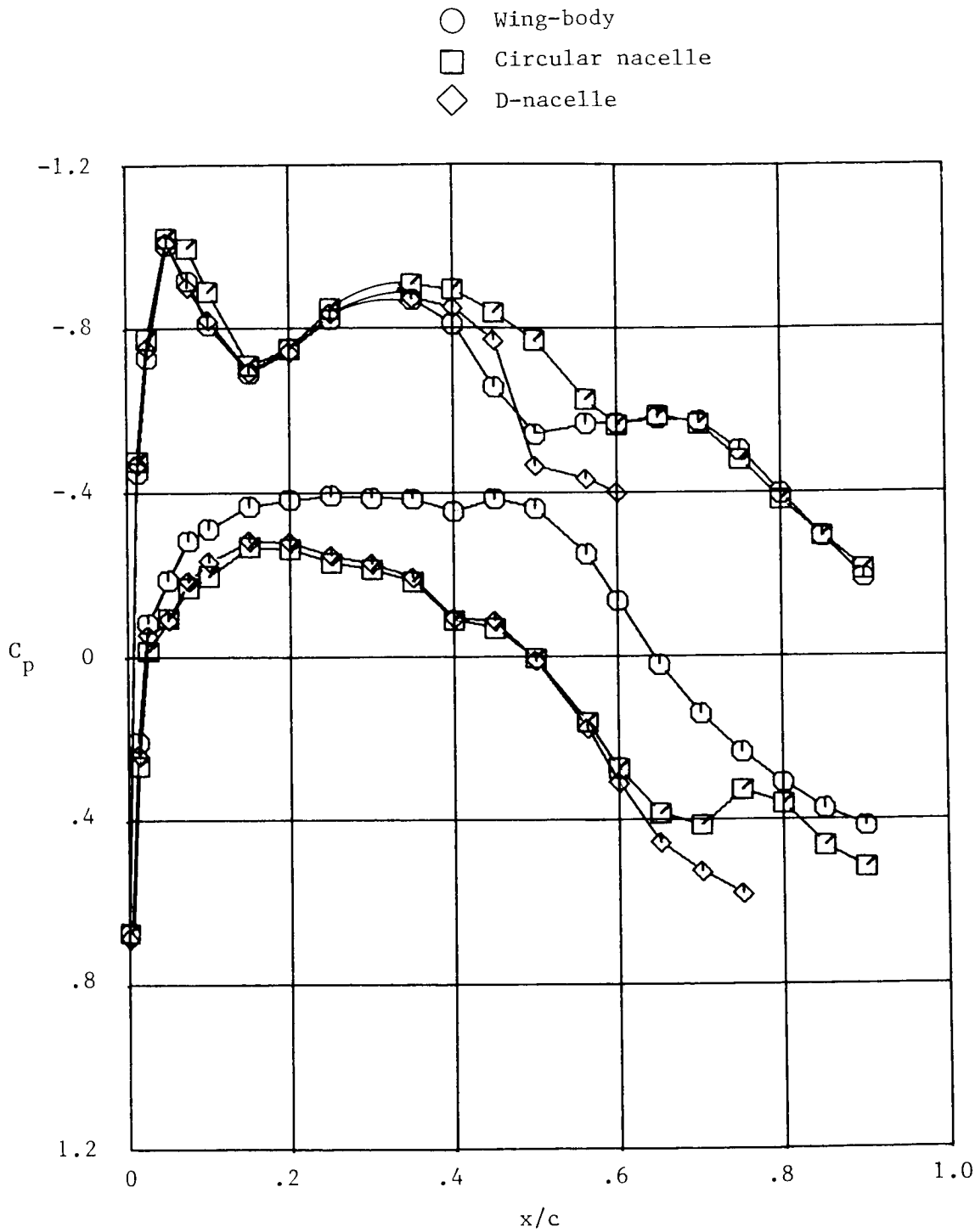

(a) η = 0.328.

Figure 21.- Effect of aft-mounted nacelles on wing chordwise pressure-coefficient distributions for basic pylon configurations.

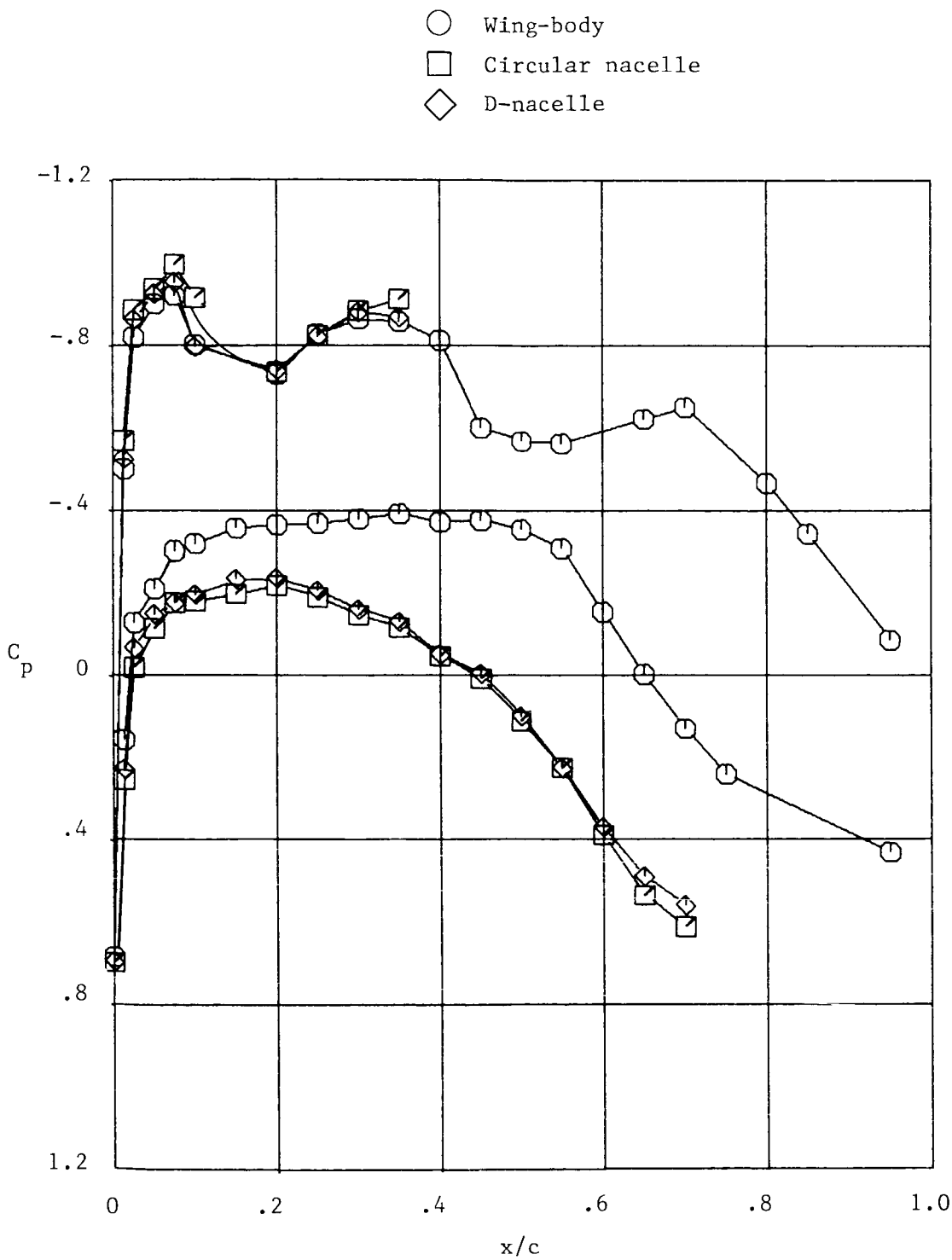

(b) $\eta = 0.370$.

Figure 21.- Continued.

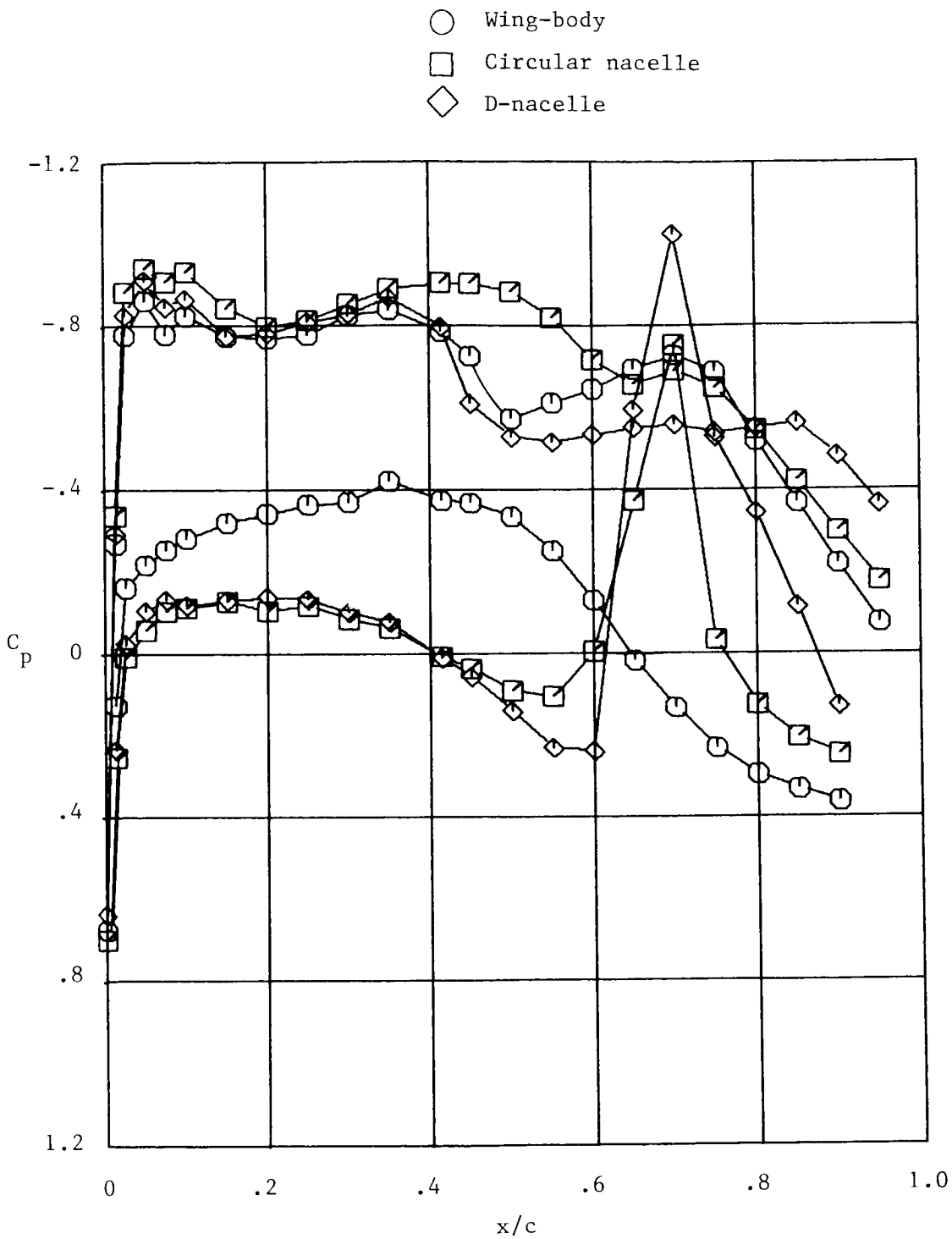

(c) η = 0.440.

Figure 21.- Concluded.

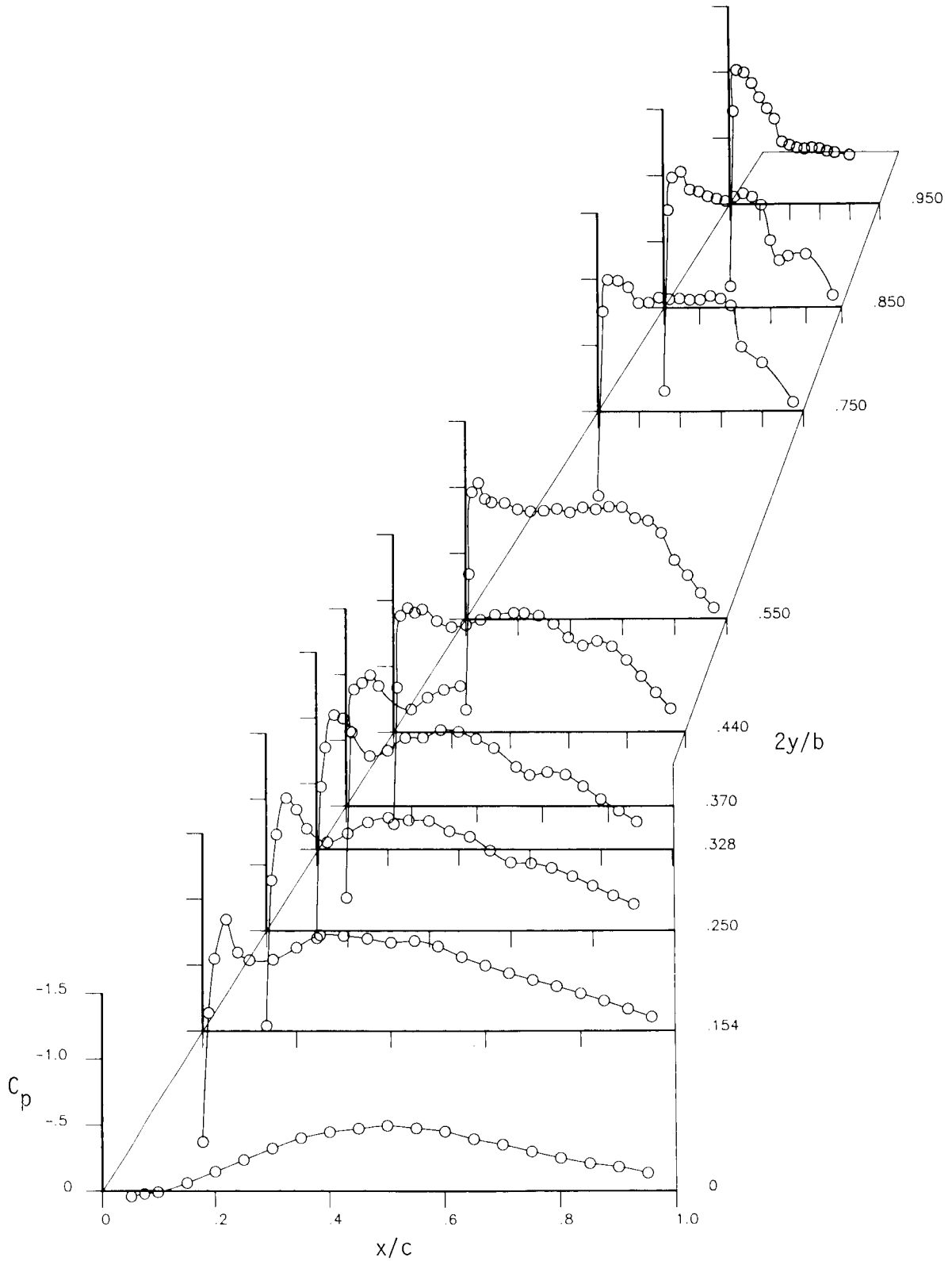

(a) Upper surface.

Figure 22.- Wing pressure-coefficient distribution for circular-nacelle/basic pylon/recessed-diverter configuration at $M_\infty = 0.80$ and $\alpha = 0.8°$.

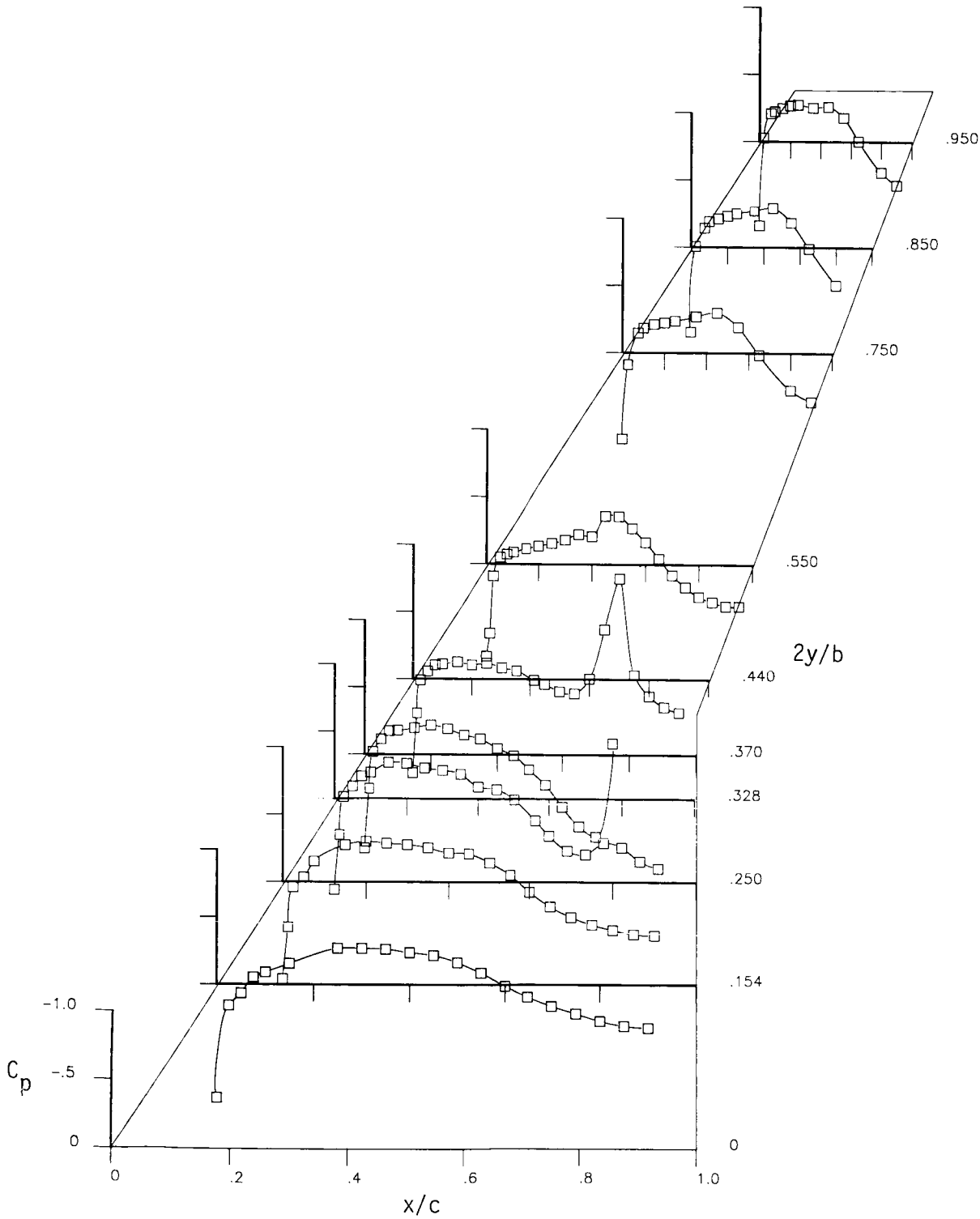

(b) Lower surface.

Figure 22.- Concluded.

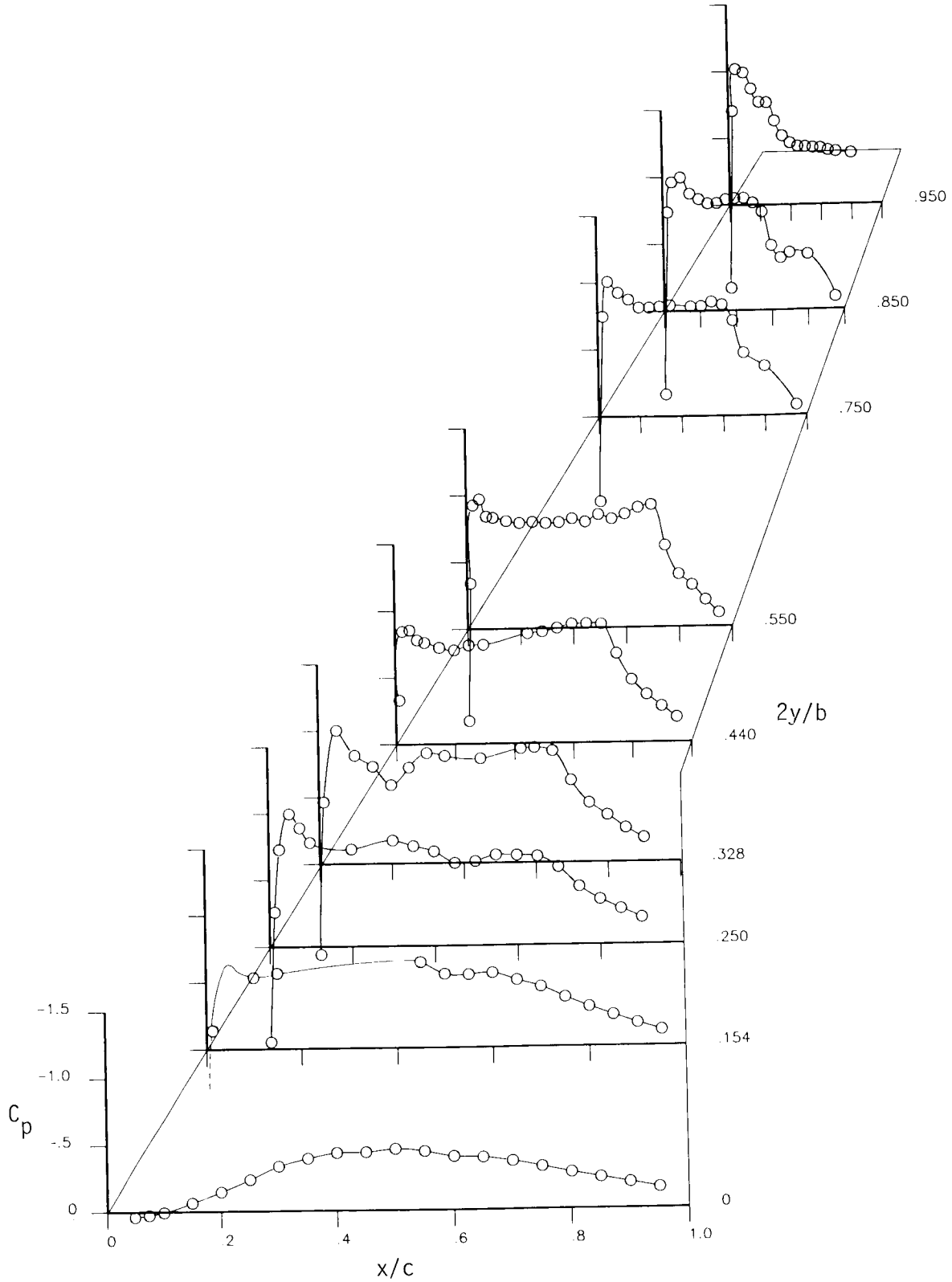

(a) Upper surface.

Figure 23.- Wing pressure-coefficient distributions for circular-nacelle/pressure-pylon/recessed-diverter configuration at $M_\infty = 0.80$ and $\alpha = 0.8°$.

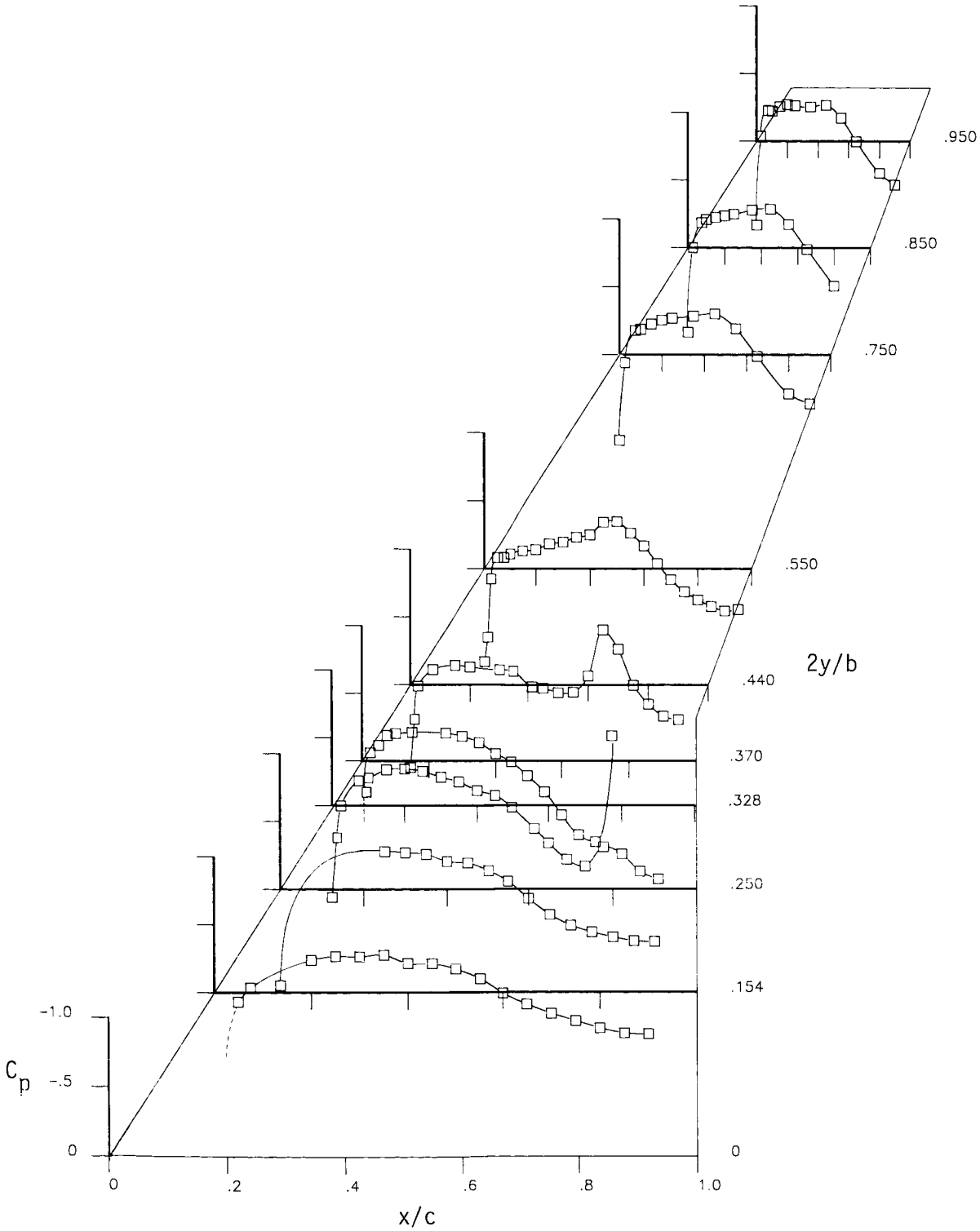

(b) Lower surface.

Figure 23.- Concluded.

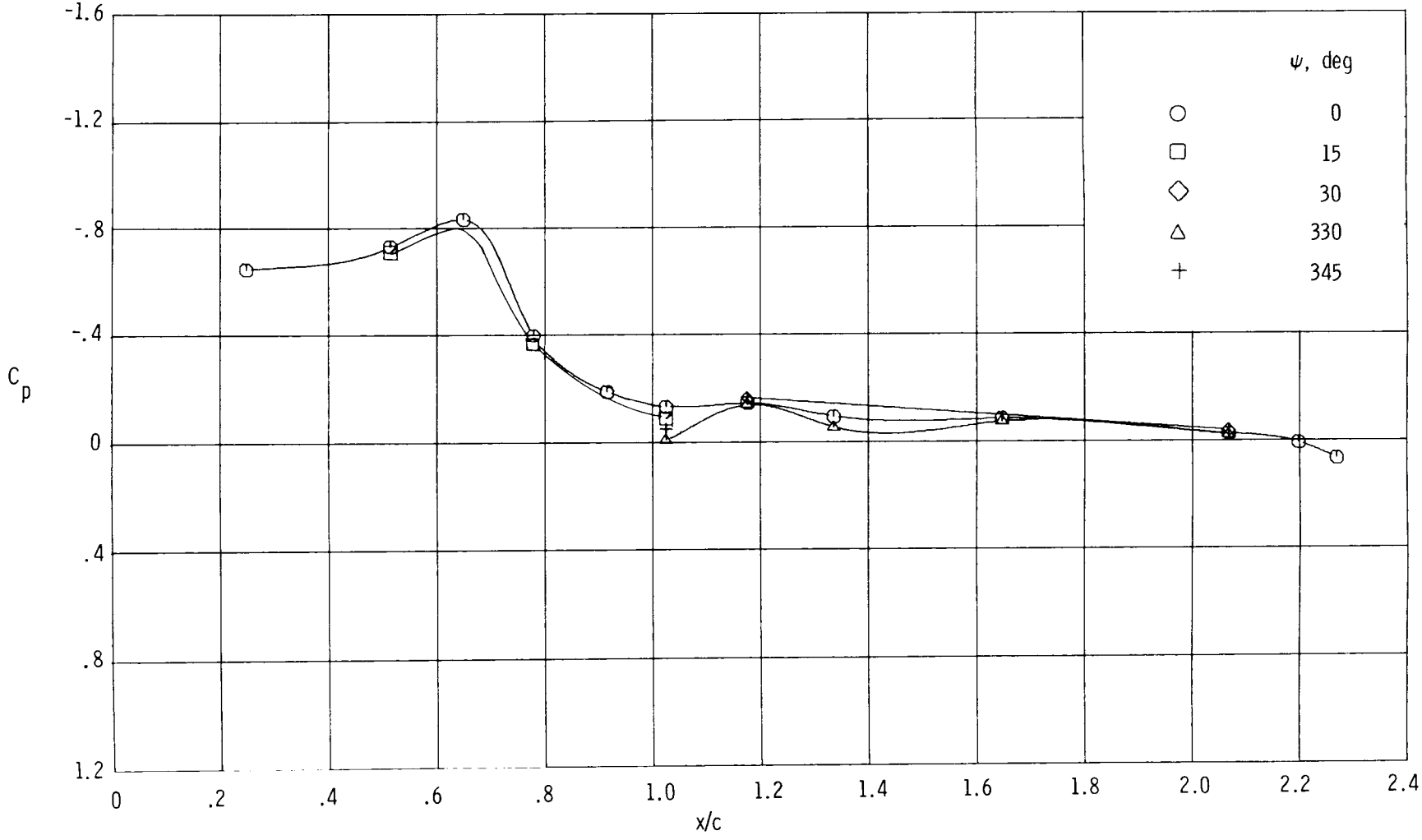

(a) Pylon and upper nacelle.

Figure 24.- Pylon and external-nacelle pressure coefficient distributions for circular-nacelle/pressure-pylon/recessed-diverter configuration at $M_\infty = 0.80$ and $\alpha = 0.8°$.

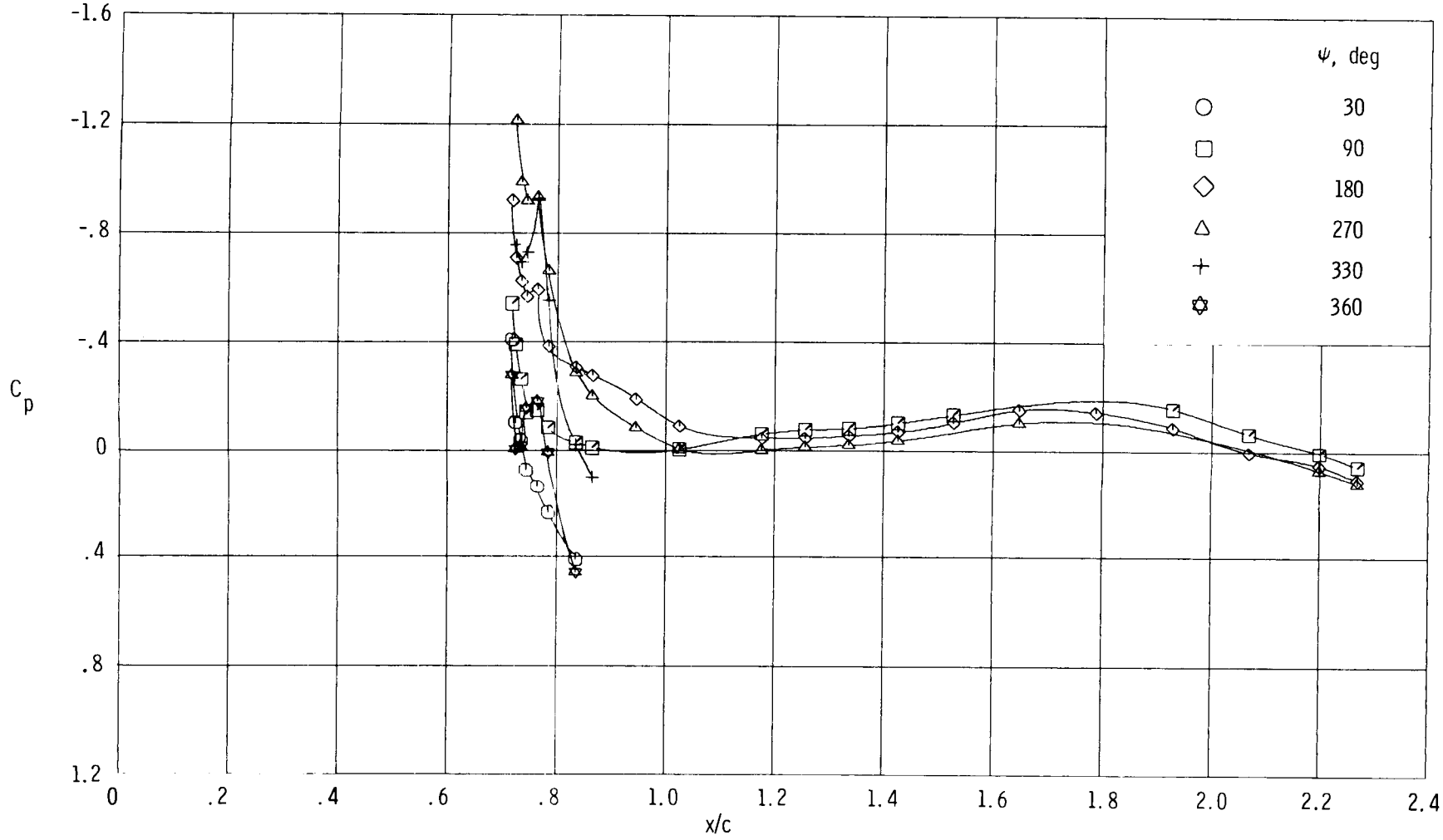

(b) External nacelle.

Figure 24.- Concluded.

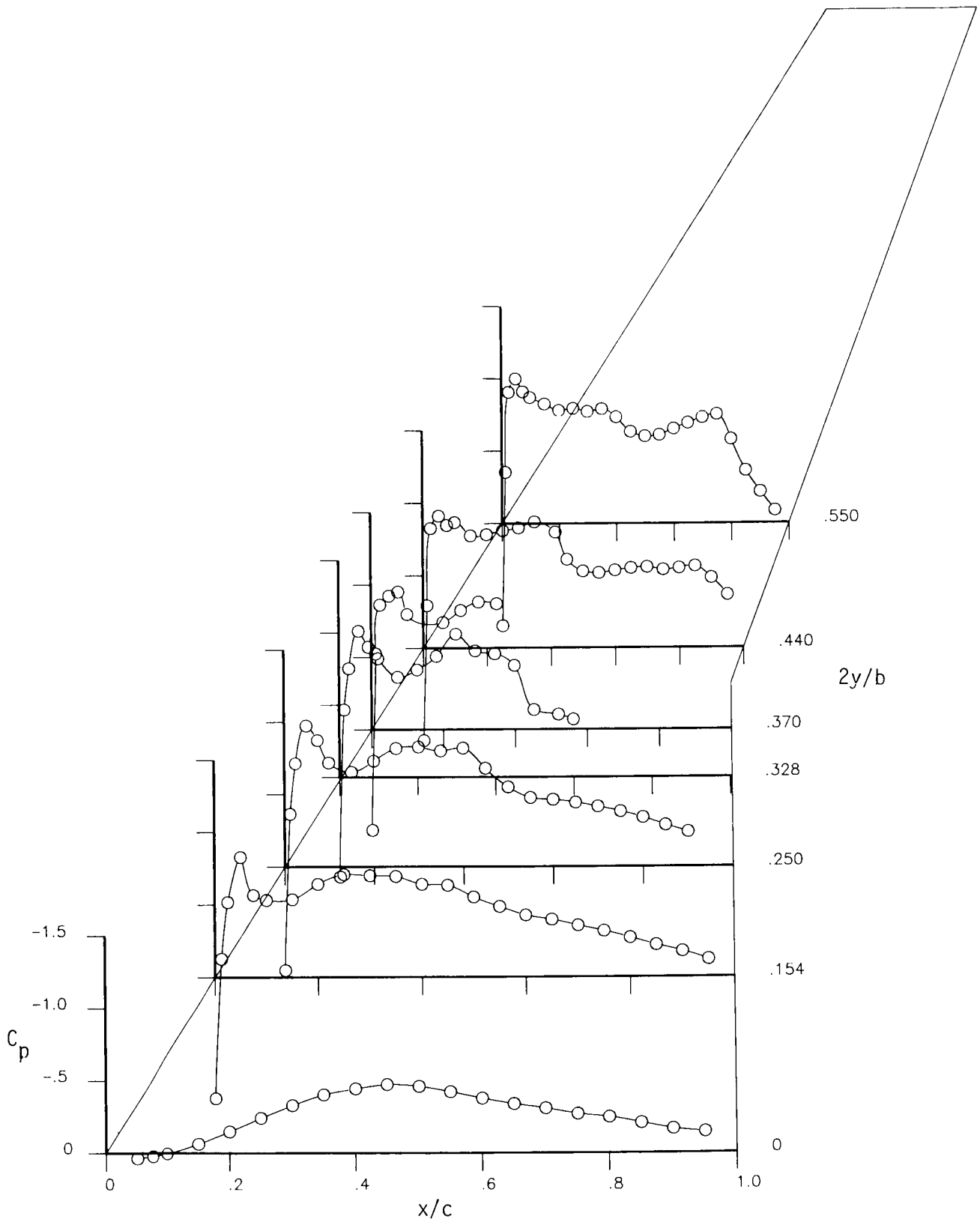

(a) Upper surface.

Figure 25.- Wing pressure-coefficient distribution for D-nacelle/basic-pylon configuration at $M_\infty = 0.80$ and $\alpha = 0.8°$.

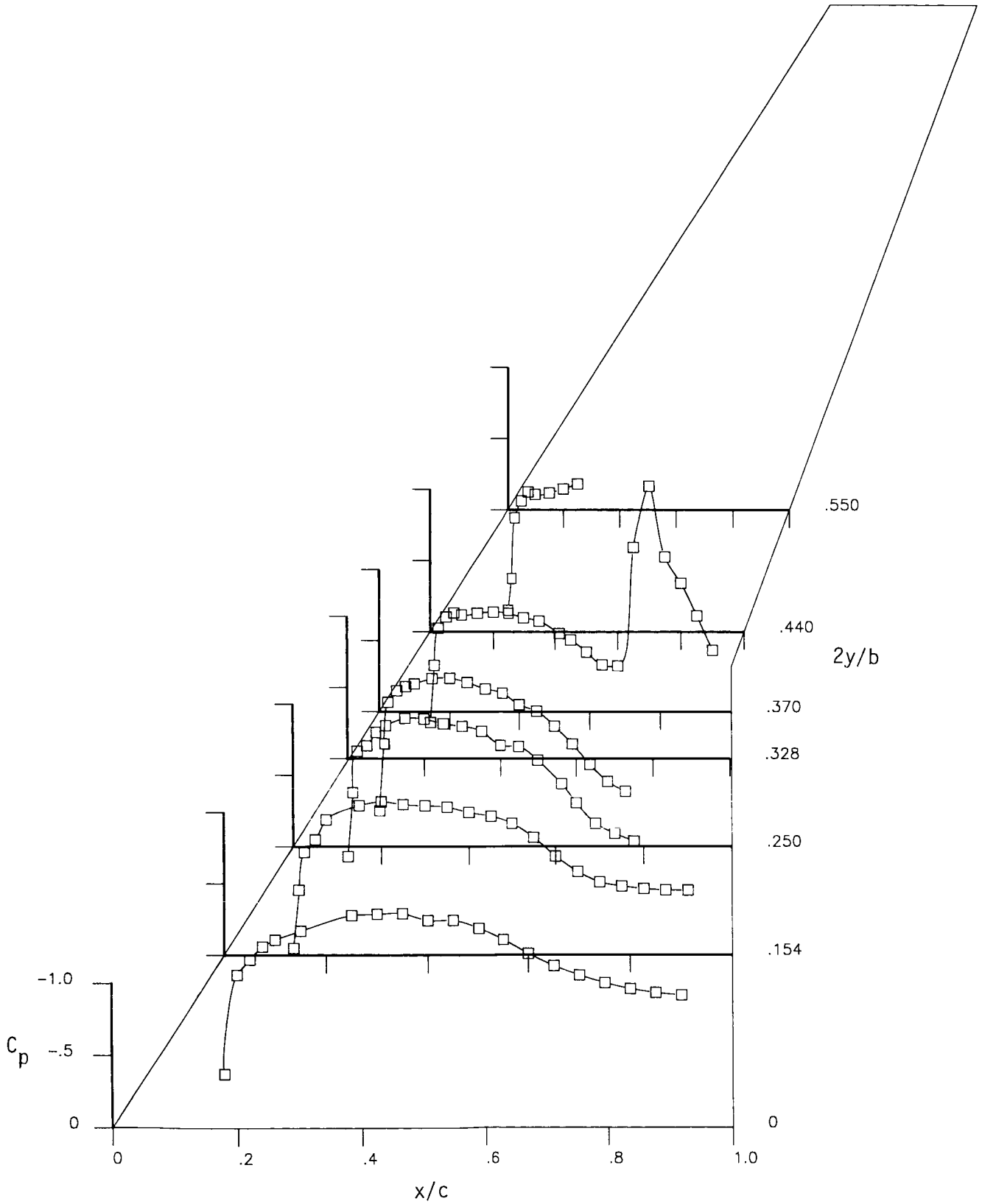

(b) Lower surface.

Figure 25.- Concluded.

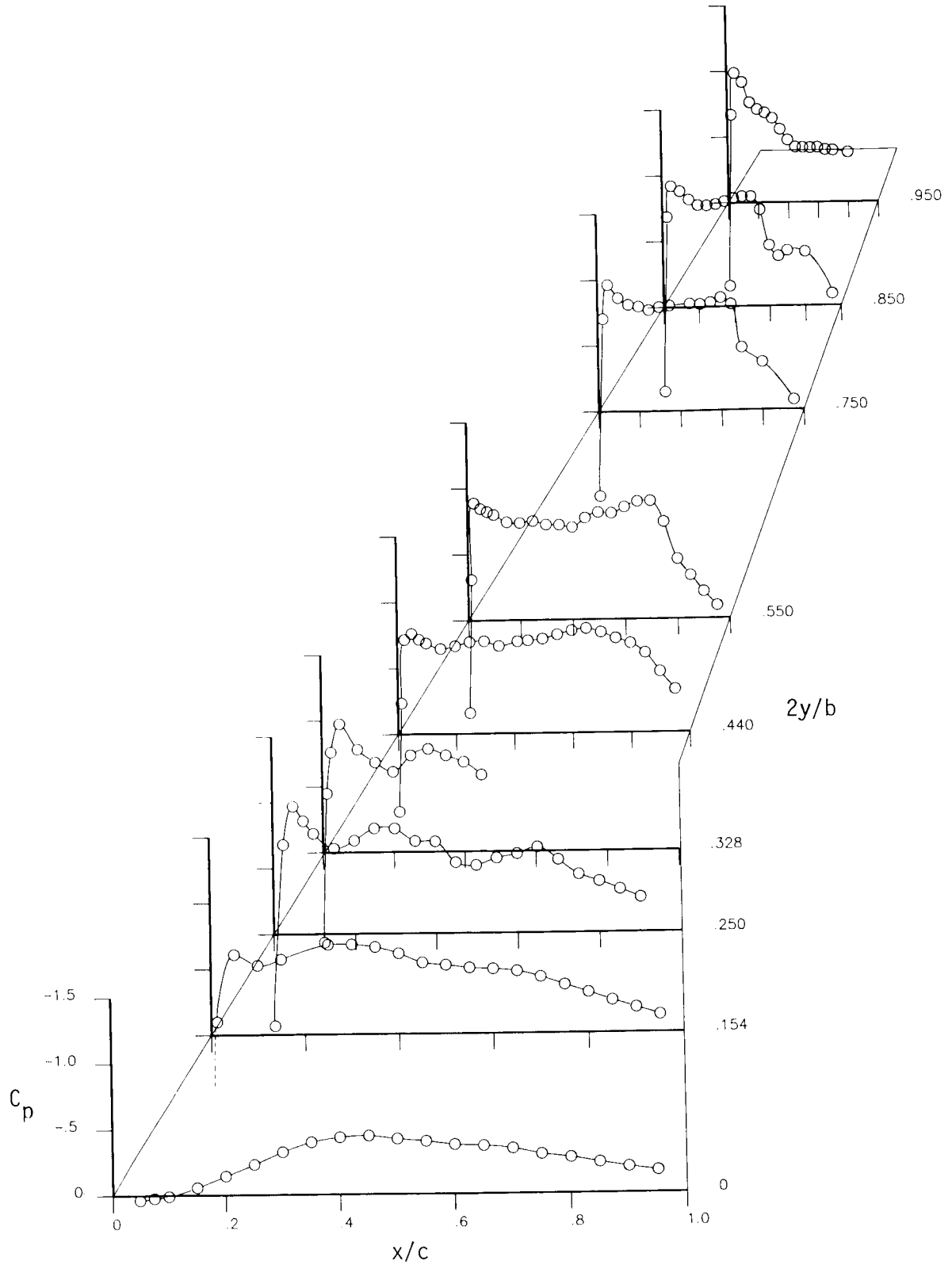

(a) Upper surface.

Figure 26.- Wing pressure-coefficient distributions for D-nacelle/pressure-pylon configuration at $M_\infty = 0.80$ and $\alpha = 0.8°$.

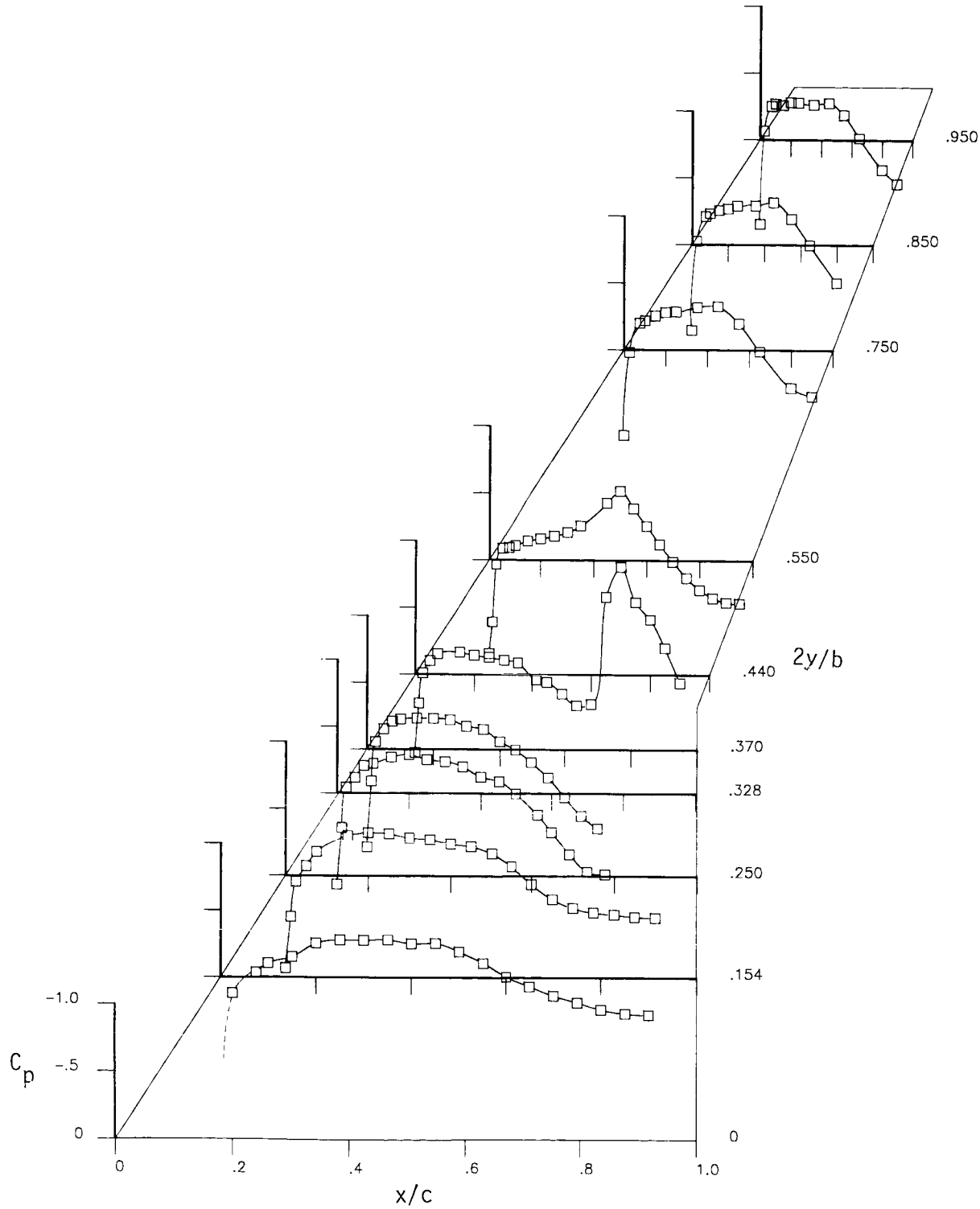

(b) Lower surface.

Figure 26.- Concluded.

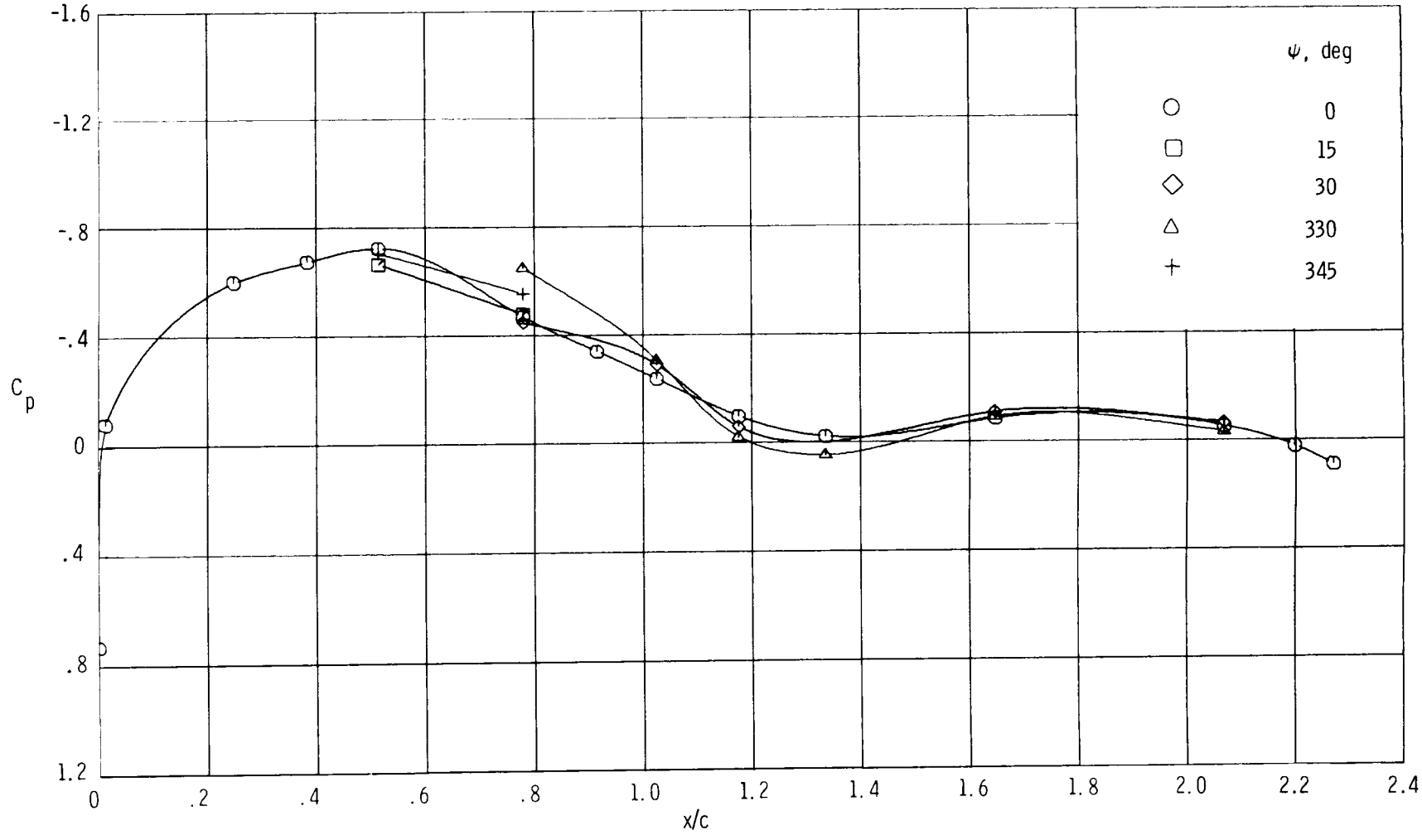

(a) Pylon and upper nacelle.

Figure 27.- Pylon and external-nacelle pressure-coefficient distribution for D-nacelle/pressure-pylon configuration at $M_\infty = 0.80$ and $\alpha = 0.8°$.

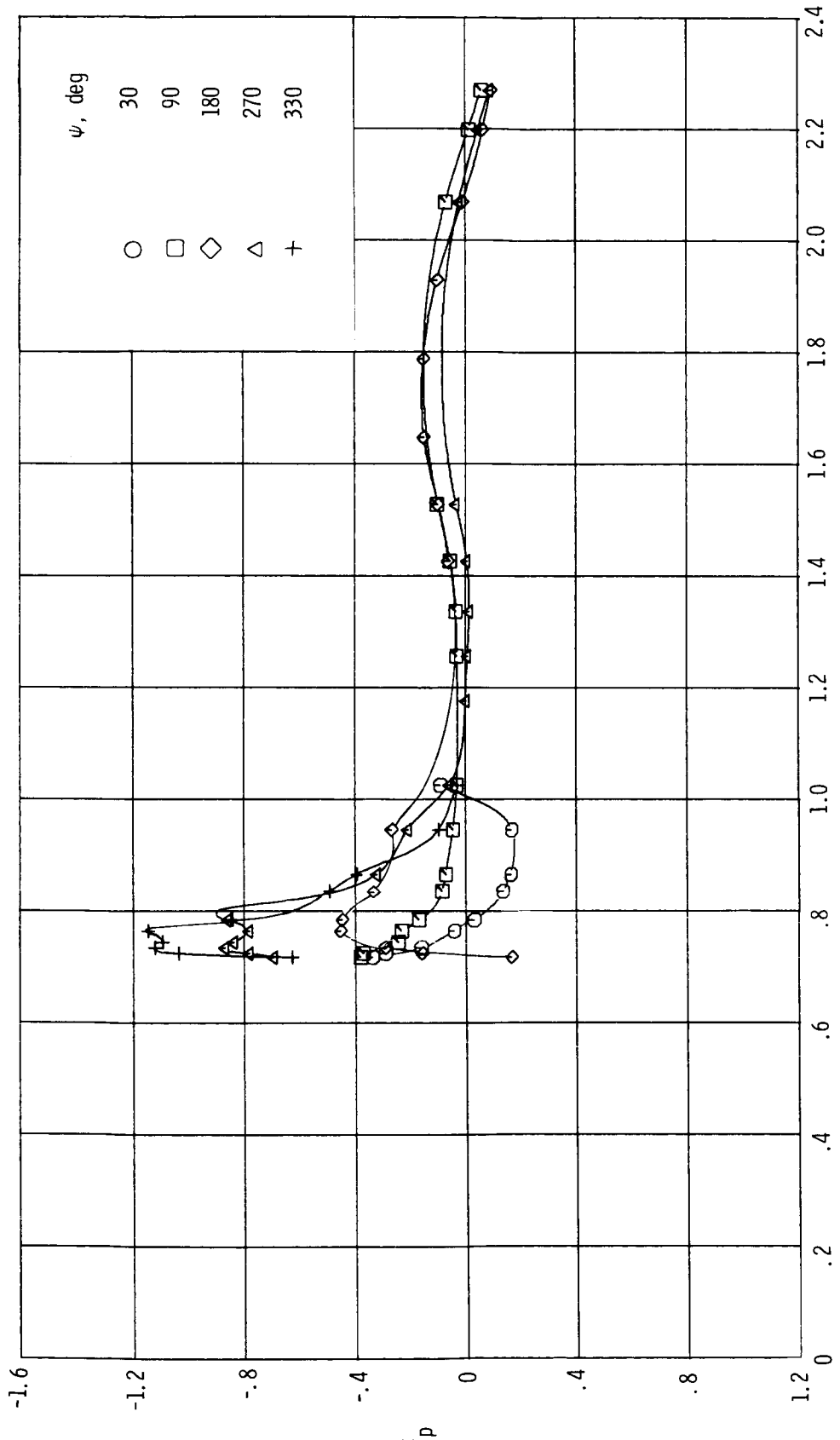

(b) External nacelle.

Figure 27.- Concluded.

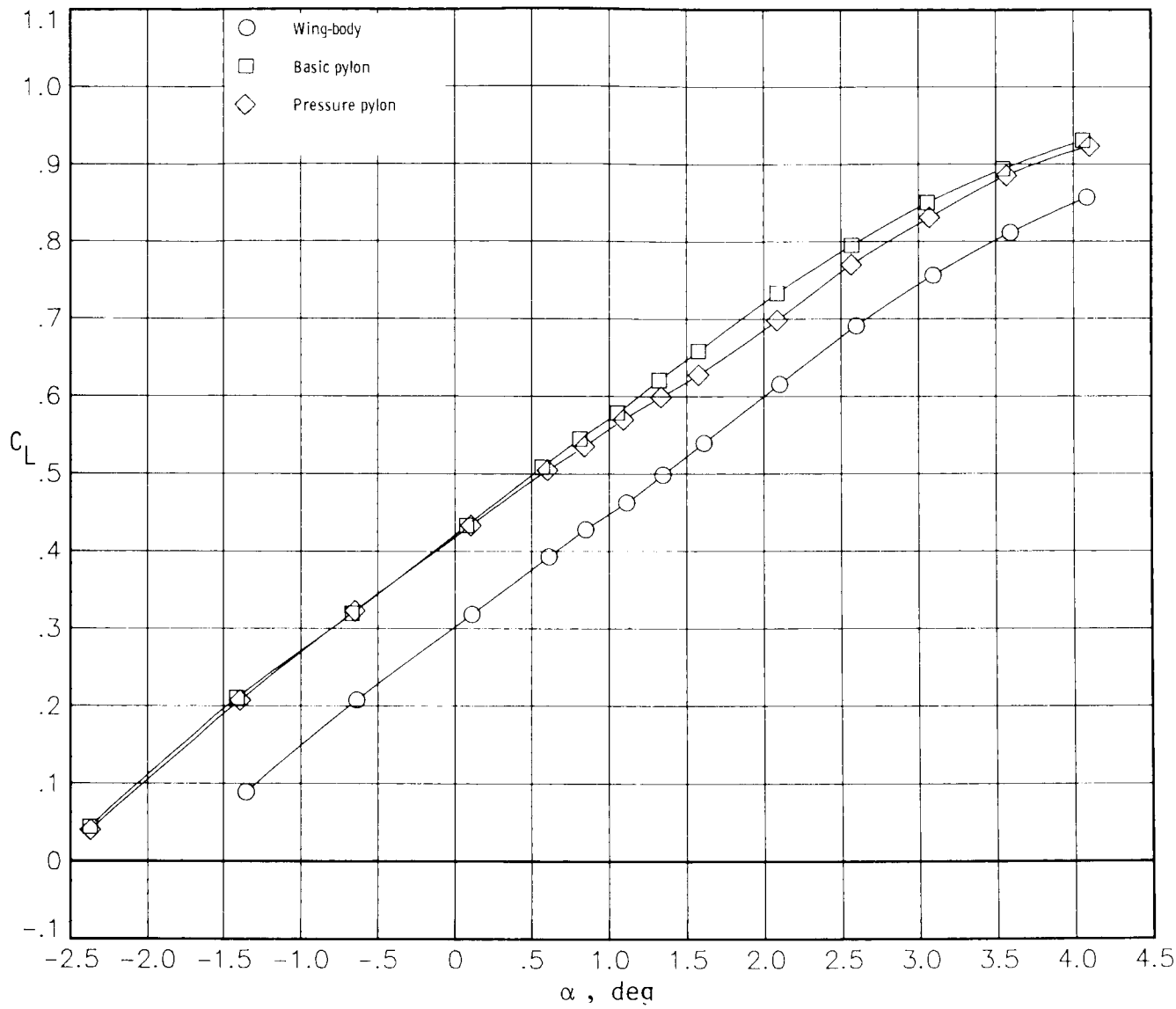

(a) Lift coefficient plotted against angle of attack.

Figure 28.- Comparison of longitudinal characteristics at $M_\infty = 0.80$ for underwing aft-mounted circular-nacelle/recessed-diverter configurations with basic and pressure pylons.

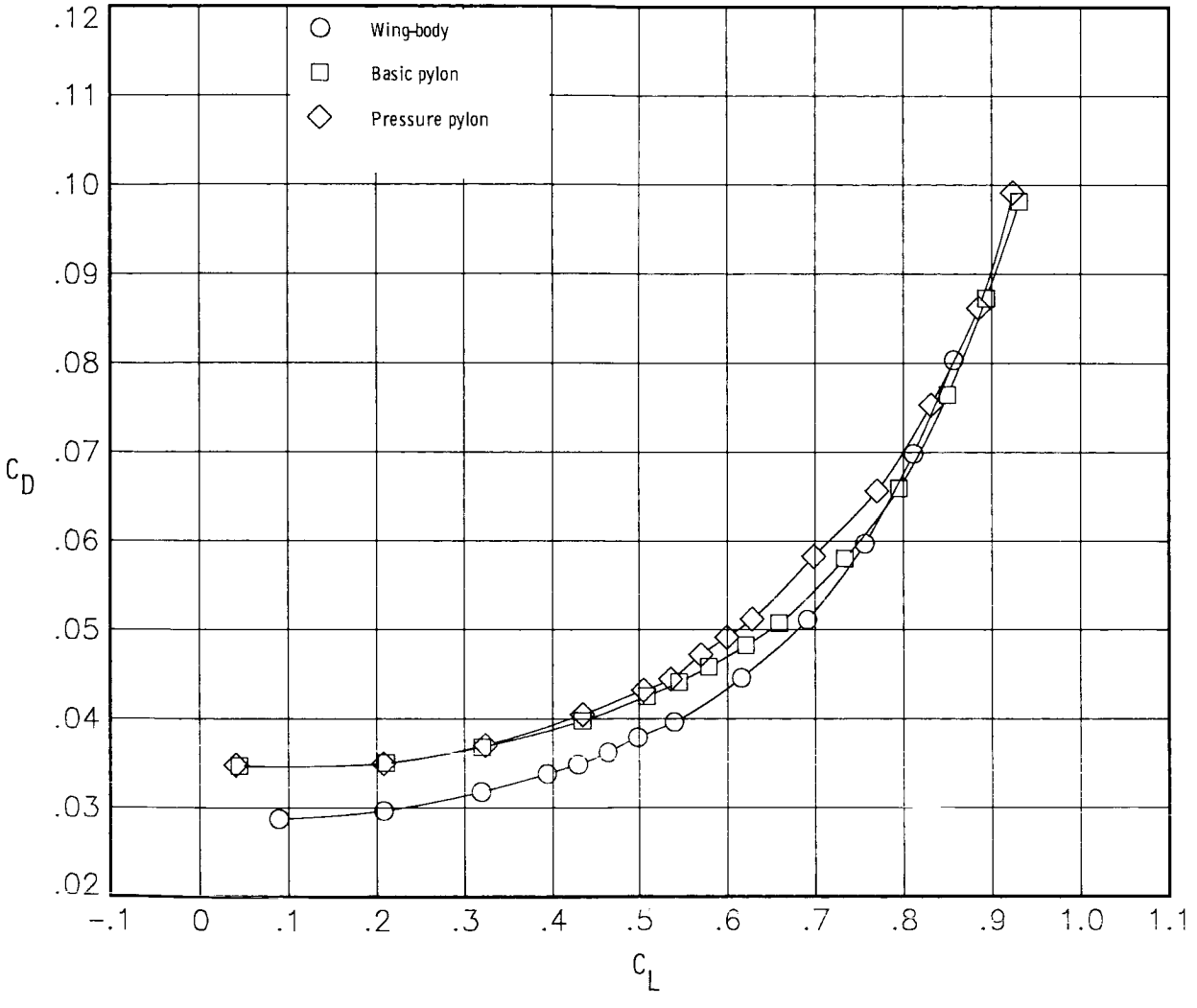

(b) Drag polar.

Figure 28.- Continued.

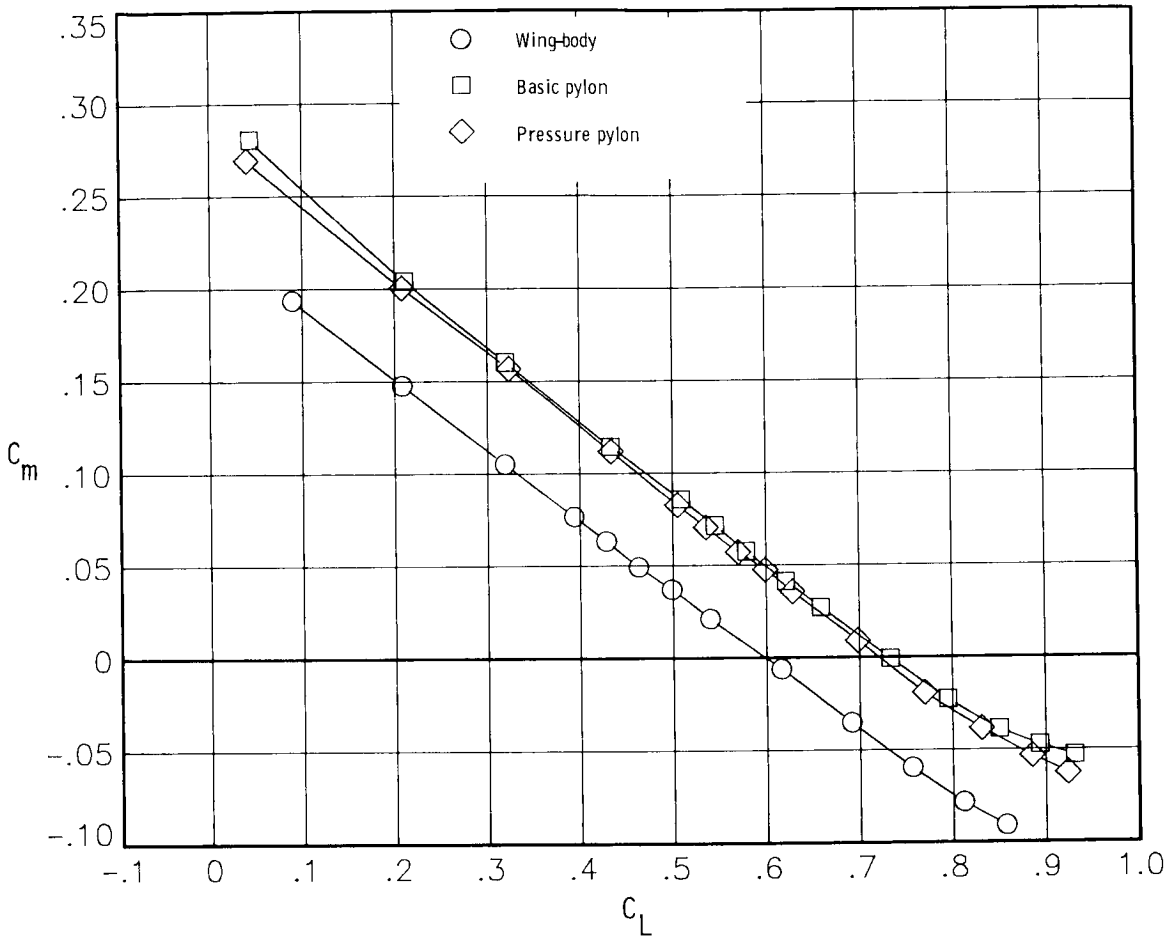

(c) Pitching-moment coefficient plotted against lift coefficient.

Figure 28.- Concluded.

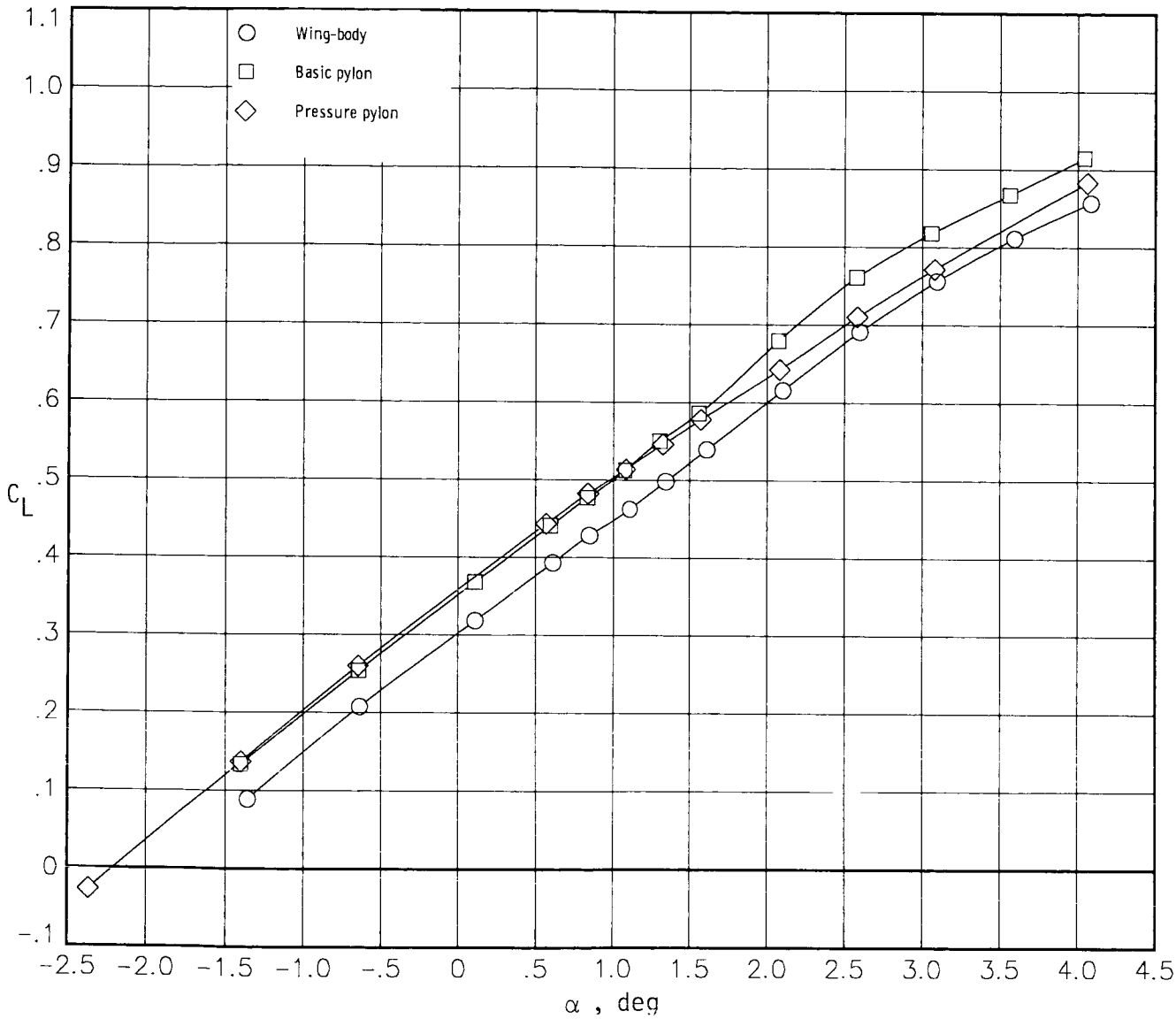

(a) Lift coefficient plotted against angle of attack.

Figure 29.- Comparison of longitudinal characteristics at $M_\infty = 0.80$ for underwing aft-mounted D-nacelle configurations with basic and pressure pylons.

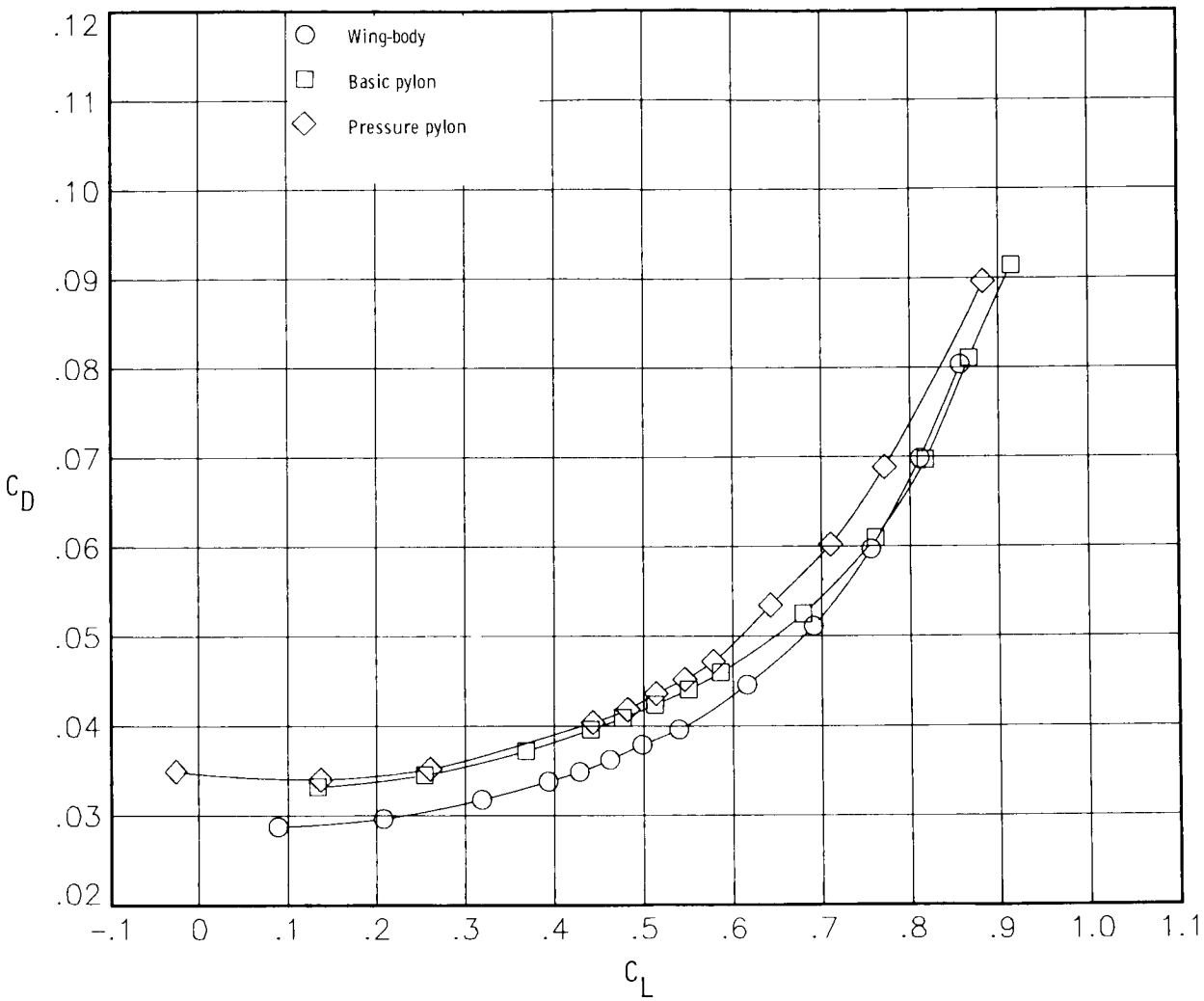

(b) Drag polar.

Figure 29.- Continued.

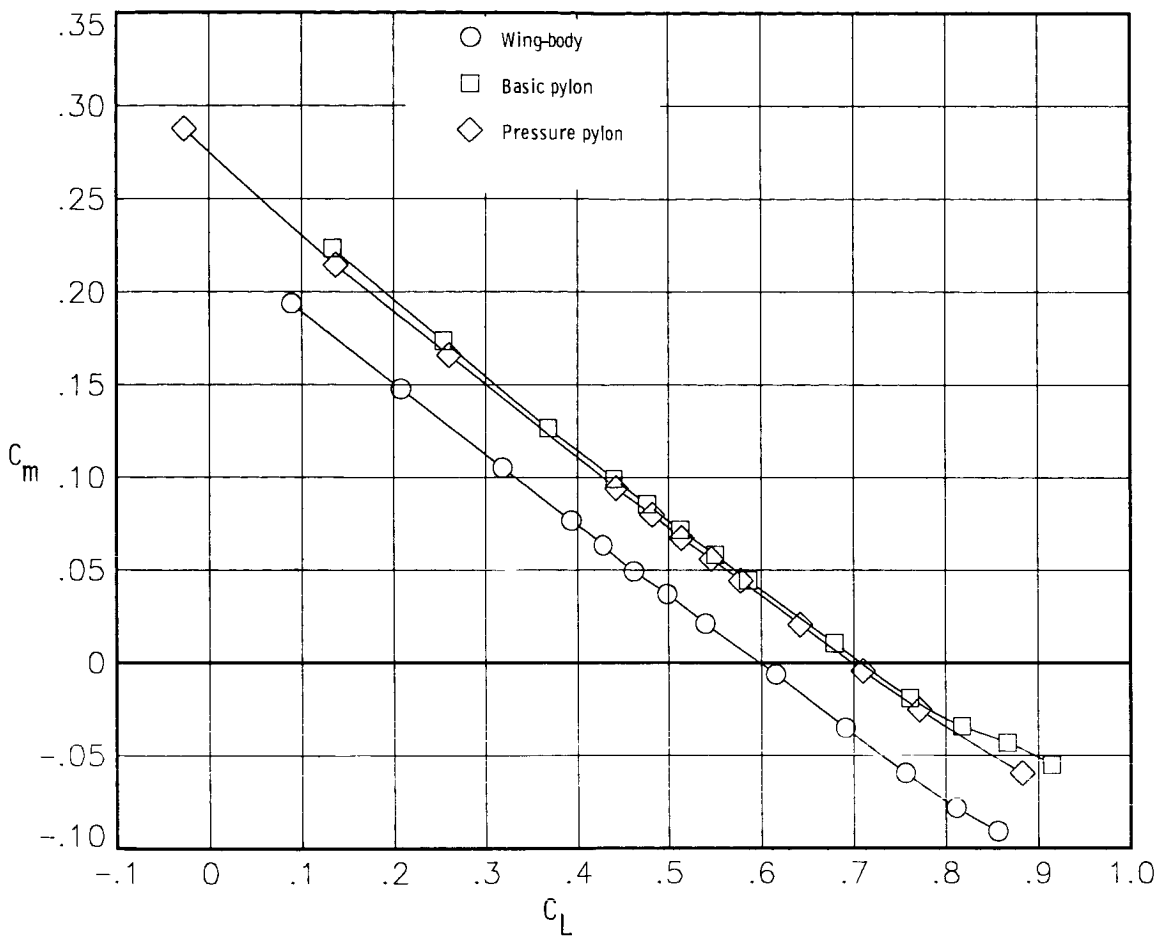

(c) Pitching-moment coefficient plotted against lift coefficient.

Figure 29.- Concluded.

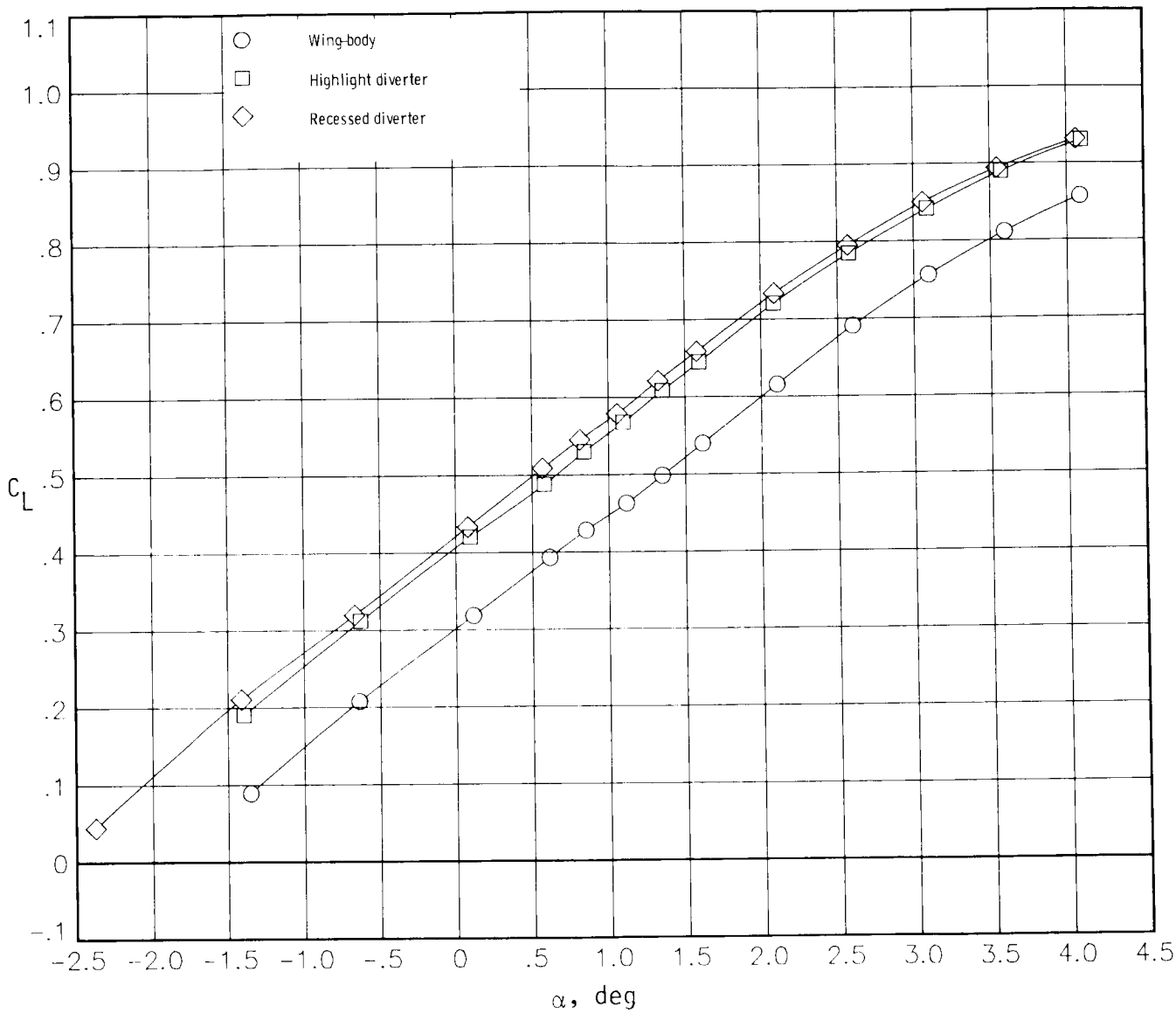

(a) Lift coefficient plotted against angle of attack.

Figure 30.- Comparison of longitudinal characteristics at $M_\infty = 0.80$ for underwing aft-mounted circular-nacelle/basic-pylon configurations with highlight and recessed diverters.

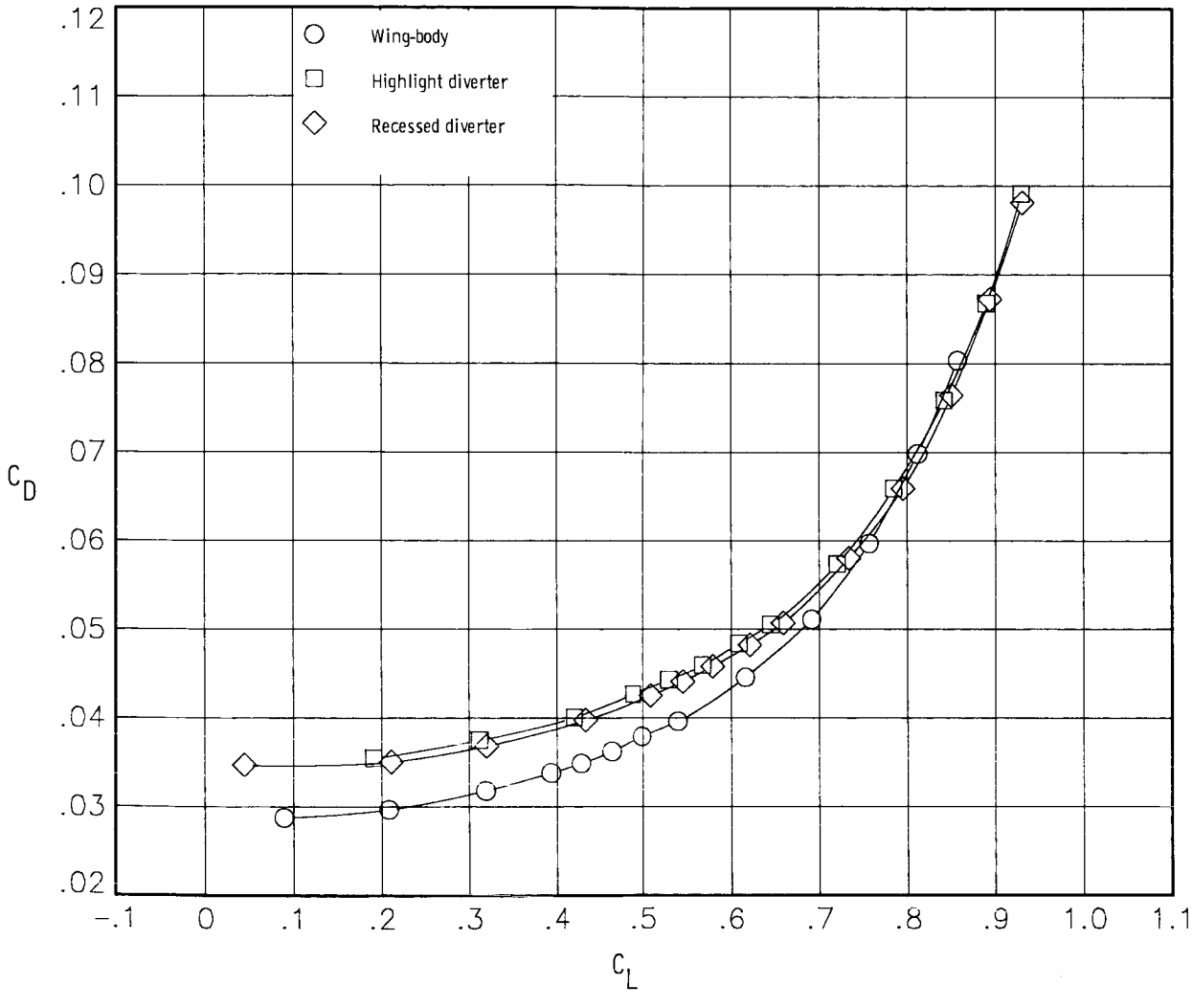

(b) Drag polar.

Figure 30.- Continued.

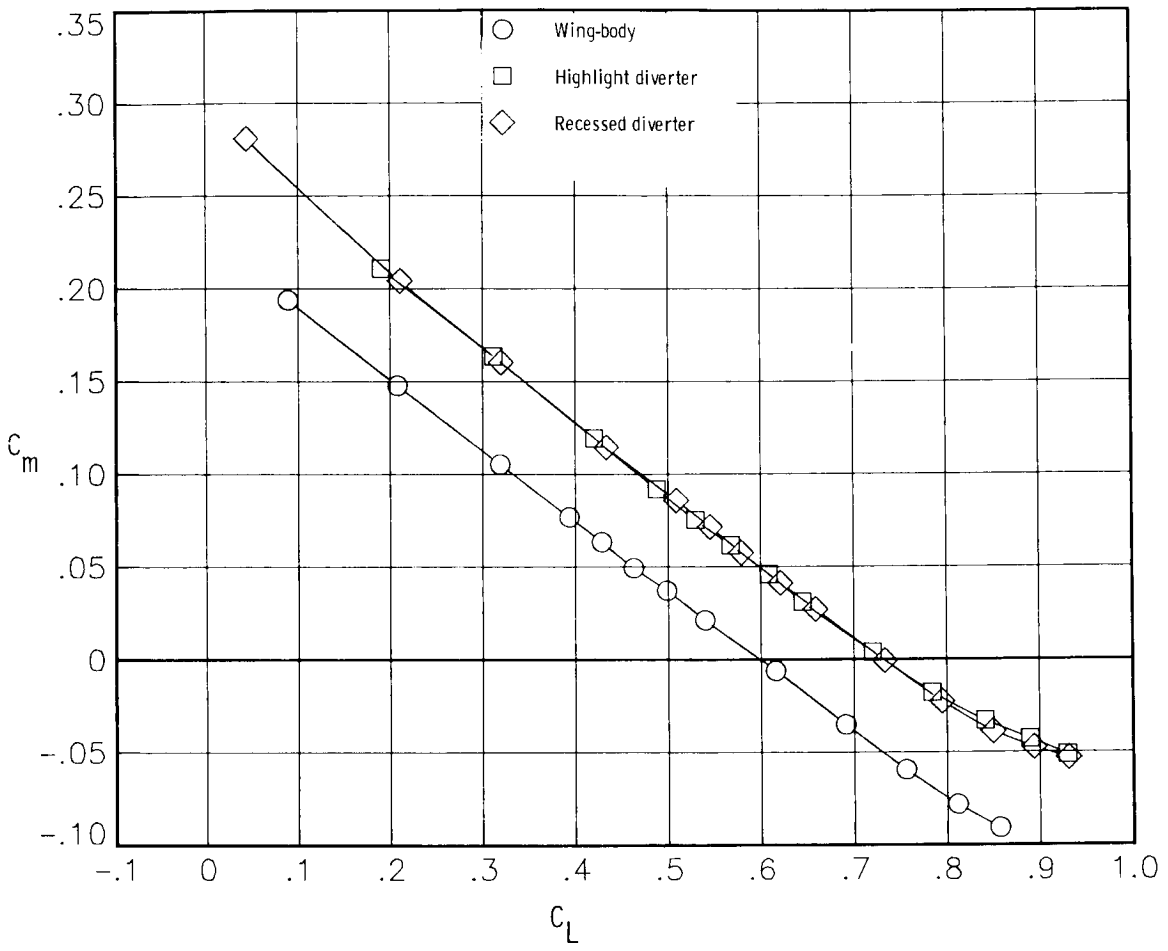

(c) Pitching-moment coefficient plotted against lift coefficient.

Figure 30.- Concluded.

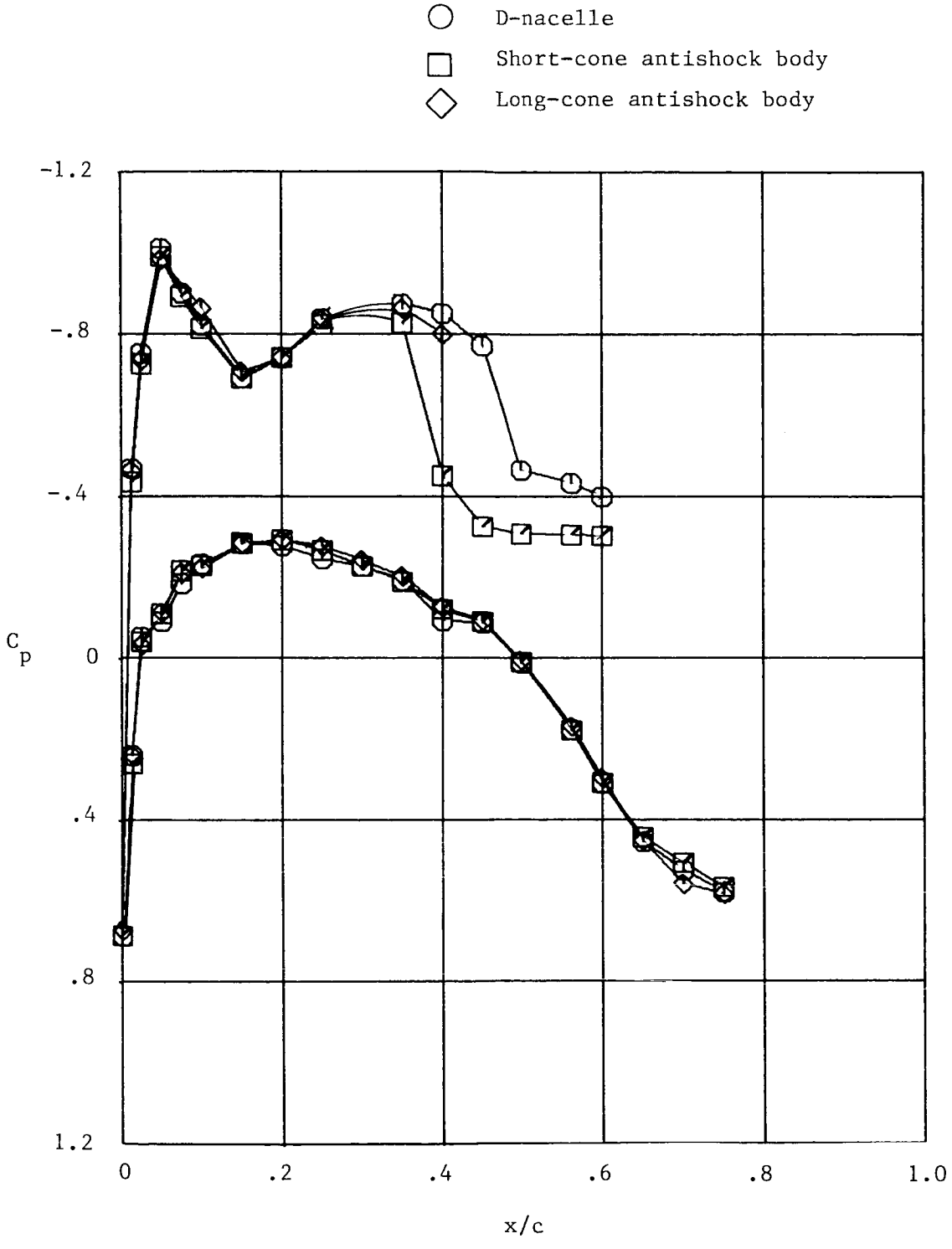

(a) $\eta = 0.328$.

Figure 31.- Effect of antishock bodies on wing pressure-coefficient distributions at $M_\infty = 0.80$.

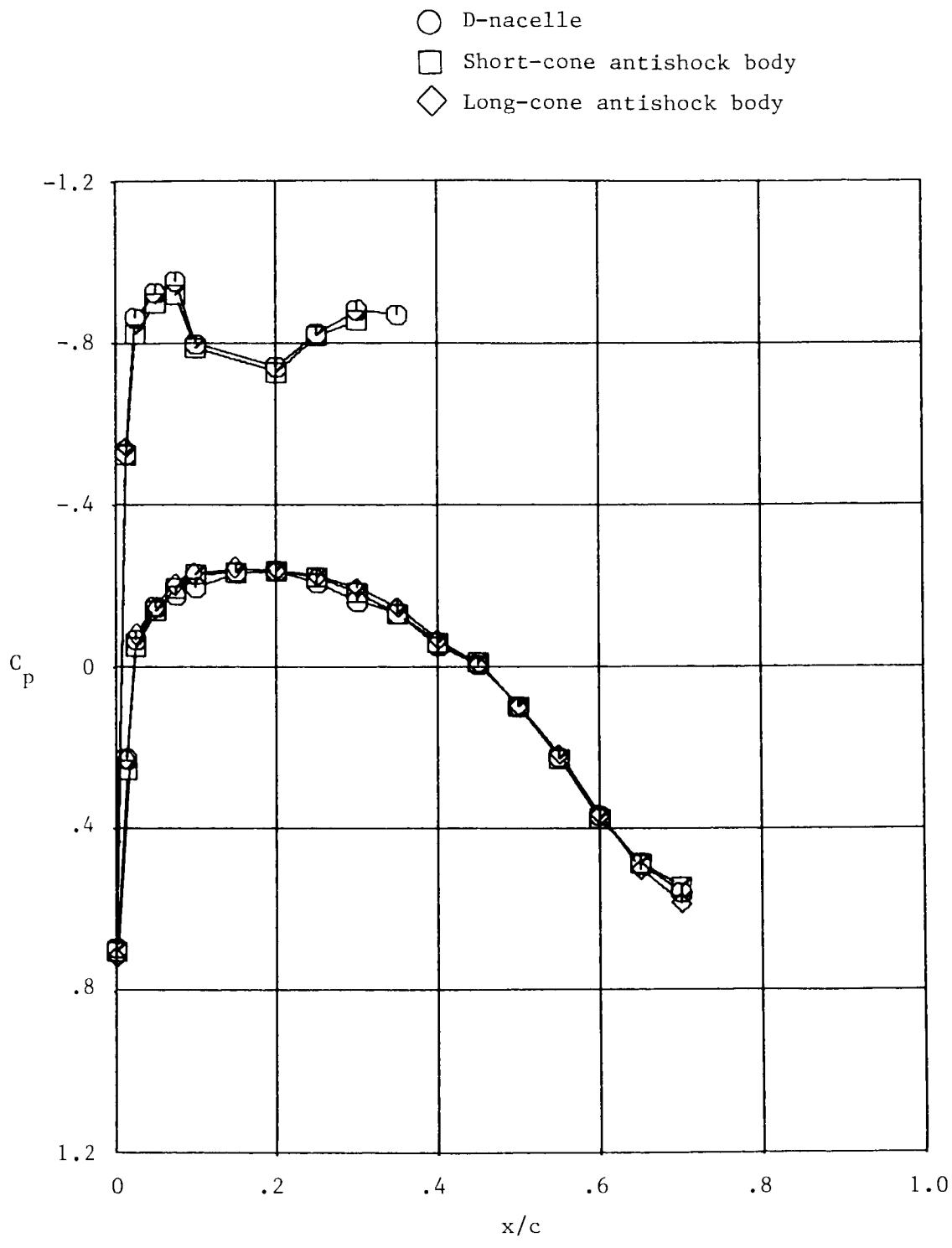

(b) $\eta = 0.370$.

Figure 31.- Continued.

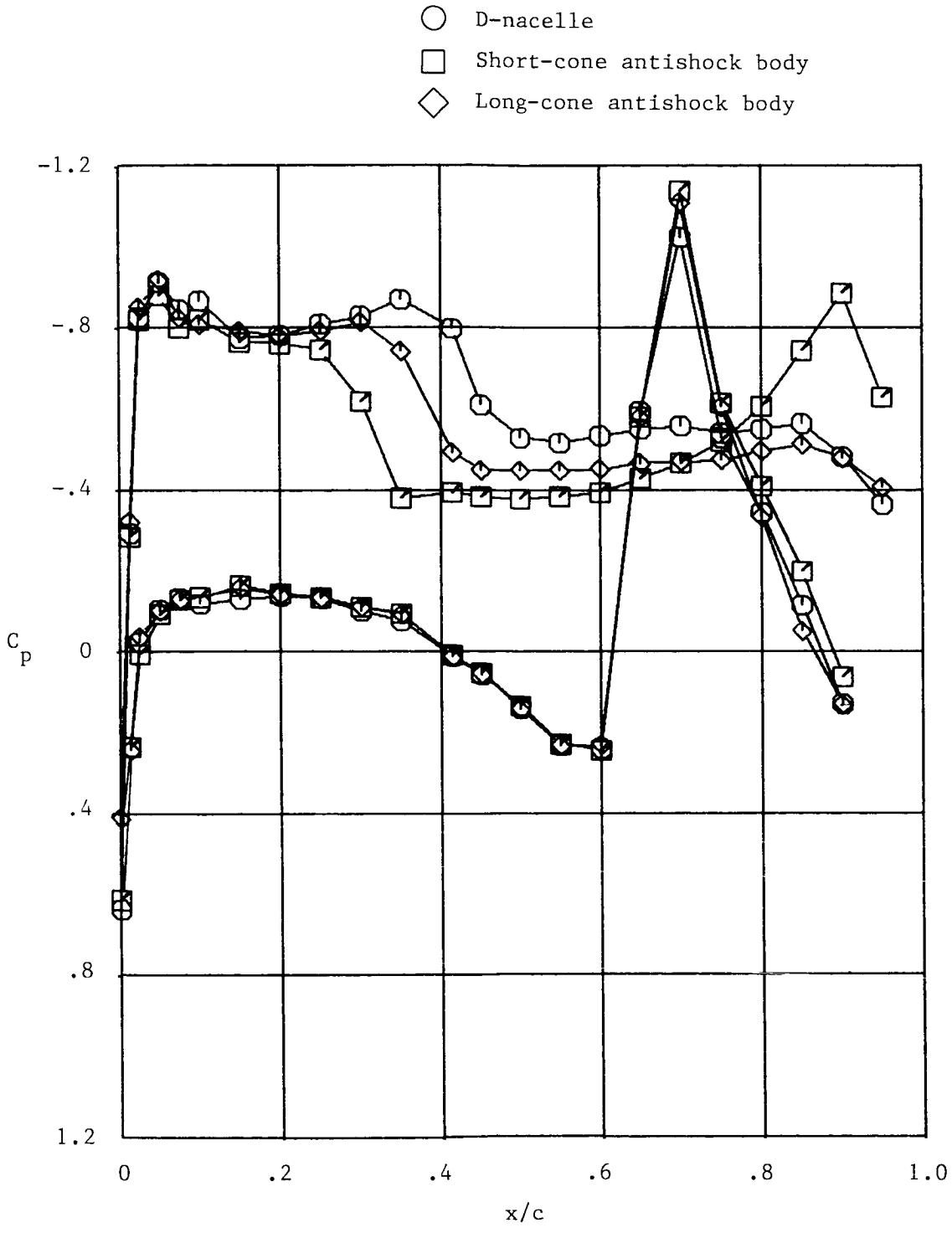

(c) η = 0.440.

Figure 31.- Concluded.

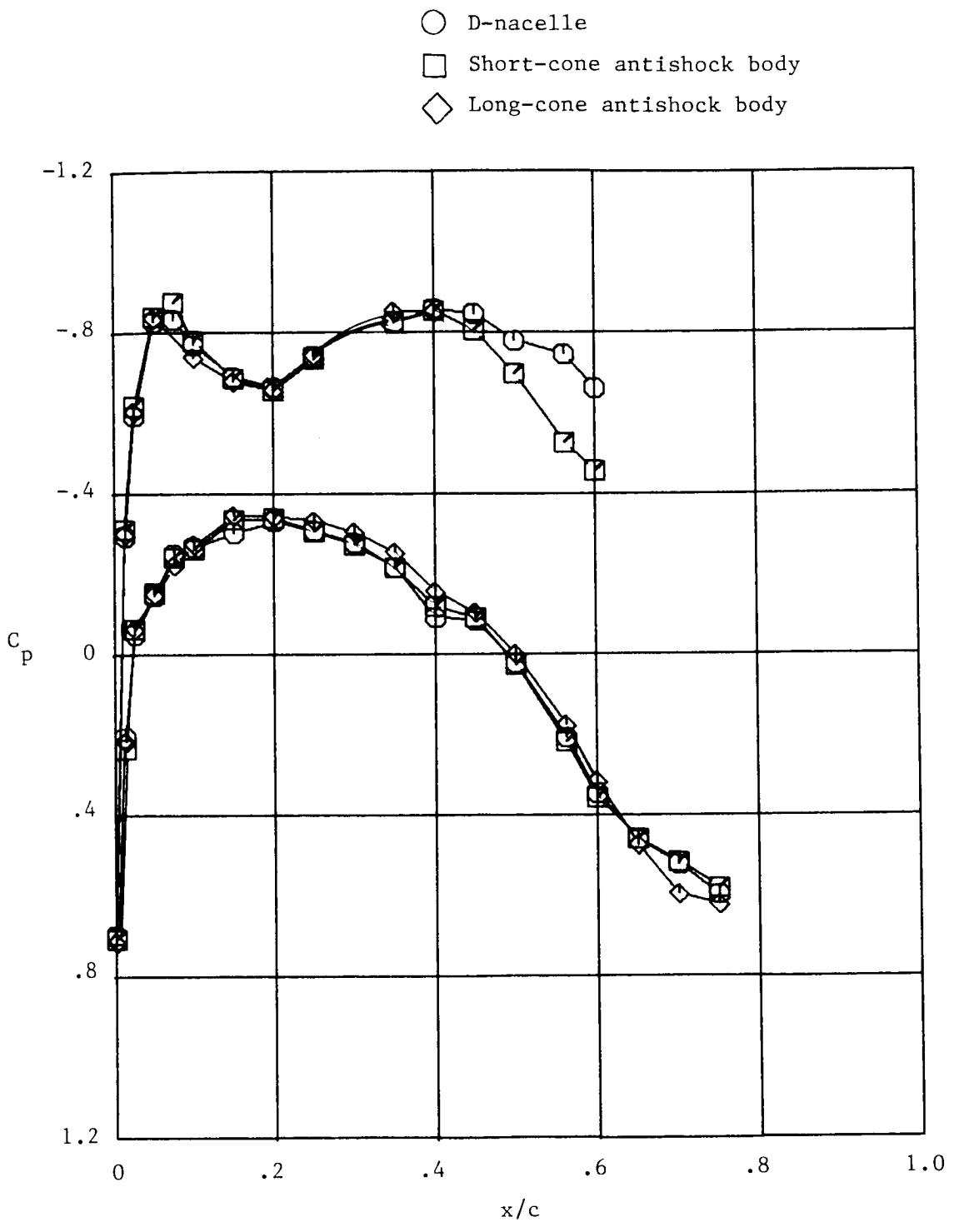

(a) η = 0.328.

Figure 32.- Effect of antishock bodies on wing pressure-coefficient distributions at M_∞ = 0.85.

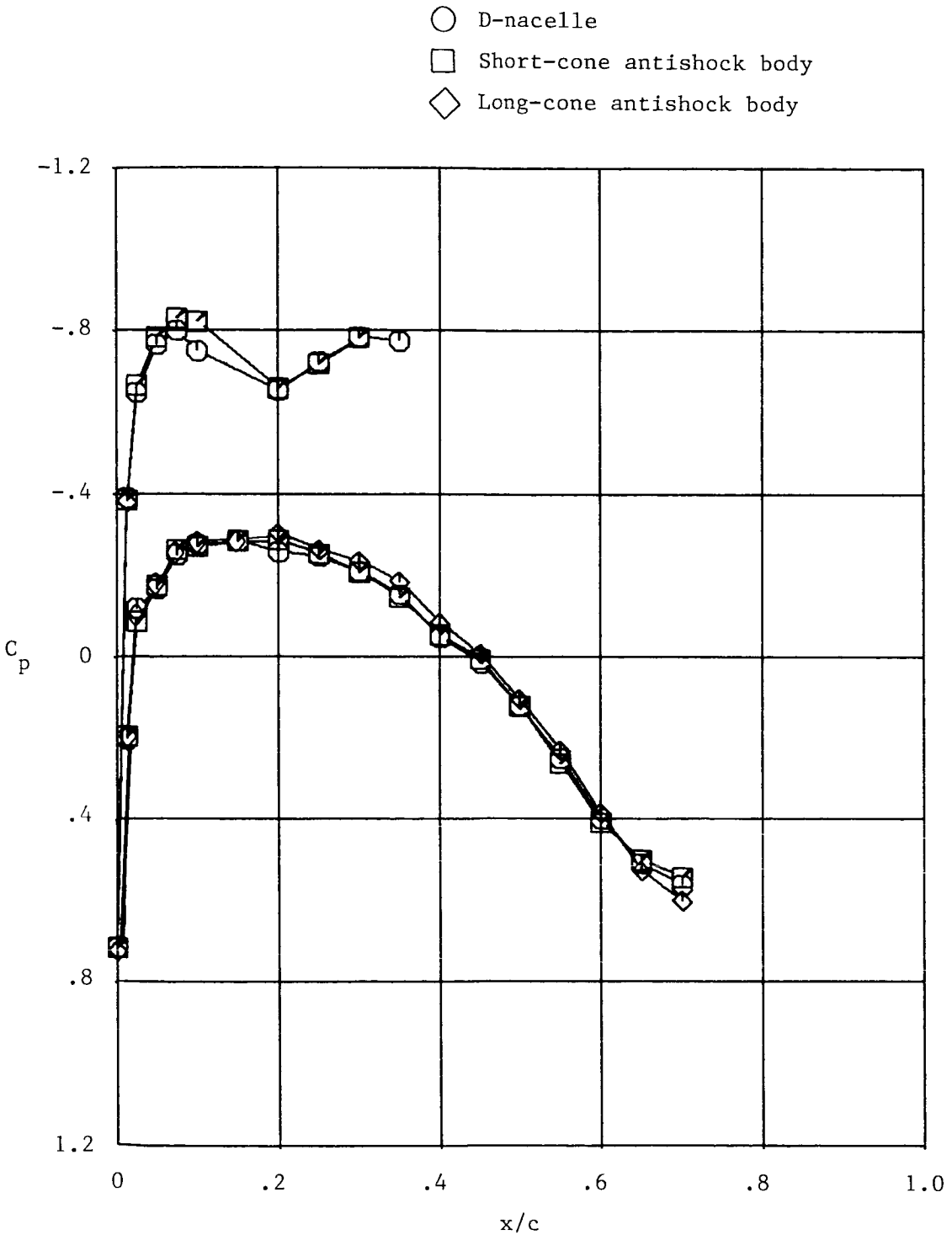

(b) $\eta = 0.370$.

Figure 32.- Continued.

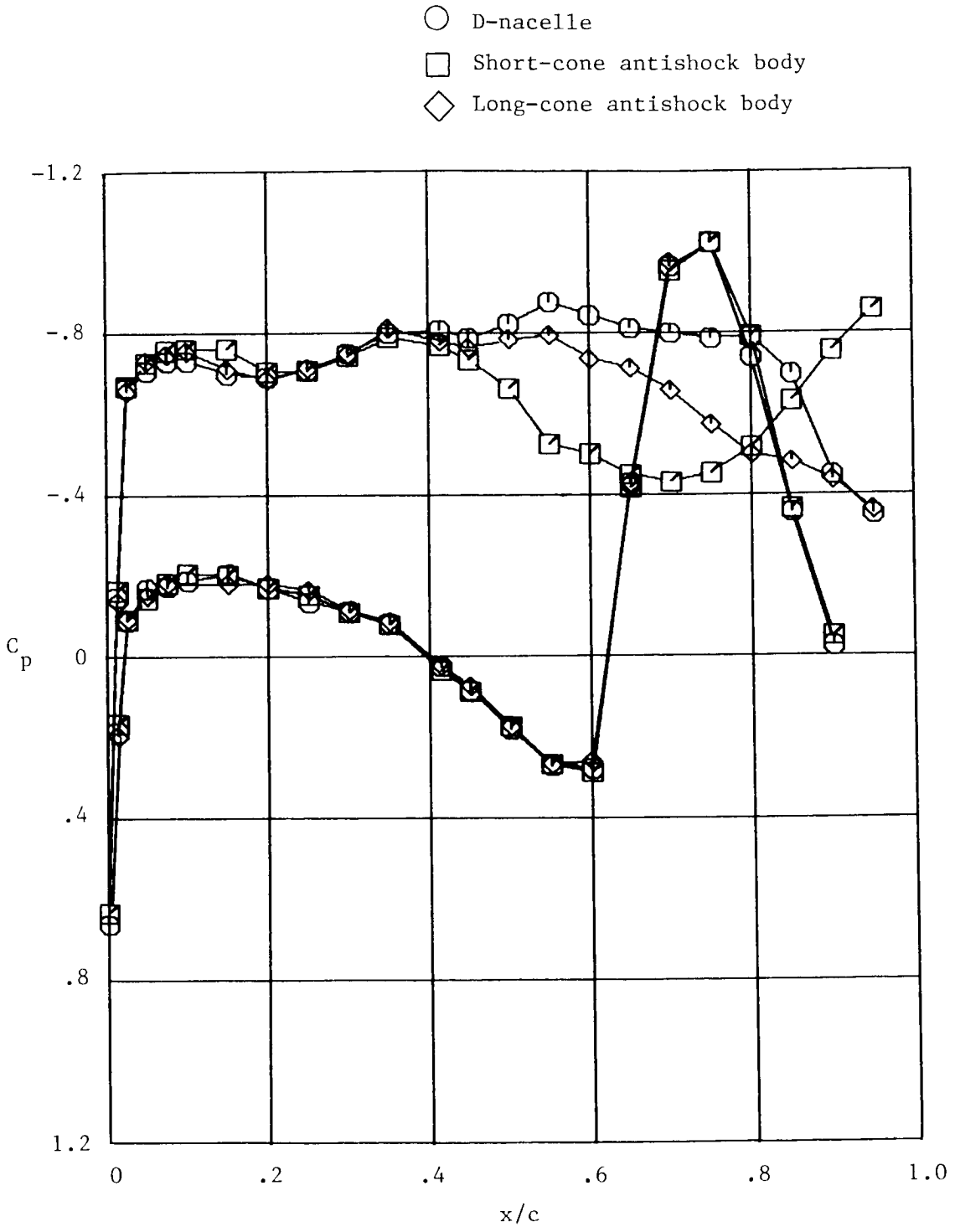

(c) η = 0.440.

Figure 32.- Concluded.

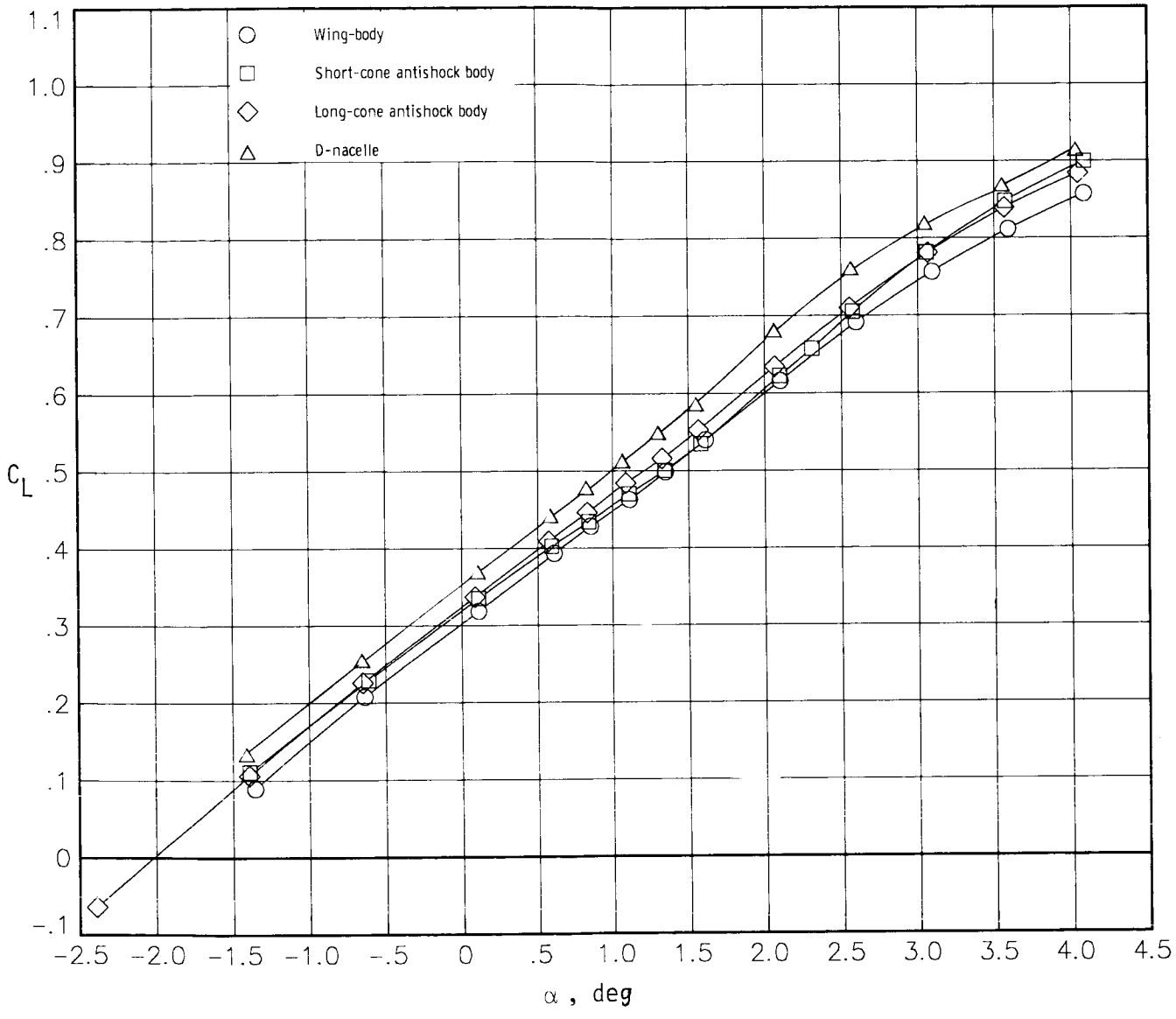

(a) Lift coefficient plotted against angle of attack.

Figure 33.- Comparison of longitudinal characteristics at $M_\infty = 0.80$ for underwing aft-mounted D-nacelle/basic-pylon configuration with short-cone and long-cone antishock bodies.

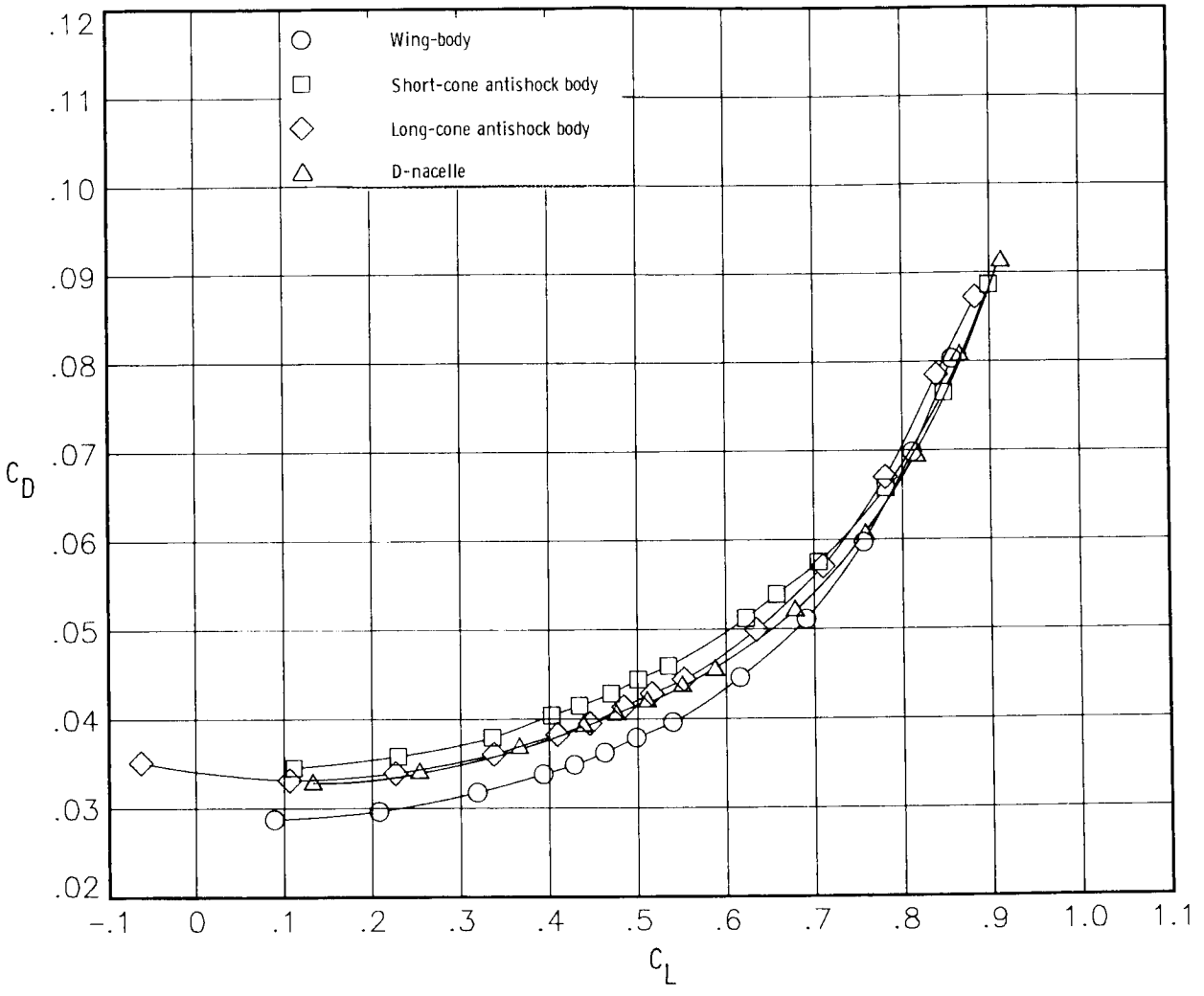

(b) Drag polar.

Figure 33.- Continued.

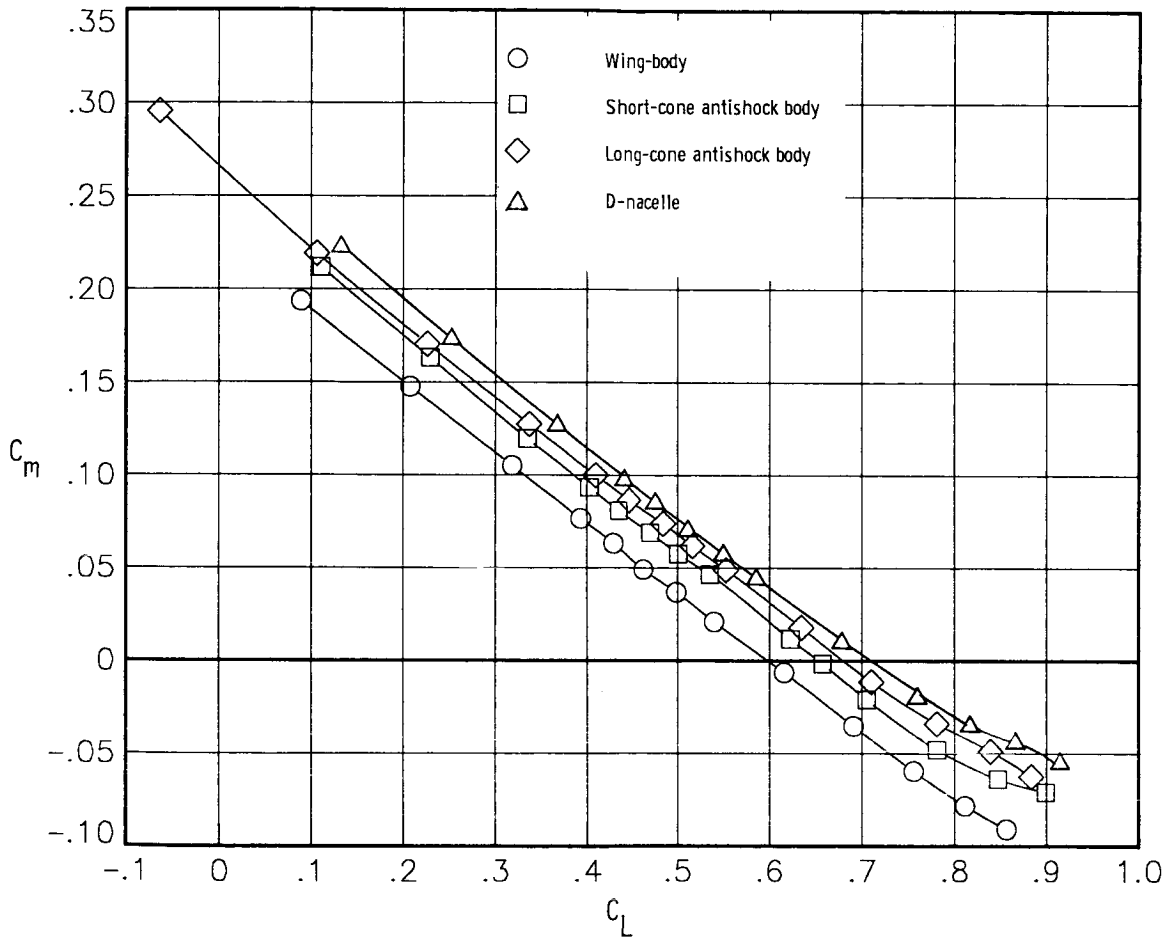

(c) Pitching-moment coefficient plotted against lift coefficient.

Figure 33.- Concluded.

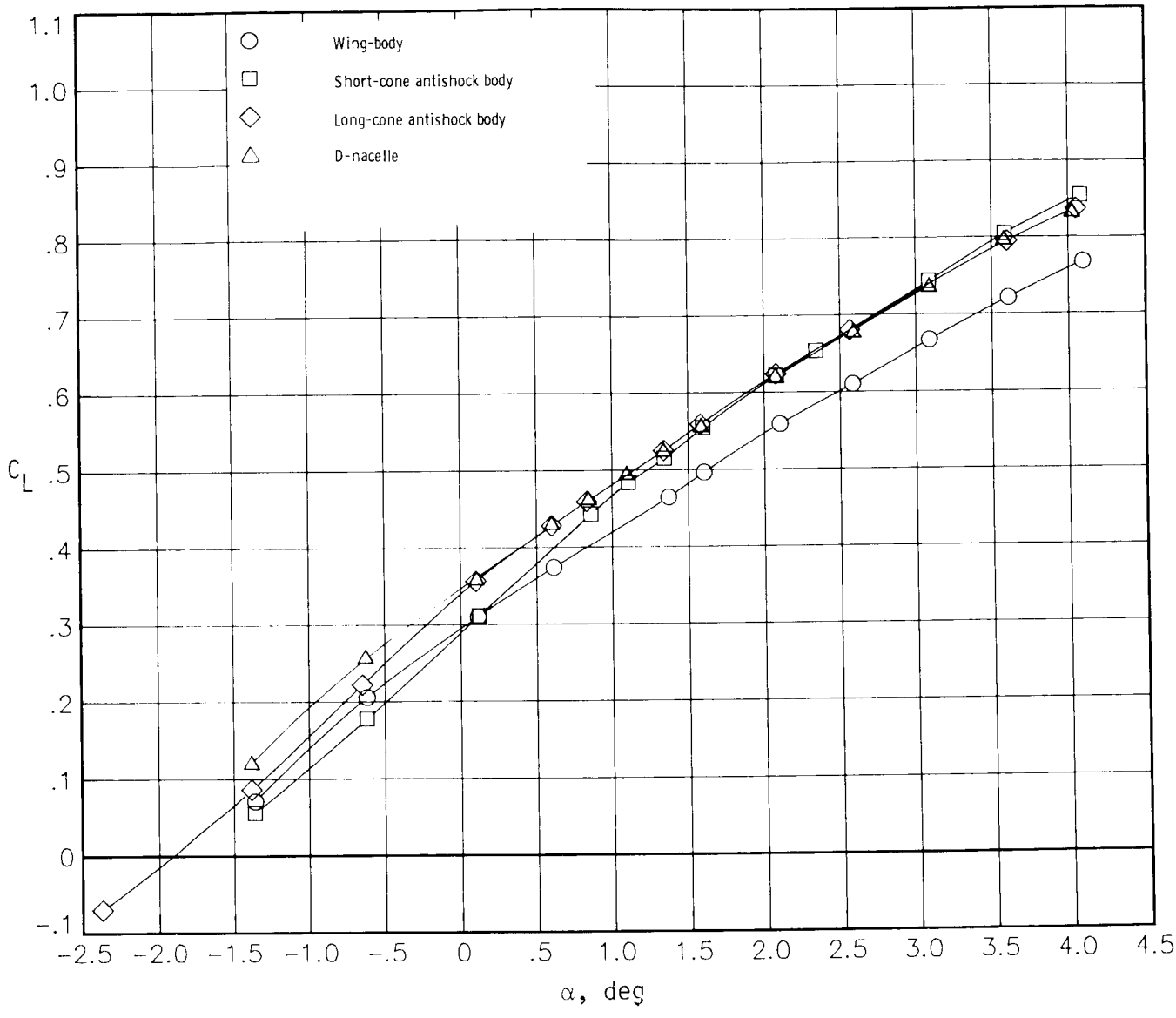

(a) Lift coefficient plotted against angle of attack.

Figure 34.- Comparison of longitudinal characteristics at $M_\infty = 0.85$ for underwing aft-mounted D-nacelle/basic-pylon configuration with short-cone and long-cone antishock bodies.

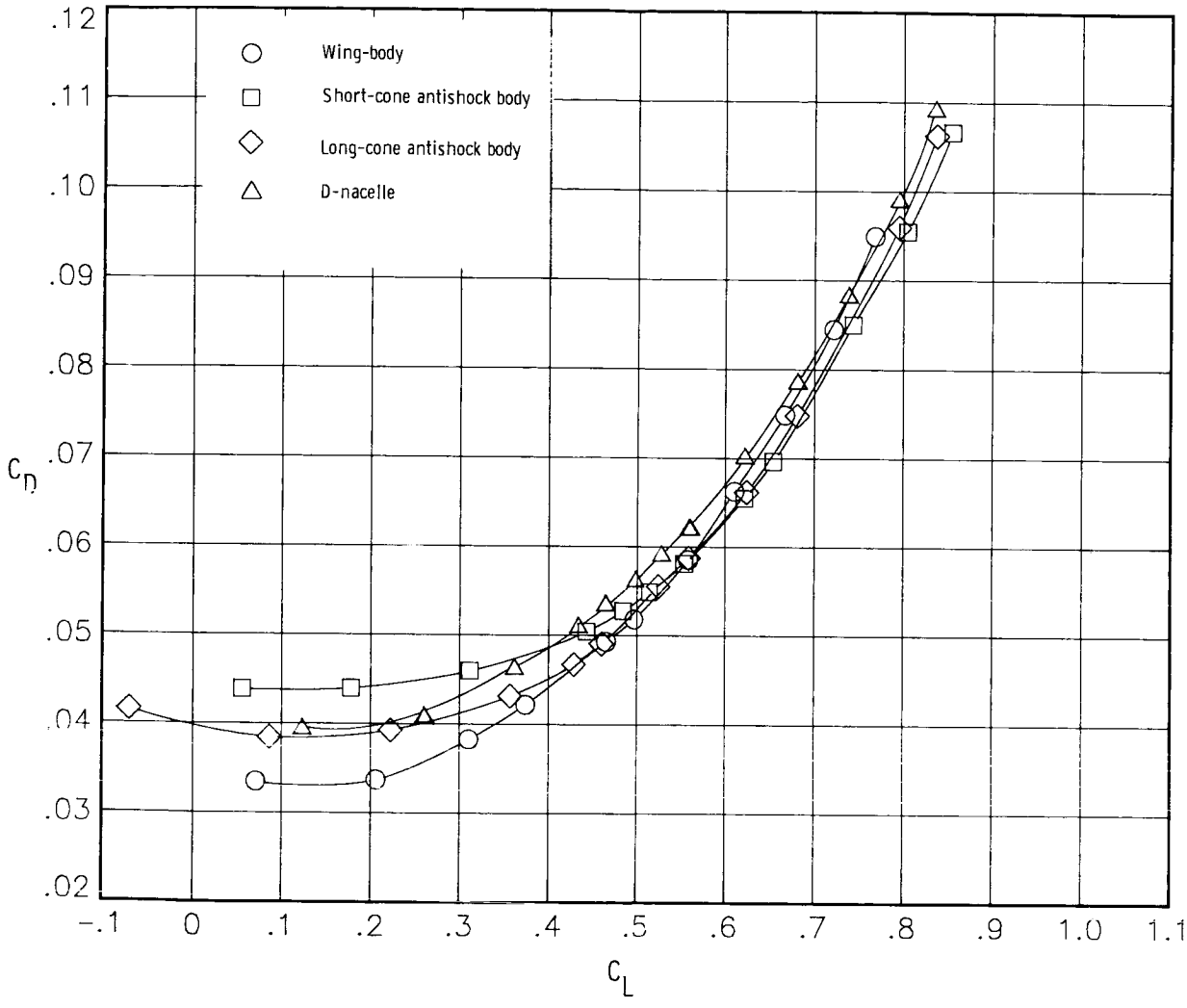

(b) Drag polar.

Figure 34.- Continued.

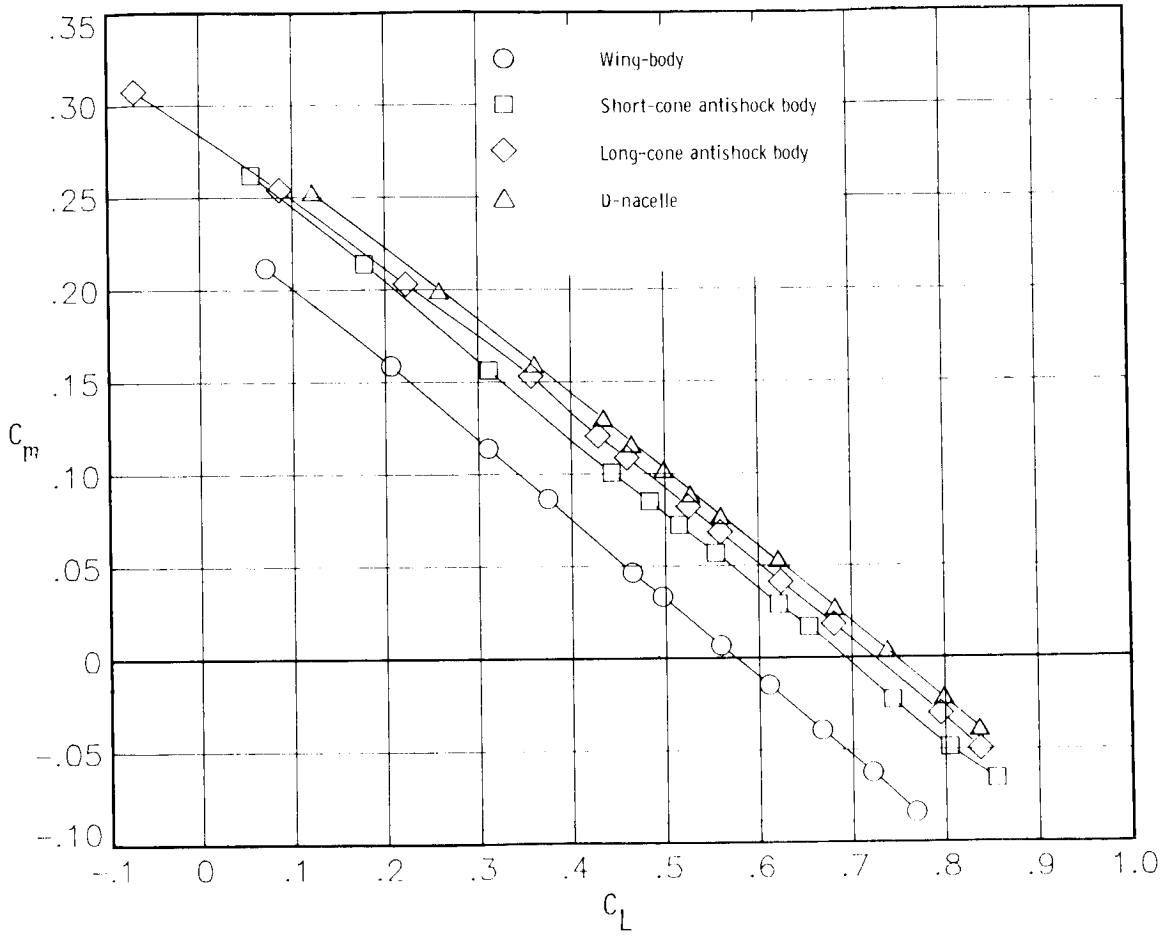

(c) Pitching-moment coefficient plotted against lift coefficient.

Figure 34.- Concluded.

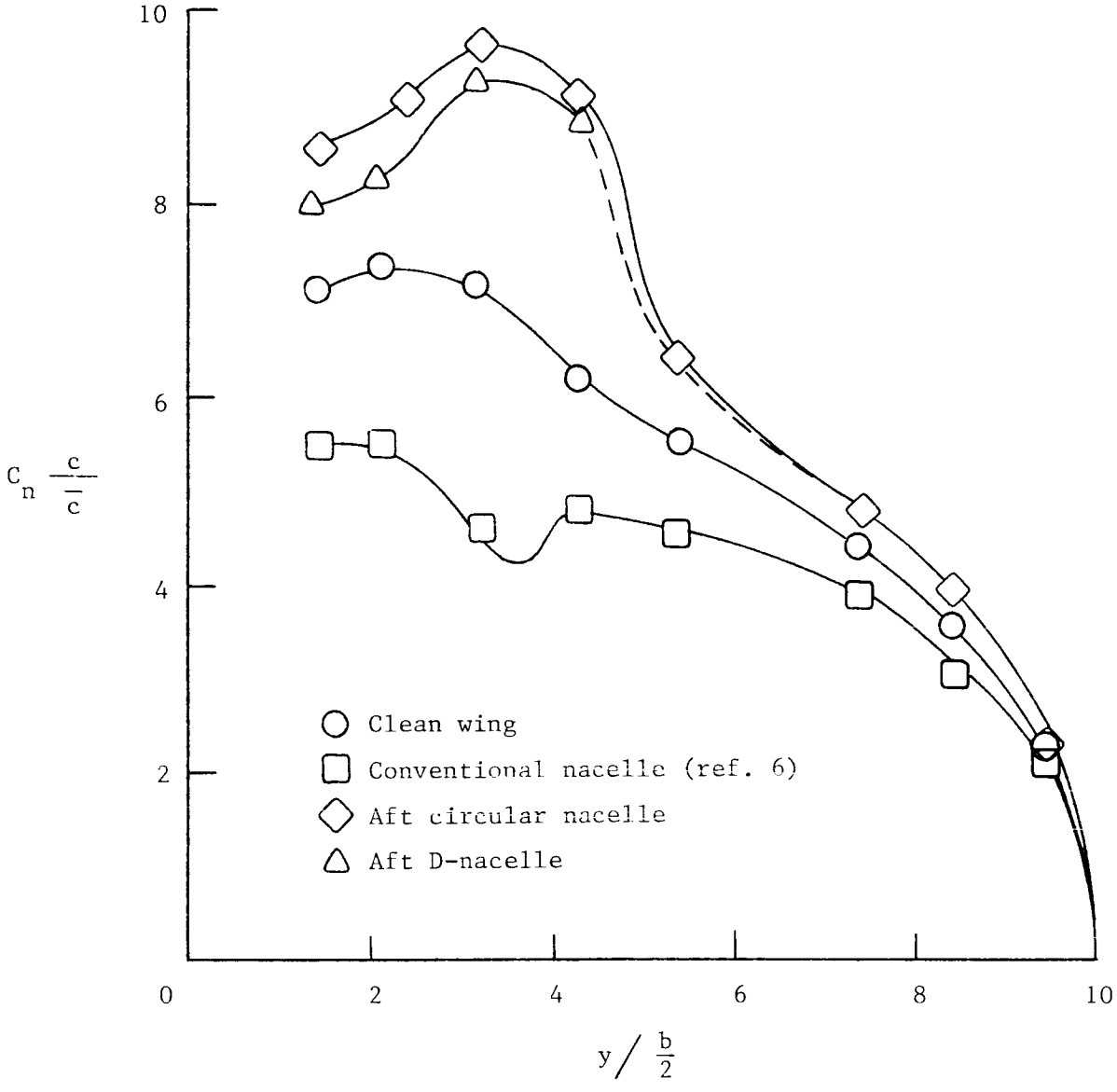

Figure 35.- Comparison of span-load distributions for aft-mounted and conventional pylon-mounted nacelle configurations at $M_\infty = 0.80$ and $\alpha = 1.0°$.

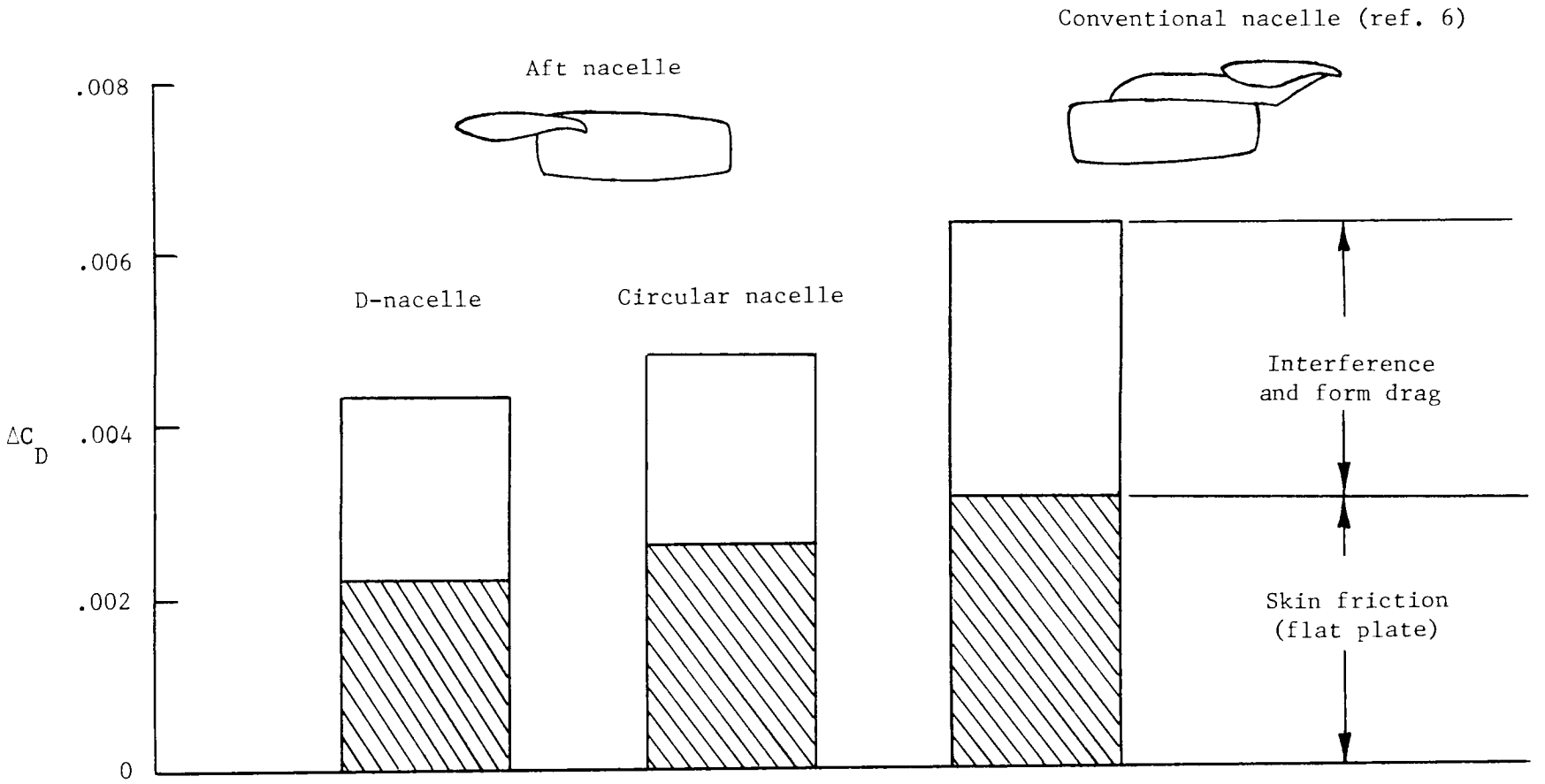

Figure 36.- Comparison of installed-drag increments for aft-mounted and conventional pylon-mounted nacelle configurations at $M_\infty = 0.80$ and $C_L = 0.43$.

1. Report No.	2. Government Accession No.	3. Recipient's Catalog No.
NASA TP-2447		

4. Title and Subtitle	5. Report Date
Effect of Underwing Aft-Mounted Nacelles on the Longitudinal Aerodynamic Characteristics of a High-Wing Transport Airplane	December 1985
	6. Performing Organization Code: 505-40-90-01
7. Author(s): William K. Abeyounis and James C. Patterson, Jr.	8. Performing Organization Report No.: L-15664
	10. Work Unit No.
9. Performing Organization Name and Address: NASA Langley Research Center, Hampton, VA 23665-5225	11. Contract or Grant No.
	13. Type of Report and Period Covered: Technical Paper
12. Sponsoring Agency Name and Address: National Aeronautics and Space Administration, Washington, DC 20546-0001	14. Sponsoring Agency Code

15. Supplementary Notes

16. Abstract

As part of a propulsion/airframe integration program at the Langley Research Center, tests have been conducted in the Langley 16-Foot Transonic Tunnel to determine the longitudinal aerodynamic effects of installing flow-through engine nacelles in the aft underwing position of a high-wing transonic transport airplane. Mixed-flow nacelles with circular and D-shaped inlets were tested at free-stream Mach numbers from 0.70 to 0.85 and angles of attack from -2.5° to 4.0°. The aerodynamic effects of installing antishock bodies on the wing and nacelle upper surfaces as a means of attaching and supporting nacelles in an extreme aft position have been investigated.

17. Key Words (Suggested by Author(s))	18. Distribution Statement
Transport airplane Favorable interference D-shaped nacelles Antishock bodies	Unclassified - Unlimited Subject Category 02

19. Security Classif. (of this report)	20. Security Classif. (of this page)	21. No. of Pages	22. Price
Unclassified	Unclassified	137	A07

For sale by the National Technical Information Service, Springfield, Virginia 22161

National Aeronautics and
Space Administration
Code NIT-4

Washington, D.C.
20546-0001